Desert dune system response to Late Quaternary environmental change in the northeastern Rub' al Khali: Advances in the application of optically stimulated luminescence datasets

Carly L. Leighton

St Catherine's College

Thesis submitted for the degree of

Doctor of Philosophy

University of Oxford

Trinity Term 2013

Approximately 74,000 words

Abstract

The application of optically stimulated luminescence (OSL) dating to desert sand dunes has allowed accumulation histories to be used as tools to infer past environmental change. In response to issues facing the interpretation of these records, two research questions are addressed in this thesis. (i) Are dune chronologies representative of dune stratigraphies? And (ii) how can we most appropriately interpret dune chronologies as records of Quaternary environmental conditions?

Five dune profiles were sampled for OSL dating at two sites in the northeastern Rub’ al Khali in the southern Arabian Peninsula. The visible stratigraphy was used to guide sampling for three of the profiles and the effectiveness of this approach is assessed. A key finding is that bounding surfaces are not always identifiable as chronological hiatuses by OSL dating, given the level of precision that can be achieved. Using hierarchical relationships visible in two-dimensional exposures is therefore not guaranteed to identify the depositional units necessary to reconstruct dune histories.

Comparison of the depositional records from three sampled profiles shows that there is significant variability in chronologies at both the dune and dunefield scales. In light of these findings, the use of ‘range-finder’ OSL dating was investigated as a method of increasing sample throughput in the laboratory. It is concluded that the use of partially prepared samples and shortened measurement techniques can be used to rapidly assess the chronological context of samples and target those units most useful in constructing dune profiles.

A new method of presenting dunefield OSL datasets as net accumulation rates, incorporating accumulation thickness rather than relying on the frequency of ages, is presented. Within the last 30 ka, regional accumulation and preservation occurred at ~30-26, 22.5-18, 16-9, 6-2.7, 2.1-1.6, 1.1 and 0.7 ka. In conjunction with numerical model results and a review of other palaeoenvironmental archives, the regional aeolian record is interpreted as a response to changing forcing factors. High rates of net accumulation between ~16-9 ka are attributed to coeval increases in sediment supply and transport capacity. A hiatus in accumulation between ~9-6 ka is interpreted as a result of reduced sediment availability due to high moisture levels. The importance of both external forcing factors and local controls on dune accumulation processes is recognised, and therefore the importance of sampling at multiple locations to distinguish these factors is emphasised.

Acknowledgements

Most thanks must go to my supervisors Dave Thomas and Richard Bailey for granting me the opportunity to be their student on this project, introducing me to the desert, and being incredibly supportive throughout.

Without a fully funded National Environment Research Council (NERC) studentship I would not have been able to have spent the last 3.5 years working on such an exciting project. In addition, I am grateful to St Cross College for a college travel grant, St Catherine's College for awarding me the C.C. Reeves Scholarship, and the British Society for Geomorphology for a postgraduate grant. And many thanks to St Catherine's College for taking me back as a student for a few more years.

Thanks to Matt Telfer for all his help in the lab and encouragement, and to the Oxford OSL group for helpful and instructive discussions on everything related to OSL. Giles Wiggs and Heather Viles for advice and guidance throughout this project, and also for Giles' assistance in the field. Mona Edwards for guidance in the lab, Ailsa Allen for much needed help with figures, Lorraine Wild, and Matthew Burn for helping to improve our workspace within the department. And to Heather Viles and Mark Bateman for kindly agreeing to be my examiners.

I'm grateful to Richard Washington and Ali Rogers who offered me the chance to become a member of Keble College. Thanks also to Andrew Barry and Richard Bailey for allowing me to be involved again in undergraduate Geography at St Catherine's College.

Thanks to everyone in the department, and particularly fellow members of the various 'DPhil rooms', including Jeremy, Caitlin, Ashley, Mari, Becky, Rachel, and Andrea. A special mention must go to Vicky, Eveliina, Tanya, and Nihan. To friends within and outside of Oxford who always provide much needed and welcome entertainment. Especially housemates (past and present), Lucy, Charlotte, Maddy, Hannah, Kylie, Katy, Sarah, Fabi, James M, Matt, and Stephen.

Alex, for encouragement, support and distraction. And to my family, particularly my parents, for everything.

Table of Contents

List of Tables and Figures

Chapter 1

Chapter 2

Abbreviations and Units

OSL	Optically Stimulated Luminescence
TL	Thermoluminescence
D_e	Equivalent dose (Gy)
SAR	Single aliquot regenerative
IR	Infrared
IRSL	Infrared Stimulated Luminescence
GPR	Ground penetrating radar
PDF	Probability density function
IOSM	Indian Ocean Summer Monsoon
ITCZ	Inter-tropical Convergence Zone
LGM	Last Glacial Maximum
MIS	Marine Isotope Stage

Units

ka	Thousands of years before present
Ma	Millions of years before present
^{14}C BP	Uncalibrated radiocarbon years before AD 1950
cal. ka BP	Calibrated radiocarbon thousands of years before AD 1950
Gy	Gray (1 Gy=1 J kg^{-1})
nm	nanometres
W	Watt (1 W=1 J s^{-1})

Time intervals

Following the International Commission on Stratigraphy

Quaternary	Since 2.6 Ma
Pleistocene	1.8 Ma until the Holocene
Late Pleistocene	130 ka until the Holocene
Holocene (MIS 1)	Since 11.7 ka

Following Martinson et al. (1987)

MIS 2	24 – 12 ka
MIS 3	60 – 24 ka
MIS 4	74 – 60 ka
MIS 5	130 – 74 ka

Following Carlson (2010)

The Younger Dryas	~12.9 – 11.6 ka

Following Hemming (2004)

Heinrich event 1	~16.8 ka
Heinrich event 2	~24 ka
Heinrich event 3	~31 ka

SECTION 1: INTRODUCTION

1 Questioning the utility of sand dunes as palaeoenvironmental records

1.1. Introduction

The study of past climatic change has fundamentally changed our understanding of the earth system. Rapid and dramatic change is recognised to have occurred at times throughout the last ~2.6 Ma (the Quaternary Period). Palaeoclimate research has contributed significantly to predicting and planning for the impacts of future climate change by providing evidence on the magnitude, frequency and spatial extent of past climatic changes and associated environmental responses. This is evident, for example, through the contribution of palaeoenvironmental studies to the fourth Intergovernmental Panel on Climate Change (IPCC) assessment report (Jansen et al., 2007).

A range of palaeoenvironmental proxies, including those from ice and marine cores, has enabled the reconstruction of past climates at a range of spatial and temporal scales. Of particular interest is the increasing use of terrestrial archives such as lacustrine records, speleothems and various geoproxies, which has enabled an appreciation of the complex responses of different parts of the terrestrial environment to climatic forcing.

Drylands are particularly important regions for study given their sensitivity to changes in climate. Under the definition of drylands classified according to an aridity index constructed by the UNEP (1992), dry-subhumid, semi-arid, arid and hyper-arid regions comprise approximately 47% of global land area (see Thomas, 2011, for more detailed discussion). Under a range of emissions scenarios for the twenty-first century, mean surface air temperatures over many of the arid subtropics including the Sahara, southern Africa, the interior of the Arabian Peninsula and central Australia are projected to rise greater than the global mean (Christensen et al., 2007; Washington and Thomas, 2011). Precipitation is expected to fall in the subtropics as the reach of subtropical anticyclones extends polewards (Christensen et al., 2007; Washington and Thomas, 2011). Rising temperatures and drier subtropics are likely to have far-reaching implications (Christensen et al., 2007), such as through the impacts of predicted increases in dune activity (Thomas et al., 2005; Wang et al., 2009) and dust emissions (Prospero and Lamb, 2003; Washington et al., 2009). Given the significance of these potential impacts and the direct importance of drylands for a large proportion of the world's population, more drylands research is required within Quaternary science. Improving understanding of the response of arid environments to climatic change is of considerable interest and relevance.

Part of the reason for a relative paucity of palaeoclimate research in drylands is that these regions are often lacking in palaeoenvironmental proxies (typically organic material or isotope records) and suitable material for radiocarbon dating. The development of optically stimulated luminescence (OSL) dating, which establishes the time since sampled sediment was last exposed to sunlight, has provided the opportunity for chronologies of the environmental histories of drylands to be established using geomorphological features or 'geoproxies' (Thomas and Burrough, 2012). Depending on the nature of the samples to be dated, OSL dating is often applicable to samples with burial ages in the range of 0.1-200 ka. This technique has been applied to a range of dryland geomorphological features, including shorelines and alluvial sediments (e.g. Burrough et al., 2007; McLaren et al., 2009), but it is dunefields that have been most extensively dated due to their often large spatial extent and a depositional environment that is most suitable for the assumptions of OSL dating.

This introductory chapter will discuss the role of sand dunes in palaeoenvironmental reconstructions and the questions that have been raised from the application of OSL dating to these features. The aims of this thesis, which are presented at the end of this chapter, are in response to these questions. Ultimately, the project is concerned with contributing towards improving understanding of the response of drylands to past climatic change. What do OSL chronologies from desert sand dunes mean in terms of palaeoenvironmental change?

1.2. Thesis structure

This thesis follows the published paper route, which involves the submission of at least four submitted papers to a range of peer-reviewed journals. As such, four submitted papers and one paper to be submitted have been incorporated into Chapters 4-8. These papers have been co-authored with supervisors (Appendix A). The papers have been partially edited in order to avoid too much repetition between chapters, which would inevitably occur because, in isolation, the papers require a degree of similarity in background material. However, some repetition is unavoidable, especially as arguments are developed in the discussion sections.

The thesis is divided into three sections. In Section 1 an *introduction* is provided to the subject of investigation, the area in which the project is situated, and the methods that will be used to address the aims of the thesis. In this chapter, the research aims are discussed in relation to the use of sand dunes as palaeoenvironmental archives. In Chapter 2 the geological and environmental history of the southern Arabian Peninsula is outlined, through a description and explanation of past and recent research using a range of palaeoenvironmental archives. The present day setting of the main study sites is also discussed. The purpose of Chapter 3 is to describe the methodologies used in this thesis, in particular OSL dating (including sample collection, preparation, and measurement, and age calculation), in more detail than possible in the papers.

Section 2 comprises four chapters that describe field and laboratory *investigations* addressing the research aims. In Chapters 4 and 6 the OSL ages from two field seasons in the northeastern United Arab Emirates (UAE) are presented (samples UAE10 in Chapter 4 and samples UAE11 in Chapter 6). Chapters 5 and 7 are short comments and investigations in response to the issues raised in these two central chapters.

The research presented in Chapter 4 (Paper 1) investigates the use of visible bounding surfaces as foci to 'target' OSL sampling as a method of increasing sampling efficiency, and to assess the extent to which dune OSL chronologies reflect the internal structure of the dunes they sample. In response to these findings, in Chapter 5 (Paper 2) the practical relevance of allostratigraphy, which defines sedimentary units through the presence of bounding surfaces, to the study of past dune dynamics is discussed. During fieldwork, the use of ground penetrating radar (GPR) was assessed as a further means of establishing dune stratigraphy in subsurface locations. This attempt was unsuccessful and is consequently explained in Appendix B, rather than in the main thesis body.

The reproducibility of chronologies at the dune and dunefield scales is assessed in Chapter 6 (Paper 3) by comparing multiple sampling profiles, and discussing some of the fundamental issues of interpretation that are frequently debated when using sand dunes as palaeoenvironmental archives. In Chapter 7 (Paper 4), the use of range-finder OSL dating, in which preparation and measurement protocols are shortened, is investigated as a tool for increasing sample throughput in the laboratory. This is a practical response to the issues raised in Chapters 4 and 6.

The *implications* of this project for the interpretation of dune OSL chronologies are presented in Section 3. Building on earlier chapters, in Chapter 8 (Paper 5) a numerical model is utilised to understand the dune chronology of the region as a response to external forcing factors, and relate the aeolian record to other palaeoenvironmental archives in the region. The main conclusions of the thesis are then presented in Chapter 9, alongside the wider implications for palaeoenvironmental research in drylands.

1.3. Sand dunes as palaeoenvironmental archives

1.3.1. Theories of linear dune development

Linear dunes occupy over 40% of sand seas (Bullard et al., 1995), and are the most ubiquitous of desert dunes. The term 'linear' describes the dune morphology rather than being used to imply particular formative processes. For example, 'longitudinal' dunes more specifically define a dune trend within 15° of the resultant transport direction, as shown in Figure 1.1 (Hunter et al., 1983). This distinction is particularly relevant to note for the investigation of past dune development processes as the morphodynamic relationship between the dune and past formative winds may be unknown (Munyikwa, 2005). Hence linear dunes can be composed of a variety of dune types formed under different climatic and environmental conditions (Bullard et al., 1995). Classification systems have been developed to describe the morphological variability of linear dunes (Bullard et al., 1995; Fitzsimmons, 2007), which is suggestive of the complexity of linear dune formation and their variability of form. They are frequently used as long-term records of environmental change as they are thought to preserve longer records than other more transitory and migratory dune types (Telfer et al., 2010; Tsoar et al., 2004). Simple dunes are individual bedforms, rather than compound or complex dunes that are composite structures of the same or different dune types respectively (Lancaster, 1988). There are two main types of simple linear dune; sinuous (also known as seif) dunes, which are sharp-crested and have no, or very limited, vegetation cover, and partially vegetated dunes which are longer, straighter and rounder in shape (Lancaster, 2011; Tsoar, 1989).

The early work of Bagnold (1941) in producing detailed investigations of grain movement and dune processes has since been built on extensively (e.g. Lancaster et al., 2002; Tsoar, 1989; Wasson and Hyde, 1983). These authors, amongst others, have attempted to relate

Figure 1.1 has been removed due to Copyright restrictions

Figure 1.1: A morphodynamic classification of linear dunes, based on the angle between resultant transport direction and average dune trend. Redrawn from Hunter et al. (1983).

Figure 1.2 has been removed due to Copyright restrictions

Figure 1.2: A summary of common types of stratification in aeolian dunes. Adapted from Hunter (1977).

field evidence of dune morphology and internal structure to formative winds and processes. However, there is still a paucity of understanding in some aspects of linear dune dynamics. Individual dune morphology is a product of the influence of wind speed, wind direction, slope morphology, sediment supply and grain size distribution, and hence the sedimentary record preserved is a function of many local and external variables (Munyikwa, 2005).

A helpful description of the types of stratification often found in aeolian dunes (Figure 1.2), and the conditions in which they form, is provided by Hunter (1977). The classifications are made using a number of properties including dimensions, grain size, and the relation of the strata to adjacent contacts and strata (Hunter, 1977).

Formation within a bidirectional wind regime

The most widely accepted mechanism of linear dune formation supported by field evidence is due to the interaction of directionally bimodal winds that create a resultant direction of sand transport parallel to the dune body (Livingstone, 1989; Rubin and Hesp, 2009; Tsoar, 1983; Wiggs, 2001). In general, there is net deposition on the plinth, which is relatively stable, whilst approximately half-way up the windward slope there is net erosion due to velocity speed-up (Figure 1.3; Lancaster, 1985; Tsoar, 1983; Wiggs, 2001). The transport capacity of the wind, q, increases as the shear velocity (u_*) increases: $q \approx A{u_*}^3$, where A is a constant (Bagnold, 1941; Wiggs, 2001). Erosion is expected to occur on the windward slope, with maximum erosion at the crest as streamlines converge, whilst net deposition occurs on the lee side of the dune (Wiggs, 2001). The stability of the bedform is maintained by a balance between the seasonal reversals of the crest line and alternation of the windward and lee side of the dune, which must seasonally respond to this switch in dominance of erosional and depositional processes (Figure 1.3b; Lancaster, 1985; Munyikwa, 2005; Wiggs, 2001). The level of reworking during each wind reversal will determine the level of continuity of the sequence. If the wind angle of incidence is less than 40° to the crest line sand transport continues in the lee-side eddy parallel to the crest, eroding the leeward slope and elongating the dune, but an angle of incidence greater than this and only deposition takes place as the wind velocity on the lee side decreases (Tsoar, 1983, 1989; Tsoar et al.,

Figure 1.3 has been removed due to Copyright restrictions

Figure 1.3: (a) Compression of streamlines over a dune. There is acceleration of the winds towards the crest and turbulence in the lee of the dune as streamlines diverge. Redrawn from Wiggs (2001). (b) Alternation of the stoss and lee side of the dune and shifting of the crest position in response to two changing wind directions. Redrawn from Lancaster (1982).

2004; Wiggs, 2001). The slip-face is therefore not the only part of the dune where deposition occurs, and hence they are not as well defined as on transverse dunes (Tsoar, 1983).

In addition to field evidence, modelling has supported the hypothesis that linear dunes and transverse dunes are formed under bidirectional and unidirectional wind regimes respectively (Parteli et al., 2009; Zhang et al., 2005). Linear dunes are stable when the angle between the two winds is greater than 90°, whilst parallel wind components will destabilise the dune form along its length (Parteli et al., 2009). Sinuous dunes are formed when sand availability is high, allowing for an initial sand pile to develop into a single crest that extends towards the resultant wind direction over time. These modelling results are confirmed by subaqueous experiments, where the smaller scale enables an examination of the long-term formation and evolution of linear dunes (e.g. Reffet et al., 2010).

Helical roll-vortices model

An alternative theory advocates the role of helical vortices in linear dune formation. Pairs of counter-rotating air currents, bounded by the top of the planetary boundary layer, are postulated to transport sand from the interdune to the crest (Bagnold, 1953; Tseo, 1993). However, it is no longer a particularly persuasive or popular hypothesis and has little evidence to support it from the field (Livingstone, 1988; Wiggs, 2001).

Wind-rift model

Recent work in Australia has seen a re-emergence of hypotheses placing significance on local erosional processes in supplying sediment for dune accumulation. The wind-rift model proposes the erosion of locally derived sediment which is deposited laterally or obliquely onto linear dunes (Hollands et al., 2006). This process is distinguishable from sediment reworking that occurs mainly on the crest of dunes (Fitzsimmons, 2007). In the northwestern Simpson Desert, sedimentological analysis at a number of sites within the Camel Flat Basin led Hollands et al. (2006) to address two aspects of linear dune development. The authors suggest that firstly, spatial differences in dune sediment characteristics show the importance of local sourcing of sediment, and secondly, there is no evidence for long distance sediment transport by linear dune extension. These findings have been supported by spectral analysis of satellite imagery in the Strzelecki and Tirari Deserts; the relationship between local substrate and dune morphology indicates that local sourcing of sediment is an important influence on dune processes (Fitzsimmons, 2007). This theory of dune development is not incompatible with that of bidirectional winds, although the latter puts a more prominent role on long-distance transport and deposition of sediment (Wopfner and Twidale, 2001). However, the distinct sedimentology and chronologies of different zones in this particular basin does question whether one theory of dune development when interpreting OSL dates is applicable to different sites, even within a single dunefield.

Whether accretion or elongation is the dominant process of dune development has important implications for the replicability of OSL chronologies along an individual dune. If vertical accretion is the dominant process, chronologies may be expected to be more similar than if dunes extend, as the latter process implies that dunes should be older upwind. Field evidence for extension of dune form consists of dipping towards the trending direction (Rubin, 1990) and younger ages towards the dune termination (Bristow et al., 2007b; Hollands et al., 2006; Telfer, 2011). Systematic OSL dating of a simple linear dune in the southwestern Kalahari leads Telfer (2011) to suggest that there is evidence of extensional growth during periods of net accumulation, but that reworking of the dune crest without significant dune extension is also prevalent independent of environmental conditions. The use of GPR may aid the answering of some of these questions at larger scales; for example, if it is possible to trace sedimentary sets downwind. However, this has previously proved difficult; for example Bristow et al. (1996) reveal the complexity of the internal stratigraphy of compound crescentic megadunes in Liwa, UAE. The migration of superimposed dunes has resulted in concave-up and concave-down reflective surfaces in the strike profiles. Similarly the downwind migration of peaks and saddles may complicate the internal stratigraphy of sinuous dunes (Tsoar et al., 2004) and result in discontinuous bounding surfaces that cannot be traced between dated samples.

Vertical accretion and lateral migration

Bagnold (1941) assumes vertical accretion of linear dunes with no net lateral migration, producing an effectively symmetrical internal structure (Figure 1.4a). This structure is envisaged as a zig-zag pattern of bimodal cross-stratification reflecting the reversing of the crest due to changes in seasonal wind direction, with steeply dipping avalanche deposits on the crest and low angle accretion laminae on the plinths (Lancaster, 1982). Thicker sets are expected to be deposited from winds blowing for a long duration (Lancaster, 1982). An increase in angle of incidence will lead to more steeply dipped avalanche cross-bedded deposits, and more sinuosity (Lancaster, 1982; Tsoar, 1989).

Rubin and Hunter (1985) argue that dunes migrate laterally when they are not aligned parallel to the long-term sand transport direction, resulting in deposits with a unimodal cross-bed dip direction which have often been mistaken for transverse dunes in the geological record (Figure 1.4b). Their predicted internal structure has been found to be very similar to structures exposed in the Tsondab Sandstone, Namibia (Kocurek et al., 1999), the Strzelecki Desert, Australia (Rubin, 1990), and in contemporary dunes in the Namib Sand Sea (Bristow et al., 2000, 2005). Combining OSL dating with GPR surveys enabled Bristow et al. (2005) to infer a time-averaged lateral migration rate of 0.12 m a^{-1} over the last 1600 years for complex linear dunes in the Namib Sand Sea. Tsoar et al. (2004) find no evidence of lateral migration of seif dunes in the Sinai desert between 1973 and 1999, but instead suggest that unimodal dipping is a result of the formation of peaks and saddles that are displaced downwind as a result of the variations in angle of incidence between the wind and the crest. Similarly, lateral migration of linear dunes has also not been supported in the Namib, by surveys between 1980 and 2001 (Livingstone, 2003), or in the southwestern Kalahari (Telfer, 2011).

Lateral migration of linear dunes may be a constraint on OSL chronologies depending on the rates of migration in comparison to vertical accretion. Consistently unimodal dip directions would also suggest preferential preservation of dune material deposited from one wind direction, producing a discontinuous record biased towards one mode of deposition. This should be acknowledged when inferring past changes in wind circulation, as one part of the bidirectional wind regime is not recorded in the dune’s internal structure. It is not solely changes in wind energy that are important but also the change in wind direction with relation to dune morphology, which determines the effectiveness of the wind in altering dune morphology and its preservation in the sedimentary record (Lancaster, 1982). Whether lateral migration is substantial enough to be captured by the precision of OSL dating or significantly reduce the temporal scale of the record is a function of the variability and strength of wind regime, the age of the dunes, and dune size and morphology, which will determine their reconstitution time.

Figure 1.4 has been removed due to Copyright restrictions

Figure 1.4: Predicted models of the internal structure of linear dunes: (a) Bagnold (1941) model showing vertical accretion of a near-symmetrical dune; (b) Rubin and Hunter (1985) model of lateral migration of a linear dune, with superimposed dunes migrating in an along-crest direction. Redrawn from Rubin and Hunter (1985).

The relationship between boundary conditions and dune system response

Recently there has been a reduction in the number of single-dune field studies, in part in recognition of the need to avoid simplifying the complexity of dune systems (Livingstone et al., 2007). The diversity of dunefields is a systematic reflection of the interaction between external boundary conditions and intrinsic processes (e.g. Derickson et al., 2008; Ewing and Kocurek, 2010). As scale increases, emergent behaviour is evident and dunefield patterns can be understood as being controlled by fewer significant controlling parameters (Thomas and Wiggs, 2008). External boundary conditions are argued to be a key forcing factor leading to dune field variability (e.g. Bullard et al., 1995):

> "Ultimately, boundary conditions impose a strong influence upon the type and frequency of bedform–bedform interactions that occur within a dune-field, which, in turn, strongly influence the resulting pattern" (Ewing and Kocurek, 2010: 176).

Variability in the relative dominance of different boundary conditions during dunefield pattern development leads to the modification of existing patterns and formation of complex dune patterns (Kocurek and Ewing, 2005). This approach supports the assumption that changes in external environmental factors are an important control upon the character of a dunefield (Ewing and Kocurek, 2010). The implication is that resultant dune patterns, and associated analyses (such as representative chronological investigation), are meaningful (rather than stochastic) and can be used to infer changes in past environmental controls.

More stable than some other dune types, linear dunes respond to changes in environmental conditions by pattern-reordering rather than reorientation and creating forms composed of multiple patterns and generations (Kocurek and Ewing, 2005). In the Sahara Desert, Mauritania, three 'generations' of superimposed dunes are interpreted to have formed in response to changing atmospheric conditions and wind regimes on the basis of distinct dune trends and depositional ages (Lancaster et al., 2002). However, OSL dating of complex dunes across multiple sites in the northeastern Rub' al Khali indicates that they accumulated over similar time periods, and hence simplified interpretations based upon discrete and altered boundary conditions cannot fully explain dune patterning in this region (Atkinson et al., 2012). Ewing and Kocurek (2010) designate antecedent conditions, such as topography, water table depth, and vegetation, as geomorphic boundary conditions. Thus, local context may be important in explaining variable responses to environmental conditions over space and time, in addition to climatic changes.

1.3.2. Aeolian sequence stratigraphy

The internal structure of sand dunes provides a valuable glimpse of past dune system dynamics. Examining stratigraphy, where available, can aid our interpretation of how a particular dune has developed, with the hope of linking this development to changing environmental conditions.

'Aeolian sequence stratigraphy' (Kocurek and Havholm, 1993) considers the accumulated record as a balance between sediment supply, transport, accumulation and preservation (Thomas and Wiggs, 2008). This approach therefore provides a useful perspective in comparing the behaviour of aeolian systems, at a range of scales, between different environmental contexts in relation to these fundamental controls.

The preserved stratigraphic record is the product of the alternation between phases of erosion, equilibrium and deposition (Selley, 1985). In addition, the influences of pre- and post-depositional processes on its preservation must be recognised. The vertical space in which sediment accumulates (accumulation space) is not inherently equal to the preservation space, in which the sediment lies beneath the baseline of erosion (Boggs, 2006). In relation to sand dunes, the lower units have the potential to be preserved whilst the upper units may be reworked (Boggs, 2006). Periods of accumulation are not necessarily preserved in the stratigraphic record. Preservation potential of an accumulated sequence is influenced by many factors including subsidence, water table level, and vegetation (Kocurek and Havholm, 1993). Whether environmental conditions are conducive to preservation will determine the continuity of sedimentary sequences.

Sediment state

Accumulation depends on the sediment budget of the system (the balance between sediment influx, q_i, and sediment outflux, q_o), with the behaviour of the accumulation surface over time ($\delta h/\delta t$), represented by the sediment conservation equation:

$$\frac{\delta h}{\delta t} = -\left(\frac{\delta q}{\delta x} + \frac{\delta c}{\delta t}\right)$$

(Eq. 1.1)

where q is the bulk volume transport rate, c is the concentration of sediment in transport above the accumulation surface, and x is the direction of transport (Kocurek, 1996). Therefore, $\delta q/\delta x$ is the spatial change in transport rate and $\delta c/\delta t$ is the temporal change in the sediment concentration in transport.

Accumulation occurs when $\delta h/\delta t$ is positive and $q_i > q_o$, a bypass super surface occurs when $\delta h/\delta t$ changes from positive to zero and $q_i = q_o$, and an erosional super surface occurs when $\delta h/\delta t$ changes from a positive to negative value and $q_i < q_o$ (Kocurek, 1996). Change in the level of the accumulation surface over time therefore produces the resultant stratigraphy.

> "A bounding surface is an erosional surface within or between sets of cross-strata" (Kocurek, 1996: 134).

A super surface is one type of bounding surface, which represents a sequence boundary of a period of overall accumulation.

Bounding surfaces mark where changes have occurred in the concentration and/or transportation rate of sediment, and/or the preservation of the accumulation sequence. Kocurek (1981, 1996) describes bounding surfaces in aeolian deposits as interdune, superposition and reactivation surfaces (first, second and third order surfaces respectively according to Brookfield, 1977). Reactivation surfaces form within the set, truncating previous foresets as the lee face is eroded periodically by wind flow fluctuations.

Superposition surfaces form as superimposed dunes or scour troughs on the lee slope of the main bedform migrate. Interdune surfaces form between sets, representing the separate accumulations of different primary bedforms. These stacked strata reflecting the migration of bedforms produce vertical sequences of cross-stratification, and which may be separated by a super surface.

At the micro-scale, processes of sediment entrainment, transportation and deposition are a function of wind velocity and direction, slope morphology, sediment availability and grain size distribution (Munyikwa, 2005). At the larger scale, accumulation and preservation dynamics are controlled by the sediment state of the system, which is a product of sediment availability, sediment supply and transport capacity within the system (Kocurek and Lancaster, 1999). These factors are influenced by a range of factors internal and external to the dunefield, and so the interpretation of the preserved dune stratigraphic record is a result of the complex interplay between these forces.

1.3.3. Summary

External forcing factors such as changes in sea level or climate are important in influencing sediment supply, sediment availability and transport capacity (Kocurek and Lancaster, 1999). These factors interact with local factors, such as groundwater level, vegetation, and topography, to determine whether at a specific point and time deposition or erosion is favoured, and hence whether the accumulation surface rises, falls or is stable. The feedbacks associated with this process allow for the build-up and movement of dunes. As sand is deposited and buried the dune chronological record datable by OSL is produced over time. Erosion may remove and bleach previously deposited sediment, potentially producing hiatuses in the chronological record, whilst the sediment is transported and eventually deposited. The balance between erosion and deposition is therefore important in producing a chronological record that is spatially variable. For example, moisture gradients within a dunefield may result in differences in dune dynamics, and hence chronologies, between different areas in the dunefield (Thomas, 2013). Accumulation and preservation are a result of both large-scale environmental controls and stochastic factors (Telfer et al., 2010; Bailey and Thomas, 2013), resulting in spatially and temporally variable dune records. Small scale variations in these numerous influencing factors can effectively be modelled by a random process (Telfer et al., 2010; Bailey and Thomas, 2013).

It is clear from the discussion of dune dynamics above that there is a similarity between different hypotheses and approaches in the recognition that sand dunes are inherently discontinuous palaeoenvironmental archives. Depositional and preservation processes vary over time and space as a function of both local and external parameters, forced at a variety of temporal scales. Long-term changes may be derived from the preserved sedimentary record, but change is also recorded over shorter temporal and spatial scales and therefore caution in interpretation is required (Thomas and Wiggs, 2008).

1.4. Constructing chronologies in arid environments

Luminescence dating has been increasingly used to date desert sand dunes since first being applied in the Thar Desert three decades ago (Singhvi et al., 1982). The technique measures the burial age of a sample (i.e. last exposure to sunlight), and hence from multiple vertical samples accumulation histories of dunes can be established. The application of drilling equipment has enabled large numbers of samples to be extracted systematically from deep within dune structures (e.g. Bray and Stokes, 2003; Preusser et al., 2002; Telfer and Thomas, 2007). Concurrently, developments in the laboratory, most notably the introduction of the single aliquot regenerative (SAR) protocol (Murray and Wintle, 2000; Wintle and Murray, 2006), have allowed more samples to be dated using OSL and improved levels of accuracy and reliability. However, alongside these developments two fundamental questions are still of relevance: firstly, how can the dependence of chronologies on sampling strategy be minimised; and secondly, what is the best approach to interpret dune(field) chronologies in relation to palaeoenvironmental change?

1.4.1. Sampling strategy dependence

As past studies attempting rigorous sampling strategies have highlighted (e.g. Stone and Thomas, 2008; Telfer and Thomas, 2007), sampling is of key importance when attempting to interpret the significance of groups of OSL ages. Stone and Thomas (2008) demonstrate how the use of different vertical sampling intervals results in distinctly different OSL dune chronologies being produced. At a larger scale, the authors also note how the addition of OSL ages to previous syntheses in the southern Kalahari has resulted in chronological gaps being filled in. At both the dune and dunefield scales, sufficient sampling resolution is required for patterns in OSL chronologies to be interpreted as independent of the sampling strategy employed. Aliasing, which is the emergence of 'false' signals by under-sampling a record, is therefore a key problem facing the interpretation of dune chronologies.

Telfer et al. (2010) use a simple accumulation model to show that rigorous sampling is a necessity in order to have confidence in interpreting the preserved dune accumulation record as reflecting external environmental forcing factors (Figure 1.5). The authors suggest "hundreds, and preferably thousands, of dates may be necessary to discern signal from noise" (Telfer et al., 2010: 207). Another facet to consider when interpreting the preserved OSL dates is that reworking biases the preserved record towards younger ages, with Telfer et al. noting a power-law decline in frequency with age. This is true not only in the consistent forcing scenario, but also under periodic forcing, when the frequency of dates during peaks of instability decreases with increasing age.

In addition to the requirement for sampling to capture the sedimentary units present, there is therefore also a necessity to be able to distinguish periods of significant accumulation as a

Figure 1.5 has been removed due to Copyright restrictions

Figure 1.5: Results from a simple accumulation model under a continuous forcing scenario (20 ka of stability, where deposition probability is equal to reworking probability). The left histogram shows the total net accumulation recorded after 20 model runs using 500 year bins, and shows the presence of peaks in preservation, despite constant forcing. The right histogram shows the same but after 1000 model runs. The peaks are much less developed but the power-law decline in preservation is evident. n represents the total frequency of depositional units. Reproduced from Telfer et al. (2010).

result of external forcing from intrinsic processes involving the recycling of sediment. Of course, the practical implications of these findings are problematic. In addition to the limitations of time and finances, sampling at the necessary high resolution may not be feasible in certain contexts.

Whilst the development and application of drilling has enabled the extraction of increasing numbers of OSL samples in some contexts (e.g. Bray and Stokes, 2003; Preusser et al., 2002), an alternative approach to addressing the problem of sampling resolution is to ‘target’ particular features within the dune. Systematically vertically sampling down a dune profile may not be the most appropriate mode of sampling in order to reflect the internal structure of a dune. Understanding and utilising visible dune stratigraphy may produce more meaningful dates in respect to past dune dynamics. When visible, stratigraphy may provide additional useful information to inform OSL sampling. For example, palaeosols and cutans (clay coatings formed around sand grains during illuviation and pedogenesis) in dune sequences have been used to infer wetter climatic conditions (Fitzsimmons and Telfer, 2008; Fitzsimmons et al., 2007). Coupling of GPR surveys and OSL dating has also enabled extensive bounding surfaces to be targeted for dating; increasing precision on the dating of stratigraphic hiatuses (Bristow et al., 2005, 2007a). This can be described as an allostratigraphic approach, which is the use of bounding surfaces to define sedimentary sets (as opposed to, for example, lithology in lithostratigraphy; Hughes, 2010). Additional information such as stratigraphy, where available, therefore may help provide a more appropriate sampling strategy together with information to aid the interpretation of resulting OSL ages. This approach may give us confidence that gaps in the chronology are not merely the result of insufficient sampling coverage, but how to then interpret these gaps in terms of their palaeoenvironmental significance remains problematic.

1.4.2. Interpretation of dune chronologies

Suites of OSL ages are often attributed to past periods of dune accumulation under arid conditions. However, dates cannot simply be extracted and transformed into meaningful discrete 'arid' periods (Chase, 2009; Chase and Thomas, 2006; Lancaster, 2008; Stone and Thomas, 2008). Recent studies have recognised past interpretations equating dune activity and aridity as a simplification of dune processes and noted the importance of the interplay of numerous factors impacting upon dune development at a range of scales (Chase, 2009; Chase and Thomas, 2006). These influences include moisture (Bray and Stokes, 2004; Chase and Thomas, 2006; Lomax et al., 2011; Wiggs et al., 2004), windiness (Chase and Thomas, 2007; Roskin et al., 2011), sediment supply (Goudie et al., 2000a; Preusser, 2009), and human activity (Goudie et al., 2000a; Yang et al., 2012). The nonlinear nature of dune response to changing controlling factors has been shown by the presence of thresholds in relation to dune activity. For example, Wiggs et al. (1995) show that at the dune scale a vegetation cover threshold of about 14% can be identified, below which surface activity increases (based on measurements of dune surface elevation change). Dune processes provide the mechanisms for the interplay between local (autocyclic) and external (allocyclic) factors to produce the dune sedimentary record. Both long-term changes and changes over shorter spatial and temporal scales are recorded (Thomas and Wiggs, 2008). As a result of this complexity, the meaningfulness of dune chronologies in terms of their relation to periods of environmental change is an on-going question, yet a fundamental one that underpins their use within Quaternary science.

Understanding linear dune processes is essential when attempting to reconstruct their development in relation to past environmental changes (Lancaster, 2008). The gap between reductionist studies of sediment transport processes and large scale assessments of palaeoenvironmental research is still prevalent, although aeolian sequence stratigraphy (Section 1.3.2) is one example of a multi-scale approach to the study of aeolian systems (Thomas and Wiggs, 2008). Linear dune dynamics, including processes of elongation/accretion and lateral migration, and the relationship between dune generations, have important implications for the sedimentary record preserved and resultant OSL chronologies, as assessed by Munyikwa (2005). For example, the bidirectional wind model of formation inherently results in discontinuous sedimentary sequences. The lower, less mobile, sections of the dune do not record all aeolian activity, yet the crest is consistently subject to reworking. Chronological hiatuses may mask the erosion of previous periods of accumulation, including deposits formed during humid events. It is therefore unclear whether chronological hiatuses represent periods of reduced aeolian activity or multiple environmental events that have been erased from the sedimentary record. Munyikwa argues that differences in chronologies may be a result of the differential preservation of stratigraphic units at different localities, and suggests that as many dune sequences as possible should be dated in the hope that a stratigraphic unit eroded at one site may be preserved at another.

Figure 1.6 has been removed due to Copyright restrictions

Figure 1.6: (a) The 'filtering' process, describing how information is lost and modified from the initial climate/forcing conditions (the 'aim' of palaeoclimatic research) when sand dunes are used as palaeoenvironmental archives. Adapted from Bailey and Thomas (submitted). (b) The removal of part of an accumulated record during linear dune development (Section 1.3), resulting in a discontinuous preserved record. Adapted from Munyikwa (2005). (c) Aliasing of climate signals as a result of under-sampling, resulting in a different apparent signal to the actual forcing signal. Adapted from Ruddiman (2001). (d) An example showing the use of a probability density function (PDF) to display luminescence ages, which implies that the frequency of ages can be used as a proxy for palaeoenvironmental significance.

The processes described in this section are part of a fundamental problem facing Quaternary science: records used for palaeoclimatic reconstruction are incomplete as information describing the actual past climatic conditions is gradually modified and lost (Figure 1.6; Bailey and Thomas, submitted). In addition, the preserved dune record is a product of both local and external controls, and so although subject to similar regional climatic forcing, internal dynamics will produce a unique record at each location. Sampling at the dunefield scale must be spatially representative, and it must be expected that a range of dune chronological profiles which will be similar, but not identical, will be found. The varying responses within and between dunefields highlights the need for caution when attempting to infer long-term and large-scale environmental change from isolated chronological stratigraphic records. Individual stratigraphies may provide useful site specific information to aid the interpretation of differences between chronologies at larger scales.

1.5. Thesis aims

Given the discussion above of the issues still prevalent in the use of dunes as palaeoenvironmental archives, this thesis aims to address two fundamental questions underlying the application of OSL dating to sand dunes.

I. Are dune chronologies representative of the preserved stratigraphy at the dune and dunefield scales?

Issues of sampling in relation to dune accumulation/preservation processes are addressed where the internal dune structure is visible (i.e. in created exposures) and at a range of spatial scales. The aim is to minimise the problem of aliasing and investigate appropriate methods to assess and communicate the dependence of chronologies on sampling resolution.

II. How can dune chronologies be most appropriately interpreted to reconstruct reliable records of Quaternary dryland environmental conditions?

Given the complexity of factors underlying dune development, other sources of palaeoenvironmental information (such as lacustrine sediments, speleothems and marine cores) are essential in providing information to decipher dune chronologies and establish the relative importance of these formative factors. However, this circularity within the interpretation process has the potential to blur the unique response of dunes as terrestrial forms to regional environmental change. Through the integration of high resolution sampling and visible internal structure, in a region where past climatic conditions are relatively well known, this project aims to improve understanding of the relationship between the preserved dune accumulation record and past environmental change.

The research questions will be addressed using the southern Arabian Peninsula as an applied case study. The results will be applied to the furthering of palaeoenvironmental knowledge of Arabia, and to investigate whether more fundamental relationships can be established between dune records in this region and external forcing factors.

2 Late Quaternary palaeoenvironmental reconstructions in the southern Arabian Peninsula

2.1. Introduction

Figure 2.1: Google Earth image of the Arabian Peninsula (© Google 2013).

The study sites are located in the northeastern Rub' al Khali sand sea in the United Arab Emirates (UAE) (Figure 2.1). The southern Arabian Peninsula experienced dramatic palaeoenvironmental and climatic changes during the Late Quaternary and the climate history is relatively well known, providing an appropriate case study for addressing the aims laid out in Chapter 1. Recent archaeological research highlights the impact of these changes on the dispersal of anatomically modern humans out of Africa (Armitage et al., 2011; Bretzke et al., 2013; Groucutt and Petraglia, 2012; Rosenberg et al., 2011) and population dynamics during the mid-Holocene (Cullen et al., 2000; Preston et al., 2012; Staubwasser et al., 2003). Improving our understanding of the response of the terrestrial environment to past climatic changes therefore has direct relevance to much current research in the region. This study explicitly examines the relationship between past climatic changes and the preserved dune record to establish what information dune chronologies can provide about past environmental conditions. The aim of this chapter is to introduce the geological and climatic setting of the area in which this study is situated, and the numerous climatic fluctuations during the Late Quaternary that have produced a range of diverse landforms.

2.2. Regional setting

2.2.1. Geological setting

Arabia began to detach from northeastern Africa from ~25 Ma to become a separate tectonic plate along ancient rift faults, forming the Red Sea and Gulf of Aden and leading to uplift of western Arabia (Edgell, 2006). The Arabian Plate lies between the Zagros Main Reverse Fault in Iran, the Owen Fracture Zone in the Arabian Sea, and the Red Sea. The Peninsula can geologically be described by the stable shelf of the interior region, including the Precambrian rocks of the Arabian Shield, and the unstable shelf of the Taurus, Zagros and Oman Mountains (Powers et al., 1966). Following subduction of the Arabian Plate under the Persian Plate during the late Miocene, the Zagros and Oman (also known as Al Hajar) Mountain belts began to form from ~5 Ma (Edgell, 2006). The main part of the Arabian Peninsula is tilted downwards towards the northeast as the Arabian Plate is subducted under the Iranian Plate and the Zagros Mountains are uplifted, although this is reversed in the southeast of the Peninsula towards the Oman Mountains (Glennie, 1998). The general northwards motion of the Arabian Plate is greater in Oman, causing an anticlockwise rotation of the plate (Edgell, 2006). The carbonate deposits were formed when the then low-lying Arabia was covered by the shallow Tethys Sea.

The Oman Mountains rise to heights of over 3000 m ASL and are dominated by limestones, dolomites, and, in the south, Semail ophiolite. They are hugely faulted and dominated by ridge and wadi features. Against the mountains stretch large alluvial fans, loess ramp deposits, and wadi channels. The extensive gravel plains span from the Oman Mountains in the UAE to underlie the sand seas in the north (Glennie, 1998). The older fluvial gravels are thought to have formed in the early Pleistocene or even Pliocene under much wetter conditions than at present (Glennie, 1998). The youngest terraces and fans are thought to have formed during the late Pleistocene or early Holocene (Al-Farraj and Harvey, 2000).

Beaches, bars, spits and coastal sabkhas are found along the coast of the UAE (Goudie et al., 2000b). Subsidence of the UAE coastline before 30 ka was followed by rapid uplift, and hence Wood et al. (2012) argue that tectonic activity has played a large role alongside sea level changes in the development of the coastline of the UAE.

2.2.2. Late Quaternary sea level change

During the Quaternary glacial periods global sea levels are thought to have fallen by ~120-130 m relative to present (Fairbanks, 1989; Siddall et al., 2003; Yokoyama et al., 2000). With a maximum depth of ~90 m (Williams and Walkden, 2002) and average depth of ~35 m (Lambeck, 1996), the Persian Gulf would have been dry during the last glacial maximum (LGM) and previous glacial periods. The exposed shelf is therefore thought to have been a large source of sediment for deflation and transportation inland, reflected by the high calcareous content of the coastal dunes in the UAE (Garzanti et al., 2003). The refilling of the Gulf after the LGM is thought to have been most rapid between 12-8 ^{14}C ka BP[1] (Figure 2.2), reaching a maximum depth 1-2 m above present sea levels in the mid-Holocene before receding to present levels after ~2.3 cal. ka BP (Lambeck, 1996; Teller et al., 2000; Williams and Walkden, 2002).

[1] 13.9-8.9 cal. ka BP (all ^{14}C ages calibrated to 95.4% on IntCal09 curve using OxCal 4.1, Bronk Ramsey, 2009a)

Figure 2.2 has been removed due to Copyright restrictions

Figure 2.2: Modelled palaeoshoreline reconstructions of the Persian Gulf at (a) 18 ^{14}C ka BP (~21.4 cal. ka BP); (b) 12 ^{14}C ka BP (~13.9 cal. ka BP); (c) 10 ^{14}C ka BP (~11.5 cal. ka BP); (d) 8 ^{14}C ka BP (~8.9 cal. ka BP)[2]. The water depth contours are at -20, -50, -75, -100 and -150 m. Adapted from Lambeck (1996).

A recent study has challenged the idea of the Gulf being completely dry during the LGM. Wood et al. (2012) used OSL to date the marine carbonates of the Fuwayrit Formation, which had previously been assumed to have formed during the last interglacial period (e.g. Williams and Walkden, 2002). The formation was found to have formed between 30 and 17 ka, whilst the region was shown to have experienced rapid uplift since ~30 ka. Uncoupling the isostatic and eustatic signals for this region is important, with implications for understanding changes in sediment supply to the deserts of the Arabian Peninsula during the Quaternary, but more precise dating and modelling is required to achieve this aim.

[2] All ^{14}C ages calibrated on IntCal09 curve using OxCal 4.2, Bronk Ramsey (2009a)

2.2.3. Present climate

The interior of the Rub' al Khali receives less than 50 mm yr^{-1} average precipitation (Glennie, 1998). However, there is significant spatial as well as temporal variability within this broad classification, with aridity and temperatures increasing towards the south and west (Böer, 1997). In the UAE mean annual precipitation is 50-100 mm, with significant variability (Edgell, 2006). The two main sources of precipitation are the winter depressions from the Mediterranean Sea and the Indian Ocean Summer Monsoon (IOSM) (Glennie and Singhvi, 2002). Mediterranean winds blow strongly from the northwest in the Red Sea, and can extend as far east as Ras al Khaimah; the cause of snowfall in February 2004 (Edgell, 2006). The inter-tropical convergence zone (ITCZ) in the Indian Ocean presently moves northwards to 30-35 °N in July and brings the influence of the IOSM to the southern part of the Peninsula (Edgell, 2006). Mean summer temperatures are greater than 30 °C, although in the desert interior summer temperatures exceed 50 °C (Edgell, 2006; Glennie, 1998).

The two main wind systems that influence the southern Arabian Peninsula are the *Shamal* from the north and northwest, and the IOSM winds which blow from the southwest across the Arabian Sea (Figure 2.3). The *Shamal* winds are a result of high and low pressure systems over northern and southern Arabia respectively, associated with the monsoonal circulation, and are strongest in summer (Edgell, 2006; El-Sayed, 1999). The *Shamal* winds blow down the Gulf towards the UAE as a northwesterly wind and then turn clockwise across the Rub' al Khali. Meteorological data from Ras al Khaimah airport, in the northeastern UAE, shows that 52% of the winds blow from the west and northwest but ~28% of winds blow from the southeast, highlighting the complexity of the wind regime (Goudie et al., 2000a). Of six identified wind regimes, the northwesterly winds from the Mediterranean during winter and the high energy *Shamal* regime in June-August dominate sand movement in eastern Saudi Arabia (Barth, 2001). The IOSM winds are presently more

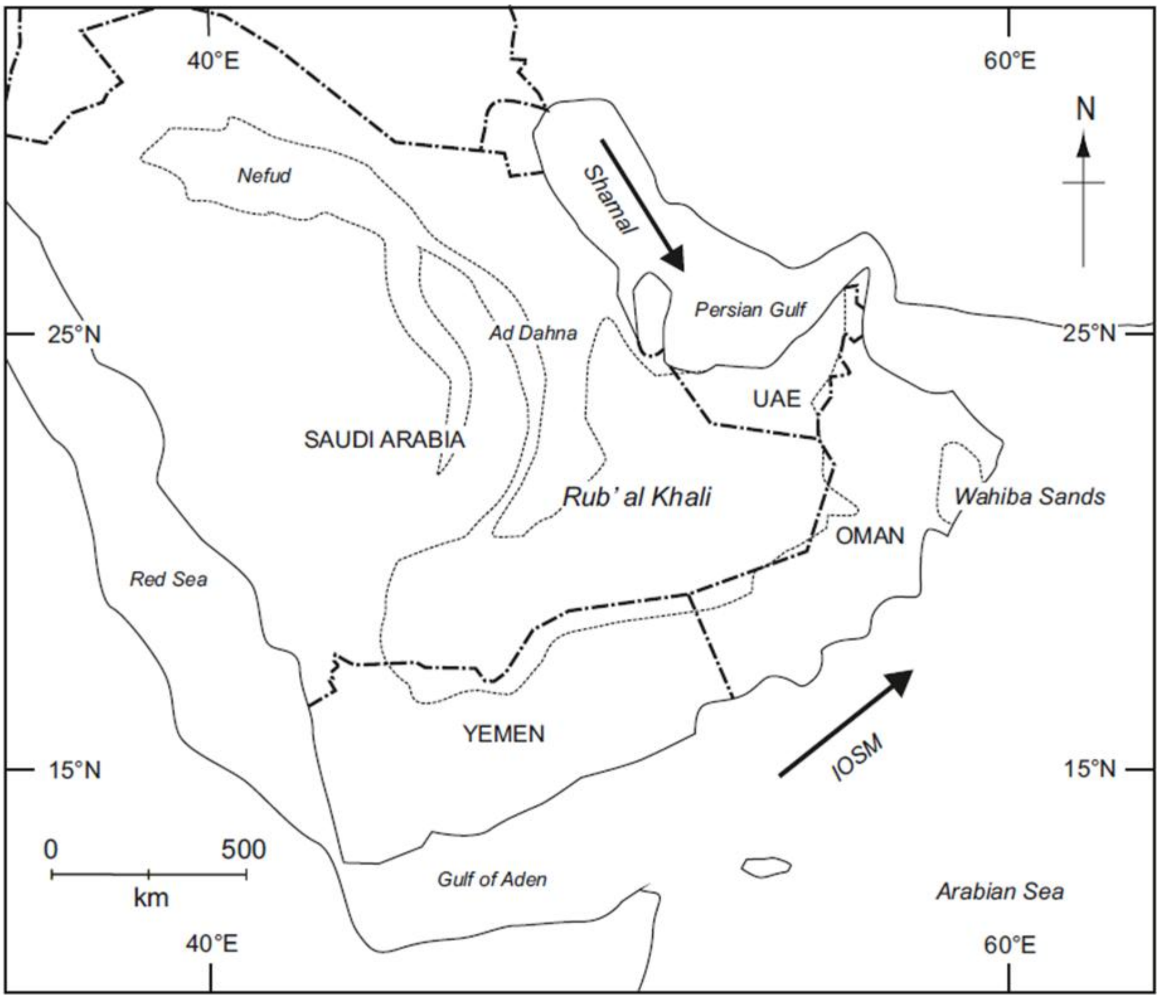

Figure 2.3: Location map showing the sand seas in the Arabian Peninsula and the dominant winds.

important in the Wahiba Sands as the winds branch northwards from the Arabian Sea across the Wahiba Sands, although these winds also reach the southern-most part of the Rub' al Khali in Oman (Edgell, 2006).

2.2.4. Sand seas of the southern Arabian Peninsula

The Rub' al Khali (also known as the Empty Quarter) is the largest sandy desert in the world, with an area of approximately 600,000 km^2 and many different types of aeolian bedform, including linear, transverse and star dunes (Besler, 1982; Goudie et al., 2000a). The sand sea is located within a large Tertiary sedimentary basin (Anton, 1983), which lies between the Hijaz-Plateau, Hadramut Highlands, Oman Mountains and Persian Gulf. To the north, via a semi-circular clockwise path the Dahna sand sea links the Nefud sand sea in Saudi Arabia to the Rub' al Khali (Figure 2.3). The Wahiba Sand Sea is located at the southeastern tip of Oman and covers an area of ~10,000 km^2.

The mixed acidic and ultrabasic heavy mineral compositions of Rub' al Khali sediments in the UAE suggest they were sourced from the Zagros and Oman mountain belts respectively, with minor local contributions (Ahmed et al., 1998; El-Sayed, 1999). In the light mineral composition, quartz and calcite dominate, with feldspar and dolomites also present (El-Sayed, 1999). The relative abundance of quartz, dolomite and calcite minerals in the sands vary with location, with calcite and dolomite most abundant near the coast. In the coastal regions, carbonate composition is as high as 70% and the presence of micrite coatings indicates the importance of a coastal source; the carbonate composition reduces to less than 10% at 40-50 km inland (El-Sayed, 1999; Teller et al., 2000). The sands of the Rub' al Khali, particularly in the northern UAE, tend to have a red iron oxide coating, but this is less distinctive in the Wahiba Sands (Besler, 1982; Juyal et al., 1998).

Arid conditions are thought to have begun in the Pleistocene, by at least 1.2 Ma (Edgell, 2006). Edgell (1989 in Edgell, 2006) has suggested that dune formation in the Rub' al Khali could have begun at around 700 ka. The earliest dune ages in the Rub' al Khali are dated to prior to the last interglacial: ~180-140 ka in Liwa (Stokes and Bray, 2005) and ~160 ka in the Emirate of Abu Dhabi, UAE (Hadley et al., 1998). In the Wahiba Sands luminescence ages of ~230 ka (Juyal et al., 1998) and ~160-140 ka (Preusser et al., 2002) from aeolianite (cemented dune sand) have been reported.

Dune orientation in the Rub' al Khali reflects the anticlockwise curvature of the *Shamal* wind across the Arabian Peninsula around Riyadh (Glennie and Singhvi, 2002; Glennie, 1998). Within the UAE, the dunes are predominantly mega linear ridges up to 70 m high, aligned southwest-northeast with crestal spacings up to 5 km apart, and modified by modern winds (Atkinson et al., 2011; Glennie, 1998; Juyal et al., 1998). Secondary dunes orientated northwest-southeast overlie the primary megaridges (Figure 2.4).

In the Liwa region, south-central UAE, the dunes are compound and complex mega-barchans up to 160 m in height with secondary smaller barchans dunes, separated by inter-dune sabkha 2-3 km in width (Bray and Stokes, 2003). The dune horns are orientated north-south, parallel to the dominant wind (El-Sayed, 1999). Liwa is separated from the Al Qâfa transverse dunes to its north by a sharp crescentic boundary, at which the height of the interdune sabkhas falls from ~150 m to ~85 m above sea level. This elevational change has resulted in large volumes of material deposited at Liwa due to the subsequent decrease in transport capacity (Stokes and Bray, 2005).

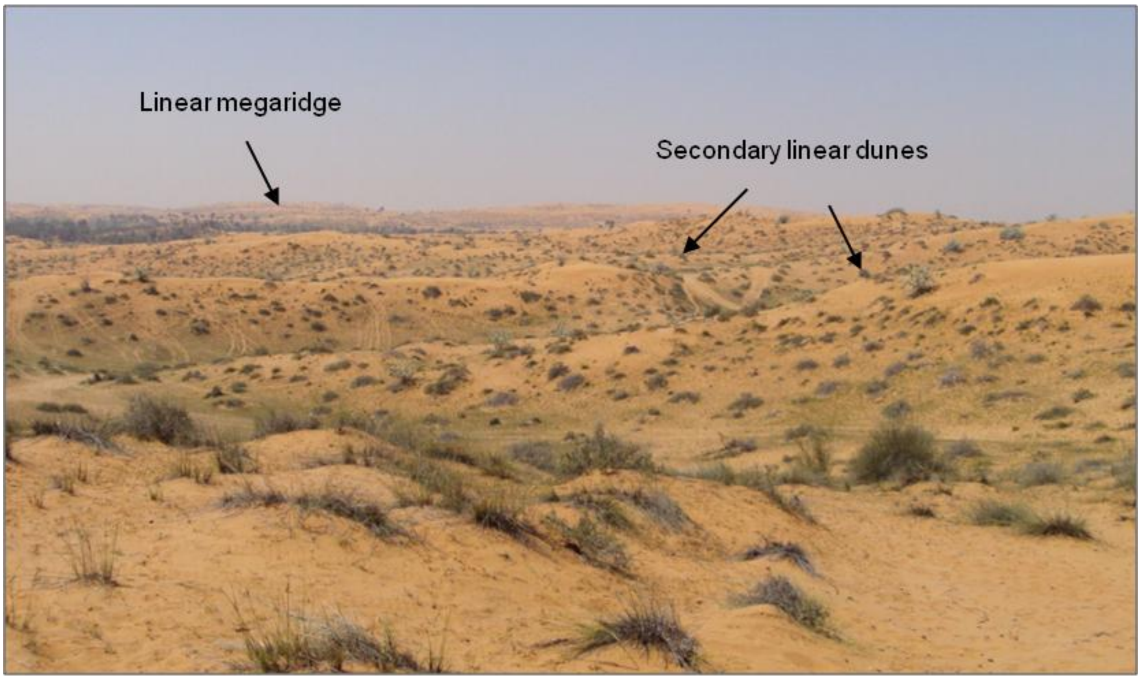

Figure 2.4: Photo of the dune landscape near Ras al Khaimah, UAE. Secondary dunes are shown in the foreground, whilst an adjacent linear megaridge can be identified in the distance.

2.3. Palaeoenvironmental reconstructions using sand dunes

2.3.1. Background

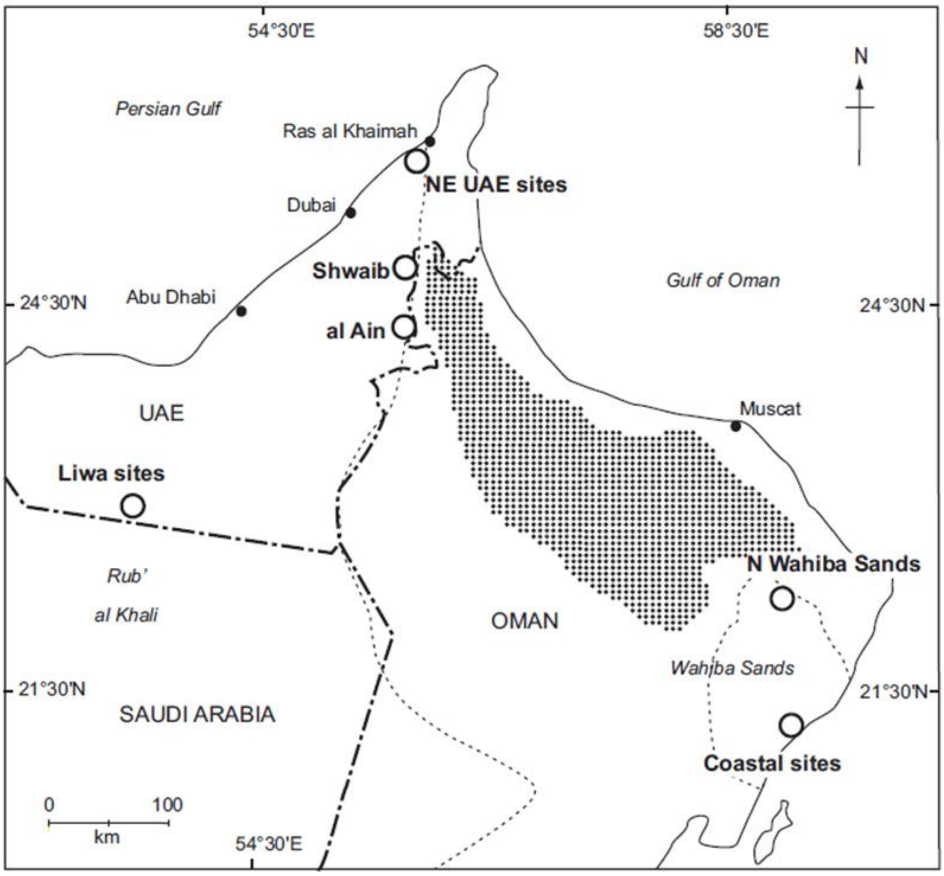

Figure 2.5: Location map of sites in the southern Arabian Peninsula from which OSL dune samples have been taken. The stippled area shows the Oman Mountains.

Initial dune OSL ages from this region, presented in unpublished theses, were from Sabkhat Matti in the northwestern UAE and Liwa (Goodall, 1995; Pugh, 1997). These ages have been interpreted as indicating arid conditions at MIS 7 (~208 ka), MIS 6/5 (between 164-113 ka), MIS 3 (~60-45 ka), and the mid-Holocene (~6 ka) (Glennie and Singhvi, 2002). Juyal et al. (1998) produced some of the first published luminescence ages (using early measurement techniques to date potassium feldspars) from this region, dating a selection of landforms in Liwa and the Wahiba Sands (Figure 2.5). In Liwa, periods of aeolian deposition

Table 2.1: Summary of interpretations from previous studies and reviews (authors in bold) of aeolian activity and preservation in the southern Arabian Peninsula during the Late Quaternary. Grouped phases are those highlighted by the authors, and do not necessarily incorporate age uncertainties in similar or comparable ways.

Authors	**Location**	**Preserved activity**		
		Grouped phases highlighted by authors (ka)	**Climate state**	**Controlling factors**
Juyal et al. (1998)	Wahiba Sands (aeolianites)	229, 117-110, 23-18, 10-6	Interglacial	Strength of SW winds
	Liwa	141, 99, 64, 40, 31, 15-12	Glacial	Sediment supply (low sea level) and preservation potential (groundwater)
Glennie and Singhvi (2002)	E Rub’ al Khali	160-130, 110, 60-50, 15-12	Glacial	Sediment supply (low sea level)
Radies et al. (2004)	Wahiba Sands	160-130, 115-105, 90-60, 35-24, 22-9, 2, 0.7	Glacial	Sediment supply (low sea level). Shift from a wet to dry aeolian system (decreasing preservation potential)
Stokes and Bray (2005)	Liwa	130-75, 6-2	Interglacial	Preservation potential (groundwater) and sediment supply (low sea level)
Preusser (2009)	E Rub’ al Khali and Wahiba Sands	186-130, 115-106, 65, 20	Glacial	Sediment supply (low sea level)
Atkinson et al. (2011)	NE Rub’ al Khali	106, 51, 22-20, 16-10, 7-3	N/A	Interaction of forcing factors. Preservation is rare

were dated to MIS 6 (~141 ka), MIS 5 (99 ka), MIS 4 (64 ka), MIS 3 (40 and 31 ka) and MIS 2 (~15-12 ka). Similar bedding directions were used to infer consistent *Shamal* wind directions from the north-northwest over this time. In the Wahiba Sands, the authors found clusters of dates for aeolianites during MIS 7 (~229 ka), early MIS 5 (~117-110 ka), the LGM (~23-18 ka) and the early Holocene (~10-6 ka), interpreted to be linked to the strengthening of the IOSM (Glennie and Singhvi, 2002). However, as Preusser (2009) highlights, these conclusions are made from a very small number of ages of dune sands from a large area, and with little information provided of the geological context of the samples.

More recent research has since built on this initial chronology. High resolution sampling for OSL dating has been focused in the northeastern UAE, Liwa and the Wahiba Sands. Over 300 luminescence ages provide a more detailed framework for reconstruction of the histories of the dunefields in the southern Arabian Peninsula. Several reviews have been published in recent years, which are summarised in Table 2.1 and discussed further in the following sections.

2.3.2. Northeastern Rub'al Khali, UAE

The northeastern Rub' al Khali within the UAE is the most extensively dated part of the sand sea (Figure 2.6). Goudie et al. (2000a) dated two dune profiles from complex, branching linear dunes near Ras al Khaimah. At Awafi, the dune accumulated rapidly between ~13-9 ka. This is linked by the authors to rising sea levels in the Persian Gulf and related changes in sediment supply. Aeolian units under- and overlying lacustrine deposits at Awafi have been dated to ~18 and 4 ka respectively (Parker et al., 2004). The Idhn dune, which is over 40 m high, accumulated over the last 1000 years; 20 m of sediment over 270 years at a calculated rate of 74 m ka^{-1}. Possible causal factors include fluvial influence from a nearby wadi, a short-term climatic fluctuation, or increased human influence (Goudie et al., 2000a). These results indicate the importance of relatively short periods of dune growth, and possibly multiple phases of activity, separated by longer periods of non-deposition.

In more recent work, Atkinson et al. (2011, 2012) have conducted high resolution sampling across a number of sites in the northeastern UAE, exploiting the occurrence of dune sections exposed by quarrying (Figure 2.7). Dune activity and preservation was found to

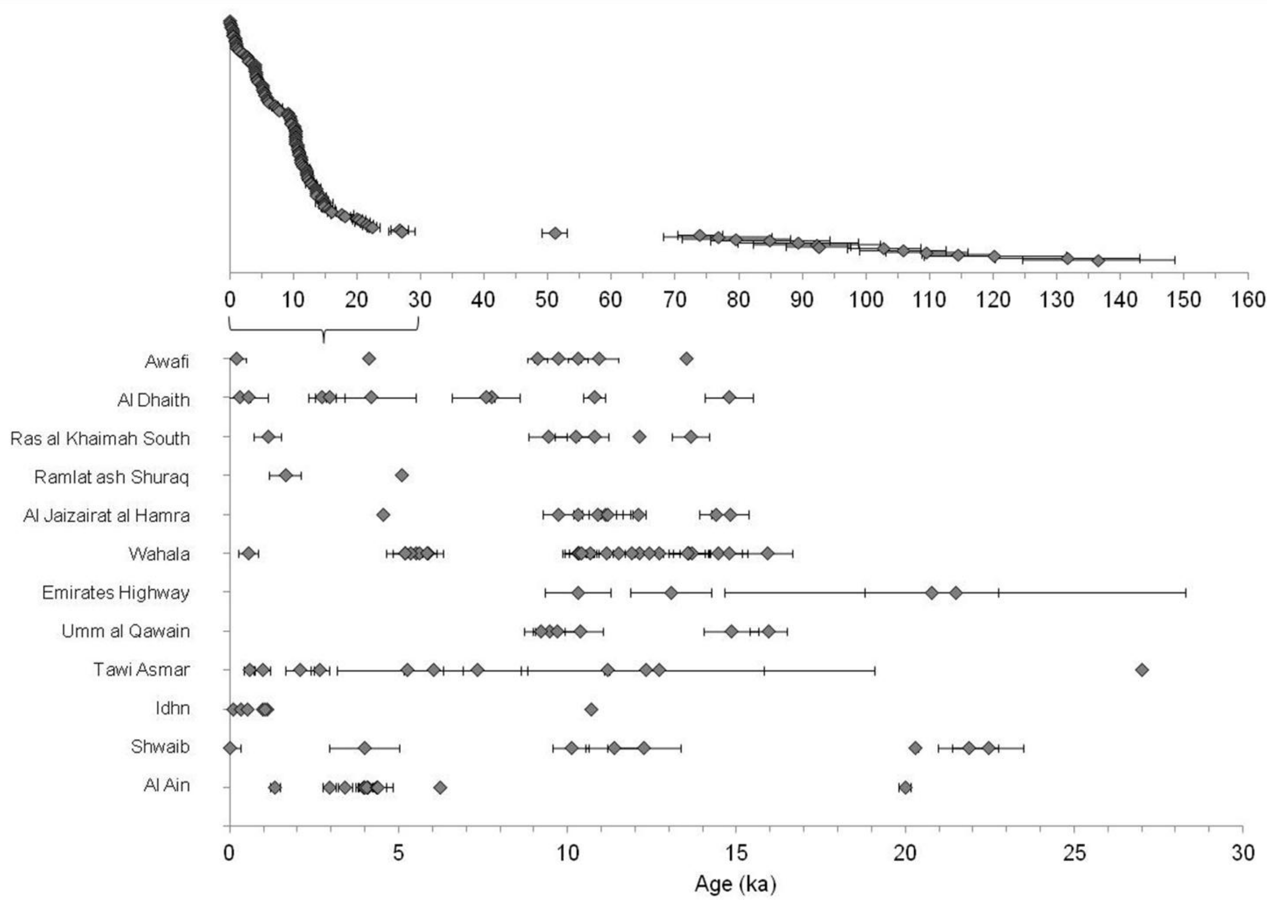

Figure 2.6: Previously published dune OSL ages from the northeastern UAE (sites separated in lower figure), Shwaib and Al Ain (Figure 2.5) within the last 160 ka (top) and 30 ka (bottom) (Atkinson et al., 2011, 2012, 2013; Goudie et al., 2000a; Parker and Goudie, 2007; Parker et al., 2004).

Figure 2.7: Photo of the quarrying activity at Shwaib, UAE. Vehicles (c. 6 m high) are for scale.

have occurred mainly during MIS 2 (22-20 and 16-9 ka) and MIS 1 (7-2 ka), although earlier deposits dated to 105 and 51 ka at one site were also found (Atkinson et al., 2011, 2012). The high degree of consistency of periods of accumulation during the Pleistocene-Holocene transition and the mid-Holocene between different sites indicates that regional forcing is a dominant control on OSL chronologies, and that inter-site variability is likely a result of the impact of localised factors, such as topography, coastal proximity, water table variability, anthropogenic activity, and vegetation cover (Atkinson et al., 2012).

Glennie and Singhvi (2002) interpret the primary linear megaridges in the northeastern Rub' al Khali as forming under winds with a west-northwest component, and hence as out of equilibrium with the present north-northwestly winds of the *Shamal*. During past glacial periods, the *Shamal* is therefore thought to have strengthened and straightened. In contrast, Atkinson et al. (2012) note the complex relationship between these generations of dunes. Dune ages of the primary and secondary dunes are found to overlap during the late

Pleistocene-Holocene transition, and hence they were interpreted not to form under distinct atmospheric circulation patterns.

2.3.3. Liwa, UAE

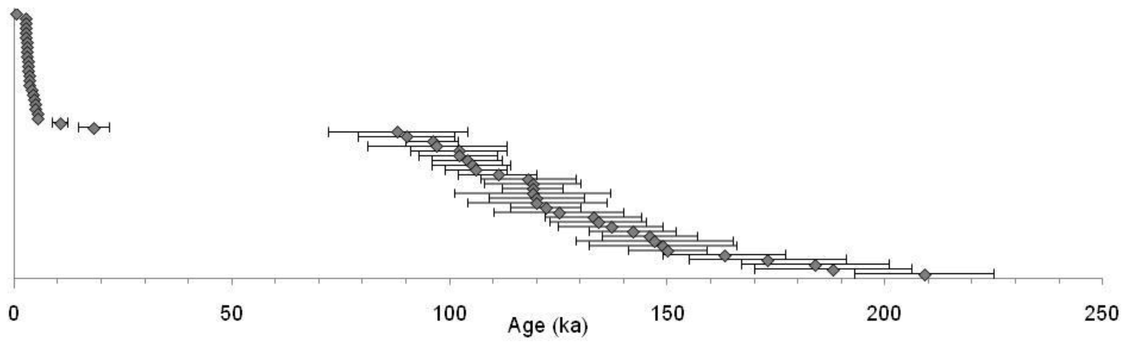

Figure 2.8: Previously published dune OSL ages from Liwa within the last 250 ka (Stokes and Bray, 2005).

As noted in Section 2.3.1, Juyal et al. (1998) provided some of the first luminescence ages from Liwa (although these included no samples of unconsolidated sand). The consistency of bedding dip directions to the south-southeast led the authors to infer that the *Shamal* winds were the dominant dune-forming winds during glaciations of the last 140 ka, and that the timings of accumulation are consistent with periods of low sea level.

More recently, Stokes and Bray (2005) extracted 56 OSL ages from four cores and two outcrops in Liwa and Al Qâfa (immediately to the north of Liwa depression). The main periods of accumulation were MIS 5 (130-75 ka) and MIS 1 (6-2 ka), with lesser periods at 180-140, 18-16 and 0.9 ka (Figure 2.8). The authors find, in contrast to some studies (Goudie et al., 2000a; Preusser, 2009; Preusser et al., 2002), that most preserved dune accumulation is recorded in humid interglacial periods (inferred during MIS 5 and 1), rather than in more arid intervals. The authors argue that the aeolian system is limited by preservation potential, correlated with sea level and precipitation, rather than sediment supply or transport capacity. Precessional changes in monsoon intensity and sea level changes, relating to the eccentricity cycle, drive these changes, and allow previously accumulated aeolian deposits to be preserved when groundwater levels are high. Due to these processes, the preserved record is out of phase with glacial periods, as it is only at the end of these phases that preservation is possible (Stokes and Bray, 2005). Bray and Stokes (2003) also highlight the dynamism of the dunes, arguing that they formed in short-lived, rapid accumulation phases.

2.3.4. Wahiba Sand Sea, Oman

Deep drilling has also been exploited in the High Sands, in the north of the Wahiba Sands, to produce sediment cores that span the last ~160 ka (Figure 2.9). Dating potassium feldspars using infrared stimulated luminescence (IRSL), intervals of aeolian activity have been identified at 160-140, 120-100 (MIS 5d; above fluvial deposits correlated with MIS 5e), 78-64 (MIS 4), 22-18 (LGM), 2 ka and 700 years (Preusser et al., 2002). Minor deposition has also been dated to 97-86 ka (MIS 5b) (Preusser, 2009).

These intervals correlate to low global sea levels during periods of high latitude glaciations and low monsoon intensity, in phases of increased sediment availability, decreased precipitation and reduced vegetation cover (Preusser et al., 2002). The north-south alignment of dune ridges, following the present summer circulation pattern, and the synchronicity of aeolian activity recognised in the UAE lead the authors to conclude that the wind regime forming these dunes was similar to the present summer circulation.

In coastal sites major accumulation occurred just before (34-24 ka) and after (16-13 ka) the LGM, and during the early Holocene (9-8 ka) (Preusser et al., 2005). Radies et al. (2004) describe the aeolian units around the LGM as Qahid subunits A and C, spanning 35-25 and 18-8 ka respectively, whereas subunit B, at 22-18 ka, has only been found in core WDR-2, an inland site. Contrasting periods of accumulation at the coast and inland are explained by the differences in preservation potential between the inland and coastal sites. Changes in the

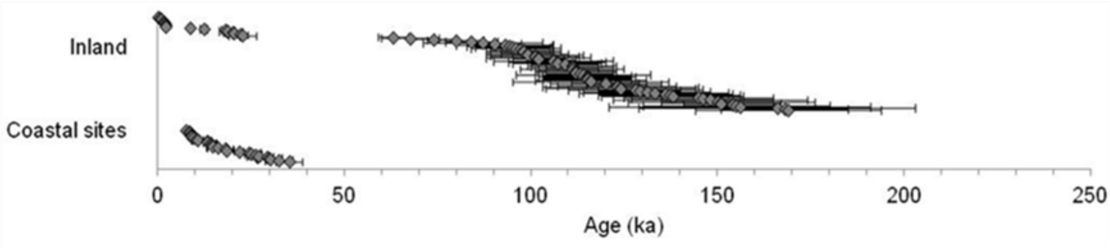

Figure 2.9: Previously published dune OSL ages from inland and coastal sites in the Wahiba Sands shown in Figure 2.5 (Preusser et al., 2002, 2005; Radies et al., 2004).

groundwater level at the coastal site as a response to sea level and precipitation (i.e. monsoon intensity) impacted upon the preservation potential of the dunes, and whether the dunes were bypassed or accumulated. This then had downwind sediment availability implications for the dunes in the north of the Wahiba Sands (Preusser, 2009). Radies et al. (2004) describe the evolution of the Wahiba Sand Sea from a wet aeolian system, in which palaeosols and supersurfaces formed during wetter phases, to a dry aeolian system around and after the LGM.

Preusser (2009) argues that it is not preservation potential but sediment supply that is the limiting control on dune accumulation. The lack of dates during MIS 4-2 at Liwa, in contrast to the Wahiba Sands, is explained as a result of stabilisation of the Persian Gulf sediments over time. The continuing lowering of the sea level exposed more of the continental shelf off the Oman coast, providing a more continual supply of sediment to the Wahiba Sands. However, as noted in Section 2.2.2, the extent of dryness of the Persian Gulf is under debate. An alternative interpretation is provided by Stokes and Bray (2005), who ascribe the differences in the records in Liwa and the Wahiba Sands as a function of the differences in preservation between dune type (transverse megabarchans and large linear dunes respectively). Transverse forms were only preserved in arid-humid transitions, whereas linear dunes, as elongating rather than migrating forms, may have been preserved in arid or humid phases if conditions allowed for accumulation.

These studies highlight the interdependent nature of the dunefields in this region. Local influences together with changes in external factors, such as sea level and wind regime change, have produced the dune record available to sample in specific localities. A number of points of contention in the interpretation of these records still remain.

2.3.5. Previous interpretations of aeolian records

The issues raised in Chapter 1 are particularly relevant to the discussion of dune OSL ages in relation to past environmental change. The response of dune systems to environmental change is more complex in periods of aridity, with issues of preservation obscuring the palaeorecord (Bray and Stokes, 2004). In addition to some of the specific interpretational discrepancies noted above, some more general points are also worth highlighting in response to the discussion in the preceding section.

First, many of the luminescence ages, particularly those from the older studies, have large associated errors. Lack of precision therefore does not allow for wide age intervals to be subdivided into multiple ages of activity (Stokes and Bray, 2005). The older dating methods used (e.g. additive-dose, multiple aliquot protocols) in some of the older studies has led to these dune ages being excluded from the syntheses presented in subsequent chapters.

Second, it is important to recognise that broad-scale climatic changes, such as the glacial-interglacial cycles of the Quaternary, are characterised by rapid fluctuations at temporal and spatial smaller scales. For example, Preusser (2009) emphasises the need to recognise the fluctuating climate within MIS 5 and the increasingly arid conditions in the late Holocene since 6 ka, rather than assume stability of interglacial conditions during MIS 5 and the Holocene as a whole. In addition to these points, the use of the terms ‘arid’ and ‘humid’ (and similarly ‘glacial’ and ‘interglacial’ conditions in reference to the lower latitudes), whilst cautiously used in this study, are constricting as they may ignore spatial and temporal relativity (e.g. antecedent conditions) and infer stability.

2.4. Terrestrial archives

2.4.1. Lacustrine and alluvial sediments

Some of the first radiocarbon dates of lacustrine sediments in the Arabian Peninsula were presented by McClure (1976), followed by further work by Gardner (1988), Sanlaville (1992), and Wood and Imes (1995). These studies produced dates of around 35-20 ^{14}C ka BP and 9-6 ^{14}C ka BP[3] for humid periods characterised by lake development in the region. However, the chronology underlying the first of these periods has since been questioned. Glennie and Singhvi (2002) show the discrepancy between shell ages from raised beaches and Shackleton's (1987) δ^{18}O sea-level curve. The possibility of diagenesis and contamination of samples by relatively young carbon has led authors to suggest that the earlier humid phase, which is inconsistent luminescence ages, may be an underestimation of age (e.g. Glennie and Singhvi, 2002; Preusser, 2009).

Most palaeolacustrine deposits are found within the interdunal areas (Parker et al., 2004). Recent radiocarbon ages produced in acknowledgement of the problems identified above and supported by the application of alternative dating methods, have produced a more robust chronology of palaeoenvironmental change in the southern Arabian Peninsula. Rosenberg et al. (2011) recently revisited some of the sites of McClure (1976), including Mundafan (Figure 2.10), to apply OSL and amino acid racemization (AAR) dating. Periods of lake presence were found at ~125, 100 and 80 ka in addition to the early Holocene, but no evidence of the late Pleistocene humid period was found. Additional palaeolake

[3] ~40-24 and 10-7 cal. ka BP (^{14}C ages calibrated on IntCal09 curve using OxCal 4.2, Bronk Ramsey, 2009a)

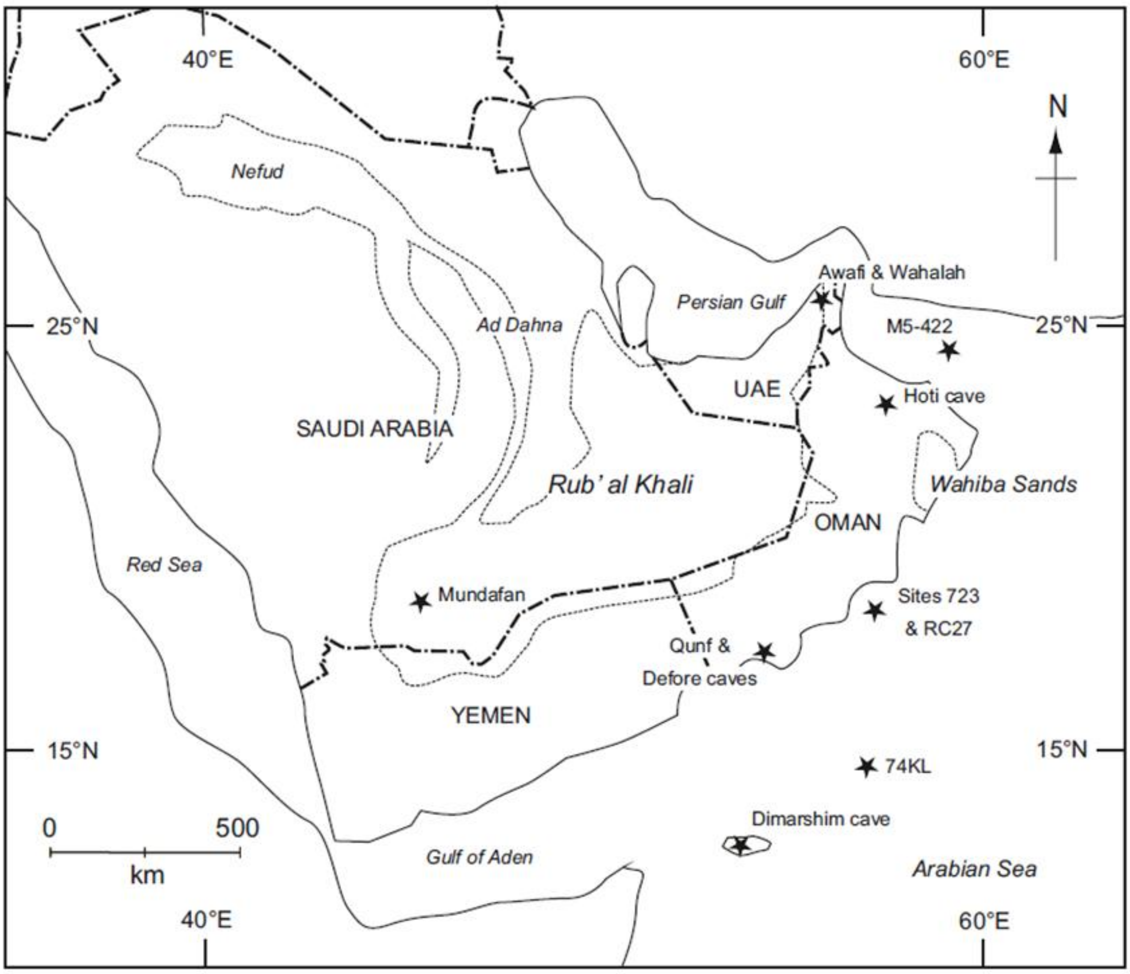

Figure 2.10: Map showing the location of some of the main palaeoenvironmental sites for the southern Arabian Peninsula discussed in Sections 2.4 and 2.5. Palaeolakes: Mundafan (McClure, 1976; Rosenberg et al., 2011); and Awafi and Wahalah (Parker et al., 2004, 2006; Preston, 2011; Preston et al., 2012). Speleothems: Hoti cave (Burns et al., 2001; Fleitmann et al., 2003b, 2007; Neff et al., 2001); Qunf and Defore caves (Fleitmann et al., 2003a, 2007); and Dimarshim cave (Fleitmann et al., 2007; Shakun et al., 2007). Marine cores: M5-422 (Cullen et al., 2000; Sirocko et al., 1993; Staubwasser et al., 2003); 74KL (Sirocko et al., 1993); and site 723 (and nearby RC27) (Anderson and Prell, 1993; Gupta et al., 2003, 2005; Overpeck et al., 1996).

sediments in Oman and the Nefud desert dated using OSL and thermally transferred OSL (TT-OSL; an OSL protocol used to overcome the problem of saturation by using an optical bleach prior to TT-OSL measurement in order to measure luminescence resulting from the thermally-driven transfer of charge into the fast OSL trap) support these findings, and extend the record further to show lake presence at ~410, 320 and 200 ka (Rosenberg et al., 2012, 2013). Wadi deposits have also been dated alongside overlying dune sediments in the

UAE, which indicate humid periods during MIS 5e, MIS 5a and the early Holocene (Atkinson et al., 2013). However, other recent work has dated lacustrine sediments (again using OSL dating) near the archaeological site at Jebel Faya to early MIS 3 (~61-58 ka), which is suggested by the authors to align with an intensification of the IOSM at ~58 ka (Parton et al., 2013). Intervals of increased humidity are assumed to align with periods of intensified and more northward influence of the monsoon (i.e. at precessional maxima), leading to increased summer rainfall (Bray and Stokes, 2004). A recent study also implicates the African monsoon in bringing additional precipitation to central and northern Arabia during these times, supported by climate model simulations of MIS 5e (Rosenberg et al., 2013). There is therefore significant debate over the timing of periods of increased moisture in the region (that allowed for permanent lake presence), the spatial extent of these changes, and the underlying mechanisms.

After the LGM the mean summer location of the ITCZ, which is sensitive to sea surface temperature (SST) anomalies (Chiang and Bitz, 2005), shifted northwards and the IOSM strengthened, in line with increasing insolation (Kutzbach, 1981). The onset of the early Holocene humid phase is reflected in the formation of palaeosols in Yemen at ~12.5 ka (Pietsch and Kühn, 2012) and ~11 ka (Davies, 2006; Lézine et al., 2007), and in lacustrine sediments at ~9.3 ka in the central Wahiba Sands (Radies et al., 2005) and ~8.5 ka at Awafi and Wahalah in the northeastern UAE (Parker et al., 2004, 2006). Playa sedimentation rates in the Oman Mountains were also high between ~10.5 and 8 ka, interpreted as a result of higher precipitation levels (Fuchs and Buerkert, 2008). Variability in timing relates in part to geographical location as the northern extent of the monsoonal influence gradually migrated, and also to the non-linear responses of systems within local environmental contexts to this forcing.

Following a period of peak precipitation during the early Holocene, the position of the ITCZ moved southwards and the IOSM weakened. There are discrepancies between different records over the timing of these changes, a reflection of the varying sensitivity of different proxies and sites to changing groundwater levels and moisture sources. Precipitation was high enough for the formation of weakly developed soils in Yemen until 6.7 ka (Pietsch and Kühn, 2012), wet lacustrine deposits in the southern Wahiba Sands until ~5.5 ka (Radies et al., 2005), and the presence of intermittent lakes in northeastern UAE until ~4 ka (Parker et al., 2004, 2006).

Throughout this period of relatively high moisture levels, climatic variability is evident (e.g. Davies, 2006; Lézine et al., 2007; Parker et al., 2006). The year-round presence of a lake at Awafi has been identified between ~8.5-5.9 ka (Parker et al., 2004, 2006; Preston et al., 2012). Geochemical, pollen and phytolith analyses, alongside chronological control provided by OSL and radiocarbon dating, have been presented for this site (Figure 2.11). With sediments resampled at higher resolution, this period has been shown to be punctuated by three phases of aridity centred on 8.0-7.8, 7.5-7.2, and 6.5-6.2 ka (Preston et al., 2012). This record is corroborated by a lacustrine sequence at Wahalah, which similarly indicates onset from ~8.5 ka, with arid periods at 8.2-7.9, 7.7-7.5, 7.15-7, 6.75-6.6, and 6.3-6.1 ka (Preston, 2011).

The lakes were present but intermittent between 5.9-3.7 ka at Wahalah and ~5.9-4.1 ka at Awafi. In comparison to earlier pluvial periods, this interval was characterised by sustained aridity rather than brief arid interludes and was marked by a peak arid event at 5.2 ka, which was also the time of the lowest levels of human activity in the region (Preston et al., 2012). The pluvial conditions between 5.2-4.1 ka (5-4.6 ka at Wahalah) may reflect an increase in precipitation from mid-latitudinal westerly systems (Parker et al., 2006). The Awafi and Wahalah lakes were desiccated at ~4.1 and 3.7 ka respectively. This increase in aridity is closely matched in timing by an increase in terrigeneous input in marine cores (Cullen et al., 2000), a reduction in Indus river discharge (Staubwasser et al., 2003), and a hiatus in the northern Oman speleothem record (Fleitmann et al., 2007), indicating a region-wide shift in climate.

Figure 2.11 has been removed due to Copyright restrictions

Figure 2.11: Awafi palaeolake record showing sediment stratigraphy, magnetic influx and iron (Fe) content (higher levels indicate increased dune activity), phytolith climate index (ratio of C3 to C4 phytoliths is presented as a climatic index, which represents warm/wet versus warm/dry conditions respectively), and the authors' palaeoenvironmental interpretation. Reproduced from Preston et al. (2012).

2.4.2. Speleothems

Speleothems are found in caves in the mountainous parts of Arabia, including the Oman Mountains and Yemen, and their growth is associated with wetter conditions. Stable isotope ratios of oxygen in speleothem calcite ($\delta^{18}O_c$) and hydrogen in fluid inclusions (δD_{FI}) can be correlated with isotope ratios of palaeo-groundwater and palaeo-precipitation. These ratios can show changes in precipitation amount, source and seasonality, as well as changes in temperature, ocean isotope ratios, and evaporation processes. The use of δD_{FI}, which is not affected by temperature, can be used to show if temperature has a dominant effect on $\delta^{18}O_c$ values. Speleothems are most commonly dated using U-Th dating.

The speleothem records show discrete periods of wetness, stretching back ~330 ka in the longest record at Hoti Cave, northern Oman. This deposit shows deposition at 330-300, 200-180, 135-120, 82-78, 10.5-6 ka, each coincident with peak interglacial conditions at MIS 9, 7a, 5e, 5a, and 1 respectively, and with little or no growth in the intervening periods (Fleitmann et al., 2003b). These records correlate with long- and short-term climatic fluctuations in the speleothem records of southern China (Wang et al., 2005) supporting the interpretation that these archives as not biased by local climate effects (Fleitmann et al., 2007).

In northern Oman there are presently three possible precipitation sources: Mediterranean frontal systems from the northwest (Dec-Mar); local thunderstorms in the mountains in very hot summers; and tropical cyclones from the Bay of Bengal and the southeastern Arabian Sea that occur approximately once every 5-10 years (Fleitmann et al., 2003b). Southern Oman presently marks the northernmost limit of the monsoonal rainbelt. The isotopic composition of moisture sources from the north and south are different, the south being more depleted. Two moisture sources can be defined by two separate water lines; the Northern and Southern Local Meteoric Water Lines (N- and S-LMWL) (Fleitmann et al., 2003b).

Ranges of the values of $\delta^{18}O_c$ and δD_{FI} from samples deposited during peak interglacial periods lie between −8 and −4 ‰ (Vienna Pee Dee Belemnite; VPDB) and −53 and −20 ‰ (Vienna Standard Mean Ocean Water; VSMOW) respectively, compared to the more positive modern stalagmites range of −2.6 to −1.1‰ (VPDB) and −7.6 and −3.3‰ (VSMOW) respectively (Fleitmann et al., 2003b). Past interglacial $\delta^{18}O_c$ and δD_{FI} values were isotopically distinct from today's groundwater, which is recharged from a mixture of sources but plotting closer to the S-LMWL. This has been interpreted that a greater proportion of precipitation was sourced from the Indian Ocean, whilst precipitation sourced

Part of Figure 2.12 has been removed due to Copyright restrictions

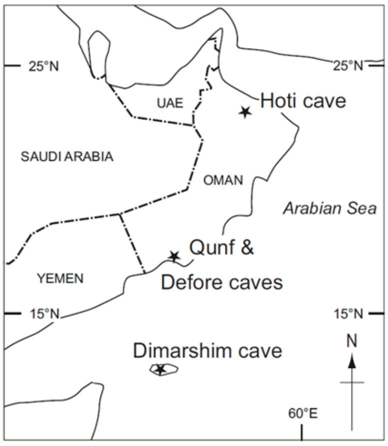

Figure 2.12: Oxygen isotope records from speleothems in northern and southern Oman, and Yemen during the Holocene. Adapted from Fleitmann et al. (2007).

from the north either decreased or was halted completely (Fleitmann et al., 2003b). It is not possible to distinguish whether this was via cyclones or monsoons, although a monsoonal cause may be more likely given that Holocene lacustrine records indicate that the ITCZ and monsoon rainbelt were located further north (Fontes et al., 1993 in Fleitmann et al., 2003b). Fleitmann et al. (2007) analysed high resolution records from four caves that cover a north-south transect between 12 to 23 °N (Figure 2.12) and have three different precipitation regimes; Hoti Cave in northern Oman (winter precipitation), Qunf Cave and Defore Cave in southern Oman (monsoonal summer precipitation), and Dimarshim Cave in Socotra, Yemen (inter-monsoonal precipitation). There is a rapid decline in $\delta^{18}O$ during the early Holocene (11-8 ka), interpreted as representing the rapid northward migration of the mean latitudinal position of the ITCZ and monsoonal rainbelt (Figure 2.12). From ~8 ka the ITCZ and monsoon rainbelt migrated gradually southwards and precipitation at the northern margins of the ITCZ migratory path decreased. At Hoti Cave, this shift in moisture source occurred ~6.3 ka. In Socotra the trend coincided with increased inter-monsoon precipitation, indicating a shortening of the duration of the summer monsoon.

The time lag between the rapid rise in the early Holocene precipitation is ~400 years between southern (~10.5 ka) and northern Oman (~10.1 ka), and longer compared to Awafi, UAE (Fleitmann and Matter, 2009; Parker et al., 2004, 2006). The records described in this section highlight the time-transgressive nature of the migration of monsoonal circulation system and the responses of different palaeoenvironmental proxies.

2.5. Marine archives

The low oxygen concentration and high sediment accumulation rates in the Arabian Sea provide a good setting for almost continuous records of changes in strength of the IOSM (Gupta et al., 2003). Marine records spanning up to 300 ka show changes in upwelling along the Oman coast, reflecting fluctuations in the strength of the summer monsoon (e.g. Anderson and Prell, 1993). Upwelling is a result of the southwesterly winds of the IOSM creating an anti-cyclonic gyre in the Arabian Sea (Ivanochko et al., 2005).

A range of proxy records from marine cores have been used in this region to reconstruct past wind strengths, circulation patterns, and continental aridity, including foraminifera abundances (particularly *G. bulloides* and *G. Ruber*) and oxygen isotopes ($\delta^{18}O$), biogenic opal (silica) flux, nitrogen isotope flux ($\delta^{15}N$), barium excess, authigenic uranium, and grain size and geochemical analyses of lithogenic material (Clemens and Prell, 2003; Gupta et al., 2003; Ivanochko et al., 2005; Pourmand et al., 2004; Schulz et al., 1998). Of the latter, aluminium, chromium and dolomite are sourced from Iran and the Persian Gulf, whilst magnesium-rich minerals (e.g. palygorskite, dolomite) are sourced from central Arabia (Sirocko, 2000).

Generally, stronger monsoon winds are recorded during interglacials and interstadials, and stronger northwesterlies in glacial and stadial periods (e.g. Ivanochko et al., 2005; Schulz et al., 1998). Orbital, millennial and centennial scale fluctuations in the strength of the IOSM have been related to changes in solar output, Eurasian snow cover, and events in the North Atlantic. Heinrich events, Dansgaard-Oeschger events, and the Younger Dryas have been identified in marine sediments as a reduction in the strength of the summer monsoon (Gupta et al. 2003; Overpeck et al., 1996; Schulz et al., 1998).

The marine record indicates a strengthening in upwelling (i.e. the southwesterly winds of the IOSM) after the LGM in a series of steps which have been dated by Overpeck et al. (1996) to 15.3-14.7 and 11.5-10.8 cal. ka BP. During the early-mid Holocene the monsoon was at peak strength before weakening gradually until ~3-2 cal. ka BP (Lückge et al., 2001; Naidu and Malmgren, 1996). However, throughout the Holocene several intervals with a weak summer monsoon have been identified at ~10.5, 9.4, 8.2, 5.8, 4.4, 3.4, 1.7 cal. ka BP (Gupta et al., 2003, 2005; Staubwasser et al., 2002; Thamban et al., 2007). Within the last 1500 years a marine core located off the coast of Pakistan records a dominant northerly winter monsoon compared to the IOSM (Lückge et al., 2001).

Discrepancies between the marine and terrestrial records highlight the problems that underlie the comparison and integration of different proxy records. For example, whilst there are parts of the speleothem record from the southern Arabian Peninsula that have been correlated to monsoonal fluctuations in the marine record, such as the 9.2 and 8.2 ka events

(Fleitmann et al., 2007), the two signals do not always coincide in timing or amplitude. Marine summer monsoon proxies (including *G. bulloides* abundance and lithogenic grain size; see Clemens and Prell, 2003, for a detailed discussion) have been interpreted as indicators of increased monsoonal wind strength, whereas speleothems have predominantly been used as records of precipitation amount and source. As Burns et al. (1998) note, whilst between 50-40 ka some marine indicators show higher monsoon intensity than during MIS 5e (e.g. Anderson and Prell, 1993; Reichart et al., 1997), speleothem growth is only recorded during MIS 9, MIS 5 and the early Holocene (Burns et al., 2001; Fleitmann et al., 2003b). These differences are also seen between different marine proxies. For example, lithogenic accumulation has a 100 ka cyclicity, which Clemens and Prell (2003) attribute to a dominant glacial-interglacial aridity signal rather than regional monsoon strength, and is out of phase with summer monsoon proxies (which show strong in-phase 41 and 23 ka spectral frequencies). Increased upwelling does therefore not necessarily align with periods of continental wetness, which has been interpreted to indicate that the ITCZ has only shifted significantly northwards to have impacted upon the interior of the Arabian Peninsula during these interglacial periods (Burns et al., 1998). Strong monsoonal winds occur in both glacial and interglacial periods (Clemens and Prell, 2003), which, in comparison to the concentration of continental pluvial periods occurring in peak interglacial periods in the speleothem record, suggests that wind intensity, dominated by the precessional signal, does not force wet continental conditions (Fleitmann and Matter, 2009).

2.6. Rationale for the study

Within this chapter the environmental context of the northeastern Rub' al Khali and previous palaeoenvironmental reconstructions of the region have been introduced. The southern Arabian Peninsula provides a useful case study for addressing the two main research questions outlined in Chapter 1. Access to the interior sediments of linear megaridges in the UAE allows the question of the representativeness of dune chronologies to be addressed by incorporating knowledge of the visibility of the underlying dune stratigraphy (Figure 2.13). The abundance of a range of palaeoclimatic records in and around the southern Arabian Peninsula recording dramatic changes in climate and sediment supply during the Late Quaternary provides the opportunity to compare and amalgamate information from different archives. This information is an important link to aid deciphering the relationship between aeolian records and past climatic change.

There are a number of recent studies located in the northeastern Rub' al Khali, Liwa basin, and Wahiba Sands that have extended the region's dune chronology. However, this is still of limited number with low sampling resolution at some sites. There is a need to further expand the aeolian chronology and to establish further the relationships between the chronologies at different locations. In addressing the research questions, this thesis also further extends the aeolian chronology within the southern Arabian Peninsula, in order to provide a more thorough terrestrial record of the environmental response to past climatic changes.

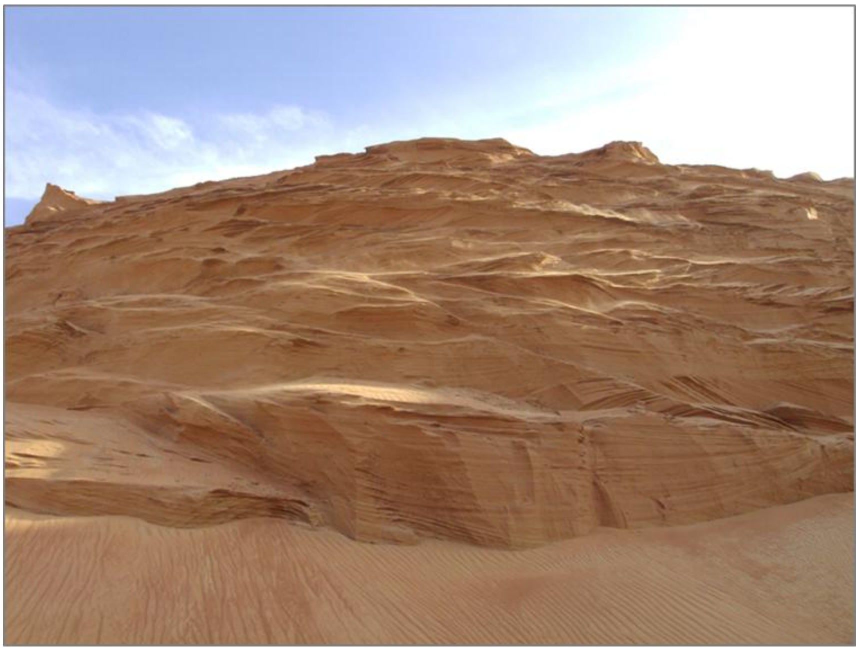

Figure 2.13: Sand dunes as visible palaeoenvironmental archives. Bottom of photograph covers a horizontal distance of c. 5 m.

3 Methodology

3.1. Introduction

In this chapter an introduction will be provided to the methods used in this thesis, in order to complement their incorporation within each of the component papers. An important objective of this thesis is to reassess previously applied methods of dating sand dunes in order to provide a more appropriate and meaningful way of collecting and interpreting data. Hence, the methods applied are of particular importance.

An introduction and justification of the study region was given in Chapter 2. This regional introduction will be built on in this chapter by describing the study sites and discussing sampling strategy, given the recognition of its importance in Chapter 1.

As the main methodological technique utilised throughout this thesis, optically stimulated luminescence (OSL) dating will be introduced. The theory underlying this dating method is discussed in relation to experimental, analytical and data presentation methods. In addition, other techniques, including laboratory analyses, will be discussed.

3.2. Site overviews and sampling strategy

Sampling in the UAE has been aided by the presence of large sand excavation quarries used by the construction industry (Figure 3.1). These pits provide an invaluable opportunity for palaeoenvironmental studies as they reveal the internal structure and stratigraphy of large linear megaridges across the region. The sites are scattered throughout the country, although due to recent economic problems active pits are less prevalent than a few years ago. These excavations have provided a unique perspective of this part of the Rub' al Khali, but at the cost of the destruction of the landscape of this part of the sand sea, including the dunes as palaeoenvironmental archives.

Figure 3.1: An example of the sand quarries in the northeastern Rub’ al Khali. Vehicles (c. 6 m high) are for scale.

Two large quarries were sampled in April 2010 (UAE10) and March 2011 (UAE11) (Table 3.1; Figures 3.2 and 3.3). The first site is a large pit near Shwaib in the east of the country adjacent to the Oman border. The second site is a pit located off the Emirates Highway approximately 20 km southwest of the city of Ras al Khaimah. The sites are located at the far northeastern extents of two northeast-southwest trending linear megaridges approximately 70 m high. These are compound dunes, with secondary linear dunes orientated northwest-southeast superimposed on them. At the time of visiting, these quarries were active, the faces had not slumped, and they provided clear visible stratigraphy to aid sampling.

Table 3.1: Details of the sampling sites referred to in this thesis.

Site	**Location**	**Sampling profile**	**Type of profile**	**Description**
Shwaib 24°47’38.85”N 55°47’24.70”E	Dhaid-Al Ain road, near Shwaib	UAE10/1	Exposure	South-facing, ~65 m in height. Sampled base of exposure. 20 samples.
		UAE10/2	Exposure	~20 m in height. 19 samples.
Emirates Highway 25°39’17.22”N 55°50’50.94”E	Emirates Highway, SW of Ras al Khaimah	UAE10/3	Exposure	~20 m in height. 19 samples.
		UAE11/1	Core 0.5 m sampling interval	Near crest of secondary dune. 14 samples.
		UAE11/2	Core 0.5 m sampling interval	Near interdune of secondary dune. 6 samples.

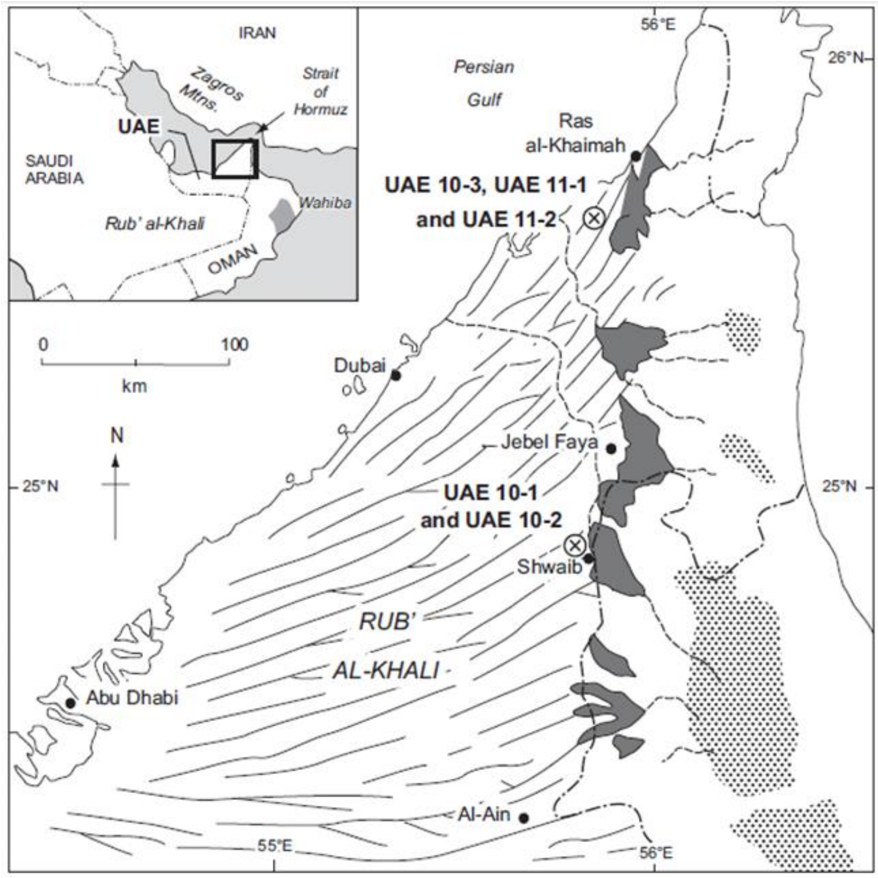

Figure 3.2: Location map of study area and the sampling sites near Shwaib (UAE10/1 and UAE10/2) and the Emirates Highway (UAE10/3, UAE11/1 and UAE11/2). Trends of linear megaridges and major alluvial fans are shown. Adapted from Atkinson et al. (2011).

The sites have previously been sampled by Atkinson et al. (2011, 2012) in 2006 and 2007, although the pits have expanded in size since then. The sites were revisited and resampled at higher sampling resolution, but due to active quarrying the sampled faces and sediments were not the same as those studied by Atkinson et al. (2011, 2012).

Sampling of three profiles in 2010 made use of the dune stratigraphy, which by usual drilling methods is not visible. This additional glimpse of past dune system dynamics allows for the assessment of how OSL chronologies relate to dune stratigraphy, and what this means for ages collected when this information is unavailable. Sampling was therefore determined by the nature of the exposed internal stratigraphy. Samples were collected in vertical and horizontal profiles at high resolution, tightly bracketing bounding surfaces and

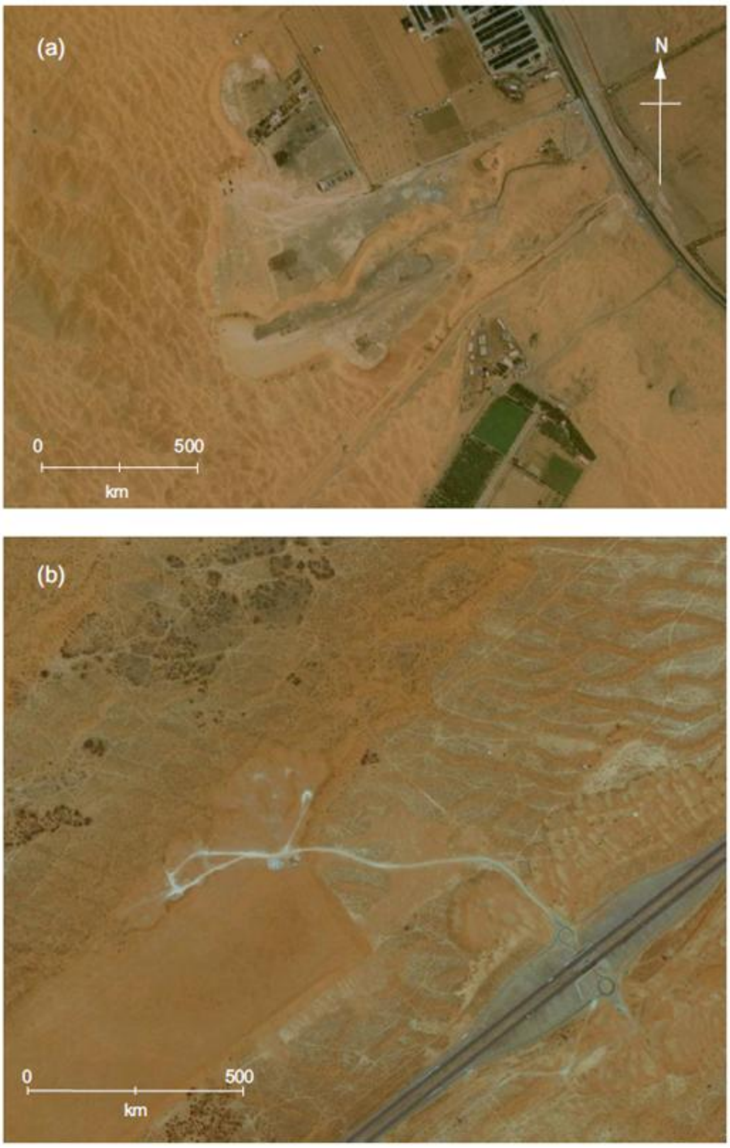

Figure 3.3: GoogleEarth images of the quarries near (a) Shwaib (©2013 Google. Image © 2013 GeoEye. US Dept of State Geographer. Imagery date: 6/10/2009); and (b) the Emirates Highway (©2013 Google. Image © 2013 DigitalGlobe. Imagery date: 29/04/2010).

stratigraphic features. The impacts of spatial location and resolution upon OSL chronologies and their interpretation could then be investigated.

Bounding surfaces and cross-laminated beds were characteristic throughout the profiles. Most of the sampling was undertaken in the basal units due to accessibility, although the vertical section at UAE 10/3 spanned the entire exposed vertical profile. The substantive chapters comprising Section 2 will include more detailed discussion of the sampling strategy of each site.

In 2011 the Emirates Highway site was revisited and two cores were extracted for OSL dating. A Dormer™ portable auger was used to extract the samples at 0.5 m vertical intervals. This sampling strategy can be described as 'blind' drilling, as the internal structure of the dune was not visible. The cores were taken from the same secondary dune, one near the crest and one near the interdune, which overlay a linear megaridge. These profiles were located only a few tens of metres from where UAE10/3 was thought to have been sampled the previous year. The aim of this second phase of sampling was to assess the dune-scale variability of OSL chronologies and investigate the implications of sampling the site blindly, which is how dune sediments are more frequently sampled.

3.3. Laboratory analyses

Previous studies in this region have shown the sediments in the northeastern Rub' al Khali to be composed predominantly of quartz and calcite, as described in Section 2.2.4. A small number of laboratory analyses were conducted in order to provide additional information about the heterogeneity of the sediments (which could be related to changes in sediment source region and environmental conditions at the source and/or depositional site) and complement the dating procedures.

Loss on ignition (LOI) was used to estimate organic and carbonate contents (following Heiri et al., 2001):

$$LOI_{550} = \frac{DW - DW_{550}}{DW} \times 100$$

(Eq. 3.1)

$$LOI_{950} = \frac{DW_{550} - DW_{950}}{DW} \times 100$$

(Eq. 3.2)

where DW is the dry weight of the sample before combustion, DW_{550} is the dry weight after heating to 550 °C, and DW_{950} is the dry weight after heating to 950 °C. LOI_{550} is proportional to the organic content of the sample. LOI_{950} multiplied by 1.36 theoretically equals the weight of carbonate in the initial sample (Bengtsson and Enell, 1986; Heiri et al., 2001). LOI has been shown to be a good qualitative indicator of organic and carbon contents, although absolutely is dependent upon sediment composition (Santisteban et al., 2004) and laboratory setting (Heiri et al., 2001).

Grain size analyses were conducted using a Malvern Mastersizer 2000 laser particle analyser and statistics were calculated using Gradistat (Blott, 2000). Comparison of pre-treated (HCl and H_2O_2 to remove carbonates and organic material respectively) and raw material showed that finer material had been preferentially removed in the pre-treatments, possibly during decanting. Given the lack of organic material and that the source of carbonate minerals is mostly likely the previously exposed Persian Gulf and coastal sediments (rather than formation in-situ as nodules), the need for HCl and H_2O_2 treatment to remove unwanted material is negligible, as the aim of this analysis is to investigate the particle size of material transported and deposited by the wind. Unprocessed sediment was therefore used for particle size analysis to fully capture the lower range of grain sizes.

Oven-dried samples were used for colour analysis in the laboratory using a standard Munsell colour chart. Colour changes may be a result of fluctuations in environmental conditions at the sediment source, a shift in dominance of a contributing source region, or changes in the conditions under which the sediment was deposited.

3.4. Introduction to OSL dating

OSL dating is used to estimate the age of burial of a sample. As minerals such as quartz and feldspar are exposed to ‘background’ radiation, electrons are displaced from their outer shells and become trapped in crystal defects. These electron populations build up over time, proportional to the level of radiation they are exposed to (the dose rate). When exposed to sufficient energy, such as sunlight or artificial light within the laboratory, the electrons return to their ground state and may emit light. The intensity of the light emitted is measured and, as it is proportional to the total trapped population, the total absorbed dose (the palaeodose) is estimated (the equivalent dose, D_e). The age of the sample can then be estimated:

$$\text{Age (ka)} = \frac{\text{Equivalent dose, } D_e \text{ (Gy)}}{\text{Dose rate, } D' \text{ (Gy ka}^{-1}\text{)}}$$

(Eq. 3.3)

3.4.1. Background radiation and dose rate

Radioactive decay from trace concentrations of radionuclides, mainly uranium (^{238}U), thorium (^{232}Th) and potassium (^{40}K) isotopes, interacts with the atoms of surrounding material, such as quartz or feldspar crystals. α-particles (two neutrons and two protons) interact strongly with electrons due to their double positive charge and slow velocity. They therefore lose energy quickly and have a short range (~20-30 μm in quartz). β-particles (high energy electron and neutrino) have a much lower linear energy transfer (LET) and hence a greater range (~3 mm). α-particles therefore have "highly localized tracks of high ionization density" (Bailey and McKeever, Unpublished: 5), whereas β-particles produce tracks where ionization is spread throughout the crystal but the energy per unit volume is low. γ-rays (photons) can travel ~30 cm through sediment. These variations in the distance of influence of ionising radiation in host sediments are important in producing spatial heterogeneity of the dose rate. In addition, buried sediments are also exposed to cosmic radiation, the extent of which is dependent on the latitude and altitude of the site and the thickness of sediment overburden.

The exposure of minerals to natural background radiation allows for the generation of free electrons (and holes), which can then become trapped in defects within the crystal lattice.

3.4.2. Trapped charge

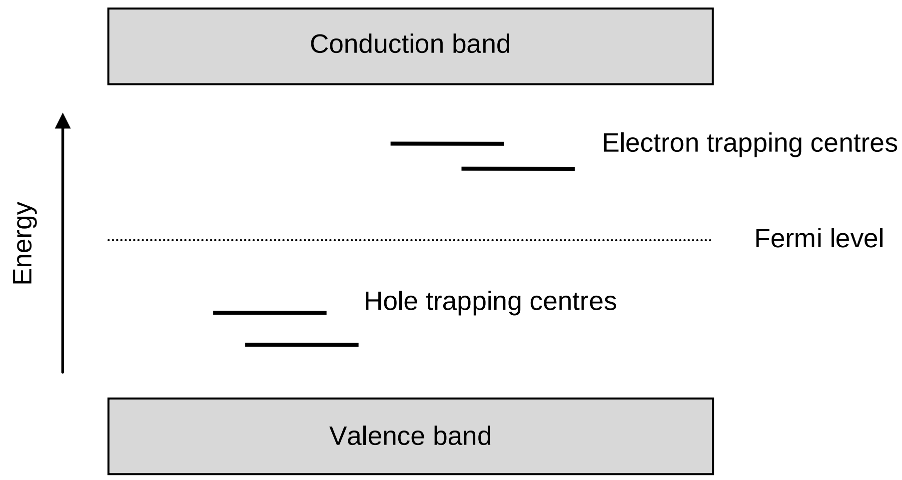

Figure 3.4: Band diagram showing the position of electron and hole trapping centres in relation to the conduction and valence bands and the Fermi level. Redrawn from Bailey and McKeever (Unpublished), permission to reproduce this figure has been granted by Richard Bailey.

The excitation of the system from a stable to metastable state as a result of ionising radiation allows for the movement of electrons and holes through the delocalised (conduction and valence) bands (Figure 3.4; Bøtter-Jensen et al., 2003b). A hole is a specific configuration of electrons where an electron is absent (Bailey and McKeever, Unpublished), such as when an electron has been displaced due to interaction with incident radiation. Loss of energy during this movement allows for the free species to become trapped within crystal defects of net opposite charge, if the potential energy due to Coulombic field of defect is greater than the kinetic energy of the free species (Solymar and Walsh, 1984, in Bailey and McKeever, Unpublished). The traps lie between the delocalised bands (Figure 3.4). These defects are due to impurities and structural imperfections within the mineral crystal lattice. For example, Al^{3+} is a common impurity within quartz (replacing

Si^{4+}) and may form a hole trapping centre. Once captured, new capture cross-sections are defined (due to a different Coulombic field resulting, for example, from an additional negative charge in the case of a trapped electron) and the probability of transitions from delocalised to localised levels changes.

3.4.3. Detrapping (1st order) and signal emission in quartz

Sufficient energetic stimulation, by light in the case of OSL or heat in the case of thermoluminescence (TL), causes the detrapping of electrons and holes. The excitation of an electron (or hole) from a trapping centre (or the valence band) may enable recombination at a recombination centre and the emission of light (luminescence). First order kinetics assumes no retrapping which, although unlikely in reality, aids description here. A number of trap sites, with different characteristics, are thought to contribute towards the OSL signal (Bailey, 2001).

The following formula describes the average time a localised charge carrier (i.e. electron or hole) is expected to spend in a trap, τ (s):

$$\tau = s^{-1}\exp(E_t/k_BT)$$

(Eq. 3.4)

where, E_t is the thermal activation energy required for excitation to delocalised band, k_B is Boltzman's constant, T is temperature (K), and s relates to the interaction of the trapped charge with the host lattice (Bailey and McKeever, Unpublished.; Bailey et al., 1997). Equation 3.4 describes the thermal eviction of carriers from traps, and is important for dating applications because τ places a limitation on the age range datable for each OSL component (Singarayer and Bailey, 2003).

'Traps' are closer to band edges and so transitions occur relatively often, whereas 'recombination centres' are towards the centre of the gap and their charges are strongly localised (Bailey and McKeever, Unpublished). It is therefore from recombination centres where the signals used for dating of quartz and feldspar are most likely to be emitted. Recombination can be described by the Schon-Klasens (mobile electron) and the Lambert-Klick (mobile hole) schemes, in which recombination process returns electrons to the valence band and holes are removed from the system (Figure 3.5; Bailey and McKeever, Unpublished).

As an electron and hole recombine, the energy loss required for the electron to relax to the valence band can be achieved by the emission of phonons to the surrounding lattice (heat/non-radiative transition) or the emission of a photon (luminescence) (Figure 3.6). If the crystal is heated during this process, there are a higher proportion of non-radiative transitions during relaxation and the luminescence efficiency (η) decreases. This is known as thermal quenching and occurs for quartz >50 °C (Bøtter-Jensen et al., 2003b; Spooner, 1994a). The likelihood of a certain route being followed, and the competition between

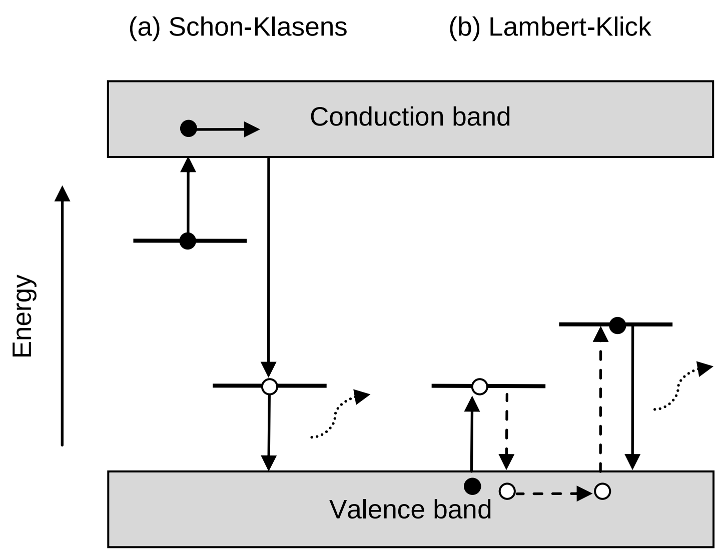

Figure 3.5: Band diagram showing the Schon-Klasens and Lambert-Klick schemes for recombination. (a) A mobile electron recombines with a trapped hole. (b) A mobile hole recombines with a trapped electron. Electron transfers are shown by solid circles and arrows, hole transfers are shown by open circles and dashed arrows. Curved dashed lines show the emission of a phonon/photon during relaxation to a ground state. Redrawn from Bailey and McKeever (Unpublished), permission to reproduce this figure has been granted by Richard Bailey.

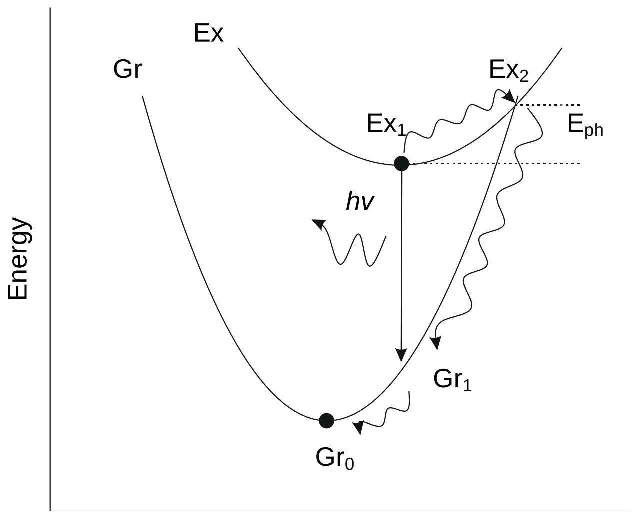

Figure 3.6: Schematic diagram of the energetic transfers that may occur during recombination. The electron in an excited state (Ex_1) returns to the ground state of the recombination centre (Gr_0) via the emission of a photon of energy *hv* to Gr_1, and then more slowly as the lattice reconfigures to Gr_0 via phonon emission. If however the crystal is heated and the electron absorbs phonon energy (E_{ph}), it may relax from Ex_2 by emitting a larger number of phonons. Redrawn from Bailey and McKeever (Unpublished), permission to reproduce this figure has been granted by Richard Bailey.

radiative and non-radiative centres, is dependent on temperature and the nature of the crystal lattice itself. The temperature at which the detrapping process takes place in a laboratory is aimed at achieving the optimum balance between reducing the contribution of thermally unstable traps to the OSL signal (such as the trap responsible for the 110 °C TL peak), rate of charge detrapping (Bailey et al., 1997), and thermal quenching.

The rate that charge is optically excited from a single trap type per s (i.e. decay rate), *f*, is described by:

$$f = \sigma\Phi \quad \text{(Eq. 3.5)}$$

where σ is the photo-ionization cross-section (probability of interaction between incoming photon and trapped electron, in which there is a strong temperature and wavelength dependence; cm^2) and φ is the incident beam intensity (photon flux; photons/s/cm^2) (Bailey and McKeever, Unpublished). The luminescence intensity is a function of the trapped charge population, which is proportional to the absorbed radiation.

Continuous wave OSL (CW-OSL) is when stimulation intensity is kept constant throughout the optical stimulation (Figure 3.7). Using a one-trap first-order model, OSL intensity, I, as a function of time can be described by a single exponential decay:

$$I(t) = n_0 f \exp\,(-ft)$$
(Eq. 3.6)

where t is time, n_0 is the initial trapped electron population at t =0, and f is the decay rate (Bailey et al., 1997).

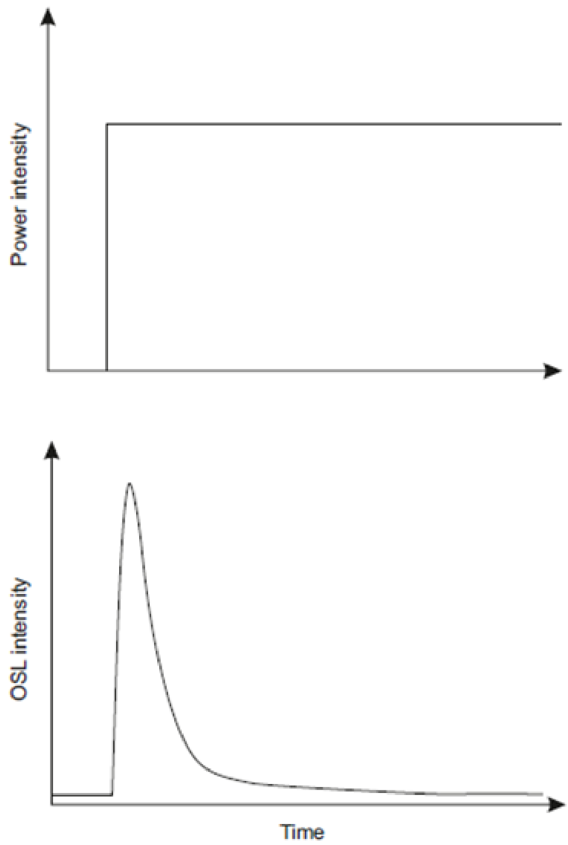

Figure 3.7: Top: CW-OSL stimulation. Bottom: Simplified OSL intensity decay curve under CW-OSL simulation.

However, as stated at the beginning of this section, models of the recombination process rely upon assumptions of short free carrier lifetimes (compared to trapped carriers), and first order kinetics. For example, the occurrence of retrapping, temporary trapping, and changes in luminescence efficiency during optical stimulation imply that non-first order kinetics are important during recombination (Aitken, 1998).

3.4.4. Quartz OSL components

The quartz CW-OSL signal can be described by the sum of several exponential components, *i*, as a function of time:

$$I(t) = \sum_{i=1}^{N} n_{0.i} f \exp{(-ft)}$$

(Eq. 3.7)

where n_0 is the initial trap concentration for N components, assuming first-order kinetics (Bailey et al., 1997).

These components have been interpreted as representing the differing rates of electron loss from multiple OSL traps. Three main components have been identified as the ‘fast’, ‘medium’ and ‘slow’ (comprising more than one) components (Bailey et al., 1997), described due to their relative decay rates, in addition to which an ‘ultrafast’ component has also been identified as present in some samples. Jain et al. (2003) identify seven components, of which between three and six are required to fit any of their twelve quartz samples. Their behaviour and the nature of their decay have been described, with the quantification of this behaviour being relatively consistent across studies (Durcan and Duller, 2011). The dominance of the different components varies substantially between samples (e.g. Bailey et al., 1997; Jain et al., 2003) and so therefore their characterisation is essential for understanding variations in OSL properties of different samples and maximising the accuracy of ages. The fast component is of most use when dating sediments, due to its relatively quick decay, bleachability (Singarayer and Bailey, 2003) and thermal stability. A fundamental assumption of most measurement procedures is that the fast component is the dominant contributor to the initial OSL decay.

Techniques for separating these components, or maximising the contribution from the fast component, include: linear modulation OSL (LM-OSL), where the stimulation power is linearly increased during OSL measurement (e.g. Choi et al., 2006; Jain et al., 2003); the use of IR stimulation at high temperatures (Bailey, 2010; Jain et al., 2005; Singarayer and Bailey, 2004); curve-fitting of the bulk CW-OSL signal into a pseudo-LM-OSL signal (e.g. Bulur, 2000; Cunningham and Wallinga, 2009; Singarayer and Bailey, 2004); and early background (EBG) subtraction (Ballarini et al., 2007; Cunningham and Wallinga, 2010). These procedures each have their respective disadvantages that have made them unsuitable for a generally applicable dating procedure. For example, LM-OSL measurement requires measurement times of over 400 s for the fast and medium components to be fully captured (Wintle and Murray, 2006); IR stimulation at high temperatures requires a bright and pure quartz signal in order for feldspar to not dominate the IRSL signal (Bailey, 2010); curve-fitting is time-consuming and labour-intensive; and the EBG subtraction method requires a bright signal or is associated with a reduction of precision.

In this thesis software written by Diana Bailey was used to decompose the CW-OSL curve into its constituent components (Bailey, 2009). A number of components are specified and these are fitted using a Levenberg-Marquardt algorithm. This process is discussed in further detail in Chapter 7.

3.4.5. Feldspar minerals

Photo-eviction from feldspars is more complex and less well-known than quartz. In addition, quantum mechanical tunnelling may occur, where electrons are transferred through sub-conduction-bands between adjacent sites. The likelihood of this process occurring is increased if the sites are close or if the electron is thermally excited. The implication of this process is that trapped charge decreases over time, which is known as 'anomalous fading' (Spooner, 1994b; see Huntley and Lian, 2006, for detailed discussion). There has been significant work in recent years to improve the reliability of using feldspar minerals for dating (e.g. Buylaert et al., 2009; Jain and Ankjærgaard, 2011; Thomsen et al., 2008), although quartz remains the most suitable mineral of choice when present in sufficient quantities for dating Late Quaternary sediments.

Whilst feldspars will not be directly dated during this study, they are often a contaminant of the samples that may be difficult to fully remove during sample preparation (Duller, 2003).

3.5. Experimental procedures

The purpose of this section is to describe the main OSL experimental procedures that have been followed throughout this study. More thorough investigation of these procedures and deviations will be described in detail in the subsequent papers.

3.5.1. Sample preparation

Prior to measurement of the D_e, chemical and physical pre-treatment was undertaken to isolate the quartz fraction. All samples were prepared and measured in the Oxford Luminescence Dating Laboratory (OLDLAB) under subdued orange (585 nm) light.

The sample preparation protocol is shown in Figure 3.8. The top (or outer edge of sample within quarry) ~3 cm of sand was removed in order to minimise the dating of samples bleached since the burial event. Samples were treated with 37% hydrochloric acid (HCl) to remove carbonates and 30% hydrogen peroxide to remove organic matter. Dry sieving

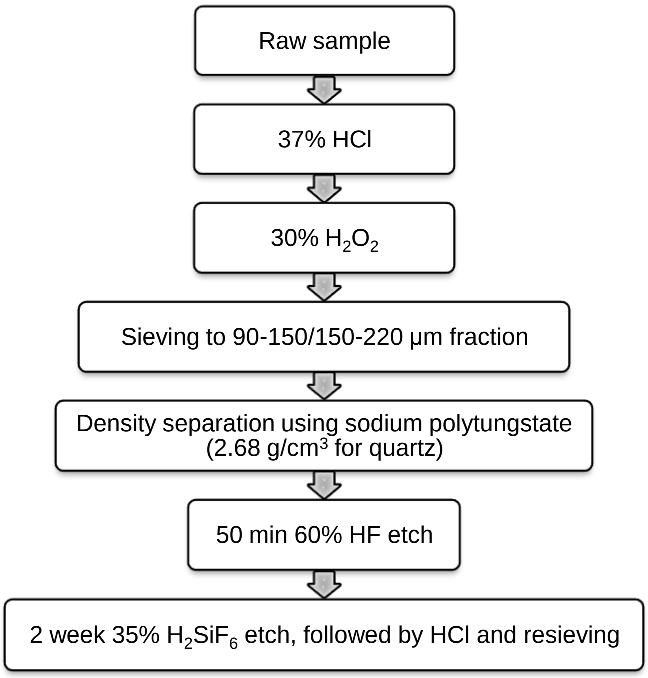

Figure 3.8: Standard sample preparation procedure to isolate quartz prior to D_e measurement.

separated size fractions of 90-150 μm and 150-220 μm. Heavy minerals were removed by heavy liquid density separation using sodium polytungstate (at 2.68 g cm^{-3} for quartz and 2.58 g cm^{-3} for feldspar). A 60% hydrofluoric acid (HF) etch for 50 min on a shaker table was undertaken to remove the alpha-irradiated shell of the quartz grains. A further 2 week treatment with 35% hexafluorosilicic (H_2SiF_6) acid was required after an initial infrared (IR) purity test revealed the presence of feldspars. Following an HCl treatment to remove fluorides and re-sieving, the samples were mounted onto aluminium discs using Silkospray® and a 5 mm diameter mask. Medium aliquot (subsample) sizes were chosen due to the unlikelihood of both partial bleaching, in an aeolian depositional environment, and significant bioturbation, given the clear visible laminations at the sites.

Size fractions of 90-150 μm and 150-220 μm were dated for multiple grain measurements, whilst only 150-220 μm grain size were used for single grain measurements. The discs were loaded onto the wheel alternately in order to minimise the effects of cross-bleaching and cross-irradiation (Bray et al. 2002).

3.5.2. Measurement of the equivalent dose

Equipment

All OSL measurements were conducted using four Risø TL-DA-15 automated readers in the OLDLAB ('Atlas', 'Bacchus', 'Cyclops' and 'Delphi'). The $^{90}Sr/^{90}Y$ source used for beta irradiation provides a dose rate for a quartz sample of approximately 0.1 Gy s^{-1}. A heating plate lifts the sample into measurement position and heats the sample prior and during stimulation.

Four arrays of seven blue light emitting diodes (LEDs) emit at 470±30 nm for optical stimulation of the sample in three of the readers, which can deliver a maximum power of >40 mW cm^{-2} to the sample (Botter-Jensen et al., 2003a). The other machine's ('Delphi') stimulation source was changed to green diodes with peak emission at 525 nm midway through this project (see Bailey et al., 2011 for a discussion of the advantages of using green diode stimulation), and the use of the longer wavelength for stimulation is explicitly stated within this thesis. In three of the readers, there are three arrays of seven IR LEDs which emit at 875 nm, producing a maximum power of ~145 mW cm^{-2} at the sample (Botter-Jensen et al., 2003a). In 'Cyclops', IR stimulation uses a solid-state 1W IR laser diode emitting at ~830±10 nm.

A bialkali EMI 9235QA photomultiplier tube (PMT) detects the luminescence emission. A 7.5 mm Hoya U-340 detection filter prevents any scattered stimulation light from reaching the PMT. This filter transmits between 250 and 390 nm, with peak transmission at 340 nm (Bøtter-Jensen et al., 2003b). The UVA-violet emissions (~360 to 420 nm) of quartz are of most importance for OSL measurement (Bøtter-Jensen et al., 2003b).

One of the machines ('Cyclops') has a single grain OSL attachment, allowing for the measurement of single grains. Each grain is situated in a 300 μm diameter and 300 μm deep hole within an aluminium disc. The 100 holes are located 600 μm apart. The stimulation source is a 10 mW green (532 nm) laser diode which focuses to <20 μm diameter, with a maximum estimated energy at the sample of 50 W cm^{-2} (Duller et al., 1999; Risø DTU, 2009).

SAR protocol

The single aliquot regenerative (SAR) method (Murray and Roberts, 1998; Murray and Wintle, 2000) was introduced to OSL dating as an improvement upon multiple aliquot techniques, in which OSL signals from different aliquots were used to construct a dose response curve. Single grain work has shown that individual grains respond uniquely to dose (Murray and Roberts, 1997), and so the use of multiple aliquot protocols is flawed. However, sensitivity change may be problematic when using repeated measurements of the same aliquot to construct a dose response curve. This occurs when repeated cycles of irradiation, preheating and light exposure cause a change in the magnitude of emission per unit dose due to changes in thermal stability and dose response, associated with competitor characteristics (Bailey and McKeever, Unpublished). The SAR protocol (Table 3.2) addresses this by introducing measurement of a signal from a test dose (T_x) after the natural and each regenerative dose, and the change in the response to this test dose is used to standardise the preceding natural/regenerative OSL signal (L_x).

Before each L_x and T_x measurement the sample is heated (a 'preheat') in order to remove thermally unstable signals. A preheat in the range of 160-300 °C empties the unstable 110 °C trap in quartz whilst not depleting the OSL trap. Using the SAR protocol, in which the test dose is used to account for sensitivity change, allows for higher preheat temperatures to be used. A lower temperature preheat is used prior to the test dose measurement in order to reduce sensitivity change between the measurement of L_x and T_x, although it is the change in T_x relative to L_x being constant independent of measurement cycle that is important,

Table 3.2: The SAR protocol, in which steps are repeated in order to construct a dose response curve (adapted from Wintle and Murray, 2006).

Step	Treatment	Observed
1	Give dose, D_i *(zero dose is given for the natural dose)*	
2	Preheat (260 °C for 10 s, after cooled to <60 °C)	
3	Stimulate for 100 s (dependent on light intensity and wavelength) at 160 °C	L_x
4	Give test dose, T_D	
5	Heat (220 °C for 10 s, after cooled to <60 °C)	
6	Stimulate for 100 s (dependent on light intensity and wavelength) at 160 °C	T_x
7	Stimulate for 50 s (dependent on light intensity and wavelength) at 280 °C	
8	Return to 1	

rather than the sensitivity change itself. It is part of standard procedure to do a preheat plateau test in order to assess the dependence of the D_e on preheat temperature (Wintle and Murray, 2006). A preheat plateau test was conducted on three of the samples from the UAE following the procedure outlined in Table 3.2 but using a range of temperatures between 220-280 °C prior to measurement of the L_x (step 2). The results are shown in Figure 3.9 and indicate no dependence of D_e on temperature in the range 220-280 °C. 260 °C and 220 °C were subsequently selected as preheat temperatures prior to L_x and T_x measurements respectively.

The suitability of the SAR protocol in correcting for sensitivity change is tested by the integration of four quality assurance ratios: the recycling ratio, zero dose ratio, dose recovery test, and OSL IR depletion ratio.

The recycling ratio repeats a measurement (usually the first, smallest dose) towards the end of the sequence to give a measurement of the widest range of sensitivity change. Aliquots

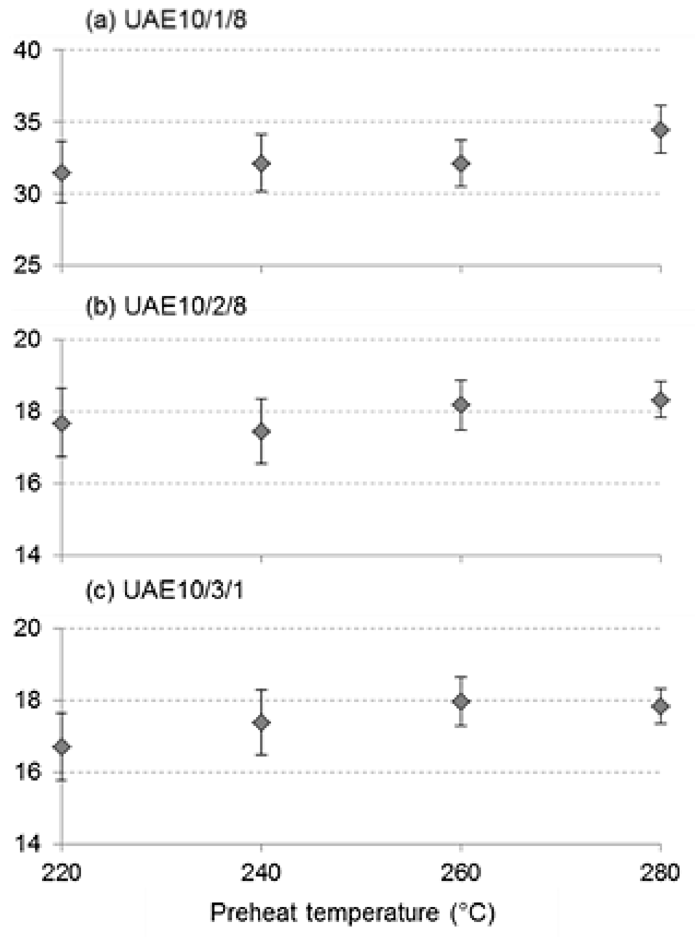

Figure 3.9: Preheat plateau test results for three samples from the sample sites: (a) UAE10/1/1; (b) UAE10/2/8; and (c) UAE10/3/1. The D_e values for each preheat temperature are calculated using a minimum of 6 aliquots.

were excluded from D_e calculation if this value was outside of 10% of unity, as recommended by Murray and Wintle (2000).

The zero dose ratio (recuperation test) measures the OSL signal for which a zero dose has been given. Thermal transfer is when charge is released from a shallow, optically insensitive trap during preheating and is subsequently captured by an OSL trap, leading to a larger OSL signal than would be expected from the initial trapped charge prior to the preheat. The value of the zero dose ratio should be zero, but if thermal transfer has occurred it may be larger. Aliquots were excluded from D_e calculation if this value was above 5% (Murray and Wintle, 2000). In addition, the incorporation of a high temperature optical bleach within the SAR protocol (Step 7 in Table 3.2) has been shown to reduce transfer between regeneration cycles (Murray and Wintle, 2003), and was followed here.

A dose recovery test is composed of optically depleting the natural OSL signal at room temperature, giving a known dose to the sample, and assessing whether the known dose can be recovered using the SAR protocol. The dose recovery ratio is the ratio of the measured dose to the known dose, and should be unity if the SAR protocol is appropriate for the sample in question. It is particularly useful for indicating if thermal transfer or major sensitivity change occurs during the first preheat. Dose recovery results were within ±10% of unity for 96% of the samples dated in this study.

The OSL IR depletion ratio is used as an efficient method of identifying whether feldspar is contaminating the OSL signal, as at room temperature only feldspar (and not quartz) emits a significant IRSL signal (Duller, 2003). Aliquots were excluded from D_e calculation if this value was outside of 10% of unity.

Following the administration of the SAR protocol the D_e is calculated by fitting the dose response curve using a single saturating exponential, and interpolating the natural L_x/T_x signal. A dose response curve can be described by:

$$I = I_0 + I_\infty\left(1 - e^{-D/D_0}\right)$$
(Eq. 3.8)

where I is the OSL intensity corresponding to dose, D, I_∞ is the maximum signal, I_0 is the offset from zero at zero dose, and D_0 is the characteristic dose (Roberts and Duller, 2004). The uncertainties on the L_x/T_x measurement are based on Poisson counting statistics (i.e. $n \pm \sqrt{n}$). These are propagated in the calculation of the D_e uncertainty by using a Monte Carlo curve-fitting procedure and by adding a systematic uncertainty of 3% to account for calibration uncertainty and machine reproducibility (Grine et al., 2007). This procedure was conducted using software written by Richard Bailey.

Double-SAR protocol

The double-SAR protocol includes additional steps immediately prior to L_x and T_x measurement when an IR bleach (125 °C) is administered (Roberts and Wintle, 2001). During IR stimulation the IRSL signal from feldspar is removed whilst there is not significant depletion of the quartz OSL traps, leading to a post-IR OSL signal that is relatively more dominated by quartz. This protocol has been used predominately for mixed mineralogy samples in order to isolate a quartz-dominated post-IR OSL signal (e.g. Roberts and Wintle, 2003, 2001; Roberts, 2007). However, it has been concluded that part of the feldspar signal is only bleachable by blue or green light and that some form of chemical pre-treatment of samples is usually required for accurate D_e estimations (Duller and Bøtter-Jensen, 1993; Lai and Brückner, 2008; Roberts, 2007). This protocol is further discussed in Chapter 7.

Single grain measurement

Single grain measurements were all made using the Risø reader with a single grain OSL attachment ('Cyclops'). Further technical details can be found earlier in this section. Optical stimulation using a focused green laser diode was conducted for 1 s for each grain, but otherwise the same protocol was followed as shown in Table 3.2.

Standardised growth curves

The investigation of the utility of a universal dose response curve has led to the development and application of standardised growth curves (SGCs) (Roberts and Duller, 2004). Their use relies on the assumption that all quartz responds similarly to radiation and optical stimulation. The OSL signal is standardised by the size of the test dose, T_D:

$$Standardised\ OSL = (L_x/T_x) \times T_D$$
(Eq. 3.9)

This correction assumes that the test dose is sufficiently small to be in the region of the dose response curve that can be described by a straight line (Roberts and Duller, 2004).

The advantage of using a SGC is that measurement time is reduced, as only the signals of the natural (L_n and T_n) and one regeneration point (L_x and T_x) are required. The additional measurement of a regeneration point signal to assess whether the sample is behaving as expected according to the SGC has been recommended due to the variability in dose response curve shape between some samples (Burbidge et al., 2006; Telfer et al., 2008). The SGC can be described by the same dose response curve shape given in Equation 3.8, where I is the standardised OSL (Roberts and Duller, 2004).

Models for equivalent dose calculation

Different models can be used to calculate the D_e of a sample depending on the choice of most likely assumptions of the depositional environment. The central age model assumes there is a normal distribution of the logarithmic D_e values (i.e. not a single common D_e) with mean, δ, and a relative standard deviation, σ (which reduces to the common age model when σ=0) (Galbraith et al., 1999). This parameter represents the overdispersion *after* within-aliquot (or within-grain) measurement errors (σ_{wi}, based on photon counting statistics) have been accounted for (Galbraith and Roberts, 2012; Galbraith et al., 2005). The standard error of the overdispersion, σ_b, is the estimate of the overdispersion between aliquots known to have the same D_e (Galbraith and Roberts, 2012; Galbraith et al., 2005). For single grains an overdispersion value (σ) of <20% has been suggested as representative of a single-dose population (Galbraith et al., 2005; Olley et al., 2004); i.e. the dispersion is explained by intrinsic rather than extrinsic factors such as dose rate heterogeneity, partial bleaching or post-depositional mixing.

Alternative models for consideration include the minimum age model, appropriate when it is thought that partial bleaching or mixing of older sediments may have occurred, or the finite mixture model, where multiple populations are estimated from the D_e distribution (Galbraith and Green, 1990; Galbraith et al., 1999).

As aeolian samples tend to be well bleached and the preserved stratigraphy in the sampling sites in the UAE shows little evidence of post-depositional mixing of the sediment, the central age model has been applied to calculate all sample D_e values. This is supported by single grain dating of two samples, which gives D_e values within errors of the multiple grain estimates, indicating that mixing or incomplete bleaching are unlikely to be significant for these samples. The generally low overdispersion values ($\sigma \leq 20\%$ for 87% of samples measured as single aliquots) also indicate that the D_e distributions can be explained by intrinsic factors (i.e. measurement errors) rather than environmental factors.

3.5.3. Dose rate calculation

Dose rate estimations can be based on either field measurements of the radiation received or laboratory measurements of radioisotope concentrations. In this study, both of these approaches were addressed by the application of field gamma spectrometry and inductively coupled plasma mass spectrometry/atomic emission spectrometry (ICP-MS/AES). These measurements allow for estimation of the beta and gamma dose rates. The alpha contribution is assumed negligible following the removal of the rind of the quartz grains during the HF stage of sample preparation. Therefore the estimated dose rate can be calculated as the sum of the beta, gamma and cosmic contributions. The cosmic contribution was calculated following Prescott and Hutton (1994), which incorporates sample depth (i.e. overburden density), altitude, longitude and latitude. The effective cosmic contribution to the total dose rate is ≤20% for all samples, and ≤10% for 63% of samples. Given this relatively small contribution to the overall dose rate, the cosmic dose was assumed to constant over time. Water absorbs radiation, but, as the average moisture content over the whole time of burial cannot be known, this is a major uncertainty in the estimation of the dose rate (Aitken, 1998). Moisture content was conservatively estimated at 5±3% for all samples. This large range was chosen in order to allow for temporal fluctuations in moisture, as moisture content is unlikely to be less than 1-2% (e.g. Berndtsson et al., 1996) and there is evidence of significantly wetter conditions in the past (e.g. Fleitmann et al., 2007; Parker et al., 2006).

Gamma Spectrometry

Given that gamma radiation reaches a range of tenths of a metre within the dune sediment (Aitken, 1998), gamma spectrometry is important in order to assess whether the dose rate estimations based on sample geochemical analyses are representative of the gamma dose received in the field. Field gamma spectrometer measurements were undertaken for 40 min using an Ortec® DigiBASE™ and a 2" sodium iodide detector. The spectra were converted to K (1.45-1.60 MeV window, ^{40}K peak), Th (2.56-2.95 MeV window, ^{208}Tl peak) and U (1.80-1.95 MeV window, ^{214}Bi peak) concentrations using in-house software written by Matt Telfer.

Gamma spectrometry measurements were undertaken at sites UAE10/1 and UAE10/2, but only for four samples due to time and battery constraints. The gamma dose rates were relatively homogeneous and within 15% of those based on ICP-MS/AES measurements. Previous work suggests field gamma spectrometry measurements at less regular intervals in homogeneous sediment show identical results within errors to ICP-MS and ICP-AES measurement calculations (Stevens et al., 2007), and so are likely to be sufficient for this study. Preusser and Kasper (2001) also find good agreement (generally within 10%) between ICP-MS and high resolution gamma spectrometry. Given the limited number of gamma spectrometry measurements, the ICP-MS/AES gamma dose rates are used in all subsequent age calculations for consistency.

ICP-MS/AES

Dose rates were determined by ICP-MS/AES, conducted at the Department of Geology, Royal Holloway, University of London and SUERC, East Kilbride. The conversion factors of Adamiec and Aitken (1998) were used to calculate dose rates from elemental concentrations.

Samples UAE10/1/19 and 1/20 are from the same sedimentary set, share homogeneous sedimentological characteristics and have indistinguishable D_e values with errors. However, based on the initial ICP-MS/AES measurements, the total dose rate of 1/19 was calculated to be approximately three-quarters of the value of the dose rate of 1/20. This is accounted for by the difference in beta dose rates due to the lower K concentration (from ICP-AES determination of K_2O) reported for sample 1/19. Subsequently, repeated ICP-MS/AES measurements of 1/19 gave a dose rate in agreement with 1/20. The source of this variability is unknown and implies that additional uncertainty is required in order to more accurately estimate the precision on dose rates derived using these analytical methods. Hence, based on the relative standard deviations of repeated ICP-MS/AES measurements for sample 1/19, relatively large uncertainties of 13%, 9% and 13% were attached to K, U and Th radioisotope concentrations respectively, and were used to calculate dose rates. Given the limited number of ICP-MS/AES measurements and the difficulty in identifying outliers in usual OSL dating circumstances, the relative standard deviation is used as a conservative estimate of variability.

Assumptions in dose rate calculation

Beta heterogeneity

Dosimetry tends to be the least well-known component in OSL age calculation, and is particularly important if radioactivity is low or highly concentrated (Duller, 2008). Given their respective ranges, the alpha contribution is assumed to be negligible after the removal of the outer rind of the quartz grains prior to D_e measurement and the gamma dose rate is assumed to be relatively homogeneous for an individual sample, although variation in the latter has been noted for single grains (Guérin and Mercier, 2012). The beta dose rate varies "across spatial scales of the order of tens of microns to several millimetres" and hence is expected to be more heterogeneous (Nathan et al., 2003: 313). This effect will be amplified if the beta source is not uniformly distributed within the sediment (Cunningham et al., 2012). The radioisotope ^{40}K contributes approximately 80% to the beta dose to the UAE samples (which is >60% of the total dose), and hence variations in the concentration of this radioisotope are likely to have the most significant impact upon dose rate heterogeneity. Other reasons may be the presence of carbonate nodules or spatial variations in moisture content. Carbonates can both decrease and increase dose rates to the dated sediment by attenuation and the incorporation of mobile U respectively (Grine et al., 2007).

Particle size analysis indicates that the sediments are fairly homogeneous, and low overdispersion (≤20%) for over 87% of samples indicates that beta heterogeneity has not resulted in unaccounted variability in the D_e. However, beta variability may have had a more significant impact on the determination of the dose rate. For example, the discrepancies apparent in ICP-MS/AES results may be due to the relatively small amount (<0.2 g) of sample used for these measurements.

More research into dose rate heterogeneity and the way this is accounted for in age calculation is required for all luminescence dating studies. The use of multiple methods of analysis for dose rate determination where possible, including high resolution gamma spectrometry, is one approach to assessing the problem, although does not fundamentally solve the issue of how to deal with discrepancies. The use of subsamples provides an 'average' D_e estimate, partially accounting for non-systematic D_e variability and its description using the overdispersion parameter. In this study repeated measurements for several samples for ICP-MS/AES replicates this approach in the calculation of the dose rate, but is financially implausible to the same extent. Relatively large uncertainties have therefore been applied to K, Th and U radioisotope concentrations, although the cause of this variability remains unclear.

Decay series disequilibrium

Dose rate calculation within many luminescence dating studies assumes that the radioisotope decay chains are in secular equilibrium and constant throughout the time of burial. Disequilibrium describes when the concentrations of the parent and daughter nuclides within a decay series are unequal. This principally occurs when there is mobility of radioisotopes within an open system, for example via solution, precipitation or gaseous diffusion (e.g. ^{222}Rn in the ^{238}U series) (Olley et al., 1996). Disequilibrium in the ^{238}U decay series is particularly problematic for geological dating due to the long half-lives of the daughters ^{234}U, ^{230}Th and ^{226}Ra (Olley et al., 1996, 1997). One important mechanism is differentiation of members of the decay chain during carbonate lithification (Zander et al., 2007).

The activity of each radionuclide can be measured and then the ratios can be compared to assess if the system is currently in secular equilibrium. However there are two problems with this method. Firstly, it may not be possible to measure all the radioisotopes directly. Secondly, even if the system appears to be in equilibrium, it does not mean that this has been the case throughout the burial history. Therefore, modelling the environmental history is a complex undertaking and whilst it has been attempted by some authors (e.g. Olley et al., 1997; Zander et al., 2007) others have incorporated additional uncertainty into age estimates (e.g. Atkinson et al., 2011). Olley et al. (1996) found that the effect of ^{238}U disequilibria on dose rate is usually less than 3% if the dose rate is assumed to be constant and system closed after sediment deposition, although large disequilibria will have more significant impacts.

Disequilibria in the ^{238}U series has been found in the shallow marine and intertidal sediments in the coastal plain of the UAE (Zander et al., 2007). Given the reduction in carbonate content of aeolian deposits with increasing distance from the coast (El-Sayed, 1999), the carbonates are most likely to have been transported to the coastal fringes of the Rub' al Khali rather than having formed in-situ. The high concentration of carbonates near the coast is therefore not necessarily indicative that disequilibria is a significant problem for these sampling locations as a result of the occurrence of carbonate lithification, although this explanation of carbonate presence does not negate the assumption that the dose rate has been constant and system closed after aeolian sediment burial (i.e. the assumption described above by Olley et al., 1996).

The radioisotope concentrations of K, Th and U determined by field gamma spectrometry are calculated from the spectral peaks of ^{40}K and daughters ^{208}Tl and ^{214}Bi respectively. These are compared to the radioisotope concentrations determined by ICP-MS/AES in Figure 3.10, in which the parent isotopes are used for radioisotope concentrations. Whilst only four samples in total from sites UAE10/1 and UAE10/2 have been measured using both techniques, there is no systematic deviation in any of the radioisotope concentrations depending on the method of analysis. This indicates that there is unlikely to be significant ^{238}U series disequilibrium at sites UAE10/1 and UAE10/2.

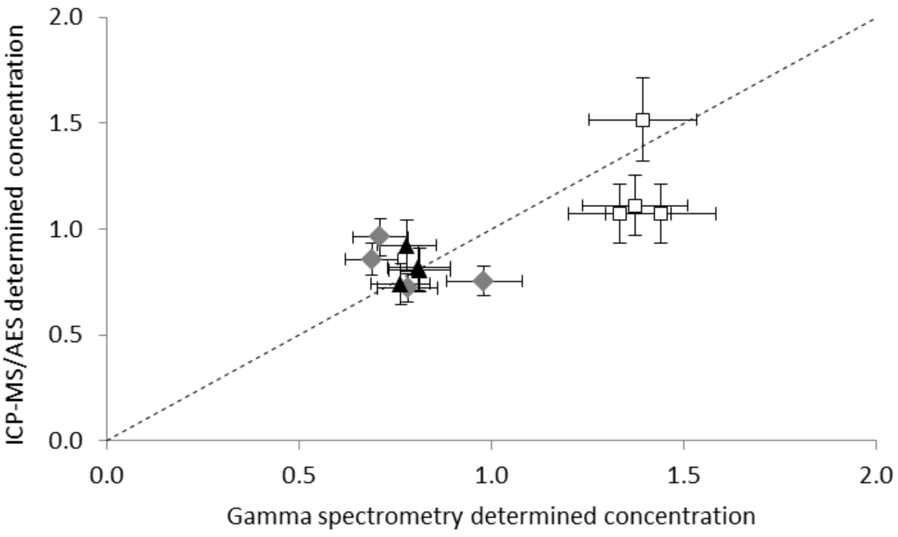

Figure 3.10: Radioisotope concentrations determined by ICP-MS/AES (13, 9 and 13% uncertainties for K, U and Th respectively) and field gamma spectrometry (10% fractional error) for four samples. K (%), U (ppm) and Th (ppm) are shown by black triangles, grey diamonds, and open squares respectively. The 1:1 line is shown.

3.6. Bayesian analysis of OSL ages

Sampling using visible stratigraphy enables the relative chronology of samples to be known. This is potentially useful both for identifying anomalous ages and to improve the precision on OSL ages by incorporating this known information. In this section, Bayesian analysis will be introduced as a technique for integrating different types of relevant chronological information and the potential of this technique for applying to OSL dune ages will be discussed.

3.6.1. Introduction to Bayesian analysis

It is given that:

$$p(\boldsymbol{t} \cap \boldsymbol{y}) = p(\boldsymbol{y}|\boldsymbol{t}) \times p(\boldsymbol{t}) \quad \text{(Eq. 3.10)}$$

$$p(\boldsymbol{y}) \times p(\boldsymbol{t}|\boldsymbol{y}) = p(\boldsymbol{y}|\boldsymbol{t}) \times p(\boldsymbol{t}) \quad \text{(Eq. 3.11)}$$

where $p(\mathbf{t})$ and $p(\mathbf{y})$ are probabilities of two sets of events occurring. Bayes' theorem states:

$$p(\boldsymbol{t}|\boldsymbol{y}) = \frac{p(\boldsymbol{y}|\boldsymbol{t})p(\boldsymbol{t})}{p(\boldsymbol{y})}$$
(Eq. 3.12)

where $p(\mathbf{t})$ is the *prior* knowledge (proposition) about the parameters, $p(\mathbf{y})$ is the probability of set of measurements describing the parameters occurring (evidence), $p(\mathbf{y}|\mathbf{t})$ is the *likelihood* of the measurements given the prior event occurring, and $p(\mathbf{t}|\mathbf{y})$ is the *posterior* probability of a particular set of parameters given the measurements and the prior. As $p(\mathbf{y})$ is difficult to describe, the following equation is used:

$$p(\boldsymbol{t}|\boldsymbol{y}) \propto p(\boldsymbol{y}|\boldsymbol{t})p(\boldsymbol{t})$$
(Eq. 3.13)

In terms of the dating of a sedimentary sequence, a Bayesian model incorporates *prior* information, $p(\mathbf{t})$, known about the sedimentary sequence (e.g. relative stratigraphy, depth information, presence of dated markers) with dating information, in the form of probability density functions (PDFs), which represent the *likelihood* of a sample having a particular age, $p(\mathbf{y}|\mathbf{t})$ (Bronk Ramsey, 2008). The application of Markov Chain Monte Carlo (MCMC) sampling, by repeatedly sampling all possible solutions using the probability of the product of prior and likelihood, produces a *posterior* probability distribution which incorporates the prior information and dating measurements, $p(\boldsymbol{t}|\boldsymbol{y})$. This method can be used to assess the most likely probabilities of certain ages given the prior.

Bayesian techniques have been increasingly applied to the analysis of radiocarbon dates and other chronological methods, in order to increase the precision of chronologies by utilising information regarding the relationships between samples (e.g. Blockley et al., 2008; Clark-Balzan et al., 2012). In part, the increased application of these methods can be tied to the widespread availability of software such as OxCal (Bronk Ramsey, 1995, 2009a).

3.6.2. Assumptions implicit in calculating the likelihood

The application of Bayesian analysis to dating methods other than radiocarbon has been noted as problematic due to the complexity of associated uncertainties (Millard, 2006; Rhodes et al., 2003). The *likelihood* describes the probability of the measurements (here, OSL ages) given the prior, and hence requires inclusion of a description of the measurement process. For this reason, Millard (2006) argues that the likelihood needs to be formulated for each dating technique. It is assumed that sample measurements are independent, whilst common parameters have negligible uncertainty (e.g. the half-life of ^{14}C in the analysis of radiocarbon ages) (Millard, 2006). When this is not the case the likelihood needs to be broken down into a series of likelihoods, with joint likelihoods utilised for shared parameters, or else age uncertainties will be underestimated (Millard, 2006). However, if there are many parameters and only few are shared, this underestimation may only be small; the relative significance of this can be weighted in the decision to calculate appropriate likelihoods (Millard, 2006).

The treatment of uncertainties in the Bayesian analysis of OSL ages has proved complex; Rhodes et al. (2003: 1237) note that "there is no easy way to treat systematic errors in a rigorously Bayesian way" as samples do not have fully independent uncertainties. Whilst there are shared parameters in the calculation of the D_e, such as radiation source calibration uncertainty, these only make a small contribution to the overall uncertainty (Millard, 2006). The main shared parameters are associated with the calculation of the dose rate, and occur at a range of scales. For example, the gamma and beta radiation dose estimations may be calculated using shared in-situ gamma spectrometry measurements, and therefore the uncertainty of each sample will not be independent (Millard, 2006). In their approach, Rhodes et al. (2003) input OSL ages with precision-only uncertainties into OxCal and recombine systematic errors after analysis. They introduce the term unshared systematic

(USS) errors to describe additional systematic errors that are unshared by the samples. These are incorporated into the age uncertainties by increasing the errors in the samples until the A_{model} value (an agreement index used to quantify the consistency of the posterior and likelihood distributions) is above the threshold value, to produce a set of ages that are internally consistent. By providing a term that accounts for all discrepancy this approach assumes that the dates should be consistent and robust, and hence potentially ignores true inconsistency (e.g. caused by post-depositional mixing), although when used alongside independent age control it can attempt to understand where these discrepancies arise.

There are examples in the application of Bayesian analysis to OSL ages where independence has been assumed. Millard (2008) models the OSL ages produced by Jacobs et al. (2003) as calendar ages in OxCal, due to the majority of the uncertainty being independent. Dosimetry was measured for each of these samples by alpha-counting for the internal alpha dose rate, beta-counting for the external beta dose rate, thick-source alpha counting (TSAC) for U and Th concentrations, and atomic absorption spectrometry (AAS) for K concentration for estimation of the external gamma dose rate. Feathers et al. (2006) also analysed OSL ages in OxCal using a simplified method. TSAC (U and Th) and flame photometry (K) were the main methods of dose rate calculation for each sample and again ensured near independent ages.

Within OxCal, parameters can be used to input OSL data as D_e estimates and dose rate parameters and their associated uncertainties (e.g. beta, gamma, and cosmic dose rate contributions, and water content), from which ages can be calculated using given equations (Bronk Ramsey, 2009a; Clark-Balzan, pers. comm.). When calculated in sequence, the shared uncertainties can then be dealt with in a Bayesian way.

3.6.3. Application of Bayesian analysis to dune OSL ages

The OSL samples collected in the UAE lend themselves to the application of Bayesian analysis due to the sampling strategy undertaken. The visible relative chronology and intensive sampling can be used as prior information to reduce the uncertainty on the individual ages.

OxCal (Bronk Ramsey, 1995, 2001, 2009a) provides a free online platform for importing ages into a Bayesian model, from which posterior distributions are calculated using MCMC sampling. OxCal v. 4.1 and 4.2 are used in the calculation of ages in this thesis. Different types of models are available, which constrain the model to varying degrees. A ‘Sequence’ defines a group of events for which the order of events is known but the deposition process is random and unknown. The prior can be more strictly enforced by incorporating uniform or defined deposition rates (Bronk Ramsey, 2008). Groupings are defined by boundaries, which are estimations of the start and end of a dated phase/sequence. The use of a ‘Boundary’ defines a uniformly distributed group, although other boundaries can be used as priors to define a normally distributed, or linear or exponential changes in, accumulation rate.

Due to the discontinuous nature of dune accumulation a ‘Sequence’, as the most conservative of sequence models, is the most appropriate method of constraining this information. A ‘Boundary’ is the most appropriate phase/sequence boundary due to the unknown nature of aeolian deposition and preservation. The dose rates were calculated using individual ICP-MS/AES measurements of U, Th and K concentrations for each sample, and hence the uncertainties on each sample are considered to be near independent. The ages for the UAE samples have been calculated by using two alternative methods: as calendar ages and as a series of OxCal parameters, with little difference in final result.

Nonetheless, all modelled ages presented in this thesis will be those calculated using parameters, where the shared uncertainties are treated explicitly.

The ages of samples that are known to belong to the same sedimentary set, and hence should have the same age of deposition (e.g. UAE10/1/19 and 20), were combined. Age populations of the different samples within the profiles were identified using a homogeneity test (Galbraith, 2003), and where present (e.g. UAE10/1) were inputted as independent sequences, each separated by boundaries ('overlapping sequences').

The agreement indices, A_i and A_{model}, are a comparison of the posterior distributions using the complete model and when no model is applied (i.e. the overlap between posterior and likelihood probability distributions) for individual ages and the whole model respectively, and 60% has been described as a reasonable minimum acceptable value (Ramsey 1995). Outlier analysis in OxCal v.4 weights samples according to how likely they are to be correct using a prior probability, and then calculates the ages alongside the other information available (Bronk Ramsey, 2009b). The model used for all the ages in this thesis uses a student's *t* distribution with 5 degrees of freedom, with the analysis determining the appropriate scale (from 10^0 to 10^4): Outlier_Model("General",T(5),U(0,4),"t"). In this model "t" describes the reason behind the offset, which in this case is that "the sample measured might not relate to the timing of the event being dated" (Bronk Ramsey, 2009b: 1023).

3.7. Presentation of OSL datasets

In this section, methods that can be used to display D_e distributions and dune OSL ages, some of which are used in this thesis, are briefly introduced.

3.7.1. Equivalent dose distributions

Radial plots are a particularly useful method of displaying D_e distributions because they incorporate a value of precision for each D_e value. Each aliquot/grain D_e value is plotted individually on a graph of precision/relative standard error against a standardised scale (usually shown as $\pm 2\sigma$, equivalent to 95% confidence interval) and log D_e scale (Galbraith and Roberts, 2012; Galbraith, 1990).

3.7.2. Dune OSL ages

Gaussian PDFs are often used to display both D_e and age data (e.g. Bateman et al., 2007; Telfer and Thomas, 2007). They are used to estimate the continuous PDF of a distribution for which the sample of ages are taken, and represent *n* ages as *n* Gaussian distributions (each component centred on the mean and associated standard error) normalised by the standard deviation, and summed pointwise (Galbraith, 2010). Without normalisation the peaks are dominated by precision, which is particularly problematic given that the standard error tends to increase with age: the shape of the PDF "is often largely determined by the error distribution… rather than by the distribution of 'true' values" (Galbraith and Roberts, 2012: 11). The peaks are frequency-based, and hence are strongly related to sampling frequency and strategy. The extent of smoothing depends upon the increment of summation (α) used, the choice of which is somewhat arbitrary. A value of α =0.6 has been suggested as a general rule, but Galbraith argues that this needs to be calculated from first principles as the choice of smoothing factor is important in determining the number of peaks (Brandon, 1996 in Galbraith, 1998). The smaller this value the less smoothed the curve and more data is visible, although it may appear more 'noisy'. The use of PDFs is criticised because they do not estimate the true distribution of ages, their peaks do not necessarily represent discrete components, good information is obscured by poor, and they are statistically untested (Galbraith, 1998).

A new method of dune age presentation is introduced in Chapter 6 based on net accumulation rates:

$$\text{Net accumulation rate, m ka}^{-1} = \frac{\text{Depth of accumulation, m}}{\text{Time interval of accumulation, ka}}$$

(Eq. 3.14)

There are numerous possible ways of calculating and constructing these graphs; the method chosen is based on the ‘as sampled’ depth and either the ‘as sampled’ or ‘minimum’ time interval (for full details see Chapter 6). The graphs have been constructed in Matlab®. The width of the bars corresponds to the time interval of accumulation (either ‘as sampled’ or ‘minimum’), centred on the weighted mean of the age group. The age groupings are samples at the same site/profile with ages within errors, tested using the homogeneity test advocated by Galbraith (2003), and are a function of sampling frequency and resolution, and dating precision.

SECTION 2: INVESTIGATIONS

4 The utility of desert sand dunes as Quaternary chronostratigraphic archives: Evidence from the northeastern Rub' al Khali

Paper One: Carly L. Leighton, Richard M. Bailey, David S.G. Thomas

Published in *Quaternary Science Reviews*
DOI: 10.1016/j.quascirev.2013.04.016

Abstract

The distributions of optically stimulated luminescence (OSL) ages from dunes are affected by palaeoenvironmental changes, complex dune dynamics and sampling strategy. Extracting the relative importance of these factors when interpreting discontinuous OSL chronologies from sand dunes has proven difficult, and is particularly hindered in contexts where the internal sedimentary structures of dunes are not visible. In this study samples for OSL dating were taken from three major dune exposures in the Rub' al Khali, United Arab Emirates, each showing clear internal structure, with the aim of addressing these problems. Specific objectives were to assess how ages of individual sedimentary units represent dune accumulation as a whole, and how the dune record in turn reflects known past environmental changes. Final ages were calculated using the OxCal software package, by incorporating the known relative stratigraphy through the application of Bayesian methods. The results show that stratigraphy alone is not sufficient at these sites to guide OSL sampling; that is, chrono- and lithostratigraphic boundaries do not necessarily coincide. Where chronological hiatuses are present, internal sediment stratigraphy can be a useful tool in identifying potential problems of under-sampling the full dune record. The implications of these findings for reconstructing Quaternary climates from dune chronologies are considered.

4.1. Introduction

Sand dune systems are important sources of palaeoenvironmental information, and are particularly useful in dryland regions where other archives may be lacking. In response to numerous developments in laboratory and field protocols (e.g. Wintle and Murray, 2006), optically stimulated luminescence (OSL) dating has been increasingly applied to these bedforms. Chronologies of dune activity and stabilisation have been collated and correlated to regional models of past climatic change, enabling the environmental response of local terrestrial systems to be further investigated (e.g. Chase and Thomas, 2007; Thomas and Shaw, 2002). However, whilst these advances have allowed for improved chronologies of palaeoenvironmental change in arid environments, current capacity to interpret ages, and the responses of geoproxies more widely, in terms of understanding past climates remains lacking (Thomas and Burrough, 2012).

Dune archives are complex records of depositional, erosional, accumulation and preservation processes, and this complexity may make them difficult to interpret as palaeoenvironmental records. Hiatuses represent a lack of net accumulation, due to a reduction in sediment deposition and/or an increase in the reworking or erosion of previously deposited units. The reworking of linear dune sediments is dependent upon the balance between the reversals of the crest line in variable wind regimes (Lancaster, 1985; Tsoar, 1983; Wiggs, 2001) and the extent of lateral migration (e.g. Bristow et al., 2000; Tsoar et al., 2004). As a result of the balance of these processes, internal dune structures are inherently discontinuous (e.g. Kocurek, 1998; Munyikwa, 2005). The interaction of many processes that influence dune development and preservation, by directly or indirectly affecting the balance between sediment supply, sediment availability and transport capacity of the wind (Kocurek and Lancaster, 1999), are difficult to distinguish within the sedimentary record. The observable stratigraphy, as the product of their interactions, is therefore not directly related to one specific variable of past climatic change by way of a straightforward process/response model (Kocurek, 1996). In addition, environmental context at a range of spatial scales is crucial in modulating dune response, which may go a long way in explaining the apparent ‘inconsistencies’ in the terrestrial palaeoenvironmental record, such as in southern Africa (Thomas and Burrough, 2012). Dune form is a product of local as well as regional environmental conditions, and different dune forms may not respond in the same way to similar forcing conditions (Chase and Thomas, 2006). Further, it is not necessarily to be expected that forcing conditions will be consistent at regional scales, given the significant spatial and temporal environmental variability observed in drylands, the tropics and subtropics (Thomas and Burrough, 2012; Thomas et al., 2005).

The question of scale is important when interpreting dune structures and chronologies. A numerical model suggests that the resolution of sampling may affect the capacity to distinguish the impact of major externally-forced events, such as regional climate transitions, from stochastic disturbances affecting sediment accumulation and preservation (Telfer et al., 2010). In practice, it has been demonstrated that sampling strategy and resolution can affect the chronology of dune accumulation produced from dated records (Stone and Thomas, 2008). This is particularly significant, given the discontinuous nature of dune sedimentary archives, both temporally and spatially.

Stratigraphic features, where present, can be used to aid environmental interpretation in order to support assessments of chronologies, especially regarding the presence of accumulation hiatuses and whether sampling resolution is sufficient to capture variability in the observable record. The incorporation of all available evidence when interpreting chronologies allows for recognition of a more complex system and a thorough assessment of the meaning of dates in terms of dune development (Fitzsimmons and Telfer, 2008). However, even the use of palaeosols, as stratigraphic features requiring surface stability for their formation, requires caution. The timescale of palaeosol formation may be uncertain as bioturbation may limit constraining the exact timing (Fitzsimmons et al., 2007), the palaeosol may only have formed at certain sites, or part or all of the units may have been subsequently reworked and removed (Fitzsimmons et al., 2007; Munyikwa, 2005). Therefore interpretation of the more obvious dune stratigraphic features is not straightforward, and where these features are not present there is even less information to guide interpretation. Where dune internal structure is not visible, which is more often than not, stratigraphy has also been used to infer dune processes and guide OSL dating with the aid of ground penetrating radar (GPR) (Bristow et al., 2000, 2005, 2007a). However, GPR is not suitable for use at all sites, due to subsurface electromagnetic properties, logistical difficulties, or a lack of internal dune structure.

The complexity of dune accumulation has led to the suggestion that many hundreds, if not thousands, of samples are required for dating if the major climatic events in the history of a dunefield are to be captured (Telfer et al., 2010). Such an approach is unlikely to be viable in practical terms. On the other hand, dune stratigraphy is seen as a vital guide to the interpretation of dune development, and has been exploited to 'target' OSL sampling of large sets of cross-stratification around inferred unit boundaries (Bristow et al., 2005). Intensive sampling and dating of a dune with exposed and clear stratigraphy may provide an opportunity to identify and explain the issues that hamper dune chronology development: representativeness and reproducibility. This paper will introduce OSL ages from three sites in the United Arab Emirates (UAE) where the stratigraphy is visible and has been used to guide sampling in the field. The relationship between chrono- and lithostratigraphy will be investigated, and the use of stratigraphy to guide sampling strategies, calculate ages using a Bayesian approach, and interpret resultant chronologies and chronological hiatuses will be assessed.

4.2. Material and methods

4.2.1. Sampling sites and strategy

The sites are located in the far northeast of the Rub' al Khali in the UAE. Large linear dunes, or 'megaridges', up to 70 m high and 1 km apart, are orientated southwest-northeast and superimposed by smaller secondary linear ridges that are up to 15 m high and orientated towards the southeast (Atkinson et al., 2011, 2012). The dunes are presently partially vegetated. Large sand quarries in the northern UAE have recently revealed the internal structure of dunes within this part of the dunefield (Atkinson et al., 2011). Three sites situated in this context, and part of the same linear megaridge dune system, were sampled for OSL dating (Figures 3.2 and 4.1).

The first two sites, UAE10/1 and UAE10/2, are both located in the same pit near Shwaib (24°47'38.85"N 55°47'24.70"E). The sites are only a few kilometres to the west of the Oman Mountains where alluvial gravels extend towards and underlie the dunes (Atkinson et al., 2011). The third site is within a large sand quarrying excavation pit located off the Emirates Highway (25°39'17.22"N 55°50'50.94"E) approximately 20 km southwest of the city of Ras al Khaimah. These sites have been previously sampled by Atkinson et al. (2011, 2012), and here they were revisited with the specific aim of using the stratigraphy to guide sampling (Figure 4.2).

Sampling was conducted at a high spatial resolution, bracketing identified structural features. Previous studies have classified aeolian bounding surfaces according to their hierarchical relationships and inferred origin (e.g. Brookfield, 1977; Kocurek, 1981). First-order bounding surfaces and super surfaces represent the migration of interdunes and a cessation of accumulation and preservation due to changing external conditions respectively (Kocurek, 1988). Most of the bounding surfaces across which sampling followed were

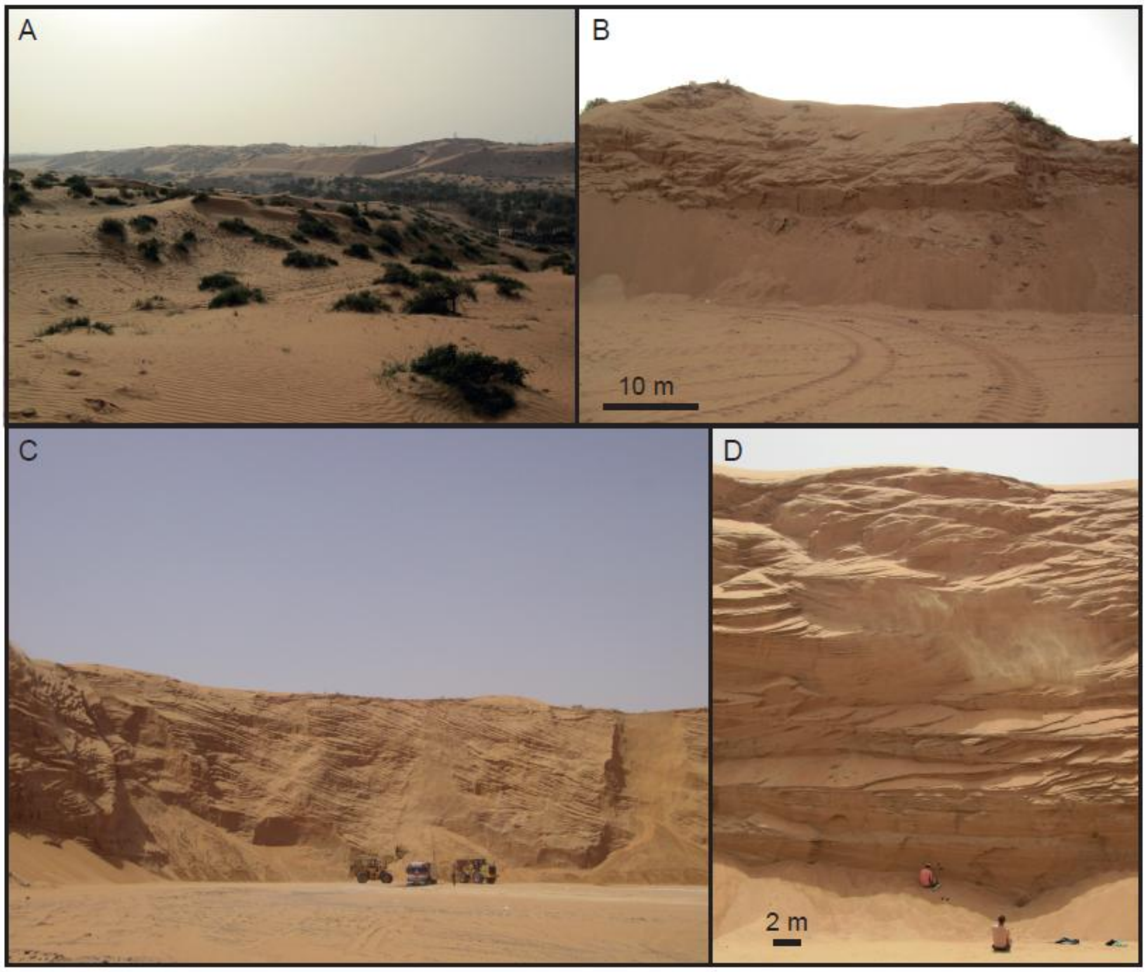

Figure 4.1: Photographs of the sampling sites. (a) Landscape at site UAE10/3 (Emirates Highway). The photo is taken from a secondary curving linear dune, with a megaridge visible in the background. (b) Sampled profile at UAE10/3 (Emirates Highway site). (c) View of the Shwaib pit (between the UAE10/1 and UAE10/2 sections), vehicles are shown for scale. The structure is dominated by unidirectional dipping towards the east. (d) Part of the sampled profile at UAE10/1 (Shwaib). The top of the section shows the presence of trough cross-stratification. Scales are approximate.

interpreted to be reactivation (third-order) surfaces representing the periodic erosion of the lee face, following Kocurek (1981). More extensive bounding surfaces sampled at one of the sites (UAE10/2) are interpreted as second-order surfaces, representing formation by the migration of superimposed dunes over the underlying bedform (Kocurek, 1981). However, without a three-dimensional view of the extent of these surfaces their significance as unconformities was unclear. Therefore allostratigraphical units, which are defined by their bounding unconformities, could not be strictly classified. Vertical and lateral sampling of

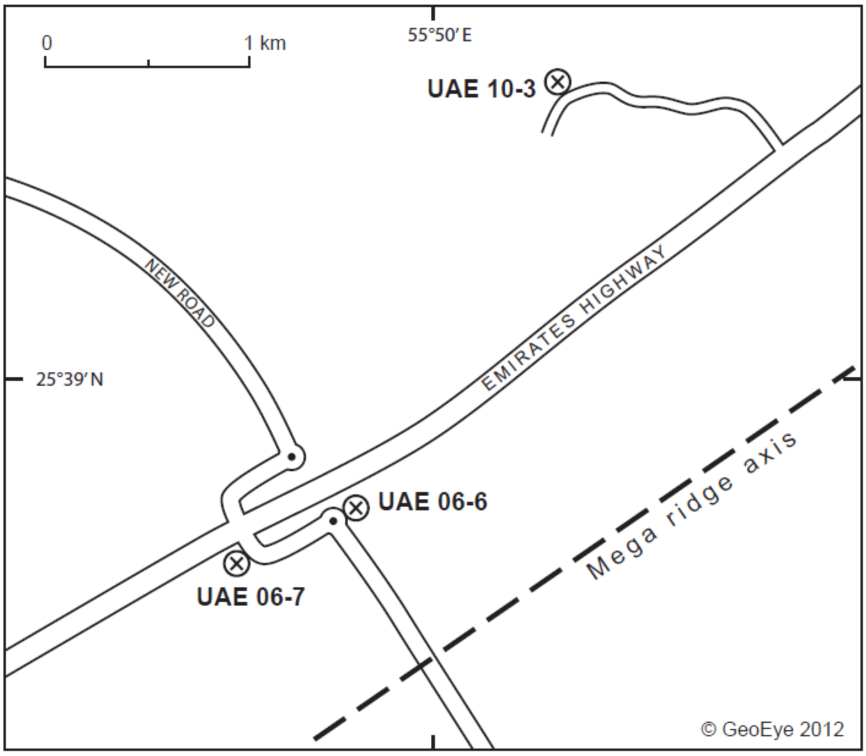

Figure 4.2: Geomorphological context of site UAE10/3, and location in comparison to sites from the Emirates Highway, UAE 06-6 and 07-7, presented in Atkinson et al. (2011).

the visible exposures, by sampling above and below bounding surfaces both with depth and horizontally, aimed to investigate the spatial variation in OSL chronologies. This method of sampling was employed in order to tie dates to dune development processes and to assess dating consistency.

4.2.2. Methods

Sample retrieval and preparation for OSL dating

Samples were extracted by scraping away the outer exposed section surface, and hammering in horizontally 12 cm sections of 50 mm diameter opaque plastic tubing. When full, the tube was extracted into a bag, and the inner end capped and sealed. All containers and bags were lightproof.

All samples were prepared and measured in the Oxford Luminescence Dating Laboratory (OLDLAB) under subdued orange light. The outer ~3 cm of sand within the sample tube (that closest to the exposure face) was removed in order to minimise the dating of grains bleached since the burial event. Following sample preparation (Section 3.5.1) the discs were mounted using Silkospray® and a 5 mm diameter mask. A large mask was used in order to maximise the OSL signal, given the low probability of partial bleaching and post-depositional mixing in this arid aeolian context where clear laminated structures have been preserved.

Sedimentology

Grain size analyses were conducted on raw samples using a Malvern Mastersizer 2000 laser particle analyser and analysed using Gradistat (Blott, 2000). Organic and carbonate contents were estimated using loss on ignition (LOI), following Heiri et al. (2001). Colour analysis was conducted on oven-dried samples using a Munsell colour chart.

D_e measurement

OSL measurement was conducted using standard Risø TL/OSL-DA-15 readers, following the single aliquot regenerative (SAR) protocol (Murray and Wintle, 2000). A preheat plateau test showed no temperature dependence in equivalent dose (D_e) (220-280 °C), and preheats of 260 °C for 10 s for natural/regenerated signals (L_x) and 220 °C for 10 s for test dose response (T_x) were subsequently adopted. Single aliquot OSL measurement was conducted using 470 nm stimulation at 160 °C, with a 280 °C OSL bleach incorporated after every test dose. Single grain measurement was conducted using 525 nm stimulation at 130 °C. Quality assurance ratios of zero-dose, recycling and IR depletion were incorporated into the protocol, and only aliquots fulfilling these criteria within ±10% of unity were included for age calculation (the majority lay within ±5%). Dose recovery results were

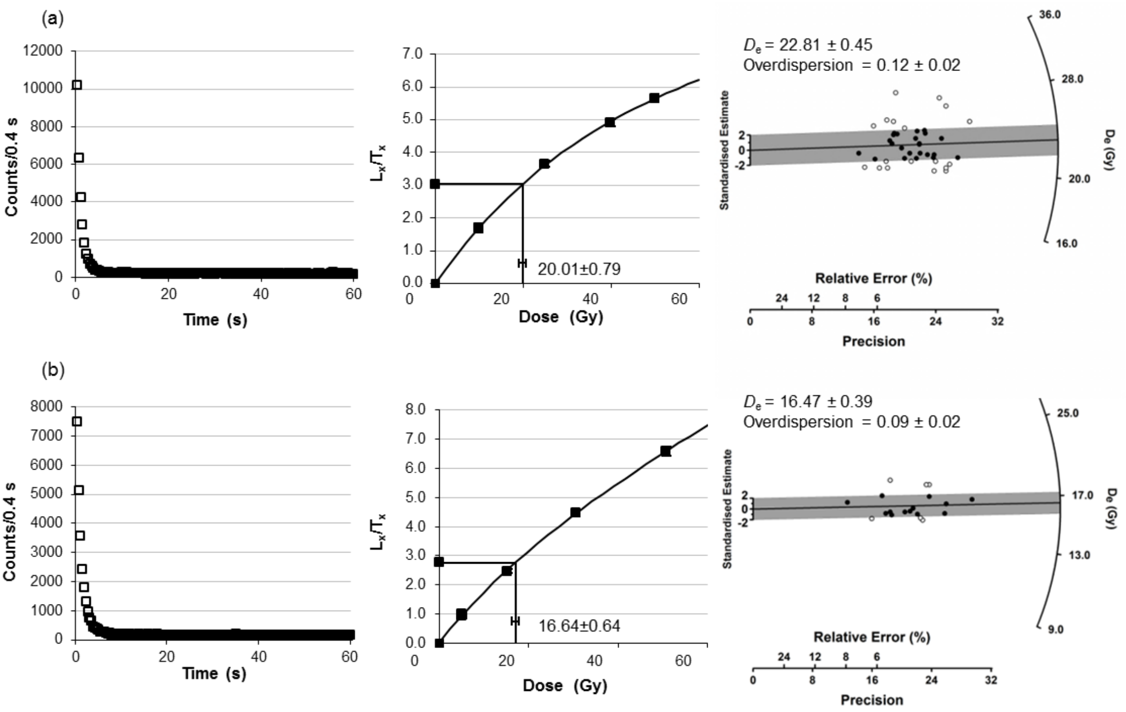

Figure 4.3: Typical OSL characteristics of the samples. From left to right: OSL decay curve; dose response curve; radial plots of D_e distributions. (a) Sample UAE10/1/20. (b) Sample UAE10/3/8.

within ±10% of the given dose for all samples, with the majority within ±5%. Typical aliquot characteristics are shown in Figure 4.3.

Dose rate calculation

Dose rates were determined by ICP-MS and ICP-AES, conducted at Department of Geology, Royal Holloway, University of London, and SUERC at East Kilbride. Gamma spectrometry was undertaken in the field at sites UAE10/1 and UAE10/2 for four samples; the results indicate relatively homogeneous gamma dose rates in agreement (within 15%) with dose rates based on the ICP-MS/AES measurements. The ICP-MS/AES gamma dose rates are used in subsequent age calculations, with moisture content estimated at 5±3% for all samples, to allow for temporal fluctuations in moisture.

The initial dose rate data for samples UAE10/1/19 and 1/20 are shown in the first row of Table 4.1. These samples are from the same sedimentary set, share homogeneous sedimentological characteristics (Table 4.2 and Figure 4.4), and have indistinguishable D_e values within errors (Table 4.3), provoking questions regarding the precision that can be confidently attached to dose rates derived from ICP-MS/AES measurements. Based on the initial ICP-MS/AES measurements, the total dose rate of 1/19 was calculated to be approximately three-quarters of the dose rate of 1/20 (accounted for mostly by the difference in beta dose rates due to the lower potassium concentration reported for sample 1/19). Subsequently, repeated ICP-MS/AES measurements of sample 1/19 were conducted, and these are reported in Table 4.1, alongside the limited repeat measurements of four other samples. Whilst the least repeatable measurements of radioisotope concentration are for thorium, repeated measurements of potassium, for which the dose rates are most sensitive, show large variability for sample 1/19. The source of this variability is unknown but the implication is that additional uncertainty, beyond the quoted analytical uncertainty, is required in order to more accurately estimate the precision on dose rates derived using these analytical methods. Hence, based on the relative standard deviations of repeated ICP-MS/AES measurements for sample 1/19, relatively large uncertainties of 13%, 9% and 13% were attached to potassium, uranium and thorium radioisotope concentrations respectively, and were used to calculate dose rates. For thorium concentrations these uncertainties may be low, but given the limited data the relative standard deviation of the sample with the most repeat measurements is thought to be the most appropriate estimate. Whilst outliers can in some instances be identified (e.g. one thorium measurement of UAE10/3/13), given the limited number of ICP-MS/AES measurements (and even fewer in usual dating circumstances) the means of the repeated measurements for each radioisotope concentration were used to calculate the dose rate for these samples (Table 4.1). Further investigation of these issues is beyond the scope of this paper, though further study is required given the significance of these findings for the calculation of dose rates in OSL dating, which commonly are given limited attention in many studies.

Table 4.1: Repeated ICP-MS/AES measurements of potassium, thorium and uranium radioisotope concentrations. Indicated in bold are the values used for dose rate calculation, usually the mean of the measurement values other than for the Th concentration of sample UAE10/3/13. In this case, the measurement in italics is interpreted as an outlier and hence the other measurement (in bold) is used for dose rate calculation rather than the mean.

	K (%)	Mean	Standard deviation	Relative st dev	**Th (ppm)**	Mean	Standard deviation	Relative st dev	**U (ppm)**	Mean	Standard deviation	Relative st dev
UAE 10/1/19	0.689	**0.953**	0.125	0.131	1.210	**1.557**	0.209	0.134	0.839	**0.947**	0.081	0.085
	1.025				1.525				0.919			
	1.042				1.911				1.107			
	0.987				1.566				0.951			
	1.018				1.483				0.934			
	0.903				1.659				0.923			
	1.010				1.545				0.956			
UAE 10/1/8	1.016	**1.005**	0.015	0.015	0.507	**1.048**	0.765	0.730	1.245	**1.137**	0.153	0.134
	0.994				1.589				1.029			
UAE 10/2/6	0.907	**0.910**	0.004	0.004	1.809	**1.501**	0.436	0.290	1.096	**0.965**	0.185	0.191
	0.912				1.193				0.835			
UAE 10/3/1	0.922	**0.915**	0.009	0.010	0.996	**1.012**	0.022	0.022	1.249	**1.265**	0.022	0.017
	0.909				1.028				1.280			
UAE 10/3/13	0.735	**0.727**	0.011	0.015	**1.393**	2.293	1.273	0.555	1.040	**1.116**	0.107	0.096
	0.719				*3.193*				1.192			

Table 4.2: Sedimentology data. Munsell colour, particle size statistics (percentages of particle size according to classifications of Blott (2000): coarse sand >500 µm; medium sand 250-500 µm; fine sand 125-250 µm; very fine sand 63-125 µm; silt <63 µm) and carbonate content based on loss of ignition (LOI). [a]RY = reddish yellow, SB = strong brown. [b]Percentage LOI at 550 °C is proportional to organic content. [c]LOI at 950 °C and multiplied by 1.36 is proportional to carbonate content (g), which is expressed as percentage of original dry sample weight.

Sample	Munsell Colour[a]	Mean particle size (µm)	Sorting (s.d.)	Skewness	Kurtosis	Coarse sand (%)	Med sand (%)	Fine sand (%)	V. fine sand (%)	Silt (%)	LOI at 550 °C (%)[b]	Carbonate content (%)[c]
UAE10/1/1	7.5YR 6/8 RY	206	1.46	-0.01	0.95	0.00	0.31	0.59	0.10	0.00	0.75	14.62
UAE10/1/2	7.5YR 6/8 RY	192	1.43	-0.01	0.95	0.00	0.24	0.65	0.12	0.00	0.91	16.49
UAE10/1/5	7.5YR 6/8 RY	222	1.42	-0.01	0.96	0.00	0.37	0.58	0.05	0.00	0.72	14.77
UAE10/1/8	7.5YR 6/8 RY	203	1.51	-0.02	0.95	0.01	0.31	0.56	0.13	0.00	0.76	14.50
UAE10/1/10	7.5YR 6/8 RY	175	1.50	-0.02	0.95	0.00	0.19	0.60	0.21	0.00	0.95	16.04
UAE10/1/11	7.5YR 6/8 RY	179	1.58	-0.02	0.94	0.00	0.24	0.53	0.22	0.01	0.91	15.97
UAE10/1/17	7.5YR 6/8 RY	154	1.52	-0.02	0.95	0.00	0.12	0.56	0.30	0.01	1.10	17.35
UAE10/1/18	7.5YR 6/8 RY	258	1.66	-0.06	0.95	0.09	0.45	0.38	0.08	0.00	0.95	16.49
UAE10/1/19	7.5YR 6/8 RY	196	1.63	0.00	0.94	0.02	0.30	0.50	0.18	0.00	0.72	16.62
UAE10/1/20	7.5YR 6/8 RY	194	1.63	0.01	0.95	0.02	0.29	0.50	0.19	0.00	0.91	15.68
UAE10/2/1	7.5YR 6/8 RY	163	1.52	0.00	0.94	0.00	0.16	0.57	0.27	0.01	1.07	17.54
UAE10/2/2	7.5YR 6/8 RY	176	1.53	-0.02	0.95	0.00	0.21	0.57	0.21	0.00	1.04	17.97
UAE10/2/3	7.5YR 6/8 RY	175	1.63	-0.02	0.94	0.01	0.23	0.50	0.24	0.01	1.03	17.63
UAE10/2/4	7.5YR 6/8 RY	170	1.52	-0.01	0.95	0.00	0.18	0.58	0.24	0.00	1.00	17.26
UAE10/2/6	7.5YR 6/8 RY	170	1.52	0.00	0.95	0.00	0.18	0.58	0.24	0.00	1.02	17.12
UAE10/2/8	7.5YR 6/8 RY	177	1.55	-0.02	0.95	0.00	0.22	0.56	0.21	0.00	0.99	18.37
UAE10/2/12	7.5YR 6/8 RY	191	1.47	-0.02	0.95	0.00	0.25	0.61	0.14	0.00	1.00	17.61
UAE10/2/15	7.5YR 6/8 RY	162	1.50	0.00	0.95	0.00	0.15	0.58	0.27	0.00	1.29	17.57
UAE10/2/19	7.5YR 6/8 RY	182	1.51	-0.01	0.95	0.00	0.22	0.59	0.19	0.00	3.29	16.11

UAE10/3/1	7.5YR 5/8 SB	209	1.50	-0.02	0.95	0.01	0.33	0.56	0.11	0.00	1.25	14.05
UAE10/3/2	7.5YR 5/8 SB	191	1.50	0.00	0.95	0.00	0.26	0.58	0.16	0.00	1.25	19.58
UAE10/3/5	7.5YR 5/8 SB	191	1.52	0.00	0.95	0.00	0.26	0.57	0.16	0.00	1.29	18.90
UAE10/3/8	7.5YR 5/8 SB	176	1.42	-0.01	0.96	0.00	0.16	0.67	0.17	0.00	1.39	20.47
UAE10/3/11	7.5YR 5/8 SB	176	1.48	0.00	0.95	0.00	0.19	0.61	0.20	0.00	1.33	18.18
UAE10/3/14	7.5YR 5/8 SB	184	1.44	0.01	0.95	0.00	0.21	0.65	0.15	0.00	1.32	16.38
UAE10/3/15	7.5YR 5/8 SB	189	1.51	0.00	0.95	0.00	0.25	0.58	0.16	0.00	1.19	20.20
UAE10/3/16	7.5YR 5/8 SB	206	1.45	0.00	0.95	0.00	0.30	0.61	0.09	0.00	1.15	17.18
UAE10/3/17	7.5YR 5/8 SB	202	1.48	-0.01	0.95	0.00	0.30	0.58	0.12	0.00	1.17	17.02
UAE10/3/18	7.5YR 5/8 SB	210	1.60	0.00	0.94	0.03	0.33	0.50	0.14	0.00	1.33	15.81
UAE10/3/19	7.5YR 5/8 SB	228	1.63	-0.04	0.95	0.04	0.39	0.45	0.12	0.00	1.36	18.77

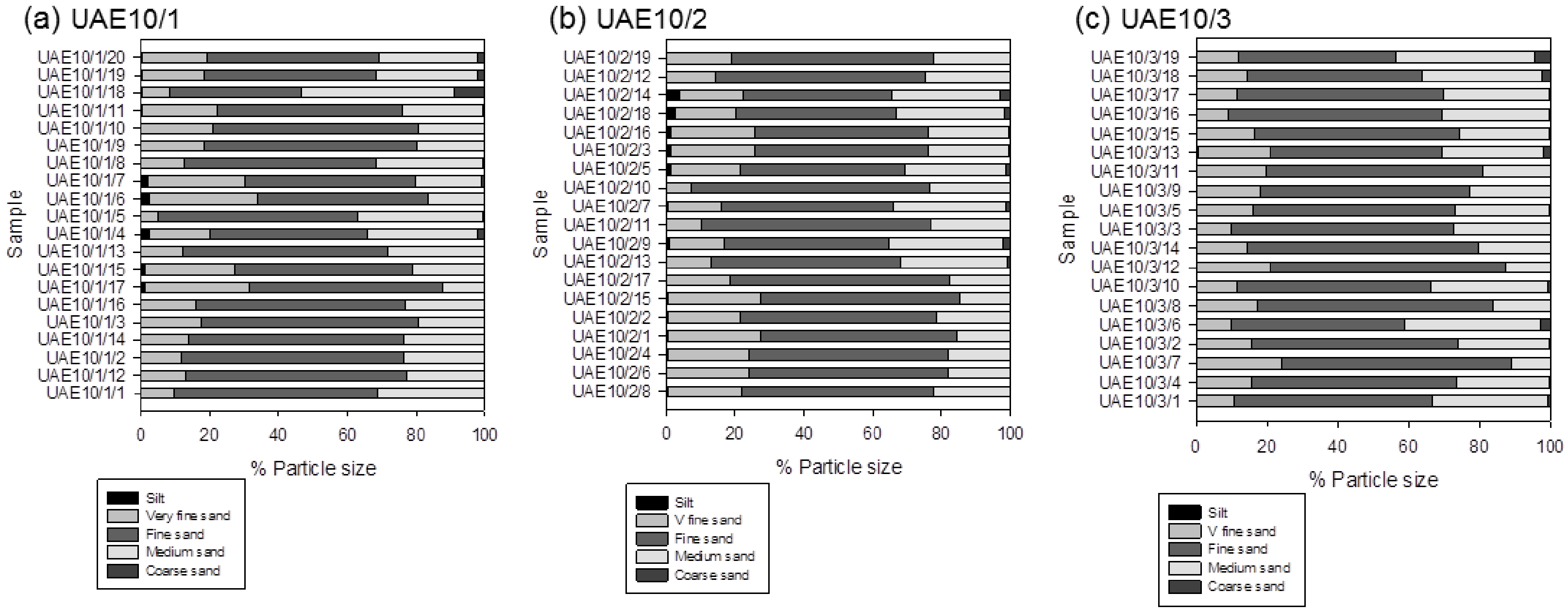

Figure 4.4: Particle size distributions for the three sample sites, shown in relative stratigraphic order (youngest samples at the top). Particle size classifications are those of Blott (2000), described in the caption of Table 4.2. Class percentage compositions are presented in Table 4.2.

Table 4.3: ICP and OSL data: n shows number of aliquots, OD shows overdispersion. Moisture content of 5±3% is used for all samples. Unmodelled ages calculated in OxCal v.4.1.

Sample	**n**	***D_e* (Gy)**	**R-ratio**	**Zero-ratio**	**IR-ratio**	**OD**	**Grainsize (µm)**	**K (%)**	**Th (ppm)**	**U (ppm)**	**Effective cosmic dose (Gy/ka)**	**Dose rate (Gy/ka)**	**Age (ka)**
UAE10/1/1	29	34.79 ± 0.97	0.986 ± 0.006	0.000 ± 0.000	0.968 ± 0.006	0.14 ± 0.02	90 - 150	1.019 ± 0.132	0.676 ± 0.088	1.232 ± 0.111	0.005 ± 0.000	1.28 ± 0.14	27.46 ± 2.75
UAE10/1/2	16	27.02 ± 1.07	0.977 ± 0.009	0.001 ± 0.000	0.950 ± 0.010	0.15 ± 0.03	150 - 220	0.866 ± 0.113	1.164 ± 0.151	0.805 ± 0.072	0.005 ± 0.000	1.05 ± 0.11	26.09 ± 2.76
UAE10/1/5	15	33.33 ± 1.45	0.984 ± 0.014	-0.001 ± 0.001	0.968 ± 0.012	0.15 ± 0.03	150 - 220	0.903 ± 0.117	0.888 ± 0.115	0.707 ± 0.064	0.005 ± 0.000	1.05 ± 0.12	32.35 ± 3.57
UAE10/1/8	24	34.28 ± 1.25	0.986 ± 0.006	0.000 ± 0.000	0.980 ± 0.006	0.17 ± 0.03	90 - 150	1.005 ± 1.131	1.048 ± 0.136	1.137 ± 0.102	0.005 ± 0.000	1.27 ± 0.13	27.39 ± 2.81
UAE10/1/10	15	31.42 ± 1.04	0.972 ± 0.014	-0.001 ± 0.001	0.968 ± 0.012	0.11 ± 0.03	150 - 220	0.770 ± 0.100	1.320 ± 0.172	0.874 ± 0.079	0.005 ± 0.000	0.99 ± 0.10	32.12 ± 3.17
UAE10/1/11	27	31.73 ± 1.08	0.983 ± 0.008	0.000 ± 0.000	0.974 ± 0.009	0.17 ± 0.02	150 - 220	0.932 ± 0.121	1.311 ± 0.170	0.934 ± 0.084	0.005 ± 0.000	1.15 ± 0.12	27.95 ± 2.87
UAE10/1/17	8	33.29 ± 2.41	0.998 ± 0.015	0.000 ± 0.000	0.964 ± 0.012	0.20 ± 0.05	150 - 220	0.899 ± 0.117	0.910 ± 0.118	0.756 ± 0.068	0.005 ± 0.000	1.06 ± 0.12	32.16 ± 4.01
UAE10/1/18	26	18.04 ± 0.39	0.977 ± 0.008	0.000 ± 0.000	0.978 ± 0.006	0.10 ± 0.02	150 - 220	0.761 ± 0.099	1.757 ± 0.228	1.037 ± 0.093	0.005 ± 0.000	1.05 ± 0.10	17.36 ± 1.58
UAE10/1/19	30	23.28 ± 0.63	1.000 ± 0.007	0.001 ± 0.000	0.988 ± 0.006	0.14 ± 0.02	150 - 220	0.953 ± 0.124	1.557 ± 0.202	0.947 ± 0.085	0.005 ± 0.000	1.19 ± 0.13	19.75 ± 1.97
UAE10/1/20	41	22.81 ± 0.45	0.976 ± 0.007	0.001 ± 0.000	0.961 ± 0.006	0.12 ± 0.02	90 - 150	0.910 ± 0.118	1.351 ± 0.176	0.991 ± 0.089	0.005 ± 0.000	1.17 ± 0.12	19.77 ± 1.92
UAE10/2/1	12	16.76 ± 0.72	0.991 ± 0.016	0.000 ± 0.001	0.968 ± 0.015	0.14 ± 0.03	150 - 220	0.922 ± 0.120	1.072 ± 0.139	0.753 ± 0.068	0.040 ± 0.006	1.12 ± 0.12	15.16 ± 1.61
UAE10/2/2	13	16.53 ± 0.63	0.997 ± 0.008	0.000 ± 0.000	0.976 ± 0.006	0.13 ± 0.03	150 - 220	0.909 ± 0.118	1.338 ± 0.174	0.958 ± 0.086	0.040 ± 0.006	1.17 ± 0.12	14.24 ± 1.43
UAE10/2/3	10	16.56 ± 0.77	1.023 ± 0.010	0.000 ± 0.001	0.996 ± 0.011	0.14 ± 0.03	90 - 150	0.850 ± 0.111	1.656 ± 0.215	1.136 ± 0.102	0.040 ± 0.006	1.20 ± 0.12	13.84 ± 1.38
UAE10/2/4	14	15.78 ± 0.51	0.961 ± 0.012	0.001 ± 0.000	0.951 ± 0.011	0.11 ± 0.02	150 - 220	0.700 ± 0.091	1.120 ± 0.146	0.884 ± 0.080	0.040 ± 0.006	0.95 ± 0.09	16.76 ± 1.58
UAE10/2/6	9	16.40 ± 0.51	0.994 ± 0.015	0.001 ± 0.001	0.961 ± 0.015	0.08 ± 0.03	150 - 220	0.910 ± 0.118	1.501 ± 0.195	0.965 ± 0.087	0.040 ± 0.006	1.19 ± 0.12	13.98 ± 1.36
UAE10/2/8	13	17.31 ± 1.09	1.002 ± 0.009	0.000 ± 0.000	0.979 ± 0.011	0.22 ± 0.05	90 - 150	0.755 ± 0.098	1.237 ± 0.161	1.117 ± 0.101	0.040 ± 0.006	1.08 ± 0.10	16.09 ± 1.74

UAE10/2/12	11	16.29 ± 1.16	1.010 ± 0.011	0.000 ± 0.000	1.004 ± 0.010	0.23 ± 0.05	90 - 150	0.876 ± 0.114	1.151 ± 0.150	1.174 ± 0.106	0.040 ± 0.006	1.20 ± 0.12	13.65 ± 1.57
UAE10/2/15	11	16.32 ± 0.46	0.991 ± 0.012	0.001 ± 0.001	0.993 ± 0.013	0.08 ± 0.02	90 - 150	0.907 ± 0.118	1.170 ± 0.152	1.203 ± 0.108	0.040 ± 0.006	1.24 ± 0.12	13.31 ± 1.26
UAE10/2/19	17	15.87 ± 0.62	0.997 ± 0.011	0.000 ± 0.001	0.999 ± 0.011	0.15 ± 0.03	150 - 220	0.724 ± 0.094	1.260 ± 0.164	0.861 ± 0.077	0.197 ± 0.100	1.13 ± 0.14	14.20 ± 1.81
UAE10/3/1	11	16.04 ± 0.65	0.991 ± 0.010	0.002 ± 0.000	0.974 ± 0.012	0.13 ± 0.03	90 - 150	0.915 ± 0.119	1.012 ± 0.132	1.265 ± 0.114	0.061 ± 0.013	1.27 ± 0.12	12.75 ± 1.26
UAE10/3/2	19	16.15 ± 0.60	1.017 ± 0.011	-0.001 ± 0.001	1.024 ± 0.012	0.13 ± 0.03	150 - 220	0.649 ± 0.084	1.380 ± 0.179	0.944 ± 0.123	0.061 ± 0.013	0.95 ± 0.09	17.03 ± 1.56
UAE10/3/5	16	15.00 ± 0.61	0.981 ± 0.011	0.001 ± 0.000	0.977 ± 0.010	0.16 ± 0.03	150 - 220	0.688 ± 0.089	1.260 ± 0.164	0.920 ± 0.083	0.061 ± 0.013	0.98 ± 0.09	15.45 ± 1.48
UAE10/3/8	20	16.47 ± 0.34	0.999 ± 0.009	0.000 ± 0.000	0.982 ± 0.009	0.09 ± 0.02	90 - 150	0.783 ± 0.102	1.289 ± 0.168	1.342 ± 0.121	0.061 ± 0.013	1.18 ± 0.11	13.99 ± 1.24
UAE10/3/11	13	15.26 ± 0.74	0.974 ± 0.014	0.000 ± 0.001	0.953 ± 0.011	0.16 ± 0.04	150 - 220	0.665 ± 0.086	1.292 ± 0.168	1.265 ± 0.114	0.061 ± 0.013	1.05 ± 0.09	14.54 ± 1.38
UAE10/3/14	11	15.79 ± 0.38	0.964 ± 0.013	0.000 ± 0.000	0.962 ± 0.012	0.06 ± 0.02	150 - 220	0.861 ± 0.112	1.068 ± 0.139	1.004 ± 0.090	0.061 ± 0.013	1.14 ± 0.11	13.96 ± 1.31
UAE10/3/15	9	14.09 ± 0.50	0.999 ± 0.015	0.000 ± 0.000	0.971 ± 0.012	0.10 ± 0.03	150 - 220	0.625 ± 0.081	1.320 ± 0.172	0.950 ± 0.086	0.061 ± 0.013	0.93 ± 0.09	15.20 ± 1.38
UAE10/3/16	22	15.32 ± 0.52	1.006 ± 0.015	0.001 ± 0.001	0.983 ± 0.013	0.14 ± 0.03	150 - 220	0.855 ± 0.111	1.076 ± 0.140	0.826 ± 0.074	0.104 ± 0.022	1.14 ± 0.11	13.60 ± 1.33
UAE10/3/17	28	14.51 ± 0.51	0.985 ± 0.012	0.000 ± 0.000	0.980 ± 0.011	0.17 ± 0.03	150 - 220	0.828 ± 0.108	2.751 ± 0.358	0.999 ± 0.090	0.125 ± 0.037	1.28 ± 0.12	11.34 ± 1.04
UAE10/3/18	13	5.07 ± 0.28	1.029 ± 0.011	0.002 ± 0.001	1.012 ± 0.009	0.19 ± 0.04	150 - 220	0.717 ± 0.093	1.200 ± 0.156	0.797 ± 0.072	0.152 ± 0.077	1.06 ± 0.12	4.80 ± 0.60
UAE10/3/19	18	0.34 ± 0.09	1.008 ± 0.036	-0.093 ± 0.051	0.955 ± 0.043	0.86 ± 0.25	90 - 150	0.905 ± 0.118	1.097 ± 0.143	1.329 ± 0.120	0.192 ± 0.129	1.41 ± 0.18	0.18 ± 0.08

Age calculation

Bayesian statistics have been applied to OSL ages in previous studies, and have been particularly useful in the comparison of OSL and radiocarbon ages from the same context (e.g. Feathers et al., 2006; Rhodes et al., 2003). The ages presented in this paper were calculated in OxCal v. 4.1 (Bronk Ramsey, 2009a). The analysis in OxCal explicitly includes the relatively large uncertainty on the dose distributions (as described above), and the shared uncertainties are considered in the age calculation by inputting the D_e and dose rate components as parameters (Bronk Ramsey, 2009a). The ages are then calculated using these parameters within the model. Known stratigraphical information is incorporated by calculating the ages within a 'sequence' model, in which the samples are input from oldest to youngest, resulting in improved overall precision in the final ages. Relative stratigraphical information is incorporated into calculation of the final age distributions, and therefore this must be acknowledged when the results of Bayesian analysis are discussed in order to avoid circularity. A general outlier model, based on a student's *t* test distribution with 5 degrees of freedom, was used for each sample (Bronk Ramsey, 2009b). All unmodelled and modelled ages presented in Table 4.4 are defined as age from measurement, using the unit ka. All modelled age ranges and uncertainties are quoted at 68.2% of the probable distribution, unless stated otherwise. The agreement indices $A_{i(/comb)}$ and A_{model} describe the agreement between the posterior distributions with and without use of the Bayesian model for individual ages and the whole sequence respectively, and a value of 60% has been described as a reasonable minimum acceptance threshold (Bronk Ramsey, 1995).

The unmodelled age parameters and stratigraphical information are inputted using sequential groups, within which the deposition process is random and unknown (Bronk Ramsey, 2008). Two sequential groups comprising the samples from 1/1 to 1/11 and from 1/18 to 1/20 were inputted for the site UAE10/1, which are thought to represent separate

Table 4.4: OSL ages modelled in OxCal. The 68.2% range is given for upper and lower modelled age limits. The agreement indices, A_i and A_{model}, compare the posterior distributions when the complete model and no model is applied for the individual ages and the whole model respectively, and 60% has been described as a reasonable minimum acceptable value (Bronk Ramsey, 1995).

Sample	***D*$_e$**	**1σ**	**Unmodelled**		**Modelled**					
			Age (ka)	**1σ**	**Mean age (ka)**	**1σ**	**Upper limit (ka)**	**Lower limit (ka)**	**$A_{i/comb}$**	**A_{model}**
UAE10/1/1	34.79	0.97	27.46	2.75	29.64	1.48	30.89	28.01	99.6	**93**
UAE10/1/2	27.02	1.07	26.09	2.76	29.30	1.33	30.64	27.78	76.9	
UAE10/1/5	33.33	1.45	32.35	3.57	28.74	1.23	30.00	27.41	89.5	
UAE10/1/8	34.28	1.25	27.39	2.81	28.42	1.23	29.69	27.10	121.1	
UAE10/1/10	31.42	1.04	32.12	3.17	28.12	1.29	29.41	26.79	72.9	
UAE10/1/11	31.73	1.08	27.95	2.87	27.74	1.45	29.28	26.39	124.4	
UAE10/1/17	33.29	2.41	32.16	4.01	29.03	1.27	30.30	27.59	107.6	
UAE10/1/18	18.04	0.39	17.36	1.58	19.03	1.20	20.09	17.72	84.8	
UAE10/1/19	23.28	0.63	19.75	1.97	18.38	1.13	19.48	17.14	121.3	
UAE10/1/20	22.81	0.45	19.77	1.92						
UAE10/2/1	16.76	0.72	15.16	1.61	14.63	0.59	15.24	13.97	124.1	**117.2**
UAE10/2/2	16.53	0.63	14.24	1.43	14.37	0.56	14.95	13.77	129.1	
UAE10/2/3	16.56	0.77	13.84	1.38	13.88	0.63	14.56	13.27	126.4	
UAE10/2/4	15.78	0.51	16.76	1.58	14.89	0.65	15.53	14.12	77.5	
UAE10/2/6	16.40	0.51	13.98	1.36	15.10	0.72	15.75	14.31	98	
UAE10/2/8	17.31	1.09	16.09	1.74	15.39	0.88	16.14	14.35	119.1	
UAE10/2/12	16.29	1.16	13.65	1.57	13.65	0.71	14.47	12.90	127.1	
UAE10/2/15	16.32	0.46	13.31	1.26	14.11	0.57	14.70	13.55	108.7	
UAE10/2/19	15.87	0.62	14.20	1.81	13.40	0.82	14.36	12.62	125.3	
UAE10/3/1	16.04	0.65	12.75	1.26	14.91	0.78	15.52	14.05	48.4	**80.6**
UAE10/3/2	16.15	0.60	17.03	1.56	14.71	0.69	15.30	13.91	58.4	
UAE10/3/5	15.00	0.61	15.45	1.48	14.05	0.52	14.55	13.49	94.3	
UAE10/3/8	16.47	0.39	13.99	1.24	14.47	0.59	15.00	13.81	118.6	
UAE10/3/11	15.26	0.74	14.54	1.38	13.83	0.52	14.32	13.28	119.5	
UAE10/3/14	15.79	0.38	13.96	1.31	14.26	0.54	14.78	13.64	126	
UAE10/3/15	14.09	0.50	15.20	1.38	13.58	0.56	14.14	13.02	79.3	
UAE10/3/16	15.32	0.52	13.60	1.33	13.24	0.67	13.97	12.61	121.3	
UAE10/3/17	14.51	0.51	11.34	1.04	12.84	0.88	13.83	12.09	61.5	

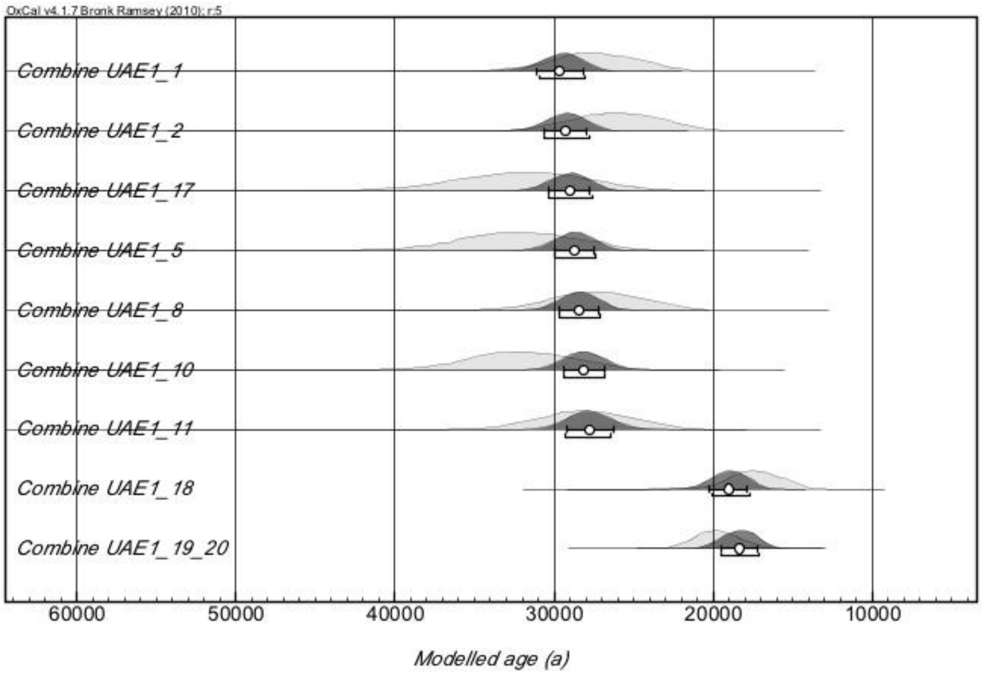

Figure 4.5: OxCal output for site UAE10/1. Prior age distribution is shown in light grey, and the posterior age distribution is shown in dark grey. The mean age and 68.2% probability age range are indicated. The oldest sample is at the top of the figure.

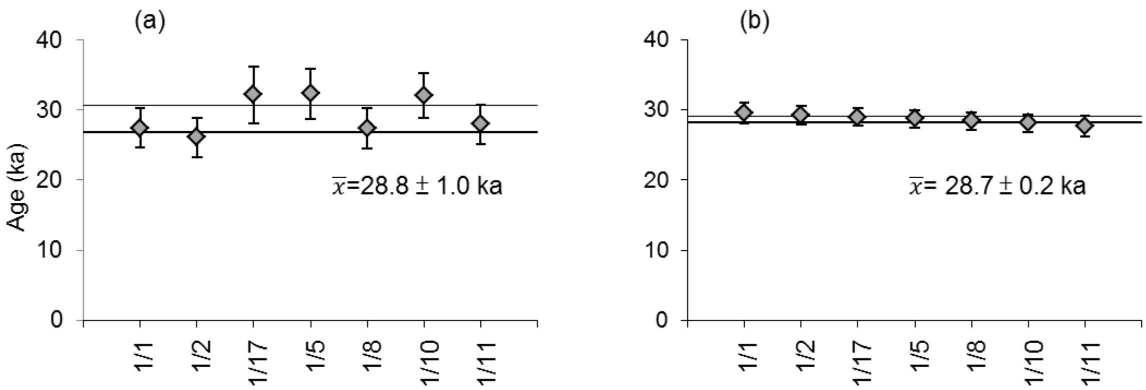

Figure 4.6: Age distribution of UAE10/1 samples and absolute weighted mean values. Upper and lower limits mark the value of the weighted standard error above and below the weighted mean respectively. Left-to-right along the x-axis indicates oldest-to-youngest samples based upon the relative chronology. (a) Unmodelled ages. (b) Ages modelled in OxCal (Bronk Ramsey, 2009a). Errors displayed and used for absolute weighted mean calculation are based on 1σ symmetrical errors.

periods of accumulation and preservation. This assumption was supported by the application of an homogeneity test at 95% confidence interval (Galbraith, 2003). It is assumed that samples 1/19 and 1/20 are of identical age due to their positioning in the same sedimentary unit; therefore they were 'combined' in the model. The mean ages for samples 1/1 to 1/11 of the prior and posterior are within errors, whilst the precision of the ages has been significantly increased (Figures 4.5 and 4.6). The model produces a combined age of 18.4±1.1 ka for samples 1/19 and 1/20 with an A_{comb} of 121.3% (despite different D_e and dose rate data being inputted into the model), which is in agreement with the relative chronology observed (Table 4.4).

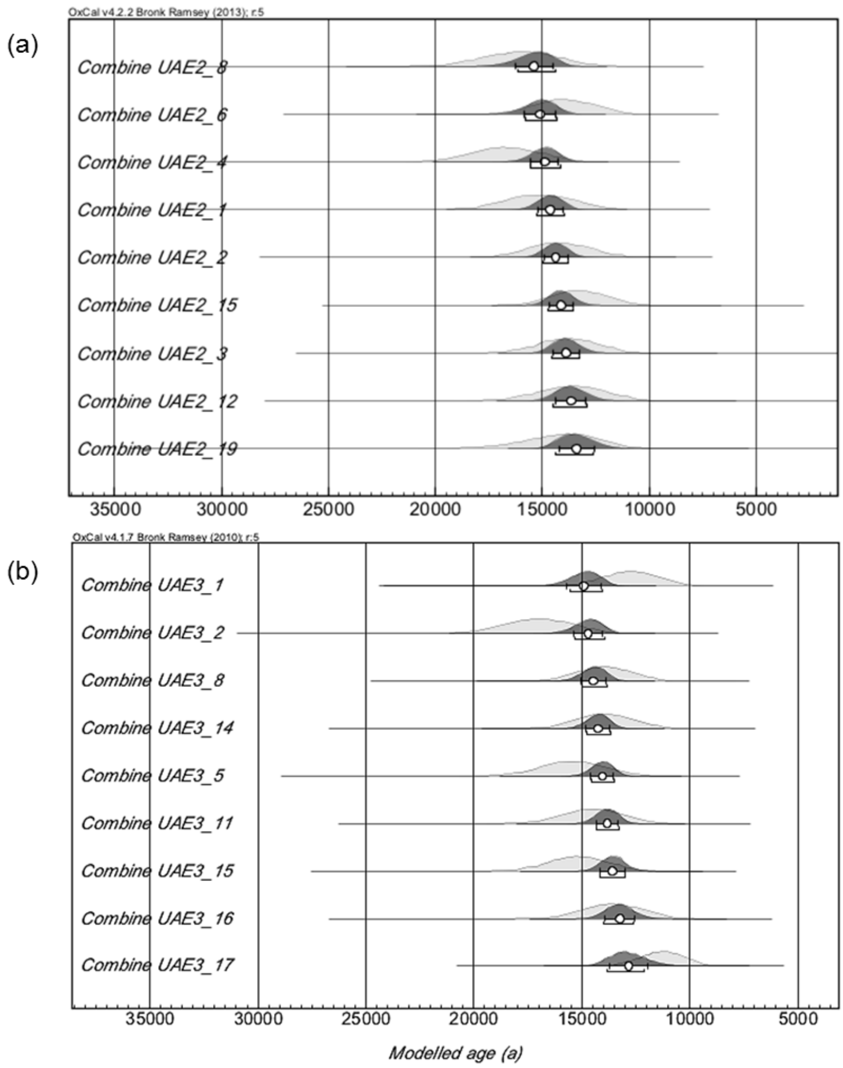

Figure 4.7: OxCal posterior age distributions (dark grey) for (a) UAE 10/2 and (b) UAE 10/3. The prior age distributions are shown in light grey. The mean age and 68.2% probability age range are indicated. The oldest samples are at the top of the figures.

The ages were inputted into OxCal as one sequence for UAE10/2 and UAE10/3. The group UAE10/3/18-19 were considerably younger and were not included in the OxCal analysis as they would not have a significant impact on the posterior distribution. Posterior age distributions for sites UAE10/2 and UAE10/3 are shown in Figure 4.7.

4.3. Results

The apparent dip direction revealed in dune exposures is towards the northeast at all three sites, parallel to the linear megaridge trend, indicating elongation of the dune in this direction. The secondary dunes may have contributed to the development of the megaridges through scouring of the underlying dune surface and deposition on their lee slopes (Rubin and Hunter, 1983), producing the compound cross-stratification that is seen at all three sites. Bidirectional dipping is prevalent, formed due to a complex relationship between primary wind directions, primary and superimposed migrating bedforms, and resultant climatic/morphological interactions.

At a smaller scale, subcritically climbing translatent stratification, rippleform lamination, and grainfall lamination are present in the cross-laminated beds (Figures 4.8a and b), indicating that tractional and grainfall deposition were the primary modes of deposition (Hunter, 1977). Towards the top of the sections, supercritically climbing translatent stratification is indicated by the curved strata.

Particle size analysis indicates that the sediments from all three sites have similar distributions (Table 4.1 and Figure 4.4). The sediments are moderately well sorted fine sand (except UAE10/1/18 for which the mean is medium sand), with symmetrical and mesokurtic distributions. There are no palaeosols present and relatively homogeneous sediments indicate a dry aeolian system (Kocurek and Havholm, 1993). There is no clear difference between the particle size distributions of the upper samples of UAE10/3, where

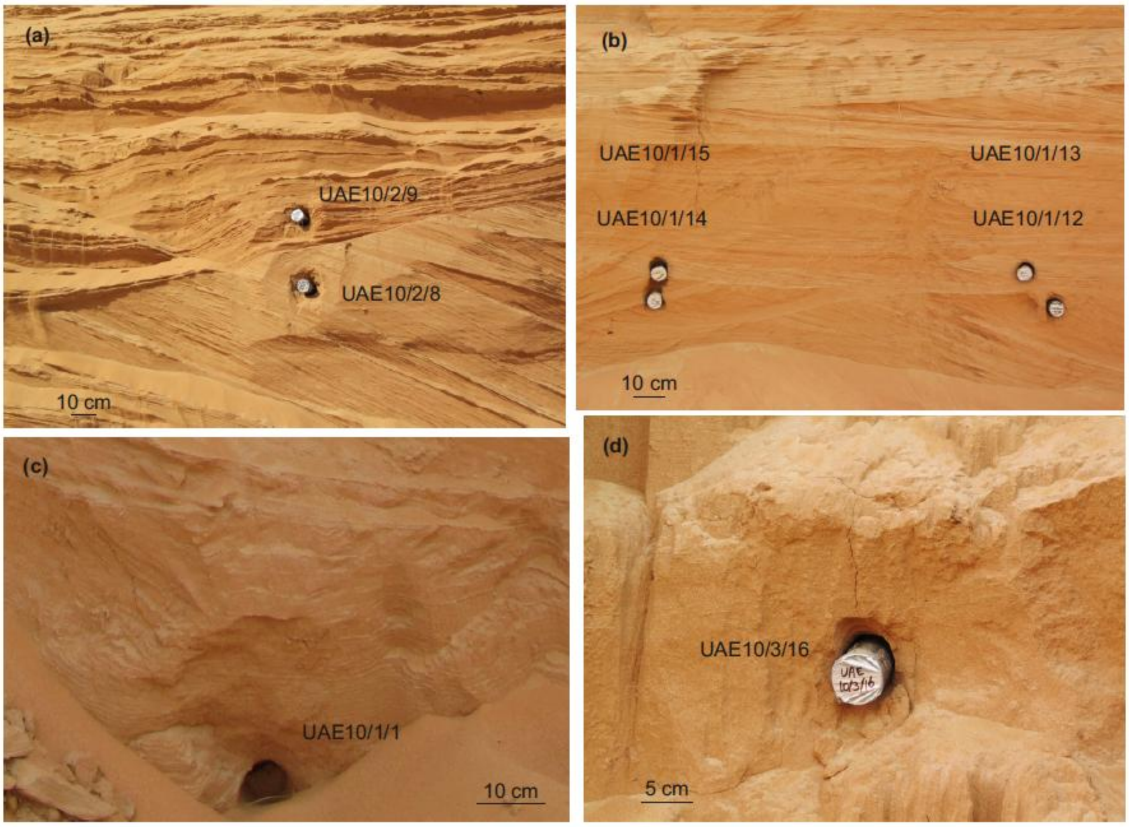

Figure 4.8: Photographs of stratigraphy at the sampling sites. (a) Samples UAE 10/2/8 and 2/9. The laminae of the bed containing 2/9 follows the underlying topography of the bounding surface below, and together with the tabular nature of the laminae, the intermediate grain size and non-erosional contacts, indicates that grainfall deposition was the dominant depositional process. Below, the erosional and sharp contacts, low/medium dip angle, distinct grading and tabular planar laminae indicate subcritically climbing translatent stratification (Hunter, 1977). (b) Bidirectional dipping and cross-lamination at UAE10/1. Rippleform lamination is present above the bounding surface beneath samples 1/13 and 1/15, whilst below the laminations are more planar, interpreted as grainfall lamination. (c) Contortion of the set at the base of UAE10/1. (d) Little or no structure in the top section of UAE10/3.

the internal structure is not clear, and for other samples where there is visible stratigraphy. Sampling at finer resolution using sampling tubes with less than 5 cm diameter may capture particle size variability at sufficiently small a scale to explain the presence of laminations. Each of the sites will be discussed individually in further detail and presented alongside the OSL dating results.

4.3.1. UAE10/1: Shwaib

This site had been sampled for dating three years previously, with site details (named Shu'ayb) and ages described by Atkinson et al. (2011). In 2010, when sampling took place for this study, the quarry had been significantly expanded. The two sampling sites at Shwaib, UAE 10/1 and 10/2, are approximately 200 m apart from adjacent edges of the pit (Figure 4.9). The site is situated at the far northeast-wards extent of a linear megaridge. The megaridges here display interdunal spacing of ~1 km, and are overlain by secondary branching northwest-southeast linear dunes. The UAE 10/1 section faces towards the northwest. The exposed face is therefore almost parallel to the direction of megaridge elongation (towards the northeast), and approximately perpendicular to the orientation of the secondary linear dunes.

Face UAE 10/1 is estimated to be approximately 65 m in height, with only the base accessible to sample. 20 samples were taken within a horizontal range of ~13.5 m and

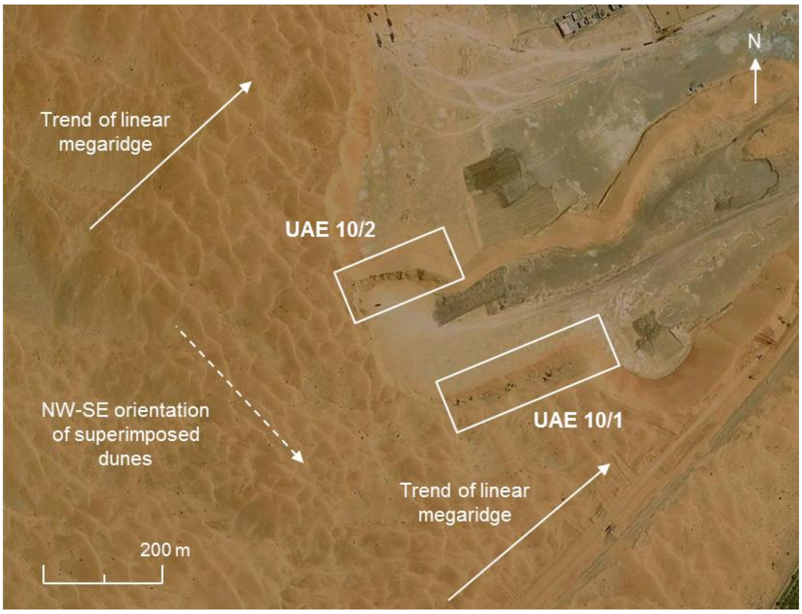

Figure 4.9: Relative positioning of the two sites at Shwaib, UAE10/1 and UAE10/2. Linear megaridges are orientated southwest-northeast, overlying secondary branching linear dunes are orientated northwest-southeast. © 2012 Google. Image © 2012 GeoEye. Imagery date: 6/10/2009.

vertical range of ~4 m (Figure 4.10). Contortion of the lowest sets is visible, but does not appear to be widespread throughout the face (Figure 4.8c).

At the macro-scale the internal structure revealed at Shwaib (Figure 4.10a) is dominated by trough cross-stratification (cf. Bristow et al., 2000) towards the top of the dune, striking perpendicular to the linear megaridge orientation. The second-order bounding surfaces that separate these laterally discontinuous lenticular features (Kocurek, 1981) may be a result of scouring of secondary dunes over the underlying linear megaridge (Rubin and Hunter, 1985, 1983). Some of these surfaces stretch tens of metres across the exposure. The apparent bedding direction is more unimodal and dips towards the northeast below approximately halfway down the profile of UAE10/1, where the samples for dating were taken from (Figure 4.2d). This is interpreted as accumulation resulting from the direct development of the primary bedform, rather than from accumulation via smaller superimposed secondary dunes. The exposed (undated) section perpendicular to UAE10/1 and UAE10/2 and facing towards the northeast is more homogeneously structured down the vertical profile, with a fairly unidirectional apparent dip towards the north-northwest, thought to align with the dip of the megaridge lee slope (Figures 4.2c and 4.9). The linear megadune structure is similar to that described by Bristow et al. (2000) in the Namib, inferred to be dominated by superimposed dunes. Here, however, due to the linear nature of superimposed dunes which stretch perpendicular to the underlying megaridge, the trough substructures are dominant across the axis parallel to megaridge elongation (i.e. UAE10/1), whilst more planar unidirectional dipping is perpendicular to the megaridge crest. Secondary dunes therefore have played a dominant role in producing the nature of the

Figure 4.10 [Next page]: (a) Photo of the UAE10/1 section. (b) Line drawing of the UAE 10/1 section, sampling strategy and OSL ages (modelled in OxCal). Bounding surfaces are represented by solid black lines, and the dip angle of laminations is represented by dashed lines. Scale is approximate.

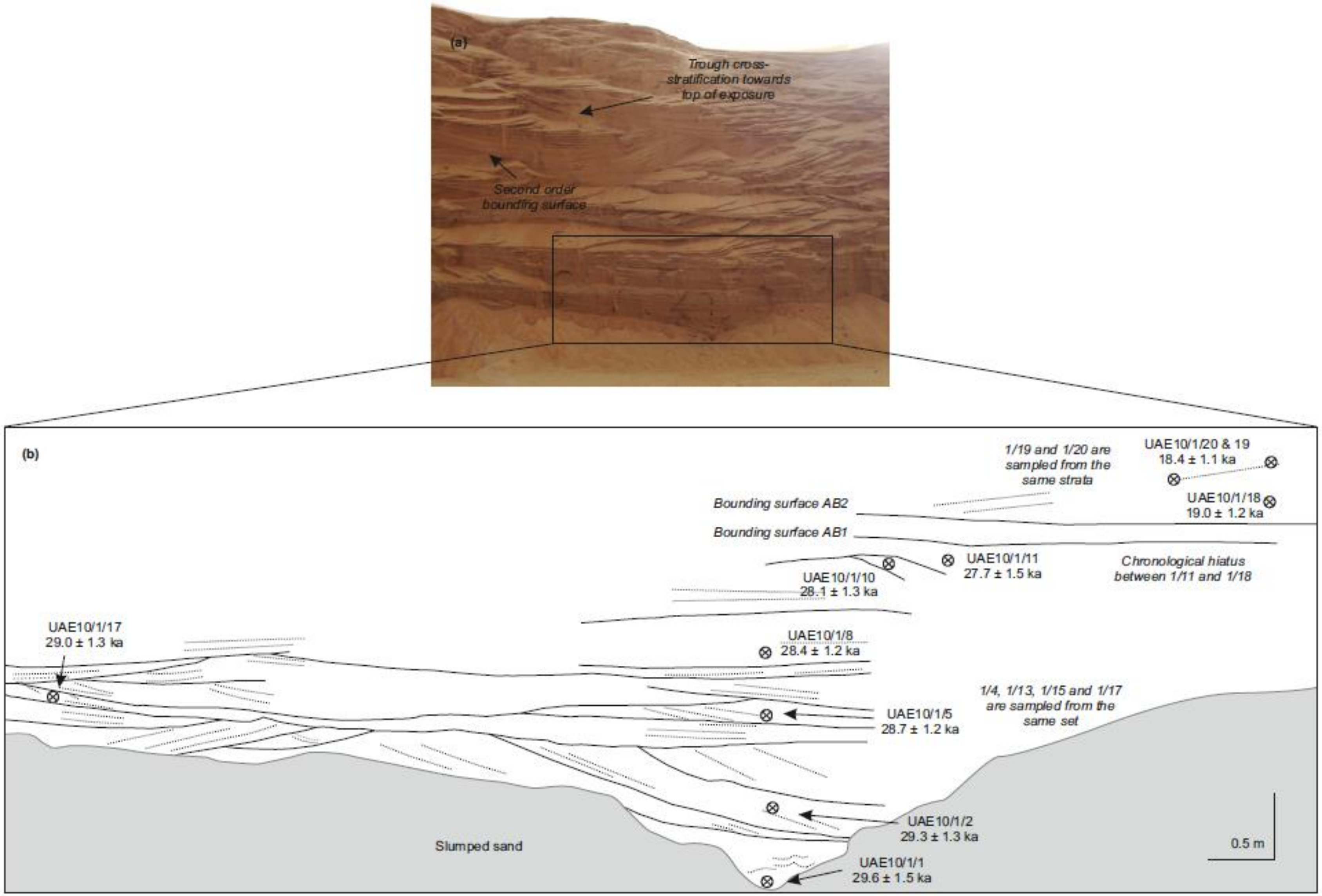
(a)
Trough cross-stratification towards top of exposure
Second order bounding surface
(b)
1/19 and 1/20 are sampled from the same strata
UAE10/1/20 & 19
18.4 ± 1.1 ka
UAE10/1/18
19.0 ± 1.2 ka
Bounding surface AB2
Bounding surface AB1
UAE10/1/11
27.7 ± 1.5 ka
Chronological hiatus between 1/11 and 1/18
UAE10/1/10
28.1 ± 1.3 ka
UAE10/1/17
29.0 ± 1.3 ka
UAE10/1/8
28.4 ± 1.2 ka
1/4, 1/13, 1/15 and 1/17 are sampled from the same set
UAE10/1/5
28.7 ± 1.2 ka
UAE10/1/2
29.3 ± 1.3 ka
Slumped sand
0.5 m
UAE10/1/1
29.6 ± 1.5 ka

underlying sedimentary record. The structure of this face indicates rapid net accumulation in an active aeolian system. Two periods of accumulation are inferred from the OSL ages from UAE10/1. The ages of samples 1/1 to 1/11 (unit A) all lie within errors of 29.6-27.7 ka (Figure 4.10). The sets of samples 1/18 to 1/20 (unit B), ~1 m directly above 1/11, have younger ages centred on 18.7 ka. There are two identifiable bounding surfaces between 1/11 and 1/18, labelled surfaces AB1 and AB2 (Figure 4.11), of which either or both may be correlated with the chronological interval between units A and B.

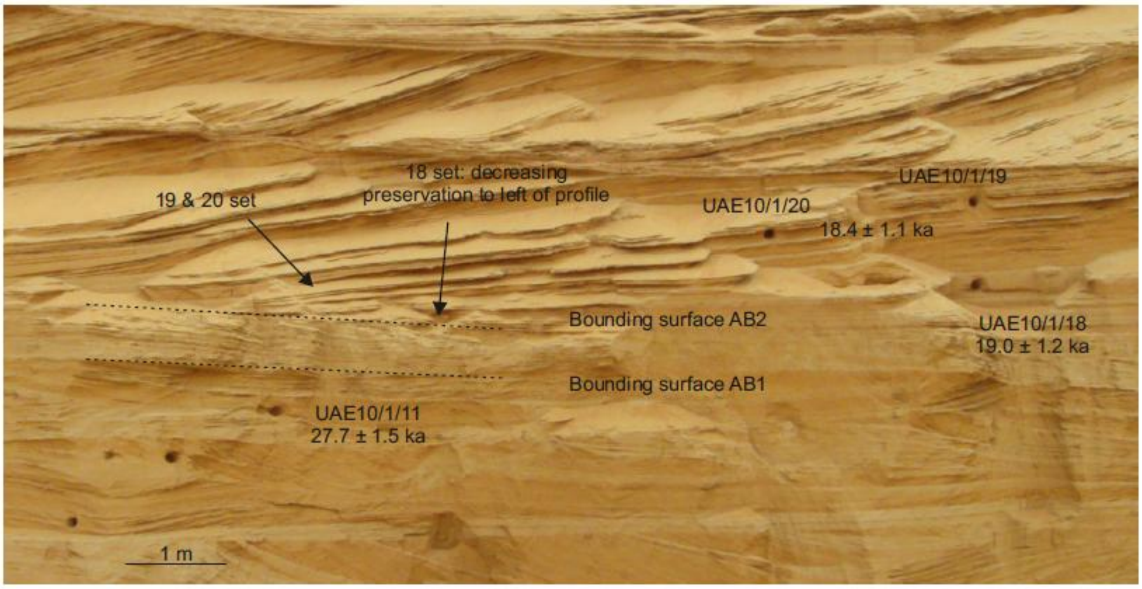

Figure 4.11: Chronological hiatus at UAE10/1. The identified bounding surfaces AB1 and AB2 are erosional discontinuities between samples 1/11 and 1/18. Scale is approximate.

4.3.2. UAE10/2: Shwaib

The exposure of UAE 10/2 faces towards the south-southeast (Figure 4.9), displaying cross-sections which cut almost parallel to the elongating direction of the linear megaridge and perpendicular to the present secondary linear dunes. UAE 10/2 stratigraphically overlies UAE 10/1, and hence represents more recent accumulation. The SSE-facing exposure is opposite that of UAE10/1 within the Shwaib quarry, and is lower at ~20 m in height above the pit floor. The structure is dominated by unidirectional dipping towards the east, with less trough cross-stratification than seen in the upper parts of profile UAE10/1. There is a second quarry pit located to the north of this section (Figure 4.9). The top of the section may therefore not correspond to the height of the present-day surface if slumping has occurred, which may explain the lack of lenticular units towards the top of the profile.

Two major bounding surfaces were sampled laterally across 53.5 m (Figure 4.12), interpreted in the field as potentially marking a chronological break due to the extent of the surfaces across the entire exposed face. The bedding laminae increase in age towards the southwest, based upon relative stratigraphic relationships. Most of the lamination is tabular and curved, with some sections following the underlying topography (Figure 4.8a). There is bidirectional dipping, although most of the bedding dips towards the east, as also seen at UAE10/1.

The ages of all samples from UAE10/2 are within errors of 15.4-13.4 ka, with individual periods of accumulation irresolvable at the resolution of OSL dating (Figure 4.12). There are no chronological differences across the two major bounding surfaces either vertically or laterally, nor the ~6 m vertical gap between the bulk of samples and sample 2/19 taken from the top of the section. The late Pleistocene age of sample 2/19, despite being taken just below the present-day surface, indicates that slumping of the uppermost sand may have occurred during sand extraction, as young ages have been dated in samples close to the surface previously at the site (Atkinson et al., 2011).

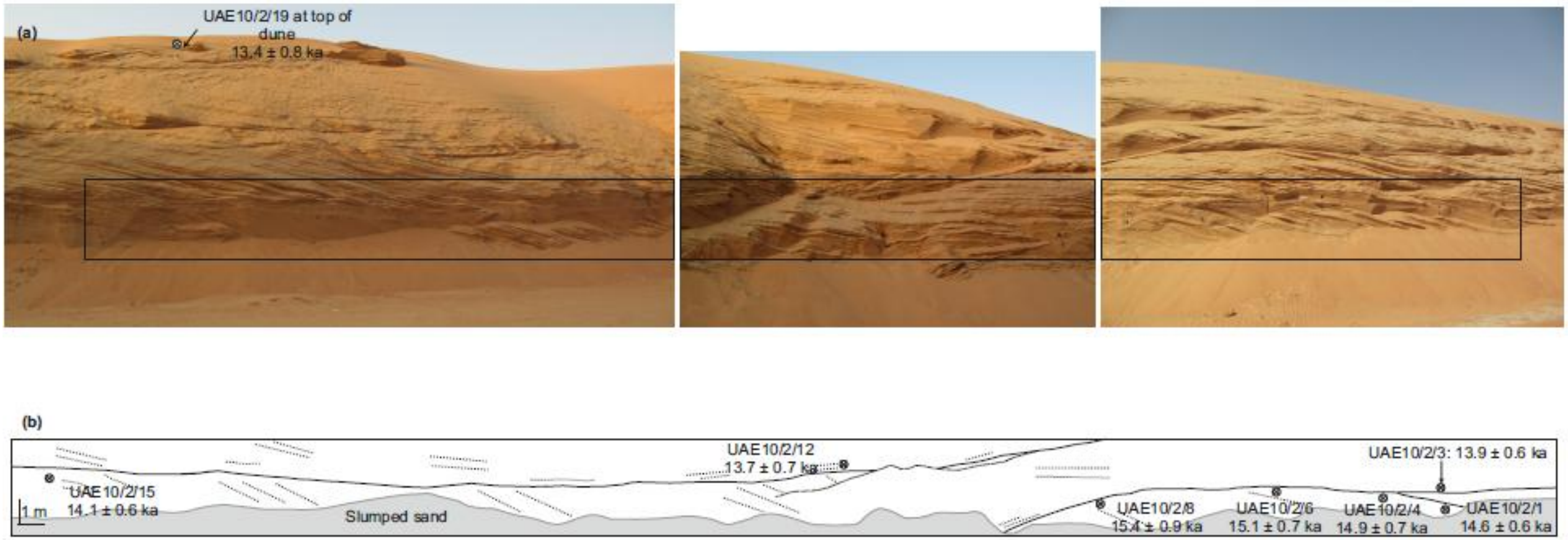

Figure 4.12: (a) Photo of the UAE10/2 section. (b) Line drawing of the UAE 10/2 section, sampling strategy and OSL ages (modelled in OxCal). Scale is approximate.

4.3.3. UAE10/3: Emirates Highway

The Emirates Highway site is approximately 2.5 km northeast of the sites sampled by Atkinson et al. (2011), located further from the core of the underlying southwest-northeast trending megaridge to the southeast (Figure 4.2). The pit is smaller than at Shwaib, with the face being ~20 m in height above the pit floor. Sampling was undertaken laterally across ~26.5 m above and below a major contact, and vertically to span the entire section. The section is curved as a result of a change in angle of the quarry wall; samples 3/1 to 3/15 and 3/19 face east whilst the section from 3/16 to 3/18 faces northeast (Figure 4.13).

Site stratigraphy is similar to that at Shwaib at both the micro- and macro-scales: compound cross-stratification and bidirectional dipping indicate similar dune processes and morphological relationships between primary and secondary dunes. Towards the top of the exposure however, the stratigraphy was less well-defined and sets were difficult to identify (Figure 4.8d). Samples 3/16 to 3/19 were taken to cover the vertical section systematically. A lack of structure has been noted at other sites previously, including in dunes near Al Ain, approximately 60 km south of Shwaib (Atkinson et al., 2011). Towards the top of the dune plant roots were present, although sampling avoided obviously affected sections.

The base of the UAE10/3 profile, sampled laterally, shows sand deposition between 14.9-12.8 ka (Figure 4.13). Samples 3/17, 3/18 and 3/19 cover a section where the stratigraphy is unclear, and the chronology is stepped with ages of 12.8 ka, 4.8 ka and a younger sample reflecting deposition in the last 200 years at the top of the dune.

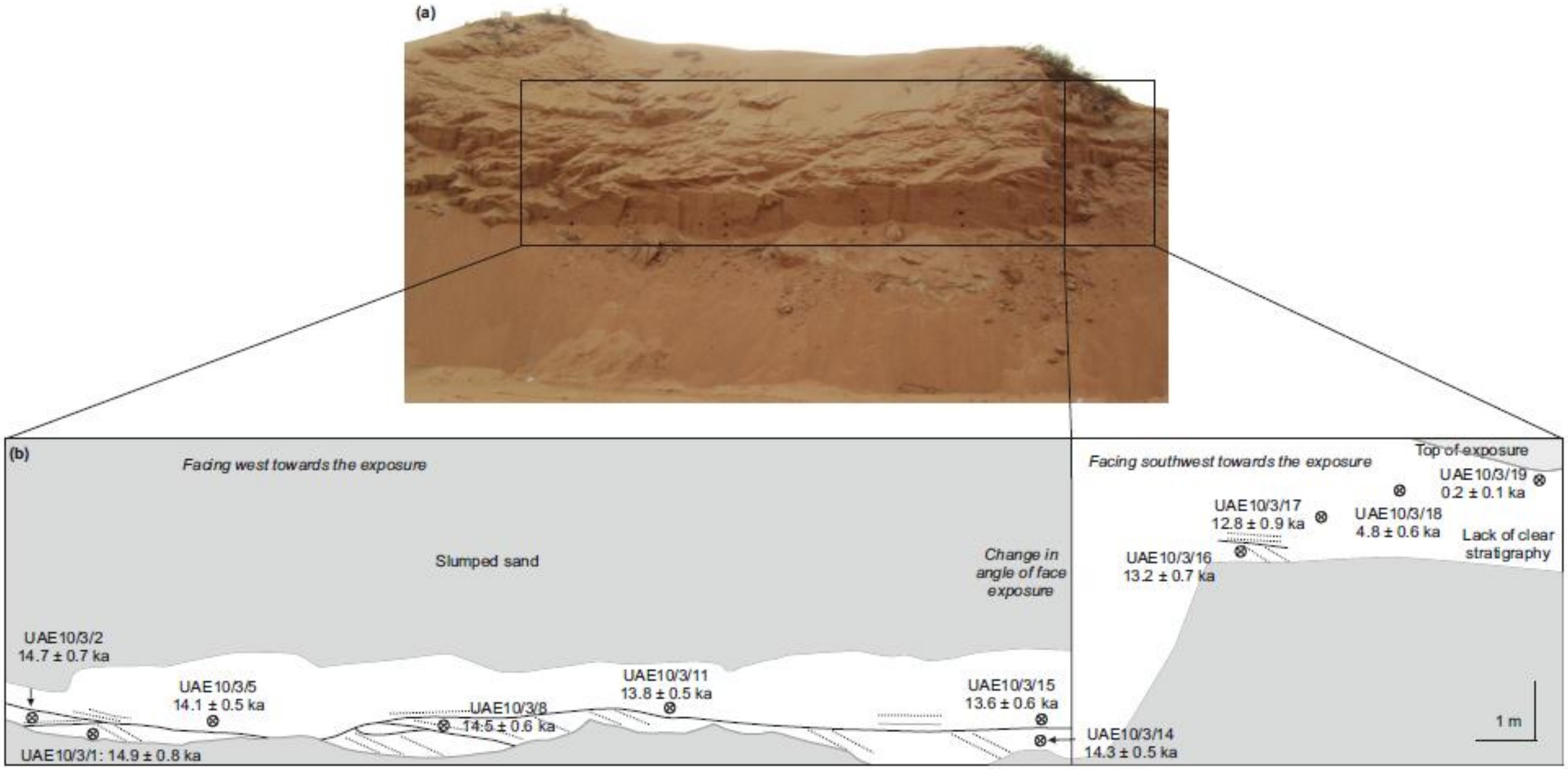

Figure 4.13: (a) Photo of the UAE10/3 section. (b) Line drawing of the UAE 10/3 section, sampling strategy and OSL ages (modelled in OxCal). Scale is approximate.

4.4. Discussion

The relevance of dune internal structure, including bounding surfaces, and its relationship to OSL chronologies of dune accumulation will be discussed in the following section, with a focus on two specific questions: can chronologically significant stratigraphic features be identified in the field; and can dunes without identifiable structure provide consistent chronologies? These questions are also significant in delimiting the optimum balance between representativeness of sampling achievable and practical constraints on fieldwork. Estimates of net accumulation rates have been calculated using the sampling interval and mean modelled ages of the oldest and youngest samples. Bracketed rates indicate the minimum and maximum rates using the time interval defined by the upper/lower and lower/upper age uncertainty limits of the oldest and youngest samples respectively.

4.4.1. Identifying chronologically significant stratigraphic features

Stratigraphical similarity of chronologically separate units

Two periods of accumulation at UAE10/1, identified as between 29.6-27.7 ka and at 18.7 ka, are distinguished by a break in overlapping age uncertainties and dissimilar D_e values which suggest that a hiatus is separating the two depositional units (Figure 4.10). Two bounding surfaces, labelled AB1 and AB2, lie between the samples of 1/11 and 1/18, dated at 27.7±1.5 ka and 19.0±1.2 ka respectively (Figure 4.11), and it is concluded that either or both of these surfaces, which represent erosional events, could be defined as a super surface (Kocurek, 1988), as they correlate with a hiatus representing a break in accumulation between 27.7 and 19.0 ka. The unit between surfaces AB1 and AB2 is an example of a relatively thin unit that could go undiscovered from blind sampling (e.g coring from above and sampling using systematic intervals), but which may yield potentially useful chronological information. However, whether or not the set between samples 1/11 and 1/18 is chronologically distinct from those above and below, we do know that at least one erosional event separates at least two chronologically distinguishable periods of accumulation. What is clear from this example is that the bounding surfaces within section A between samples 1/1 to 1/11 cannot be distinguished hierarchically from surfaces AB1 and AB2 separating samples 1/11 and 1/18. Relying on the most extensive and visually dominant bounding surfaces alone, defined as those that cut across surfaces of lesser extent (following Brookfield, 1977), to guide sampling therefore may not capture all of the sets which are chronologically distinct within the OSL chronology. However, utilising all bounding surfaces may not provide a time-efficient sampling method.

The similarity of the sets and surfaces above and below surfaces AB1 and AB2, and their indistinctiveness within the profile, suggests similar depositional and erosional processes occurred repeatedly during periods of dune accumulation between ~30 and 18 ka, which are likely to relate to the stochastic processes of dune dynamics that occur during periods of sustained dune activity, and not necessarily caused by major external forcing. Bounding surfaces that represent both chronologically significant hiatuses in dune accumulation (at the precision of OSL dating) and insignificant chronological hiatuses are reflected in the sedimentary record for this period. Additional OSL ages from this site show that 12 m of sand was deposited between ~22.5-20 ka, with an estimated net accumulation rate of 4.9 m ka^{-1} (Atkinson et al., 2011), possibly correlating with the second period of accumulation at UAE10/1. Sea-level was low in the Persian Gulf during the last glacial period (Siddall et al., 2003), implying that sediment supply is not the main factor limiting dune accumulation during MIS3-2 in this region. The lack of ages dated to ~22.5-20 ka between samples UAE10/1/11 and 1/18 may therefore be a result of erosion of a previously underlying unit at this specific site location.

The UAE10/1 example shows that chronologically resolvable hiatuses do not always correspond to visually dominant bounding surfaces, as representations in the dune sedimentary record of processes occurring at a range of scales may converge. Higher order bounding surfaces alone cannot therefore be used to 'target' breaks in aeolian accumulation/preservation, as chronological hiatuses in accumulation may be missed by sampling. Bounding surfaces therefore cannot be used to guide sampling fully, and hence the representativeness of the sampling strategy of the dune sedimentary structure must be balanced by the practical considerations of sampling and OSL measurement.

Stratigraphically dominant bounding surfaces

The two bounding surfaces sampled at site UAE10/2 extend over a combined 30 m across the exposure and are the visually dominant stratigraphical features of the face (Figure 4.12). However, the sedimentary units either side of these two features are chronologically indistinguishable. They can be explained by the occurrence of a relatively rapid erosional event between periods of high net accumulation. This indicates the highly active nature of this part of the sand sea between ~15-13 ka. Ages within this range have also been found at Wahala, Shwaib (Atkinson et al., 2011), and Awafi (Goudie et al., 2000a), indicating a regional period of aeolian accumulation. This example highlights an important difficulty for dune studies; bounding surfaces can represent single or multiple erosional events occurring over long or short periods of time, and yet may appear similar within the sedimentary record. The extent of this problem will depend upon the depth to which the erosional event excavates the sediment that has previously accumulated, the accumulated depth of the underlying sediment, and the length of the time interval during which erosion exceeds deposition.

UAE10/1 and UAE10/2 illustrate both equifinality (the potential production of similar morphological features by numerous alternative process histories) and divergence (the production of different features by similar processes) with regard to chronological timescales of process within the dune sedimentary record. At UAE10/1, the similarity of bounding surfaces for chronologically significant and insignificant hiatuses shows the convergence of structure produced by events occurring over different timescales. Chronologically indistinguishable units are separated by bounding surfaces of varying dominance within the exposure, despite homogeneous sedimentological characteristics at the resolvable scale; a divergence of form produced by processes operating at similar timescales. OSL dating here gives a good indication of the problems associated with relying upon stratigraphic form when inferring process.

4.4.2. No visible internal dune structure

Unambiguous sedimentary units are not always apparent, such as at UAE10/3 above and including sample 3/16 (Figures 4.8d and 4.13). Laminations are apparent in upper sediments, but there is a lesser degree of internal structure compared to underlying deposits, so that structure cannot be utilised easily for either guiding sampling or interpretation. Single grain measurements of samples 3/17 and 3/18 were made in order to indicate whether this lack of structure could be a result of post-depositional mixing of sediment (Table 4.5). These results show a uni-modal D_e distribution, indicating that the lack of structure is not due to bioturbation and mixing of sediment (Figure 4.14). At Al Ain, a dune with no internal structure comprised chronostratigraphic units of 7-6 ka, 4-3 ka and ~1 ka (Atkinson et al., 2011), indicating that this property is not solely site specific. Lack of internal structure where post-depositional mixing is unlikely to have occurred has also been observed in other regions (Bateman et al., 2007; Stone and Thomas, 2008; Telfer and Thomas, 2007).

The question therefore remains as to the environmental factors controlling the visibility of individual stratigraphic units. Internal structure (i.e. laminations within the sand body e.g.

Table 4.5: Single grain ICP-MS/AES and OSL data. Ages are unmodelled and calculated in OxCal v.4.1.

	Dosimetry data				**Standard aliquot data**			**Single grain data**			
Sample	**K (%)**	**Th (ppm)**	**U (ppm)**	**Dose rate (Gy/ka)**	**n**	***D*****e (Gy)**	**Age (ka)**	**n**	***D*****e (Gy)**	**OD**	**Age (ka)**
10/3/17	0.828 ± 0.108	2.751 ± 0.358	0.999 ± 0.09	1.29 ± 0.12	28	14.51 ± 0.51	11.34 ± 1.04	29	13.21 ± 0.73	0.23 ± 0.05	10.31 ± 1.05
10/3/18	0.717 ± 0.093	1.200 ± 0.156	0.797 ± 0.072	1.06 ± 0.12	13	5.07 ± 0.28	4.80 ± 0.60	21	4.96 ± 0.32	0.19 ± 0.06	4.69 ± 0.61

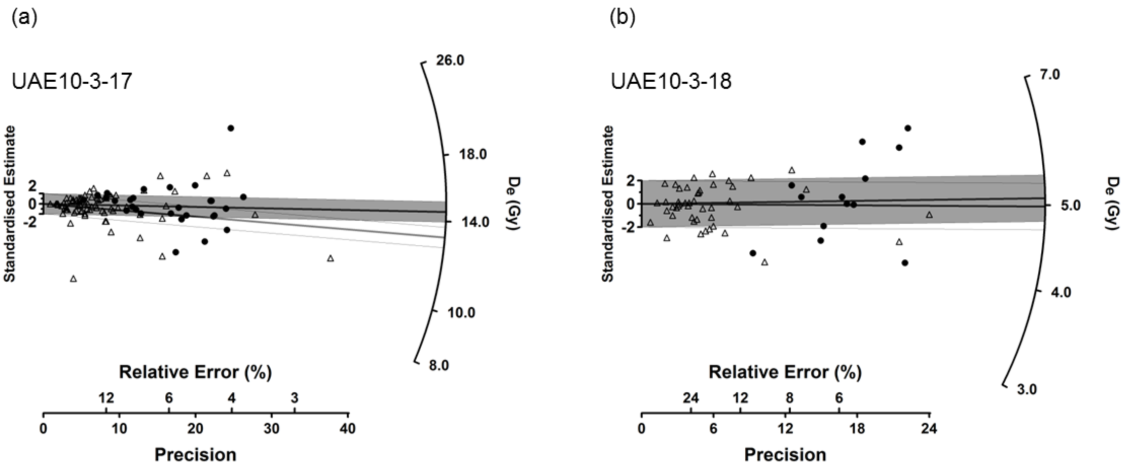

Figure 4.14: Radial plots of D_e estimates. Single grain D_e estimates are shown by open triangles, multi-grains estimates are shown by filled circles. (a) Sample UAE10/3/17. (b) Sample UAE10/3/18.

Figure 4.8d) is related to factors such as grain orientation, packing, and particle size sorting (Bateman et al., 2007). The transition from clear internal stratigraphy to no structure at UAE10/3 occurs gradually, but it is in the uppermost part of the dune where the most rapid changes in ages with depth occur. Thinner laminations indicate that it is unlikely that lack of structure is solely due to a reduction in preservation potential. The filling of the Persian Gulf, most rapid between 12-8 ka (Teller et al., 2000), is likely to have limited sediment supply to the Rub' al Khali during this time interval. Sea level change at the beginning of the Holocene was accompanied by more humid conditions in this region due to the strengthening and northward migration of the Indian Ocean summer monsoon; interdune lakes at Awafi, UAE, were at their maximum level between ~8.5-6 ka until regional desiccation at ~4.1 ka (Parker et al., 2004, 2006). Several abrupt arid events have been identified in the early to mid-Holocene (e.g. Gupta et al., 2003; Parker et al., 2006), which may have resulted in frequent reworking. Aeolian activity undoubtedly occurred when interdune lakes were present, evidenced by aeolian sediments within lake sediment sequences (Parker et al., 2006) and a small number of OSL ages from this time at Shwaib (Atkinson et al., 2011). However, aeolian activity in the region at this time was less significant compared to earlier times, and preservation was more dependent upon locally favourable conditions. The dated dune accumulation in UAE10/3 is therefore the product of a period of transitions in regional climate. This example indicates that there are multiple environmental variables that may influence bedding structure development with its absence not necessarily related to post-depositional reworking. Although beyond the scope of this paper, further investigation of the processes underlying stratigraphical visibility is required. High resolution sedimentological analysis of laminations where they are visible may be one approach to addressing this question.

4.4.3. Implications for constructing chronologies

In terms of capturing depositional records in sampling strategies, megadune structures dominated by secondary features pose potential difficulties. The composite nature of complex dunes implies increased spatial chronological variability. Increased variability of chronologies from different profiles of the same megadune will be expected if there has been significant movement of the crest, if sampling is being undertaken near the base of deep sediments, or if the dune exhibits either relatively thin chronological sets or a high variation in the thickness of chronological sets. As controls on deposition and erosion are spatially variable, so are dune chronologies. When this is coupled with the idea that chronologies are samples of unknown regional age distributions, it is clear that chronological variability between profiles should be expected. However, a thorough sampling strategy that attempts to cater for this variability, including sampling at a number of sites, may provide increased confidence when inferring environmental controls. If a number of small dunes are responding in unison, the record more likely reflects external forcing controls than internal dune variability. For example, in the northeastern Rub' al Khali, there is remarkable similarity of the timing of accumulation in sites UAE10/2 and UAE10/3, and the chronology of site Wahala, which is approximately 5 km west of UAE10/3 (~16-10, 6-5, 0.5 ka; Atkinson et al., 2011). Variability of OSL dune chronologies should be expected, and multiple sampling profiles are one way to try and capture this variability.

The complexity of dune development, both temporally and spatially, can be seen by the variability between and within the sites presented here. Where there is a lack of structure, post-depositional mixing need not necessarily be inferred. The nature of accumulation at these sites, comprised of periods of rapid accumulation together with dune sections dominated by multiple hiatuses, yields potential problems for achieving an acceptable level of sampling resolution. Stratigraphy, whilst being a useful additional tool to inform the post-dating interpretation of whether sampling strategy has been appropriate, is alone not enough to guide sampling in the field. Confidence in the suitability of a dataset to make palaeoenvironmental interpretations greatly depends upon the resolution of sampling. Techniques such as range-finder ages (e.g. Durcan et al., 2010; Roberts et al., 2009) and the use of standardised growth curves (Roberts and Duller, 2004; Telfer et al., 2008) have provided time-saving methods when producing dune chronologies, which allow for the possibility of utilising stratigraphical features, either visible in exposures or by GPR. In-situ luminescence measurements from portable readers provide the potential of addressing these issues directly when in the field (e.g. Munoz-Salinas et al., 2011; Sanderson and Murphy, 2010). In order for stratigraphy to be used effectively therefore, knowledge of internal structure must be applied without relying on assumptions of hierarchical classification (e.g.

Brookfield, 1977) based on two-dimensional exposures when designing a sampling strategy.

The methods used in this paper, whilst aided by the visibility of dune stratigraphy, could still be used when conventional coring techniques are employed; the relative stratigraphy of individual profiles will be known and cluster analysis of D_e values could be used in order to group inferred chronological sets if using OxCal or other tools employing Bayesian analysis to increase the precision dating. What is lacking without a visible internal structure is the ability to know the relative stratigraphy when sampling laterally, or to identify potentially significant unconformities between individual samples; this would be particularly useful in assessing the sufficiency of the sampling strategy. Another advantage of identifying erosional bounding surfaces which represent chronological hiatuses is the ability to infer minimum accumulation rates which, when sampling blindly, rely upon assumptions of continuity of deposition between samples. For example, two samples representing two short distinct periods of deposition could be interpreted as slower accumulation over a more extended period of time if the erosional surface between them is not visible; each interpretation with different implications for underlying environmental controls.

4.5. Conclusions

Rapid accumulation is recorded in the dated sections exposed within large linear dune features in the UAE. Complex stratigraphy reflects rapid changes in aeolian system behaviour at temporal scales that cannot be resolved by the level of precision achievable in the application of OSL dating. Where chronological hiatuses are present, internal stratigraphy can be a useful tool in identifying problems of under-sampling. It has also been used in the present study to identify issues with beta dose rate determination. The OxCal software (Bronk Ramsey, 2009a) has been used successfully to incorporate information of the relative chronology and increase the precision on each individual age. Whilst knowledge of the stratigraphy of a sampling site is useful, it is not required for these techniques to be applied when methods for obtaining samples do not provide opportunity to examine the stratigraphy (e.g. sediment coring).

Stratigraphy *alone* is not sufficient at the studied sites to guide OSL sampling; internal structure is not evident in the youngest dunes, and where the stratigraphy is clear, significant unconformities which represent a hiatus in dune accumulation/preservation are not distinguishable from bounding surfaces representing more rapid changes in dune dynamics. Unconformities separating allostratigraphic units of similar lithological properties display a range of magnitudes of stratigraphic dominance which do not align with the duration of associated hiatuses, whilst many stratigraphic signatures are not unique to specific environmental conditions/histories and exhibit convergence of form.

5 Allostratigraphy and Quaternary dune sediments: not all bounding surfaces are the same

Paper Two: Carly L. Leighton, David S.G. Thomas, Richard M. Bailey

Submitted to *Aeolian Research*

http://dx.doi.org/10.1016/j.aeolia.2013.09.001

Abstract

A lack of knowledge of the underlying stratigraphy is often cited as a limitation of dunefield optically stimulated luminescence (OSL) sampling campaigns. Here we examine the role of allostratigraphy in characterising aeolian structural sequences, and the implications of the relationship between visible internal structure and dune accumulation chronologies. We argue that whilst allostratigraphy offers the most appropriate approach to the description of dune internal structure, there are fundamental limitations of this approach which limit its direct application to constructing chronologies of dune accumulation. "Allostratigraphical units are not synonymous with chronologically-distinct accumulation units, and not all significant bounding surfaces are unconformities. Therefore, the utility of an allostratigraphical approach in guiding sampling for OSL dating is limited."

5.1. Introduction

An oft-cited criticism of the sampling of sand dunes for optically stimulated luminescence (OSL) dating is that the internal structure of the dunes is not visible to guide sampling locations, except in a limited number of cases (e.g. Atkinson et al., 2011). In recent years, dune sampling has become dominated by drilling using a range of portable equipment, from hand-operated (e.g. Stone and Thomas, 2008; Telfer and Thomas, 2007) to mechanical (e.g. Bray and Stokes, 2004; Bristow et al., 2005; Preusser et al., 2002). Linear dune sedimentary accumulation is inherently discontinuous (Munyikwa, 2005; Telfer, 2011). This is problematic when research aims to establish the history of dune accumulation and its relationship to climatic and environmental changes, and one that may be compounded by an unrepresentative and insufficient sampling strategy relying upon relatively few samples. If dune internal structure and bounding surfaces relating to breaks in accumulation/preservation are not visible, the resultant chronology is at risk of being a function of sampling resolution rather than a true representation of the dune sedimentary structure.

One approach in the field to reduce the chance of aliasing is to increase the number of samples taken to a level considered sufficient to represent the dune sedimentary record; this is a difficult threshold to define and a solution limited in practical terms by both time and expense. In recent years these issues have come to light (e.g. Stone and Thomas, 2008), but the problems faced are highly variable between sampling sites. In some regions, narrow and normally distributed single aliquot equivalent dose (D_e) distributions demonstrating low overdispersion are found in structureless sands, indicating that a lack of sedimentary structure is not necessarily the result of significant bioturbation (Bateman et al., 2007). Sites where dunes lack internal dune structure, and hence where being able to see the stratigraphy (or lack of) will have no impact upon the choice of site for sample collection or the interpretation of resultant OSL dates, can therefore still produce reliable chronologies. However, in other contexts where there is clear internal structure, there is a question of whether using stratigraphy to guide sample locations could provide useful information.

In several regions, aspects of the internal structure, including stratigraphy, sedimentology and micromorphology, have been used to guide sampling and/or infer changes in environmental and dune development conditions (e.g. Atkinson et al., 2011; Fitzsimmons and Telfer, 2008; Fitzsimmons et al., 2007). Where sedimentological variations are present, lithostratigraphic boundaries may coincide with significant palaeoenvironmental changes. For example, at a site recently sampled near Shwaib in the UAE, a near-horizontal bounding surface separating red-brown and orange-brown sand units and marked by a horizon of coarse sand and small pebble-sized clasts was dated above and below to during and before the Last Glacial Maximum (LGM) respectively (Atkinson et al., 2011). In other locations periods of environmental stability may allow for pedogenesis to occur (Fitzsimmons et al., 2007). However, the advantage of having a visible indication of where environmental changes are represented within a sequence may be negated by associated concerns over the occurrence of bioturbation (Bateman et al., 2007; Fitzsimmons et al., 2007). In other environments however, depending on factors such as grain orientation, packing and grain size distribution (Bateman et al., 2007), clear sedimentological variations may not be present.

The application of ground penetrating radar (GPR) to dunes in some studies has enabled their subsurface three-dimensional (3-D) internal structure to be viewed and used to guide sampling strategy, as well as to make inferences on processes of dune development (Bristow et al., 2000, 2005). However, in addition to the need for specialist equipment and knowledge, this technology cannot be applied to all dune systems, either due to a lack of internal structure altogether or as a result of sedimentological characteristics. The greater the relative permittivity of a material the higher the resolution achievable, whilst high magnetic permeability and electrical conductivity increase attenuation, and reduce the depth of profiling possible; therefore GPR is most effective in electrically and magnetically resistive materials with a high relative permittivity (Baker et al., 2007; Daniels, 2005). Whilst sand is potentially an ideal material for GPR profiling, high attenuation can result from high clay and silt content, or traces of iron (Bristow et al., 2007b). In Saudi Arabia, where internal structures were known to be present, no bounding surfaces were detected, leading the authors to conclude that GPR is not effective in detecting surfaces which are defined by variations in grain packing density only (Harari, 1996). Reflections enabling the detection of bounding surfaces are determined by relative permittivity; water content is therefore a crucial parameter. Wave attenuation is greater in wet sand, but when the sand is too dry there may not be a significant variation in relative permittivity across sedimentary boundaries in order for internal structures to be identified. In light of these limitations in the widespread application of GPR, at some sites exposures may provide the only indication of dune stratigraphy.

5.2. Allostratigraphy and Quaternary landforms

Stratigraphy is "…the description of all rock bodies forming the Earth's crust and their organization into distinctive, useful, mappable units based on their inherent properties or attributes in order to establish their distribution and relationship in space and their succession in time, and to interpret geologic history" (Murphy and Salvador, 1999: 256).

When a clear dune internal structure is visible, stratigraphic description provides an additional sedimentary parameter and a conceptual framework through which to develop a suitable sampling strategy. A variety of stratigraphical approaches have been applied to Quaternary deposits, such as lithostratigraphy, morphostratigraphy, and allostratigraphy, each with their respective advantages and disadvantages in specific environments (Hughes, 2010). Allostratigraphical units “are defined and identified on the basis of… bounding discontinuities” (NACSN, 2004: 1578). One assumption of this approach is that the bounding discontinuities have a time-stratigraphical significance, for both homogeneous and hetereogeneous sediments (Hughes, 2010), and so the term ‘unconformity’ is perhaps more useful here, to describe an erosional surface that “represents a significant hiatus… in the stratigraphic succession” (Murphy and Salvador, 1999: 261). Allostratigraphy therefore has an advantage in its application to many dune systems in that it can be used to distinguish between lithologically similar units that are separated by a significant chronological hiatus. Secondly, with the increasing application of technologies such as GPR which allow a 3-D assessment of the subsurface structure, the application of a classification system which is based upon meaningful 3-D characteristics is required (Räsänen et al., 2009). Allostratigraphy has therefore been identified as a more useful tool in some stratigraphic settings than lithostratigraphy. For example, Räsänen et al. (2009) advocate the adoption of an allostratigraphical approach in the classification of Quaternary glacial deposits, seconded where necessary by lithostratigraphical additions, whilst Gutteridge (2008) calls for the abolition of lithostratigraphy altogether. In practice, it seems an integration of approaches when addressing a specific problem is likely to yield the most appropriate framework for a particular environmental context (e.g. Hughes, 2010; Räsänen et al., 2009).

Allostratigraphy is related to sequence stratigraphy, which similarly defines units according to their bounding discontinuities and is usually practised at a larger scale. It has been recognised that aeolian systems are dissimilar to marine-coastal systems to which sequence stratigraphy was first applied, and require a unique stratigraphical framework; ‘aeolian sequence stratigraphy’ is the application of this approach to dune systems (Kocurek and Havholm, 1993). The behaviour of the depositional surface is described in relation to changes in the control volume; a function of accumulation and preservation. Accumulation and preservation space are not necessarily equal and vary over time. Where preservation does not occur, a bounding surface must be present (Kocurek and Havholm, 1993). Super surfaces form during periods when the sediment budget is prevailingly negative, and can be expected to be spatially and temporally more extensive as they are a function of changing external conditions (Kocurek, 1988). Super surfaces, and the accumulation units they define, are the fundamental units within aeolian sequence stratigraphy (Kocurek and Havholm, 1993). It is these surfaces that should be the target of OSL dating, in order to establish relatively large-scale changes in environmental forcing factors which are reflected in the dune sedimentary record. Within the accumulations bounded by super surfaces, internal bounding surfaces have been related to dune processes, with classification based upon extensiveness and their nature of formation. Interdune, superposition, and reactivation surfaces (relating to the 1st, 2nd, and 3rd order bounding surfaces defined by Brookfield, 1977; Figure 5.1) form due to the migration of primary bedforms and interdunes, secondary bedforms, and periodic erosion of the lee face respectively (Kocurek, 1981, 1996). Super surfaces are the most extensive of these bounding surfaces, and would be expected to be present in all dunes within a certain area, whereas internal bounding surfaces are more dependent upon site-specific processes of dune development and therefore more randomly distributed, such as along the length of a single linear dune.

Figure 5.1 has been removed due to Copyright restrictions

Figure 5.1: Simplified hierarchy of bounding surfaces in aeolian dune sediments, viewed parallel to the palaeowind direction (adapted from Kocurek, 1988).

5.3. Application of allostratigraphy to dune sedimentary deposits

The nature of dune deposits as discontinuous records of dynamic systems implies that allostratigraphical units have particular relevance to the processes underlying their formation and preservation. However, as in the application of aeolian sequence stratigraphy, dune systems also require an adaptation of the allostratigraphical approach; aeolian unconformities do not represent the spatially extensive unconformities that are classified in the rock record. Aeolian systems are more local in their processes, characterised by fluctuations in accumulation rate and periodic episodes of accumulation and erosion.

The relationship between allostratigraphy and chronology is not straightforward. Whilst allostratigraphical units are defined by the 'gaps' in the stratigraphy, and hence are defined by temporal hiatuses in accumulation, these gaps may represent rapid changes and so units may be closely related in both process and time (Hughes, 2010). Within aeolian sequence stratigraphy this is addressed by the classification of super surfaces and internal bounding surfaces on the basis of their mode of formation. Hughes (2010) argues that although in theory allostratigraphical principles can be successfully applied based upon the correct hierarchical classification of the stratigraphic architecture, in the field precise definitions are often difficult (see Chapter 4 and Section 5.4). There are numerous difficulties therefore in the practical application of allostratigraphy to dune sedimentary records, which represent depositional and erosional processes varying at a range of temporal and spatial scales, displaying equifinality of form in the resultant stratigraphy. Whilst in certain sites there may be sedimentological characteristics to aid the identification of a super surface, such as the presence of palaeosols or micromorphological features such as cutans which have been used to infer periods of soil development in central Australia (Fitzsimmons and Telfer, 2008; Fitzsimmons et al., 2007), at many locations these physical clues are not available. In these cases, when the bounding surfaces visible cannot be distinguished on the basis of process or chronological significance, it may be the dating method that provides means for distinction of sedimentary surfaces, rather than vice versa.

Sets and boundaries in dune structures are not isochronous; the allostratigraphical units which can be identified are diachronic in that they comprise “unequal spans of time either by a specific… unit, or by an assemblage of such units... A diachronic unit is not extended beyond the geographic limits of the stratigraphic unit or units on which it is based” (NACSN, 2004:1584). ‘Targeting’ OSL sampling therefore is dependent on the ability to assess the chronological significance of bounding surfaces *locally*, in addition to the task of being able to physically identify them in the field. In more heterogeneous sediments, lithostratigraphy may play an important supplementary role in identifying unconformities which represent a change in environmental conditions (e.g. Atkinson et al., 2011; Fitzsimmons et al., 2007).

5.4. Case study: Shwaib, United Arab Emirates

Two sites in the northeastern Rub’ al Khali, United Arab Emirates (UAE), expose the internal structure of linear mega-ridges within sand quarries (Figure 5.2). Sampling was undertaken at relatively high spatial resolution, sampling above and below the structural features of interest. A full description of procedures and results can be found in Chapters 3 and 4.

The chronology from this site reveals the variation in the chronological significance of these sedimentary surfaces; only the bounding surface(s) between samples 1/11 and 1/18 may be classified as a defining unconformity, as a chronological hiatus of ~10 ka separates these allostratigraphical units (Figure 4.10). Below sample 1/11 the samples are chronologically indistinguishable. At this site therefore, knowledge of the internal structure from a two-dimensional (2-D) exposure does not yield any key information that would be

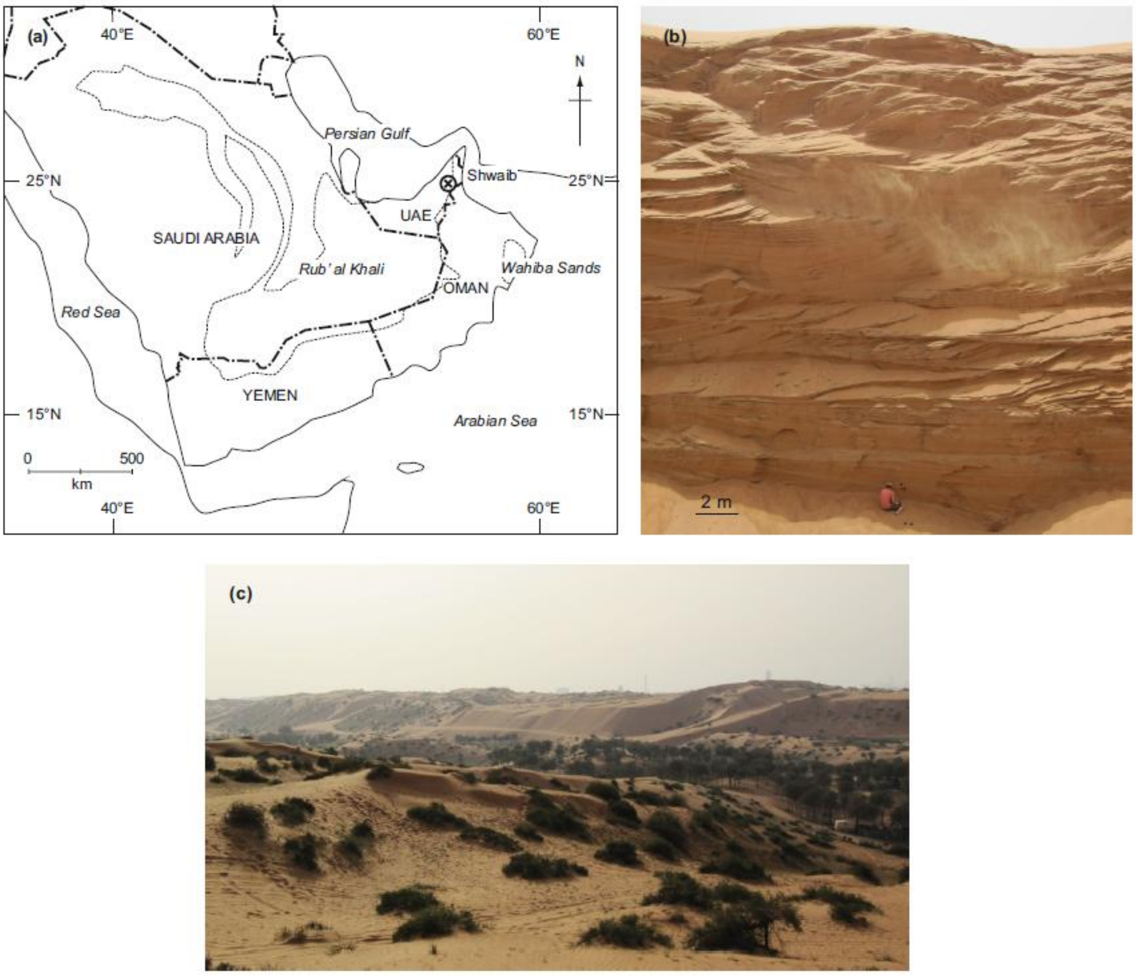

Figure 5.2: (a) Map of the study region and location of the sampling site near Shwaib; (b) Exposed profile within the Shwaib pit. UAE10/1 was sampled at the base of the exposure; (c) The landscape of the northeastern Rub' al Khali, characterised by linear megaridges and superimposed secondary linear dunes.

unobtainable when sampling blindly (for sampling for OSL dating purposes). The breaks of accumulation that do not represent a chronologically significant hiatus at the precision of OSL dating cannot be distinguished visibly from unconformities, which are identified in the chronology, by the application of an allostratigraphical approach.

At site UAE10/2 two bounding surfaces, which dominate the exposure and appear hierarchically an order above those sampled in UAE10/1, are chronologically insignificant (at the precision of OSL dating). All ages are within errors, deposited between 15.4-13.4 ka (Figure 4.12). Here, the inverse of the problem at UAE10/1 is highlighted; an apparently significant sedimentary break in accumulation based upon an allostratigraphical approach cannot be inferred as representing a significant chronological hiatus.

These two examples show the mismatch between the significance of bounding surfaces in visible 2-D exposures and their chronologies. At this site, the visible stratigraphy cannot easily be used to guide sampling for OSL dating around bounding surfaces as the chronological significance of these surfaces cannot be assumed

5.5. Conclusions

On the basis of a 2-D exposure of a dynamic dry aeolian system, allostratigraphical units are not synonymous with chronologically distinct accumulation units, and not all significant bounding surfaces are unconformities. Field classifications of stratigraphic units can therefore be unreliable and somewhat arbitrary (Miall, 2012). A 3-D view of the internal structure may allow for the extent of conformities to be better ascertained, but this needs further investigation; the application of GPR to sample for OSL dates has utilised this assumption without testing its viability. Whilst allostratigraphy provides in theory the most appropriate approach to classifying dune stratigraphy, there are fundamental limits in its application. Aeolian sequence stratigraphy addresses some of these issues by focussing on the dune processes underlying the formation of different types of bounding surface, but in the field its utility is flawed as different surfaces do not always manifest themselves as distinguishable visibly in a 2-D exposure. In light of these limitations, whilst stratigraphy can and should be used to provide additional information when interpreting dune accumulation chronologies, in most studies where this information is not available this does not mean that vital information has been lost. Range-finder dating (Durcan et al., 2010; Roberts et al., 2009) or use of a portable OSL reader (Sanderson and Murphy, 2010) could provide techniques which provide a time-efficient and practical approach to utilising stratigraphy to guide sampling.

6 Reproducibility and utility of dune luminescence chronologies

Paper Three: Carly L. Leighton, David S.G. Thomas, Richard M. Bailey

Submitted to *Earth-Science Reviews*

http://dx.doi.org/10.1016/j.earscirev.2013.11.007

Abstract

Optically stimulated luminescence (OSL) dating of dune deposits has increasingly been used as a tool to investigate the response of aeolian systems to environmental change. Amalgamation of individual dune accumulation chronologies has been employed in order to distinguish regional from local geomorphic responses to change. However, advances in dating have produced chronologies of increasing complexity. In particular, questions regarding the interpretation of dune ages have been raised, including over the most appropriate method to evaluate the significance of suites of OSL ages when local 'noisy' and discontinuous records are combined. In this paper, these issues are reviewed and the reproducibility of dune chronologies is assessed. OSL ages from two cores sampled from the same dune in the northeastern Rub' al Khali, United Arab Emirates, are presented and compared, alongside an analysis of previously published dune ages dated to within the last 30 ka. Distinct periods of aeolian activity and preservation are identified, which can be tied to regional climatic and environmental changes. This case study is used to address fundamental questions that are persistently asked of dune dating studies, including the appropriate spatial scale over which to infer environmental and climatic change based on dune chronologies, whether chronological hiatuses can be interpreted, how to most appropriately combine and display datasets, and the relationship between geomorphic and palaeoclimatic signals. Recommendations for fieldwork protocols and the presentation of multiple datasets of OSL dune ages are put forward. Chronological profiles reflect localised responses to environmental variability and climatic forcing, and amalgamation of datasets, with consideration of sampling resolution, is required; otherwise local factors are always likely to dominate. Using net accumulation rates to display ages may provide an informative approach of analysing and presenting dune OSL chronologies.

6.1. Introduction

6.1.1. Application of luminescence dating to desert dunes

The development and application of optically stimulated luminescence (OSL) dating has provided an increasingly significant tool for the study of past climatic and environmental conditions, and the establishment of depositional histories of landforms, particularly desert dunes. Developments in field and laboratory protocols have enabled the output of a large number of dune ages from many of the world's sand seas. In particular, the application of drilling methods that retain sample integrity has enabled samples to be extracted systematically from deep within dune bedforms, in some cases reaching their basal sediments (e.g. Bray and Stokes, 2003; Preusser et al., 2002; Telfer and Thomas, 2007).

The use of these methods has produced large datasets in which the dune internal structure is often unknown, as opposed to dated stratigraphic sequences where visible information can be used to guide interpretation of dune development (Stone and Thomas, 2008). Alongside reconstructions of Quaternary environmental changes, luminescence dating has aided understanding of geomorphic processes such as linear dune formation, extension and migration (e.g. Bristow et al., 2005; Hollands et al., 2006; Telfer, 2011). These advances have raised many questions with regard to the utility and interpretation of dune ages, principally related to the discontinuous nature of linear dune records, the representativeness of the accumulation units present in OSL datasets (i.e. sampling strategy-dependence), and the representativeness of sampled dune OSL chronologies for regional palaeoclimatic signals, especially from local 'noisy' records (Stone and Thomas, 2008). This paper aims to address some of these issues, including the appropriate spatial scale over which to infer environmental and climatic change based on dune chronologies, whether chronological hiatuses can be interpreted, how to most appropriately combine and display datasets, and the relationship between geomorphic and palaeoclimatic signals.

6.1.2. Linear dunes as discontinuous records of dune development

Linear dunes are frequently used in Quaternary palaeoenvironmental studies due to their widespread occurrence, relative morphological stability, and tendency to preserve longer-term records of sediment accumulation and environmental change (Kocurek, 1998; Nanson et al., 1992). As ‘accumulating’ dunes, linear dunes are important geoproxy records (Thomas and Burrough, 2012). However, sediments can still be subject to reworking during active phases; for example, by the upper sections of a dune being mobilised and deposited further along the dune body, or through an element of lateral migration impacting on longer term morphological stability (e.g. Bristow et al., 2000; Telfer, 2011; Tsoar et al., 2004). Consequently, accumulated records are inherently discontinuous, and this can hinder the interpretation of clusters of ages and the chronological gaps between them. The question of whether a hiatus in the dated sedimentary record represents a period of reduced dune accumulation or an erosional event is a significant one, and one that may be unanswerable, at least at the scale of the individual dune. These complex issues will be discussed further in this section.

The extent of reworking is dependent upon the processes underlying linear dune formation, which are to some degree still under debate (Bristow et al., 2007b; Hollands et al., 2006; Munyikwa, 2005; Telfer, 2011). Classification systems have been developed to describe the morphological variability of linear dunes (e.g. Bullard et al., 1995; Fitzsimmons, 2007), which is suggestive of the complexity of linear dune formation and their variability of form. However, these processes have clear implications for the sedimentary structure preserved, and hence the chronologies that may be obtained. Gaps in understanding the fundamental controls of linear dune formation complicate understanding of individual dune development and their relation to dunefield dynamics, and, in turn, how past environmental conditions are reflected in the landscape at these two scales of analysis.

The most widely accepted theory of linear dune formation is in the context of bimodal wind regimes, which generate or extend other dunes into elongated bedforms orientated parallel to the resultant direction of sand transport (Rubin and Hesp, 2009; Tsoar, 1984, 2001; Wiggs, 2001). In general there is net deposition on the plinth, which is relatively stable, and on the lee side of the dune, where gravity becomes the dominant mode of grain transportation, whilst the windward slope is active with net erosion reaching a maximum at the crest (Lancaster, 1985; Tsoar, 1983; Wiggs, 2001). The stability of the bedform is maintained by a balance between the seasonal reversals of the crest line and alternation of the windward and lee side, which must respond to this alternation of erosion and deposition (Lancaster, 1985; Munyikwa, 2005; Wiggs, 2001). The level of reworking during each wind reversal, as the balance between erosional and depositional processes, is a function of multiple influences including wind speed and direction, slope morphology and sediment supply, and will determine the nature and level of continuity of the sequence (Munyikwa, 2005).

In a consideration of the impact of these processes upon luminescence-dated sequences, Munyikwa (2005) argued that there is considerable potential for previously deposited sediments to be completely lost from the sedimentary sequence depending on the depth to which reworking occurs, and the end of periods of aeolian accumulation also cannot be well constrained as a result of this reworking. Further, a longer imbalance between the two dominant wind directions may lead to slow lateral migration of linear forms, as evidenced in luminescence-dated sequences from the northern Namib Sand Sea (Bristow et al., 2005). Interdune sediments and the lower slopes of linear dunes do not necessarily record all periods of aeolian activity and therefore cannot be targeted for dating in a response to the concern over reworking of the crest, which in turn raises questions of the completeness of records of accumulation in light of evidence, at least in some dunefields, of the potential contribution of lateral migration to longer term dune development. This model of linear dune formation may therefore explain the discrepancies between chronologies of different dunes within a dunefield by their incompleteness, as a result of local conditions and their impact upon the extent of reworking of sequences (Munyikwa, 2005).

Other formation mechanisms have also been suggested, with varying implications for the preservation of stratigraphic sequences. The generation of helical roll vortices and creation of parallel linear dunes in zones of updraft suggests a net depositional system with more optimistic implications for the dating of sequences, but this model of formation has not been supported by field evidence (Munyikwa, 2005; Wang et al., 2004). The wind-rift hypothesis of linear dune formation places importance upon erosion in proximal sources for the supply of material, which is then deposited laterally or obliquely onto nearby dunes, rather than the importance of long distance sediment transport resulting in dune elongation (Hollands et al., 2006). This model is supported by the dating of linear dunes and sedimentological evidence in the Simpson Desert, which suggests that dunes have not extended by more than a few kilometres, and that vertical accretion is a dominant process within the basin (Cohen et al., 2010; Hollands et al., 2006). In the southwestern Kalahari, OSL dating provides evidence for extensional growth, certainly at the scale of 10 km, but that localised reworking of sediment at any point in the dune, without resultant dune extension, has been and still is a regular occurrence (Telfer, 2011).

The importance of reworking, in addition to external forcing, indicates the complex nature of dune records and suggests that there may be two scales of dune activity recorded in the sediments of linear dunes: external forcing, as a result of regional climatic and environmental changes, and localised forcing, that may be more transient. The spatial scale over which each mode operates may have a distinctive effect on dune sedimentary records, and the implications this may have on reconstructing environmental histories requires further investigation.

It has been noted by Kocurek (1998: 333) that in the Sahara "the frequency of events has far outpaced the net potential for preservation, so that much of the potential stratigraphic record has been removed, and the accumulation surface overlies strata representing a laterally discontinuous amalgamation of events". Without an infinite supply of sediment, nor the constant capacity for preservation of deposited sediment, linear dunes do not have the potential to be gross accumulators in response to aeolian activity (McFarlane et al., 2005; Munyikwa, 2005). What is clear from the above discussion is that dunes are likely to provide localised and discontinuous records of accumulation, and hence interpretations need to consider not just the palaeoenvironmental importance of the units identified, but what significance, if any, can be placed upon chronological hiatuses. Given the high likelihood of reworking and potentially problematic interpretation of hiatuses, it is particularly important that any given sampling strategy is sufficient to capture as complete a chronology as possible.

6.1.3. Representativeness of dune OSL ages

An important aim of sampling is that the sample set is representative of the complete set of preserved sediments. This can be assessed at two spatial scales of analysis: first, the extent to which sampling coverage reflects individual dune sedimentary structure; and second, the relationship of this structure to the larger spatial unit, such as the dunefield. At the individual dune scale, multiple units of dune accumulation can be preserved in the same dune and captured by multiple coring (e.g. Telfer and Thomas, 2007), although spatial variability of these units highlight the importance of a rigorous sampling strategy (Telfer, 2011). A situation to be avoided, and one that developments in OSL analytical protocols are allowing to be addressed, is the dependence of chronologies on sampling location and vertical sampling resolution. Systematic sampling intervals of 1 m have been shown to be inadequate for capturing fully the sets within the dune dated at 0.5 m intervals in the southwestern Kalahari (Stone and Thomas, 2008). The ‘critical sampling interval’, which is sufficient to capture the variation in accumulation with depth, will be dependent upon sediment accumulation rate and depth of reworking, and hence variable in space and time. A generally applicable minimum sampling interval cannot be defined, as a unit may be smaller than the sampled diameter, and so without continuous coring there is always a possibility of missing a unit. This interval is also reliant on the associated uncertainties of OSL ages; units may be unidentifiable as a result of insufficient precision, but where smaller age uncertainties are attainable more thorough assessment of whether sampling is sufficient is possible.

Recognising these limitations, in order to identify whether the sampling interval is sufficient to capture vertical differences in unit ages, or if a significantly different chronology is likely to be produced if more samples were to be dated, it is necessary to consider the change in age represented by the bracketed unsampled sediment. Targeted sampling, by utilising bounding surfaces and stratigraphic features to apply a sampling strategy that can more appropriately reflect the dune sedimentary structure, has also been used in response to the need for more representative sampling (e.g. Chapter 4; Bristow et al., 2007a; Fitzsimmons et al., 2007). However, there is need for caution in equating dominant erosional surfaces in the sedimentary structure to considerable chronological hiatuses, or inversely assuming lower order bounding surfaces are insignificant chronologically in active aeolian systems (Chapter 4). In many field sites though, the internal structure of the dune is not visible and so systematic sampling is the norm. There are currently no standard guidelines as to a generally applicable sampling strategy for luminescence dating of dunes, and hence the amalgamation of datasets and data interpretation is also hindered by non-uniform methodologies.

For larger dunefields, whether palaeoenvironmental interpretations are meaningful is likely to be dependent on the spatial scale of analysis, as spatial differences in external forcing conditions may sufficiently explain spatial differences in dune chronologies. However, contemporary observations and OSL ages indicate significant spatial variability of aeolian system response to similar environmental forcing *within* dunefields (e.g. Cohen et al., 2010; Thomas and Leason, 2005). Also, present-day arid environments exhibit a large degree of climatic variability at rapid temporal and relatively small spatial scales (e.g. Bullard et al., 1997) which may be irresolvable by the precision of the applied dating technique. This may be represented by apparent discrepancies in palaeoclimate reconstructions (Thomas and Burrough, 2012), and may explain why significant bounding surfaces are not always clear chronostratigraphic boundaries. Due to these processes, records which appear inconsistent should perhaps be expected when compiling and interpreting different records, and may in themselves provide valuable information in the identification of periods of environmental variability (Thomas and Burrough, 2012).

Studies attempting to move from local records of past dune dynamics to those representing records of past changes in external forcing have tended to assimilate multiple records from within a dunefield (e.g. Glennie and Singhvi, 2002; Thomas and Shaw, 2002). In practice this has had the tendency to lead to the chronological breaks separating clusters of ages being filled in, as sites are compared and more sampling has been undertaken (Bateman et al., 2003; Stone and Thomas, 2008). A recent numerical model highlights that in highly variable systems, large numbers of samples are likely to be required in order to identify and separate periods of external forcing from local forcing (‘noise’) (Telfer et al., 2010). Whilst this calls for optimism in that linear dunes can be modelled to record periods of major environmental change, there are practical limitations upon extracting the required number of samples to avoid 'false positives' in many contexts. Developments in the application of 'range-finder ages' (Durcan et al., 2010; Roberts et al., 2009) and portable OSL readers (e.g. Munoz-Salinas et al., 2011) may aid the collection of sufficient samples for these purposes. Alongside these developments, a strategy of amalgamation that includes a thorough assessment of the individual sampling contexts of each chronological component will be required for the interpretation of ages as representing regional environmental changes to be more meaningful.

6.2. Study aims, rationale and methods

The issues discussed in Section 6.1 can be distilled into several fundamental questions concerned with the reproducibility of chronologies and scale that frequently arise in the application of OSL dating to desert dunes.

1) How significant are localised erosion/reworking and preservation in producing spatially variable chronologies?
2) What is the most appropriate method of presenting data in order to avoid over-emphasizing the effect of numerous dates from synchronous units, thus revealing the accumulation history rather than the choice of sampling location and resolution?
3) Can chronological hiatuses be interpreted?
4) Can a climate signal be extracted from the geomorphic signal that is represented by the preserved sedimentary record?

The aim of this paper is to address these issues through consideration of the reproducibility of dune chronologies in the northeastern Rub' al Khali, United Arab Emirates (UAE). The Rub' al Khali is the world's largest active sand sea and covers approximately 600,000 km^2

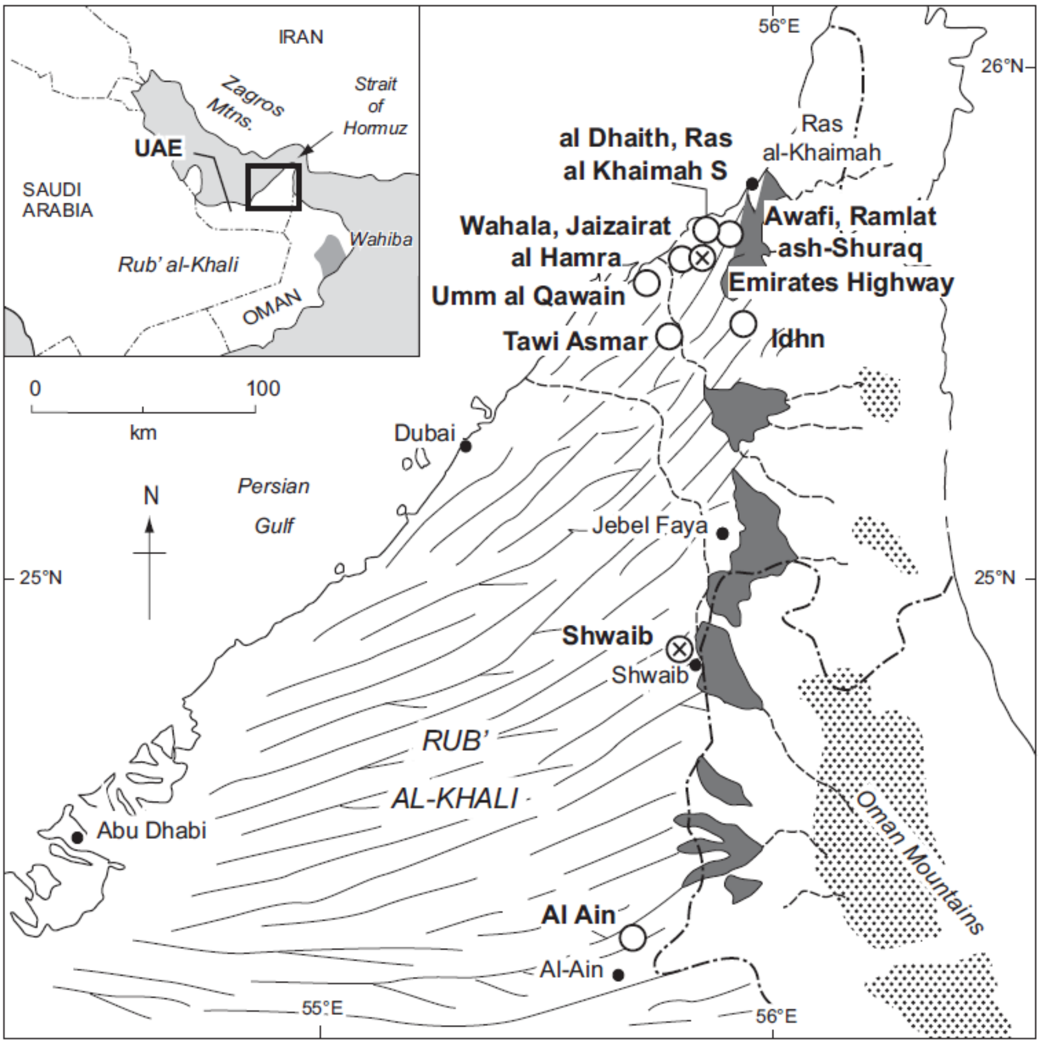

Figure 6.1: Map of the Arabian Peninsula and sample sites, from this paper (crossed symbols) and other studies. Sampled sites of previous dune dating studies in the southern Arabian Peninsula are from: Goudie et al. (2000) (Awafi, Idhn); Parker et al. (2004) (Awafi); Parker and Goudie (2007) (Al Dhaith); Atkinson et al. (2011; 2012) (Ramlat ash Shuraq, Wahala, Emirates Highway, Shwaib, Al Ain; Al Dhaith, Ras al Khaimah South, Al Jaizairat al Hamra, Umm al Qawain, Tawi Asmar, Al Ain); Chapter 4 (Emirates Highway, Shwaib). Adapted from Atkinson et al. (2011).

of the southern Arabian Peninsula (Figure 6.1). This region possesses important proxy data attesting to significant environmental changes during the Late Quaternary, relating to migrations of the inter-tropical convergence zone (ITCZ), which allowed the penetration of the southwesterly Indian Ocean summer monsoon (IOSM) into this presently arid area

(Fleitmann et al., 2011; Glennie and Singhvi, 2002). These significant climatic fluctuations may have led to hiatuses in dune accumulation, and provide a relatively well-known palaeoclimatic context to test the response of aeolian systems to fluctuating external forcing conditions. In addition, the internal structures of the dunes have been exposed as a result of quarrying for construction, allowing for assessment of dune chronologies utilising visible stratigraphic information (Chapter 4; Atkinson et al., 2011). The primary southwest-northeast linear ridges, up to 70 m in height, are overlain by partially vegetated secondary linear dunes, generally orientated northwest-southeast (Atkinson et al., 2012). OSL ages show that the dune forms do not represent distinct and separate palaeoclimatic phases, as the ages represented by them overlap, and a recent study suggests that the relationship between these dune generations is more complex than previously supposed (Atkinson et al., 2012).

The data analysed in this paper come from sites UAE11/1 and UAE11/2, taken from a dune next to a large sand quarry located off the Emirates Highway approximately 20 km southwest of the city of Ras al Khaimah. These are supplemented by datasets sampled in exposed quarry faces at the same location (UAE10/3) and at Shwaib (UAE10/1 and UAE10/2), presented in Chapter 4. For this study, the additional sampling was undertaken in March 2011 by 'blind' drilling, using a Dormer™ portable auger. Two cores were extracted from the same secondary dune, near the crest and near the interdune. This secondary dune was in turn located towards the crest of the underlying primary linear mega-ridge. Prior to sampling, water was poured into the dune in order for the sand to be consolidated enough to be augered without the hole collapsing. The samples were extracted at 0.5 m intervals using a stainless steel sampling head before being transferred to opaque plastic tubing, and capped and sealed. All containers and bags were lightproof. A total of 20 samples were collected; 14 from UAE 11/1 to a depth of 7 metres, and six from UAE11/2 to a depth of 3 metres.

6.2.1. Age calculation

For OSL dating, all samples were prepared according to the protocol outlined in Section 3.5.1 under subdued orange (585 nm) light in the OLDLAB. OSL measurements were conducted using standard Risø TL/OSL-DA-15 readers, following the single aliquot regenerative (SAR) protocol described in Section 3.5.2. Single aliquot OSL measurement was conducted using 470 nm stimulation at 160 °C (125 °C for samples UAE11/1/1 and UAE11/1/2). Zero-dose, recycling and IR depletion quality assurance ratios were incorporated into the measurement procedure, and only aliquots fulfilling these criteria within ±10% were included for age calculation (the majority lay within ±5%). Dose recovery results were within ±10% of the given dose for 93% of samples. Dose rates and final modelled ages (using OxCal) were calculated as described in Chapters 3 and 4.

6.3. Results and discussion

OSL ages presented in this paper and in other studies are displayed in Figure 6.2. Sedimentological analyses show that the sediments from both cores are relatively homogeneous, and are mainly composed of moderately well sorted, fine sand (Table 6.1). The ages for cores UAE11/1 and UAE11/2 are presented in Tables 6.2 and 6.3.

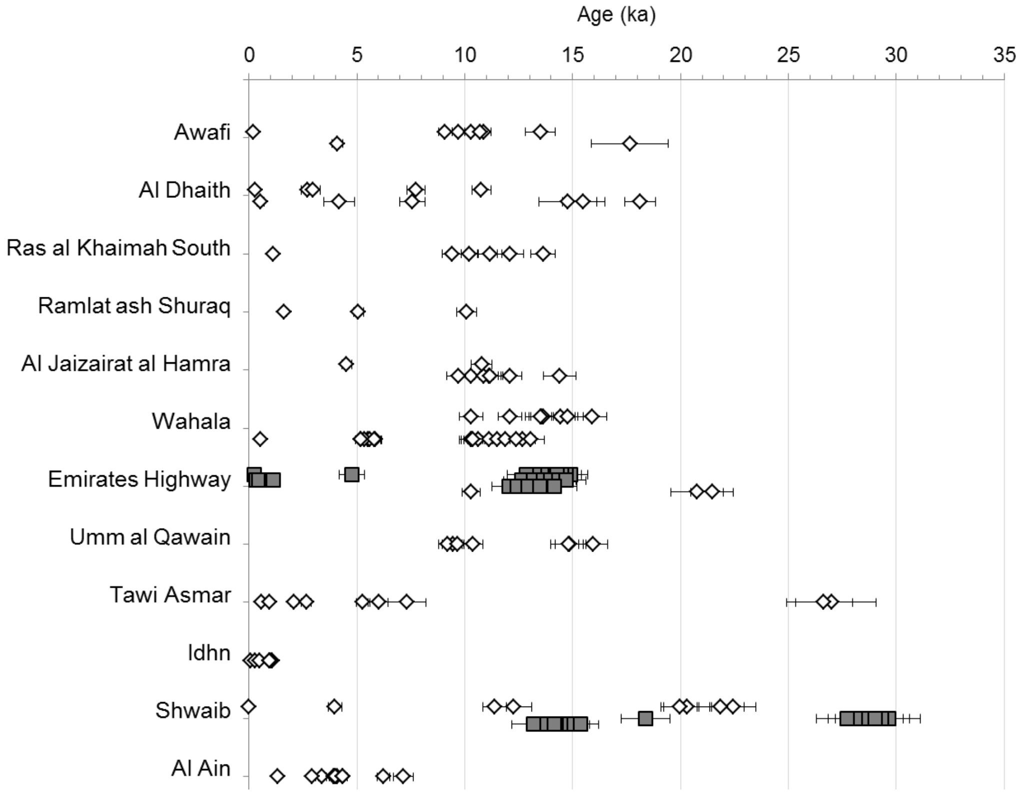

Figure 6.2: OSL dune ages from the southern Arabian Peninsula. The ages from this thesis (UAE10/1-3 and UAE11/1-2) are shown as grey squares. Ages from other published papers are from: Goudie et al. (2000); Parker et al. (2004); Parker and Goudie (2007); Atkinson et al. (2011; 2012). Site locations are shown in Figure 6.1.

Table 6.1: Sedimentology data. Munsell colour, particle size statistics and carbonate content based on loss of ignition (LOI) (Chapter 3).

Sample	**Depth (m)**	**Munsell colour**	**Mean particle size (µm)**	**Sorting (s.d.)**	**Skewness**	**Kurtosis**	**V. coarse sand (%)**	**Coarse sand (%)**	**Med sand (%)**	**Fine sand (%)**	**V. fine sand (%)**	**Silt (%)**	**LOI at 550 °C (%)**	**Carbonate content (%)**
UAE11/1/1	0.5	7.5 YR 5/8 SB	187	1.64	0.06	0.98	0.0	2.1	24.4	51.0	21.1	0.2	1.3	19.4
UAE11/1/2	1.0	7.5 YR 5/8 SB	178	1.49	0.01	0.95	-	0.1	20.1	60.3	19.5	-	1.0	19.3
UAE11/1/3	1.5	7.5 YR 5/8 SB	162	1.56	0.03	0.96	-	0.3	16.7	54.3	28.1	0.5	1.3	19.5
UAE11/1/4	2.0	7.5 YR 5/8 SB	164	1.58	0.04	0.96	0.3	0.6	17.5	53.0	28.0	0.6	1.4	18.2
UAE11/1/5	2.5	7.5 YR 5/8 SB	249	1.61	-0.04	0.94	-	6.5	44.0	41.6	7.9	-	1.2	17.9
UAE11/1/6	3.0	7.5 YR 5/8 SB	184	1.42	-0.01	0.95	-	-	19.8	66.1	14.1	-	1.2	16.4
UAE11/1/7	3.5	7.5 YR 5/8 SB	198	1.42	-0.01	0.96	-	0.1	26.1	64.1	9.7	-	1.3	16.9
UAE11/1/8	4.0	7.5 YR 5/8 SB	174	1.49	-0.01	0.95	-	-	18.6	60.5	20.9	0.1	1.4	17.4
UAE11/1/9	4.5	7.5 YR 5/8 SB	184	1.42	0.00	0.94	-	-	19.8	66.4	13.8	-	1.2	18.0
UAE11/1/10	5.0	7.5 YR 5/8 SB	180	1.39	0.00	0.95	-	-	16.7	69.6	13.7	-	1.3	17.4
UAE11/1/11	5.5	7.5 YR 5/8 SB	196	1.38	0.00	0.96	-	-	22.9	69.1	7.9	-	1.3	16.8
UAE11/1/12	6.0	7.5 YR 5/8 SB	187	1.55	-0.02	0.95	-	0.3	25.7	55.2	18.6	0.2	1.3	17.5
UAE11/1/13	6.5	7.5 YR 5/8 SB	171	1.49	-0.01	0.94	-	-	17.3	60.4	22.2	0.1	1.3	19.1
UAE11/1/14	7.0	7.5 YR 5/8 SB	173	1.52	-0.01	0.95	-	-	19.4	58.3	22.0	0.3	1.4	19.2
UAE11/2/1	0.5	7.5 YR 5/8 SB	184	1.51	-0.01	0.95	-	0.2	23.7	57.7	18.3	0.1	1.3	18.8
UAE11/2/2	1.0	7.5 YR 5/8 SB	240	1.47	-0.02	0.95	-	1.9	44.7	49.0	4.4	-	1.3	13.1
UAE11/2/3	1.5	7.5 YR 5/8 SB	192	1.47	-0.02	0.94	-	0.1	25.6	60.2	14.1	-	1.1	17.2
UAE11/2/4	2.0	7.5 YR 5/8 SB	195	1.42	0.00	0.96	-	-	24.5	65.0	10.5	-	1.2	16.6
UAE11/2/5	2.5	7.5 YR 5/8 SB	193	1.37	0.00	0.96	-	-	20.8	70.3	8.8	-	1.2	18.5
UAE11/2/6	3.0	7.5 YR 5/8 SB	194	1.39	0.00	0.96	-	-	22.6	67.9	9.6	-	1.0	18.0

Table 6.2: OSL data and unmodelled ages. Moisture content for all samples is taken as 5±3 %. n is number of aliquots measured, and OD is overdispersion. Unmodelled ages calculated in OxCal v.4.1 and 4.2.

Sample	**Depth (m)**	**n**	**D_e (Gy)**	**R-ratio**	**Zero-ratio**	**IR-ratio**	**OD**	**U (ppm)**	**Th (ppm)**	**K (%)**	**Effective cosmic dose (Gy/ka)**	**Dose rate (Gy/ka)**	**Age (ka)**
UAE11/1/1	0.5	14	0.49±0.05	0.97	-0.03	1.02	0.21±0.12	1.07±0.10	1.25±0.16	0.80±0.10	0.19±0.04	1.24±0.11	0.34±0.05
UAE11/1/2	1.0	34	0.63±0.04	1.00	0.01	0.96	0.21±0.05	1.02±0.09	1.25±0.16	0.83±0.11	0.18±0.02	1.24±0.11	0.45±0.05
UAE11/1/3	1.5	20	1.50±0.07	0.97	0.00	0.98	0.09±0.05	1.71±0.15	1.41±0.18	0.79±0.10	0.16±0.02	1.36±0.11	1.05±0.96
UAE11/1/4	2.0	14	1.47±0.13	0.91	0.01	0.98	0.24±0.08	1.08±0.10	1.47±0.19	0.84±0.11	0.15±0.01	1.26±0.11	1.11±0.14
UAE11/1/5	2.5	8	13.08±0.35	0.97	0.00	0.91	0.04±0.03	0.92±0.08	1.08±0.14	0.75±0.10	0.14±0.01	1.10±0.10	11.96±1.05
UAE11/1/6	3.0	16	16.54±0.78	1.00	0.00	0.96	0.16±0.04	1.06±0.10	1.20±0.16	0.87±0.11	0.13±0.01	1.25±0.12	13.37±1.30
UAE11/1/8	4.0	15	17.60±0.56	1.00	0.01	0.94	0.10±0.03	1.00±0.09	1.25±0.16	0.85±0.11	0.12±0.01	1.20±0.11	14.82±1.34
UAE11/1/10	5.0	12	16.37±0.77	0.98	0.00	0.94	0.12±0.04	0.92±0.08	1.03±0.13	0.88±0.12	0.10±0.01	1.18±0.12	13.96±1.40
UAE11/1/12	6.0	23	17.17±0.41	0.98	0.00	1.01	0.08±0.02	0.96±0.09	1.11±0.14	0.82±0.11	0.09±0.01	1.13±0.11	15.37±1.40
UAE11/1/14	7.0	12	17.53±0.83	0.96	0.00	0.95	0.14±0.04	1.42±0.13	1.50±0.20	0.84±0.11	0.08±0.01	1.26±0.11	13.94±1.31
UAE11/2/1	0.5	17	15.89±0.72	0.98	0.00	0.98	0.17±0.04	1.14±0.10	1.36±0.18	0.77±0.10	0.19±0.04	1.24±0.11	12.94±1.23
UAE11/2/2	1.0	16	15.66±0.74	1.00	0.00	1.00	0.15±0.04	1.19±0.11	1.37±0.18	0.92±0.12	0.17±0.02	1.37±0.12	11.51±1.09
UAE11/2/3	1.5	21	16.54±0.35	0.98	0.00	0.97	0.08±0.02	0.99±0.09	1.34±0.17	0.90±0.12	0.16±0.02	1.29±0.12	12.89±1.12
UAE11/2/5	2.5	14	16.99±1.13	0.97	0.00	0.97	0.23±0.05	1.28±0.12	1.17±0.15	0.89±0.12	0.14±0.01	1.31±0.12	12.99±1.37
UAE11/2/6	3.0	16	18.20±0.52	0.97	0.00	0.96	0.10±0.02	1.19±0.11	1.25±0.16	0.80±0.10	0.13±0.01	1.21±0.11	15.09±1.29

Table 6.3: OxCal (v.4.1 and 4.2) modelled ages. Samples UAE11/1-4 are not modelled as ages as they are already in relative chronological order. The 68.2% range is given for upper and lower modelled age limits.

Sample	D_e	Error	Unmodelled Age (ka)	Unmodelled Error	Modelled Mean age (ka)	Modelled Error	Modelled Upper limit (ka)	Modelled Lower limit (ka)	A_i	A_{model}
UAE11/1/5	13.08	0.35	11.96	1.05	12.65	0.86	13.60	11.94	95.5	105
UAE11/1/6	16.54	0.78	13.37	1.30	13.17	0.68	13.89	12.50	123.2	
UAE11/1/8	17.60	0.56	14.82	1.34	13.63	0.63	14.31	12.92	96.0	
UAE11/1/10	16.37	0.77	13.96	1.40	13.99	0.67	14.64	13.26	125.4	
UAE11/1/12	17.17	0.41	15.37	1.40	14.37	0.76	15.06	13.53	101.9	
UAE11/1/14	17.53	0.83	13.94	1.31	14.71	0.90	14.49	13.65	103.2	
UAE11/2/1	15.89	0.72	12.94	1.23	12.06	0.81	12.91	11.34	104.2	102.5
UAE11/2/2	15.66	0.74	11.51	1.09	12.44	0.69	13.17	11.78	91.9	
UAE11/2/3	16.54	0.35	12.89	1.12	12.95	0.64	13.60	12.29	121.3	
UAE11/2/5	16.99	1.13	12.99	1.37	13.47	0.73	14.11	12.66	117.3	
UAE11/2/6	18.20	0.52	15.09	1.29	14.16	1.03	15.00	12.93	94.3	

6.3.1. Localised variability of chronologies

The main aim of a sampling strategy is to capture dune-scale variability so that the chronology is an accurate representation of the underlying sedimentary structure. If this is achieved, the chronology can be understood as the 'true' preserved geomorphic response to environmental conditions at a specific time and place, and provides as close to a complete (although discontinuous) record as possible. The amalgamation of chronologies from different sites highlights a spatially varied geomorphic response, as also shown in other deserts (e.g. Cohen et al., 2010). Capturing this variability is important for the reasons given above, but raises interpretive questions regarding apparent contradictions in geomorphic response to particular climatic forcing conditions. Assuming that uncertainties are fully accounted for, these chronologies cannot be 'wrong', but instead describe a complex picture of geomorphic response and varying levels of sensitivity to a range of environmental factors rather than one directly traceable to a regional climatic signal; an issue that is further addressed in Section 6.3.4.

Figure 6.3 shows the dated cores and their sampling contexts from the Emirates Highway site, including the ages of samples from the exposed section UAE10/3 first presented in Chapter 4. The comparison of these samples from the same secondary linear dune, located within ~30 m of each other, provides a test of the reproducibility of these chronologies: when the same dune is sampled, can the same chronologies be extracted?

The age population of ~15-12 ka is identified at all three sites. Spanning a vertical interval of ~6 m at UAE10/3, this unit appears to be a pervasive feature of the dune accumulation history at this site. It is the variability in the presence of younger units within the three chronologies that highlights the possible structural differences between the sampled profiles. UAE10/3 yields ages of ~4.8 ka and ~0.2 ka within the top ~2 m of the dune (Chapter 4). At UAE11/1 ages of ~1.1, 0.5 and 0.3 ka are identified within this depth.

Whilst the top of the UAE10/3 section was sampled less systematically, and so it is plausible for the units identified in UAE11/1 to be present in the 1.5 m or 2 m intervals between samples 3/17-18 and 3/18-19 respectively, the core UAE11/1 was sampled at 0.5 m intervals; a frequently used interval in many coring studies. It is not possible to establish whether the unit dated to ~4.8 ka that is ‘missing’ between UAE11/1/5 and 1/4 is due to the narrow thickness of the sedimentary unit, or simply not being present at this specific location on the dune as a result of either localised non-deposition or erosion as part of the ongoing process of dune sediment transport and reworking. Variability of chronologies between different sampling profiles of the same individual dunes has also been shown in other studies (e.g. Telfer & Thomas, 2007) and supports the need for extensive sampling and where possible more than one sampling profile at each site, even with use of a 0.5 m vertical sampling interval. This is necessary in order to capture the variability that reflects

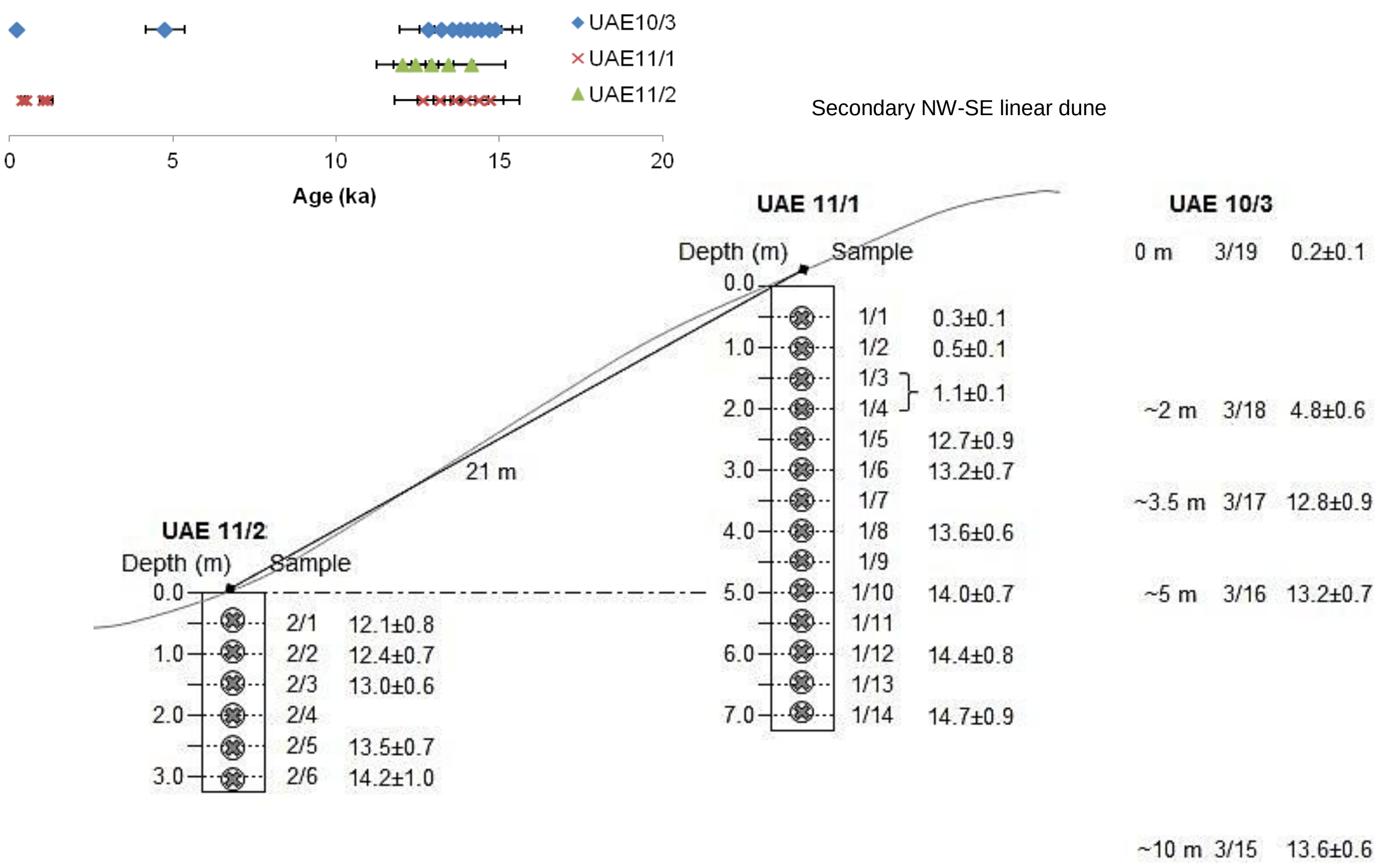

Figure 6.3: Sampling context and OSL ages (OxCal modelled, ka) at the Emirates Highway site.

the impact of spatially localised dune development processes and to distinguish this variability from the more pervasive units perhaps more indicative of externally forced changes in dune activity.

At UAE11/2 ages of ~15-12 ka are dated between 3 to 0.5 m depth. The lack of younger units can be interpreted as a result of either no recent aeolian deposition, or erosion of previously deposited units. We do not have enough information however to establish whether, if the ground surface does represent an erosional surface, the interdune has acted as sediment source for the proximal dunes, which would support the wind-rift hypothesis of linear dune development, or the material has been transported from further afield.

The lack of younger ages at the interdune site has implications for the interpretation of chronologies from complex dune systems. The complexity of the sedimentary structures underlying the megaridge/secondary dune system can be seen in dune exposures (Figure 6.4). Towards the top of the megaridge structures perpendicular to the orientation of secondary linear dune trough cross-stratification is dominant, indicating the importance of secondary features in the formation of the resulting complex feature (Chapter 4; Bristow et al., 2000). The patterns of crest-interdune chronological variability are therefore potentially important when sampling these structures at great depth. Effectively, the complex structure is composed of the superimposition of dune forms over thousands of years, whilst sampling location is chosen carefully to reflect more recent dune processes (i.e. those visible in geomorphic form at the surface). There is no reason to doubt that the variability present in the surficial sediments also occurs throughout the megaridge sedimentary structure during the period when secondary dunes have been present. This may account for some of the variability in chronologies. Sampling several profiles of complex structures is therefore important in order to minimise the potential impact of this localised variability upon the dune chronology.

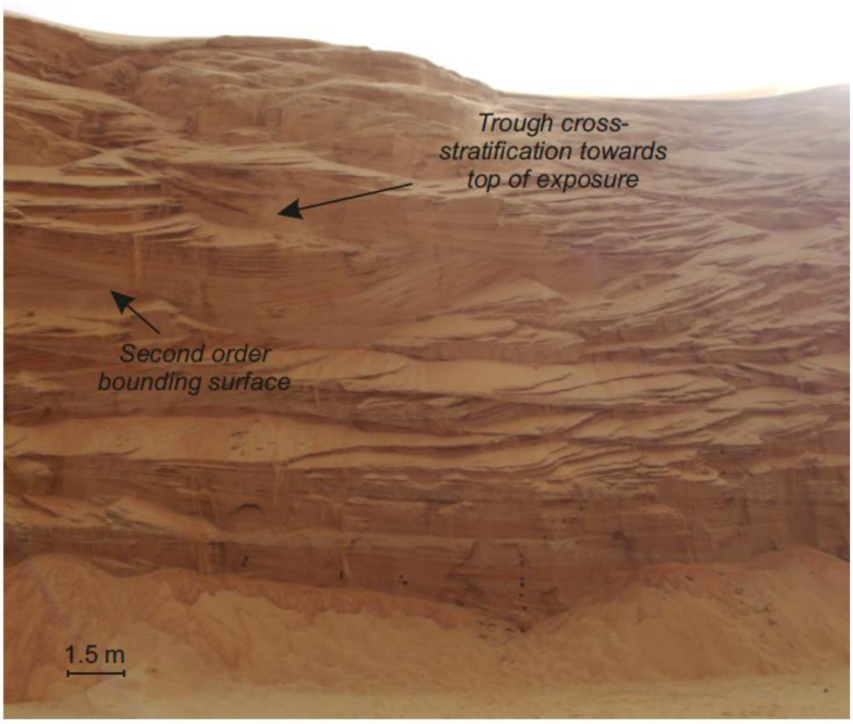

Figure 6.4: Dune exposure at Shwaib (UAE10/1). Scale is approximate.

In an assessment of the dunefield as a whole, it is clear that there is a great deal of variability between the different records (Figure 6.2), particularly within the late Holocene, indicating that localised influences play a dominant role in producing resultant sedimentary structures. After ~6 ka there are periods of rapid deposition at Wahala (~6-5 ka), Al Ain (~4-3 ka), and Idhn (<1 ka) (Atkinson et al., 2011; Goudie et al., 2000a). Lake sedimentation was recorded at Wahala from ~8.5 cal. ka BP (Preston and Parker, unpubl. in Preston et al., 2012), and shows a period of aridity at 5.9-5.1 cal. ka BP alongside evidence of increased dune mobility (Preston et al., 2012). This arid phase may therefore have seen the mobilisation of a larger supply of sediment that could have then been preserved during the wetter phases of climatic fluctuations, such as between 5.1-4.1 cal. ka BP (Parker et al., 2006; Preston et al., 2012). Idhn and Al Ain are located further south, where sediments derived from the Persian Gulf, the supply of which was cut off following the late glacial as sea level rose, may be less important. Therefore a wider sediment source area may have allowed the accumulation and preservation of thicker units in the mid-late Holocene. In addition, they are also located towards the northeastern edge of the sand sea, closer to the Oman Mountains, and the relatively high moisture levels at these sites may have allowed for greater preservation of accumulated units during brief periods of increased aridity, as inferred by Goudie et al. (2000a). Localised chronological variability is therefore evident, and possible reasons for inter-site differences have been put forward for these cases.

The above discussion of chronological variability at a range of scales indicates the importance of sampling a number of profiles using a narrow vertical sampling interval. The relative importance of requiring many samples from multiple profiles is site-dependent, as accumulation and preservation potential are spatially and temporally variable. However, the site specific nature of accumulation is only known once samples have been dated, and hence it is important to sample sufficiently at the initial fieldwork stage. The persistence of the ~15-12 ka age population across multiple profiles in comparison to the variability of younger units reflects this, as the sedimentary units of different ages display varying levels of prominence across multiple dated cores. Where sets are narrow, it is unlikely that all of the units present will be sampled and therefore more samples are required. In practice, these findings call for a cautious sampling strategy where logistics allow, potentially incorporating the use of portable readers or range-finder methods. These techniques may allow for a quick and cheap method for obtaining lots of ages to initially identify chronostratigraphic units, which can be dated precisely using usual full OSL dating protocols. Chapter 4 shows that assumptions of the chronological significance of bounding surfaces in order to 'target' samples are not necessarily valid. This strategy is particularly important for complex dunes, where sub-surface spatial variability may be significant.

There are several periods within the amalgamated northeastern Rub al' Khali dataset for which interpretation of aeolian activity is limited due to insufficient sampling resolution.

The compiled 30 ka record from Shwaib is from three sampled exposures and indicates periods of accumulation at ~29-27, 23-18, 15-11 and 4 ka (Chapter 4; Atkinson et al., 2011). Taking account of the individual profiles used to construct this combined chronology, the hiatus between 17-16 ka is between samples from different sampling profiles rather than from a single core, and could be a function of sampling. Thus, despite this small part of the northeastern Rub' al Khali being relatively well-dated, with numerous recent studies using multiple sites and small vertical sampling intervals where possible (e.g. Chapter 4; Atkinson et al., 2011, 2012), interpretation is still limited by insufficient sampling coverage. Interpreting ages in tandem with acknowledging gaps in the record is therefore an important approach for assessing if more samples are required and focussing future research. In order to produce the best estimate of the unknown distribution (i.e. the complete preserved sedimentary record) as many samples as possible are needed with the data presented in an appropriate way; to be discussed in the following section.

6.3.2. Data display

Given the issues discussed in the preceding sections, consideration of data representation and display is important in order to avoid the propagation of misleading assumptions. Ages from multiple studies are often combined and interpreted using frequency-based distributions, such as histograms or probability density functions (PDFs) (e.g. Telfer and Thomas, 2007). A criticism of this approach is that it introduces a bias towards dated units that have been sampled more frequently. Only if sampling location was chosen at random might this approach reflect the nature of the deposited record. Peaks in such PDFs therefore do not necessarily truly reflect the dunefield environmental history. Figure 6.2 shows data from this study and other published regional records, the sites of which are shown in Figure 6.1. Similarly, whilst Figure 6.2 displays and emphasises the variability in ages between sites, to facilitate the identification of patterns in the data emphasis is implicitly placed upon the presence/absence of ages rather than potentially more useful metrics such as the amount of accumulation. Alternative interpretations can be made from the total dataset depending on the scale of analysis. Localised processes can be emphasised by focusing on the uniqueness of each individual site chronology. No chronology of dune accumulation at one site records the same response to forcing as another, and hence each record could be assessed individually as the result of its specific context. In an assessment of the dunefield as a whole, throughout the last 30 ka there has almost always been recorded activity somewhere within the dunefield, but identifying and correlating discrete events is problematic. Figure 6.2 retains the individual site chronologies within the total dataset, highlighting the need to synthesise chronologies whilst retaining the ability to consider localised contexts. In this synthesis, consideration of sampling approach and resolution is also required, such as sampling interval and incorporation of stratigraphic information. Whilst issues of discontinuity remain problematic, incorporating depth information (i.e. net accumulation rates) in data display is potentially more meaningful than relying solely upon frequency of occurrence.

The net (vertical) accumulation rate represents the average rate (m ka^{-1}) that a preserved depth of sediment was deposited at assuming continuous accumulation. This assumption is of course unlikely to hold true, and hence the net accumulation rate masks periods of potentially rapid accumulation interspersed with periods of non-deposition or erosion. A method for calculating net accumulation rate is represented in Figure 6.5, and results from application of this method are shown in Figure 6.6 and Table 6.4. Each bar in Figure 6.5b (A, B and C) represents a distinct age grouping in one sampling profile within which the ages overlap within their uncertainties (Figure 6.5a). The groups are a function of dating precision and sampling interval. Figure 6.5 summarises two methods for calculating the net accumulation rates. The *'as sampled' net accumulation rate* (Figures 6.5c and 6.6b) is the minimum depth spanned by a group of samples, treated as 0.05 m for individual samples

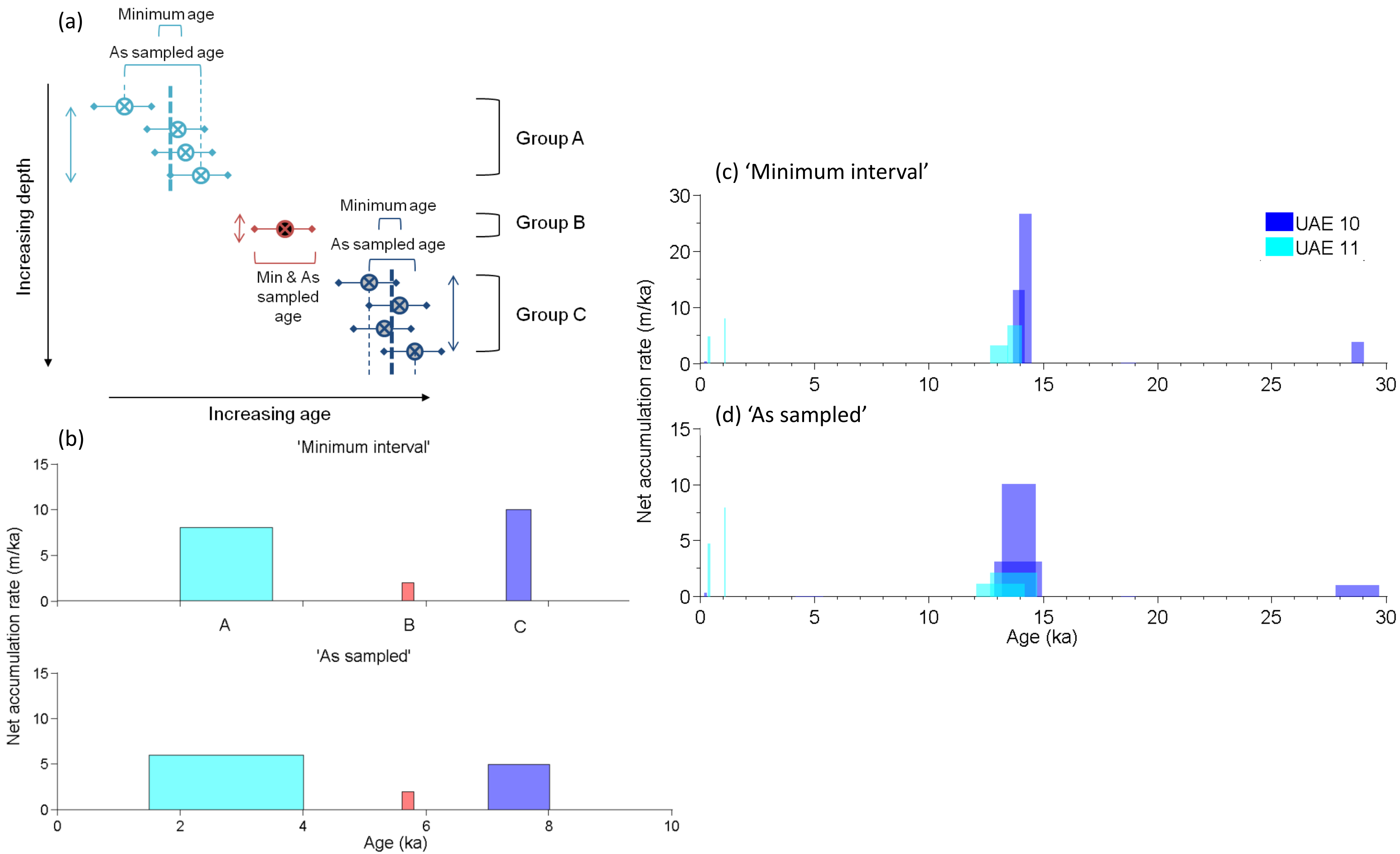

(a)
Minimum age
As sampled age
Group A
Group B
Minimum age
As sampled age
Min & As sampled age
Group C
Increasing depth
Increasing age
(b)
'Minimum interval'
Net accumulation rate (m/ka)
A
B
C
'As sampled'
Age (ka)
(c) 'Minimum interval'
UAE 10
UAE 11
(d) 'As sampled'
Net accumulation rate (m/ka)
Age (ka)

Figure 6.5 [previous page]: Method of net accumulation rate calculation. An example of the (a) sample grouping and (b) presentation of net accumulation rates. In (a), age intervals are indicated by horizontal brackets ('minimum interval' and 'as sampled'), minimum depth intervals are represented by double-headed vertical arrows. The net accumulation rate = depth interval/age interval. The width of the bar in (b) is equal to the respective age interval used and the height of the bar is equal to the respective net accumulation rate. (c) 'Minimum interval' and (d) 'as sampled' net accumulation rates, calculated using UAE10 and UAE11 samples (shown in Table 6.4).

Table 6.4: Calculation of net accumulation rates. Ages are divided into age groups, represented in Figures 6.5c and d by the light blue bars. The weighted mean is calculated for each age group, and plotted as the centre of each bar. The 'as sampled' and 'minimum interval' net accumulation rates are calculated by dividing the depth between the samples by the age interval and minimum age interval (the weighted standard error of each group multiplied by two) respectively.

Sample	**Age (ka)**	**Error**	**Age group**	**Weighted mean**	**Oldest age**	**Youngest age**	**Age interval**	**Minimum age interval**	**Depth (m)**	**As sampled rate (m/ka)**	**Minimum interval rate (m/ka)**
UAE11/1/1	0.34	0.05	1	0.40	0.45	0.34	0.11	0.11	0.50	4.72	4.72
UAE11/1/2	0.45	0.05									
UAE11/1/3	1.05	0.10	2	1.07	1.11	1.05	0.06	0.06	0.50	7.94	8.55
UAE11/1/4	1.11	0.14									
UAE11/1/5	12.64	0.84	3	13.73	14.71	12.64	2.07	0.56	4.50	2.17	8.08
UAE11/1/6	13.17	0.68									
UAE11/1/8	13.63	0.63									
UAE11/1/10	13.99	0.67									
UAE11/1/12	14.37	0.76									
UAE11/1/14	14.71	0.90									
UAE11/2/1	12.06	0.81	4	12.91	14.16	12.06	2.10	0.64	2.50	1.19	3.91
UAE11/2/2	12.44	0.69									
UAE11/2/3	12.95	0.64									
UAE11/2/5	13.47	0.73									
UAE11/2/6	14.16	1.03									

(similar to a sampling tube diameter), divided by the time interval between the mean ages of the oldest and youngest samples within each age group, or the upper/lower bounds as defined by two sigma for individual samples. The '*minimum interval' net accumulation rate* (Figures 6.5b and 6.6a) is the minimum depth interval as defined above (see also Figure 6.5), divided by the minimum time interval, taken as twice the weighted standard error of the group of ages or two sigma for individual samples when Galbraith's (2003) homogeneity test indicates similarity (otherwise, the 'as sampled' time interval is used). Mean ages are used to calculate age intervals and age uncertainties are not included. This is because the mean represents the most likely age of burial for each sample, rather than the less probable tails of the age distributions. Uncertainties are therefore not fully shown using this method and this should be considered in interpretation. However, as bars are made up of the ages within a single profile which overlap within uncertainties, those with larger errors are likely to be in bigger groups and hence have lower net accumulation rates.

The 'minimum interval' net accumulation rate allows the most precise identification of possible time periods of accumulation (within dating precision limits), which can be used as the optimum potential geomorphic signal. The 'as sampled' rate assumes more gradual accumulation. The '*maximum' net accumulation rate* is presented in Figure 6.7. This is the maximum depth that could potentially represent the same age of burial divided by the minimum time interval. It therefore includes unsampled sediment between age groups. A 'cut-off' depth has been used when calculating the 'maximum' depth of accumulation in order for the chronological intervals of the age groups depicted in the graphs to be indicative of significant accumulation rather than insufficient sampling resolution: 5 m between different age groups from the same profile/core and 0.5 m between the youngest age group and the surface. These intervals are arbitrary, in this case chosen in response to the vertical sampling resolutions used in previous research in this region. Increasing the vertical resolution of sampling in future research would help reduce these intervals.

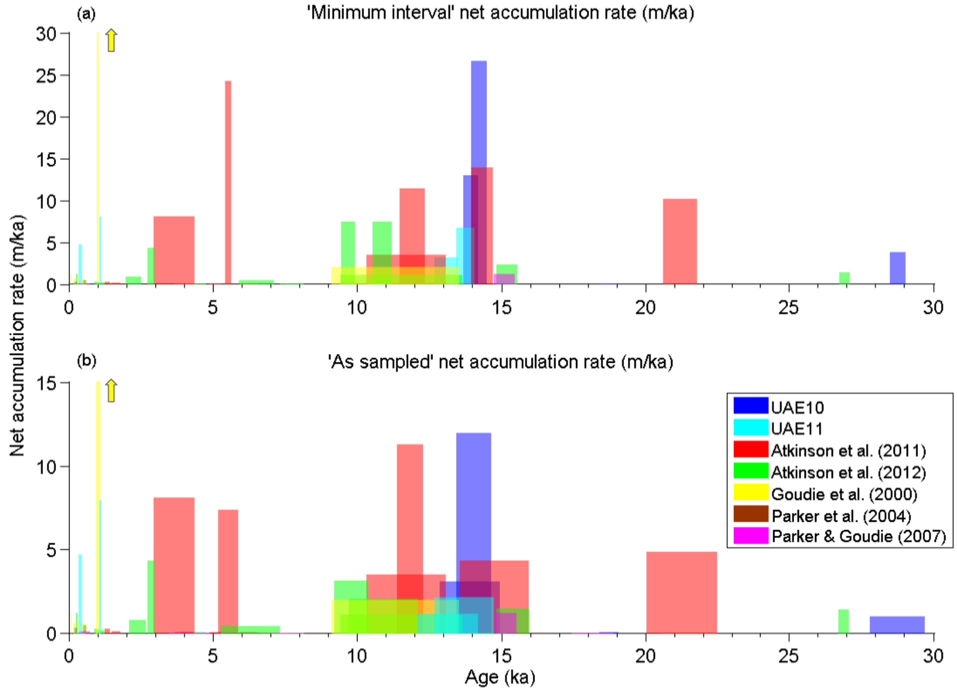

Figure 6.6: Change in net accumulation rate over time: (a) 'minimum interval' net accumulation rate; (b) 'as sampled' net accumulation rate.

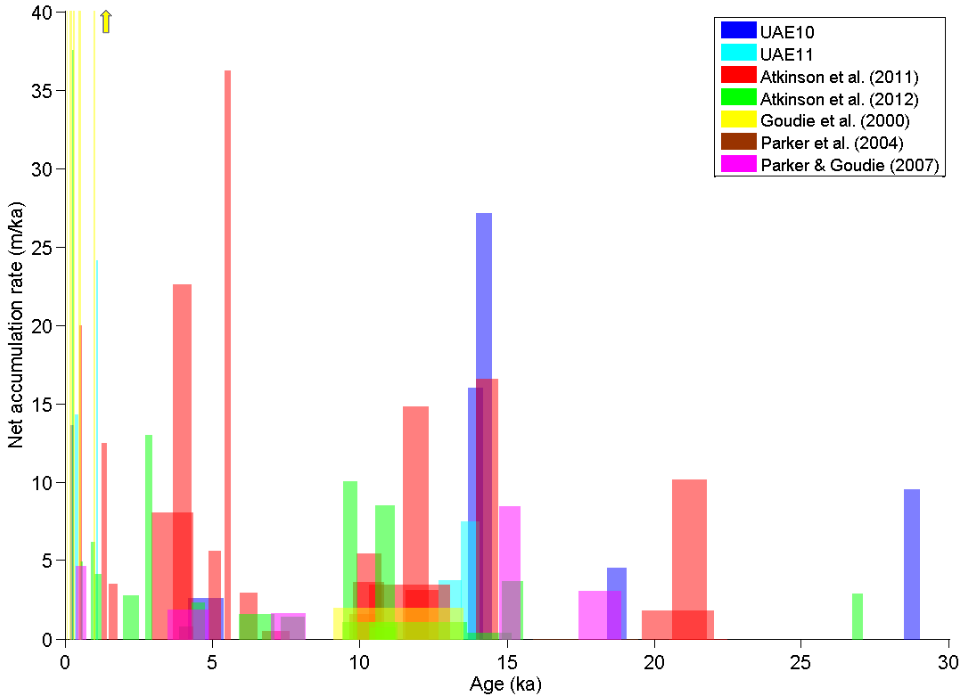

Figure 6.7: Change in 'maximum' net accumulation rate over time.

Comparison of these different graphs can be used to assess whether sampling interval is sufficient (maximum vs minimum interval) and the importance of the assumption of gradual vs contemporaneous accumulation (minimum interval vs as sampled).

The ‘as sampled’ rate is perhaps the most useful in identifying periods of regional activity, as the ‘maximum’ net accumulation rate includes unknown information whilst the ‘minimum interval’ assumes instantaneous deposition, which may be unlikely. If there are large differences between the graphs, it may suggest that the assumptions in net accumulation rate calculation are important in determining the final output, and therefore that sampling resolution or precision of dating may be inadequate. To assess which is the more likely explanation, consultation of original studies is recommended. It should be emphasised that the biggest bars are not necessarily the most important, as dating precision and sampling resolution play a role in determining both their height and width.

Figure 6.6 shows the variation in net accumulation rate over time by incorporating associated depth information with ages from sites in the northeastern UAE (Chapter 4; Atkinson et al., 2011, 2012; Goudie et al., 2000a; Parker et al., 2004). Whilst not negating the issue of sampling frequency completely, this method of data display incorporates additional information of the depth of units sampled. At individual sampling sites this places more emphasis on the thickness of units rather than sampling frequency. Displaying the age groups separately allows for overlapping of bars when similar ages are found at multiple sites indicating regional accumulation, which is potentially a more useful tool for interpretation than the absolute rates. Temporal variations in the climatic-geomorphic relationship and a reduction in preservation potential with age are incorporated, and so comparison of the absolute values in accumulation rate at different periods of time is not necessarily meaningful in terms of comparing aeolian activity directly. Telfer et al. (2010) have noted an approximate power-law decay in frequency of preservation with time. This relationship is also visible in Figures 6.6 and 6.7; the highest rates are all recorded in the last ~1 ka and there appears to be a reduction in net accumulation rate with increasing age. This is a result of the lower precision of the older ages, leading to calculated rates using larger age groupings. Wider age intervals inevitably produce lower accumulation rates, even if the underlying processes occurred at similar rates, and therefore is a signal overlying true changes in rate. It is also possible that where larger standard errors produce larger age groups, more periods of erosion may be incorporated, resulting in lower net accumulation rates but wider age intervals. It is the temporal positioning of the peaks and troughs therefore that is of most interest. If the relative positioning of the peaks and troughs remains consistent with increasing numbers of samples, the sample dataset might be interpreted as a representative reflection of the total population. It has long been recognised that sedimentary sequences are composed of “more gaps than record” (Ager, 1973), and hence stratigraphy has been described as fractal (Miall, 2012). Calculated accumulation rates are therefore scale-dependent and not generalisable (Miall, 2012). Again, it is emphasised that the absolute values of the calculated net accumulation rates should be interpreted with caution, as they represent *net* accumulation rates including periods of erosion, not continuous periods of accumulation and preservation.

Figure 6.8 displays the same data using a PDF and allows a direct comparison of these two methods of representation. At ~30 ka, accumulation appears to be of similar significance to that at ~5 ka, despite only two sites being dated to this time period. The peak in accumulation between ~16-9 ka is clear, and, as in Figure 6.6a, the accumulation is centred on two peaks with a period of potentially lower accumulation rates at ~12 ka. Whilst the early Holocene reduction in accumulation is identifiable in the PDF, the hiatuses in general appear less obvious, particularly between ~20-16 ka. The peaks at ~5 ka are also identified in both graphs, but smoothing of the data in the PDF obscures the more variable nature of accumulation in the late Holocene, when the highest net accumulation rates are all recorded.

The visibility of multiple age groupings as separate bars allows for a more thorough assessment of the significance of ages across multiple sample sites, which is not possible using a PDF. The PDF presents data in a less transparent way than the graphs of net accumulation rate, which we argue to be a more useful method of data display due to the additional information they are able to convey.

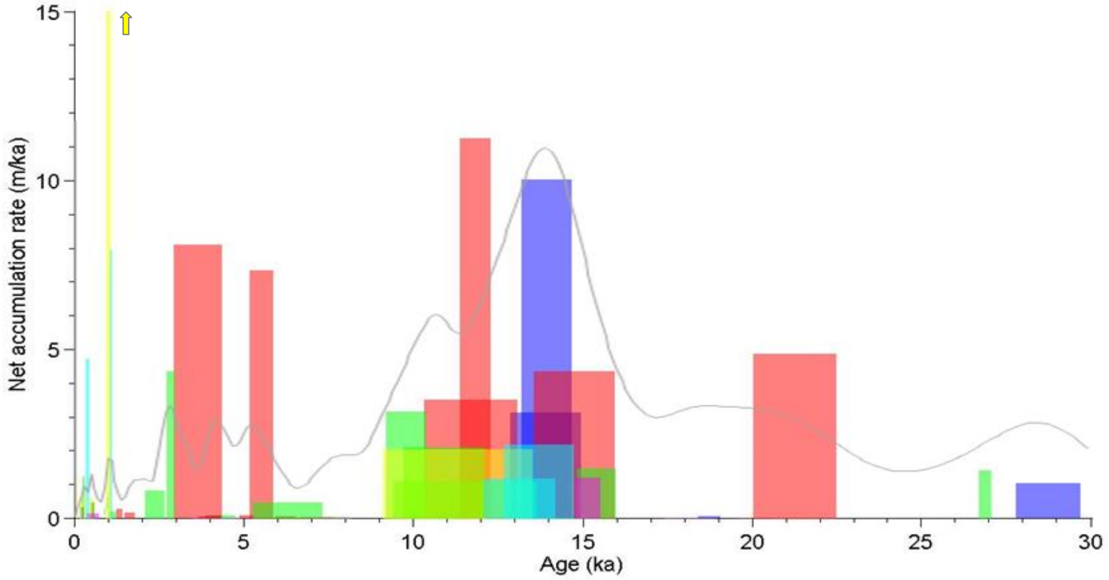

Figure 6.8: A probability density function (PDF) overlying the 'as sampled' net accumulation rate (Figure 6.6b). Constructed using 228 datapoints and normalised to the standard error (peaks represent the frequency of ages). Key as in Figure 6.6.

6.3.3. Interpretation of chronological hiatuses

As indicated in Section 6.3.1, there are chronological hiatuses that cannot be interpreted in a meaningful palaeoenvironmental context because of insufficient sampling resolution. Where hiatuses are tightly constrained by sampling however, a pertinent question is whether inferences can be made as to whether this represents a reduction in accumulation (which may be due to a number of environmental reasons), or an erosional event?

A bounding surface at Shwaib (UAE10/1) separates two samples ~1 m apart dated at 27.5 ka and 18.2 ka (Chapter 4), but in between these periods units at other sites have been dated at ~22-20 ka (Emirates Highway) and ~23-20 ka (~12 m deposition recorded in a separate record at Shwaib: Atkinson et al., 2011). Specific hiatuses are unlikely to be indicative of inactivity when many metres have been deposited at the same time at other sites in such close proximity; synthesising records is therefore crucial in order to see beyond these localised responses to environmental conditions. Chapter 4 showed that the presence of bounding surfaces cannot be easily interpreted in terms of chronological significance. These comparisons further suggest that the presence of a bounding surface that is tightly constrained chronologically within one profile does not allow for the extrapolation of the assumption of that surface's presence and representativeness of the same chronological interval within other profiles. Sedimentary surfaces that represent regional breaks in dune activity, i.e. sequence boundaries (Kocurek et al., 1999), are more likely to be persistent across multiple profiles than those caused by erosional events, which may be a result of localised processes. Distinguishing these surfaces has proved difficult in this part of the Rub al' Khali, and may be problematic in dry aeolian systems more generally where identifiable stratigraphic features other than bounding surfaces, such as palaeosols, are not present.

At the individual profile level, hiatuses can be interpreted in terms of representing localised rather than regional erosion or non-deposition. With rigorous vertical and horizontal sampling and consideration of depth and stratigraphy in data analysis, there can then be an assessment of whether chronological hiatuses are present persistently in a synthesis of results. Figure 6.6 indicates that there do appear to be periods of reduced accumulation regionally at ~26-23, 20-16, and 9-7 ka. The shared nature of this accumulation pattern from a number of studies and sites is indicative of a regional environmental constraint upon dune accumulation and/or preservation at these times. Although Section 6.3.1 shows that 17-16 ka cannot be extracted from sampling strategy at Shwaib, the lack of ages of this period at other sites representing a significant accumulation rate and the abruptness of transition from a period of rapid accumulation ~16-9 ka, indicates a reduction in accumulation rate during this period. The older the samples, the more difficult it will be to infer whether hiatuses are regionally significant given the sampling bias towards younger ages. The persistence of the peaks and troughs of Figure 6.6 with increasing addition of OSL ages would indicate that it is representative of the dunefield geomorphic history. Once the regional geomorphic record has been established, the next question is what do the peaks and troughs represent in terms of palaeoenvironmental change?

6.3.4. Extracting a climatic signal from a geomorphic signal

The establishment of a preserved geomorphic signal may then allow for a climatic signal to be derived. A period of significant accumulation between ~16-9 ka is prominent in Figure 6.6: at almost all sites there is accumulation (Figure 6.2), with some sites showing high accumulation rates. Whether this period is composed of two foci of accumulation at ~14 and ~12-11 ka and a period of lower accumulation rates at ~13 ka, indicated in Figure 6.6a, will require further investigation. Interestingly this period aligns with the presence of undated lacustrine deposits at Awafi (Parker, 2009), and is prior to, and perhaps contemporaneous with, the onset of the Younger Dryas.

Whilst a broad period of accumulation has been identified, there may have been similar periods of aeolian activity at other times not preserved to such an extent, perhaps due to a lower availability of sediment, deposition over a shorter period of time leading to a lower total thickness of deposited sediment, or the following environmental conditions being less conducive to preservation. The issue of preservation therefore requires consideration when assessing the significance of an extended period of accumulation in comparison to the rest of the record. In this case, there can be cause for optimism in that extended accumulation between 16-9 ka can be identified, but this does not provide certainty over its relative importance in comparison to other times in the dunefield's development history.

A paucity of OSL ages between ~9-6 ka aligns with an established humid period in the region as a result of the incursion of the IOSM (Fleitmann et al., 2007; Parker et al., 2006). There is presumably overlap in response to the influence of the IOSM between the different archives, further complicated by local contexts; the nature of these relationships requires further investigation but is beyond the scope of this paper. There are dated units of accumulation within this period, and it is known that there was activity during this time from dune material identified within lacustrine sediments (Parker et al., 2006; Preston et al., 2012).

Figure 6.9 shows the changes in 'as sampled' net accumulation rate at the different sites across the northeastern Rub' al Khali. The presentation of the regional OSL dataset in this way highlights the uniqueness of each individual site record. Tawi Asmar (Figures 6.1 and 6.2) has a particularly unusual chronology in comparison to others from the region; there are no dated sediments between ~25-8 ka and then accumulation is recorded at ~7-5 ka (Atkinson et al., 2012). It is the most centrally located of the field sites within the sand sea, and more arid due to the increased distance from the coast and mountains (Glennie, 1998). This relative aridity may have meant that the incursion of the IOSM had less of a stabilising influence; the dunes could have been more prone to reactivation than the other sites, whilst increased moisture brought by the IOSM may have allowed for more preservation than in the preceding period. Periods of aridity have been noted in the speleothem and lacustrine records, including at ~8-7.8 and 7.5-7.2 ka (Fleitmann et al., 2007; Preston et al., 2012), and this site may have been sensitive enough to respond to these fluctuations. More samples within the sand sea in more central locations are needed in order to investigate these differences further, and to assess whether these factors can be incorporated into the choice of sampling locations at the planning stage of fieldwork.

Figure 6.9 [Next page]: 'As sampled' net accumulation rate over time divided by site location. Key as in Figure 6.6.

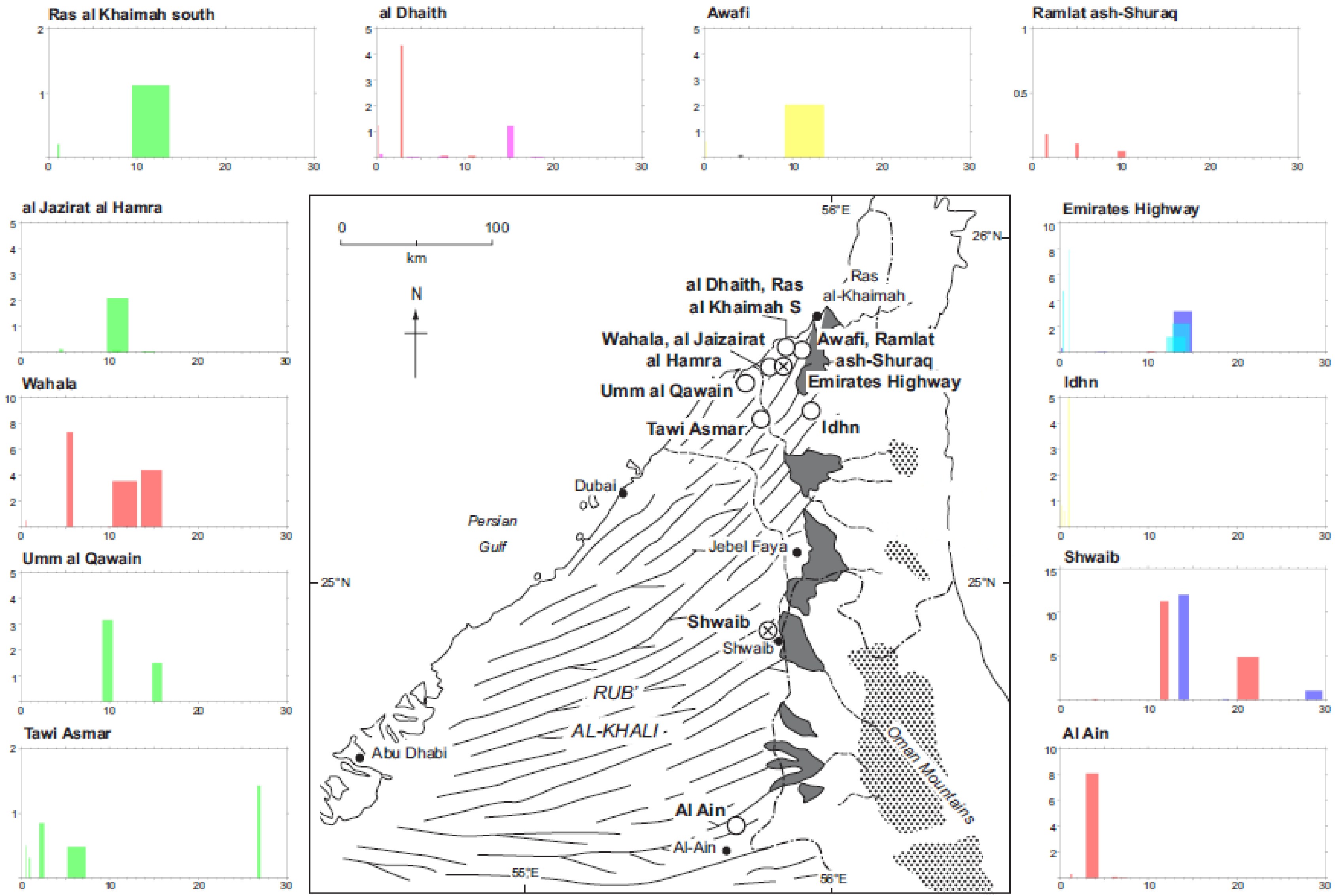

Ras al Khaimah south
al Dhaith
Awafi
Ramlat ash-Shuraq
al Jazirat al Hamra
Wahala
Umm al Qawain
Tawi Asmar
Emirates Highway
Idhn
Shwaib
Al Ain
0
100
km
N
56°E
26°N
25°N
55°E
al Dhaith, Ras
al Khaimah S
Ras
al-Khaimah
Wahala, al Jaizairat
al Hamra
Awafi, Ramlat
ash-Shuraq
Emirates Highway
Umm al Qawain
Tawi Asmar
Idhn
Dubai
Persian
Gulf
Jebel Faya
Shwaib
RUB'
AL-KHALI
Abu Dhabi
Al Ain
Al-Ain
Oman Mountains

Identified periods of reduced net accumulation rate require interpretation in order to infer whether this is a result of reduced activity or lack of preservation potential. Independent proxies can aid in this interpretation, and differentiate between environmental conditions which are represented similarly in the geomorphic signal. For example, the early Holocene can be inferred as a period of reduced activity, compared to the late Pleistocene hiatuses which are more likely due to reduced preservation potential, and potentially align with the Younger Dryas and Heinrich events. Corroboration with other proxies is essential, and dunes as archives cannot be used alone to infer forcing conditions given their complexity.

In the mid-late Holocene following the southward migration of the IOSM, there are significant spatial differences in net accumulation rates. As these are young ages, this is unlikely to be due to sites not being sampled, and more likely due to units of reduced thickness in comparison to those deposited during the late Pleistocene. Comparison of Figures 6.6b and 6.7 shows that a large number of young ages have been sampled, but there are few groups that span a significant ‘as sampled’ depth. One possibility is that this may be due to the differences in the quantity of sediment that accumulated during these respective periods of activity. It is inferred that the lack of sedimentary structure within some Holocene sediments (Chapter 4; Atkinson et al., 2012) is a result of thinner deposited units that can be more effectively reworked. During the late Pleistocene the upper dune sediments may have been subject to similar reworking processes, but a larger volume of underlying sediment, or more continuous depositional events, allowed for greater preservation of structure as proportionally less was reworked. This is supported by the nature of the less structured section in UAE10/3, for which there is not a clear structural or chronological transition, as the base has been dated to pre-Holocene (Chapter 4). Less structured sections appear to be thinner chronological units. It is unclear whether the generally thicker units during the late Pleistocene relative to the Holocene were a result of greater sediment supply, transport capacity, and/or reduced sediment availability. The temporal scale of the variation in these processes is unclear; the less structured unit could either represent periods of rapid accumulation which was then persistently reworked, or the depositional and reworking processes may have occurred gradually. As a result of reduced unit thicknesses, external forcing signals may be more difficult to extract from reworking processes.

From the amalgamation of datasets, distinct periods of regional aeolian accumulation can be identified. Interpretation of these characteristics requires corroboration with other datasets, but the records provide a unique perspective by providing a signal of geomorphic response to environmental influences. The nature of the relationship between climatic forcing and geomorphic response is complex and both spatially and temporally variable. There are immediate and broader local and regional factors that may be the cause of a preserved depositional event (Cohen et al., 2010), and hence recognising this variability is essential. If a regional pattern can be discerned and differences explained in terms of local context, as indicated in this part of the Rub' al Khali, the regional dune chronology may be related to forcing conditions in order to establish a regional signal, in addition to the local record of terrestrial response to environmental variability that more generally dunes represent. Some (parts of) dune records are inherently more useful for inferring information of past climatic change than others. In some cases, inferences regarding climatic forcing may be possible (e.g. Roskin et al., 2011), whilst in others local variability may mask any climatic signal. A more thorough assessment of these issues is required in order to improve understanding of the relationship between climatic change, environmental variability, and terrestrial (and dune) response.

6.4. Conclusions

A number of issues have been raised regarding the reproducibility of chronologies at a range of spatial scales in the Rub' al Khali, with important wider considerations for OSL sampling and interpretation.

Chronological profiles reflect localised responses to environmental variability and climatic forcing at both the dune and dunefield scales, highlighted by the presence/absence of units and hiatuses at different sites. Chronological variability identified in surficial sediments is also likely to occur throughout large complex dune structures. Amalgamation of datasets is required in order to allow for regional interpretations that can make inferences beyond this localised response. There is also no simple answer to how many samples are required, as this will vary both spatially and vertically within the dune system. There are however an increasing availability of methods to allow practical steps to increase the number of samples that can be extracted and dated. Extracting cores using narrow vertical sampling intervals at multiple locations across a dune is a thorough starting point. In data presentation and interpretation, and for the calculation of net accumulation rates, narrow sampling intervals constrain any underlying assumptions.

Displaying ages as net accumulation rates, and incorporating depth, stratigraphy, and sampling strategy within discussions of the interpretations of ages, may provide a more informative and less misleading approach of analysing and presenting dune OSL chronologies.

Erosional bounding surfaces representing large chronological hiatuses are identified at some, but not all, sites. This highlights the requirement for dating multiple profiles, which may be used to distinguish hiatuses caused as a result of localised factors and those due to regional forcing. Regional amalgamations of chronologies require more rigorous sampling in order for conclusions to be made regarding the nature of hiatuses in the chronological record.

For well-sampled dunes and temporal periods, conclusions regarding the regional significance of aeolian accumulation can be made when corroborated by independent proxies. Three distinct periods in the southern Arabian Peninsula have been identified within the last ~16 ka: regional accumulation ~16-9 ka; a reduction in accumulation associated with the incursion of the IOSM ~9-7 ka; followed by an increase in aeolian activity with more notable spatial variability of the chronologies until the present day. Hypotheses suggesting the importance of local context are raised to address the reasons behind why sites not aligned with this pattern show different environmental responses. Periods of environmental transition are not necessarily well recorded in the dune record at the local scale, but can be identified to some extent when data is amalgamated. The question of what OSL dune ages mean in terms of environmental and climatic conditions needs to be investigated further by a comparison with climatic information derived independently.

In summary, local and regional signals, with consideration of sampling resolution, must be amalgamated; otherwise local factors are always likely to dominate. Assimilation of sampling profiles and depth information with OSL ages can constrain and provide more nuanced interpretations of dune chronologies. Narrow vertical sampling intervals and multiple sampling profiles at each site are recommended in order to more readily identify localised signals and to minimise the influence of insufficient sampling resolution on the calculation and presentation of net accumulation rates. These considerations are recommended to be followed for all dune OSL dating studies, as the issues are likely to be applicable for most aeolian systems.

7 Investigating the potential of HCl-only treated samples using range-finder OSL dating

Paper Four: Leighton, C.L. and Bailey, R.M.

To be submitted to *Quaternary Geochronology*

Abstract

Rapid sample preparation and measurement protocols for optically stimulated luminescence (OSL) dating have been investigated as a method of increasing the throughput of samples (e.g. Durcan et al. 2010; Roberts & Duller, 2004; Roberts et al. 2009). Here, we investigate the potential of dating samples treated using only hydrochloric acid (HCl) for providing accurate range-finder ages for quartz. The equivalent dose (D_e) is underestimated for older samples using a standard single aliquot regenerative (SAR) protocol, but measurement of the post-IR OSL signal (e.g. Roberts and Wintle, 2001) provides D_e estimates within 15% of the 'target D_e' for two-thirds of samples. The application of a standardised growth curve (SGC) is also investigated. For these dune samples, the quickest preparation and measurement procedure from which accurate D_e estimates can be obtained is treatment with HCl, measurement of the natural and regenerative post-IR OSL signal, and calculation using a region-independent SGC. A slightly longer protocol incorporating an additional preparation stage of heavy liquid density separation can be used to improve D_e estimates in samples where feldspar-contamination is thought to be particularly problematic. In practice, these time savings in the preparation and measurement protocols mean that a large number of samples can first be rapidly treated with HCl, the post-IR blue OSL signal measured using a shortened double-SAR protocol, and D_e calculated by applying an independent SGC before then deciding which samples require full preparation and measurement, rather than the inefficiency of committing time and resources to all samples if this is unnecessary for the context of a particular suite of samples. The potential of this rapid preparation and measurement protocol is discussed in relation to sand dune dating studies.

7.1. Introduction

The applications of optically stimulated luminescence (OSL) dating require detailed and high resolution chronologies. The preparation of samples for dating and the dating procedure itself are both time- and labour-intensive processes. Minimising these stages, in particular when high resolution sampling strategies are employed, diminishes the time required for preliminary dates to be obtained, as well as potentially reducing the total number of samples that need be fully dated if, for example, a number of samples within a depth column share the same age of burial. The ineffectiveness of sampling strategies in representing depositional histories occurs as sampling frequency rarely aligns with chronological significance; clusters of dates and apparent hiatuses are therefore at risk of being a function of sampling strategy rather than a true reflection of the sedimentary structure that is being dated (Stone and Thomas, 2008). This is particularly relevant considering the increasing application of coring methods to the extraction of samples for dating from aeolian dunes (e.g. Preusser et al., 2002; Stokes and Bray, 2005; Telfer and Thomas, 2007), which requires a systematic approach to sampling as the underlying sedimentary structure is typically not visible.

There are potentially two research tactics available to address the issue of representativeness of sampling strategy. Firstly, where the dune internal structure is visible or made visible by the application of GPR (e.g. Bristow et al., 2007a), sampling can be conducted by strategically targeting depositional units around bounding surfaces in order to reflect the sedimentary structure (Chapter 4; Atkinson et al., 2011). However, this approach is not widely applicable, as it depends on relatively rare dune excavations or sediments conducive to the use of GPR, as well as the presence of clear stratigraphy. It has also been shown that reliable chronologies can be obtained from dunes with a lack of clear internal structure (Chapter 4; Bateman et al., 2007), and hence there are numerous sites where using dune internal structure as a guide is infeasible. In addition, bounding surfaces classified hierarchically are not necessarily equivalent to significant chronological hiatuses in dune accumulation (at the level of precision allowed by the application of OSL dating), and therefore this approach may require a large number of samples in order to capture all significant chronological hiatuses present (Chapter 4).

The second approach is to use a high sampling frequency sufficient to reflect likely variations in sedimentary deposition. From these samples it may then be possible to strategically select representative samples for dating. This chapter is focused on the second approach, and specifically the means by which the initial batch of samples might be reduced to those for which dating will represent accurately the preserved depositional history. Chapters 4 and 6 showed that high resolution sampling is required in order to capture dune and dunefield variability of OSL chronologies, and that targeting of bounding surfaces in the field may not always be an appropriate method of increasing efficiency. Increasing the throughput of samples in the laboratory may therefore provide one practical approach to addressing the implications of these findings.

7.1.1. Previous investigations of shortened preparation methods

The possibility of quickening preparation and measurement components of the OSL dating protocol has been investigated and put forward as a promising method for increasing sample throughput, in order to enable the selection of a few samples requiring full preparation (e.g. Durcan et al., 2010; Roberts and Duller, 2004; Roberts et al., 2009). 'Luminescence profiling' has been used as a preliminary step to assess the suitability of sites and samples for luminescence dating using shortened preparation and measurement procedures (Burbidge et al., 2007; Sanderson et al., 2001, 2003). This has been advanced by using partially prepared samples for 'range-finder' estimates of the equivalent dose (D_e), which are at lower levels of accuracy and precision than estimates from fully prepared samples (e.g. Durcan et al., 2010; Roberts et al., 2009). Roberts et al. (2009) concluded that the optimum range-finder dating procedure composed of a 1 hour safety pre-treatment of hydrochloric acid (HCl) before 45 min in 45% hydrofluoric acid (HF), followed by 45 min in 37% HCl, providing an average D_e estimation to 'target D_e' ratio of 74% (±38). Thick-source beta counting for 4 hours, and relating the beta count to the gamma dose rate, was judged as a sufficient estimate for calculating the dose rate and another way to speed up the dating process for range-finder ages (Durcan et al., 2010; Roberts et al., 2009). Using these processes to quicken the preparation and measurement procedures, Roberts et al. (2009) found that the average value of the ratio of range-finder to target ages for eight out of nine aliquots was 0.9±0.3, with a recommended minimum uncertainty for range-finder ages of 30%.

Raw samples have proven problematic to date, producing D_e estimates of 65-70% of the target D_e (Roberts et al., 2009). The presence of feldspar has proved to be a barrier to accurate ages, even after the incorporation of an IR bleach prior to blue OSL measurement within the single aliquot regenerative (SAR) protocol (the double-SAR protocol) (Durcan et al., 2010; Roberts, 2007). Dose recovery tests using the double-SAR procedure have been shown to be within ±15% of the known dose (Roberts and Wintle, 2003). For some samples the double-SAR protocol alone may not be suitable for D_e estimation, and chemical pre-treatment may be required in order to recover a quartz-dominated post-IR OSL signal (Roberts, 2007). It has been concluded that part of the feldspar signal is only bleachable by green or blue light (Duller and Bøtter-Jensen, 1993; Lai and Brückner, 2008), making it difficult to remove the feldspar signal from mixed mineralogy samples prior to measurement of the quartz signal. An HF or hydroflourosilicic (H_2SiF_6) treatment is therefore argued to be important in order to minimise feldspar contamination in samples with a significant feldspar proportion.

7.1.2. The use of standardised growth curves

In addition to the preparation of samples for standard OSL dating, the SAR dating protocol and following analyses can be lengthy procedures. Standardised growth curves (SGCs) have been investigated as a method of shortening the necessary machine time for samples by requiring only the measurements of the natural signal (L_n and T_n) and, ideally, the regenerated signal (L_x) and test dose response (T_x) of one regeneration point (Burbidge et al., 2006; Chen et al., 2013; Lai, 2006; Roberts and Duller, 2004; Telfer et al., 2008; Yang et al., 2011). This protocol is based on the assumption that quartz responds similarly to radiation regardless of its source, and hence the dose response curve of a standardised signal (standardising for changes in sensitivity, brightness, signal intensity due to mass, and measurement system) should be equivalent for all quartz samples (Burbidge et al., 2006; Roberts and Duller, 2004). The standardised OSL signal (I) is calculated as follows:

$$Standardised\ OSL\ (I) = (L_x/T_x) \times T_D \qquad \text{(Eq. 9.1)}$$

where T_D is the test dose. SGCs have been shown to produce accurate D_e estimates. The measurement of one regeneration point, to assess the consistency of each measured aliquot with the SGC, and the investigation of luminescence growth curves for local samples before the application of an SGC has been recommended, due to the recognition of distinctive growth curve characteristics of some samples (Burbidge et al., 2006; Telfer et al., 2008). Roberts et al. (2009) constructed a SGC using 12 aliquots of HF-HCl-treated material, but noted a variety of forms of the dose-response curve with approximately twice the scatter seen of fully prepared samples (Roberts and Duller, 2004), and hence concluded that using an SGC was not appropriate using these partially prepared samples.

In this paper a method is put forward for retrieving reasonable D_e estimates ('range-finders') from partially prepared samples, treated only with HCl, and by shortening the measurement protocol through use of a SGC.

7.2. Material and methods

7.2.1. Sample preparation and measurement

Five samples were chosen for investigation at a range of preparation stages due to their range of ages and significance for sampling applications; UAE10/1/1, UAE10/1/8, UAE10/3/16, UAE10/3/17, UAE10/3/18 (Table 7.1). These samples are from two sites located in sand extraction quarries that reveal the internal structure of the linear megaridges and overlying secondary dunes: UAE10/1, near Shwaib, and UAE10/3, ~20 km southwest of Ras al Khaimah city. Seven additional samples from the same region were measured using a rapid measurement procedure for D_e calculation using a SGC (as described below).

All samples were prepared in the Oxford Luminescence Dating Laboratory (OLDLAB) under subdued orange (585 nm) light. The top ~3 cm of sand were removed in order to minimise the dating of samples bleached since the burial event. The full sample preparation procedure is composed of: 35% HCl treatment until the reaction is complete in order to remove carbonates; 30% hydrogen peroxide (H_2O_2) treatment until the reaction is complete to remove organic matter; wet sieving to isolate the 90-150 and 150-220 µm fractions; heavy liquid density separation using sodium polytungstate to remove heavy minerals (at 2.68 g cm^{-3} for quartz, additional separation at 2.58 g cm^{-3} was used to remove the feldspar fraction); a 50 minute 60% HF etch on a shaker table to remove the alpha-irradiated shells of quartz grains; and a further 2 week 35% hexafluorosilicic (H_2SiF_6) acid etch (after an IR bleach revealed the presence of feldspars). At each stage of preparation, samples were extracted from the process for dating (Figure 7.1). The numbering system introduced in Figure 7.1 will be referred to in the rest of the paper in order to identify the level of preparation received by the sub-sample. Whilst Roberts et al. (2009) undertake HF treatment on raw samples as part of their shortened preparation procedure, here this was not

Table 7.1: OSL data for the five main samples discussed in this chapter. OD is overdispersion (as defined by Galbraith and Roberts, 2012), n is number of aliquots measured. Further details of these samples can be found in Chapter 4. [a] Loss on ignition (LOI) at 950 °C and multiplied by 1.36 is proportional to carbonate content (g), which is expressed as % of original dry sample weight. [b] Moisture content estimated at 5 ± 3% for all samples, in order to allow for temporal fluctuations. Potassium (K), thorium (Th) and uranium (U) concentration uncertainties are 13%, 13% and 9% respectively, based upon the relative standard deviations of repeated ICP-MS/AES measurements.

Sample	**n**	**D_e (Gy)**	**OD**	**Grainsize (µm)**	**Carbonate content (%)[a]**	**Dose rate (Gy/ka) [b]**	**Age (ka)**
UAE10/1/1	29	34.79 ± 0.97	0.14 ± 0.02	90 - 150	14.6	1.28 ± 0.14	27.46 ± 2.75
UAE10/1/8	24	34.28 ± 1.25	0.17 ± 0.03	90 - 150	14.5	1.27 ± 0.13	27.39 ± 2.81
UAE10/3/16	22	15.32 ± 0.52	0.14 ± 0.03	150 - 220	17.2	1.14 ± 0.11	13.60 ± 1.33
UAE10/3/17	28	14.51 ± 0.51	0.17 ± 0.03	150 - 220	17.0	1.28 ± 0.12	11.34 ± 1.04
UAE10/3/18	13	5.07 ± 0.28	0.19 ± 0.04	150 - 220	15.8	1.06 ± 0.12	4.80 ± 0.60

undertaken due to potential safety hazards and the relatively high calcium carbonate content of the samples (Table 7.1), which may form calcium fluoride on reaction with HF and from which D_e values cannot be determined (Roberts et al., 2009). An additional benefit to removing this stage of preparation is that, whilst the treatment is quick, it is the most dangerous in the sample preparation procedure and, depending on institution regulations, may be labour intensive. Prior to measurement the samples were mounted onto aluminium discs using Silkospray® and a 5 mm diameter mask.

All OSL measurements were conducted on one of two Risø TL/DA 15 readers, detecting using a 7.5 mm Hoya U-340 filter. Following a preheat plateau test using fully prepared samples which showed no dependence of D_e on temperature (220-280 °C), preheats of 260 °C for 10 s for natural/regenerated signals (L_x) and 220 °C for 10 s for T_x were subsequently adopted. Single aliquot OSL measurement was conducted using 470 nm stimulation at 160 °C for 100 s, with a 50 s OSL bleach at 280 °C incorporated after each regeneration cycle, which has been shown to reduce recuperation (Wintle and Murray, 2000, 2006). In addition, two samples were also measured using green diodes (peak stimulation at 525 nm),

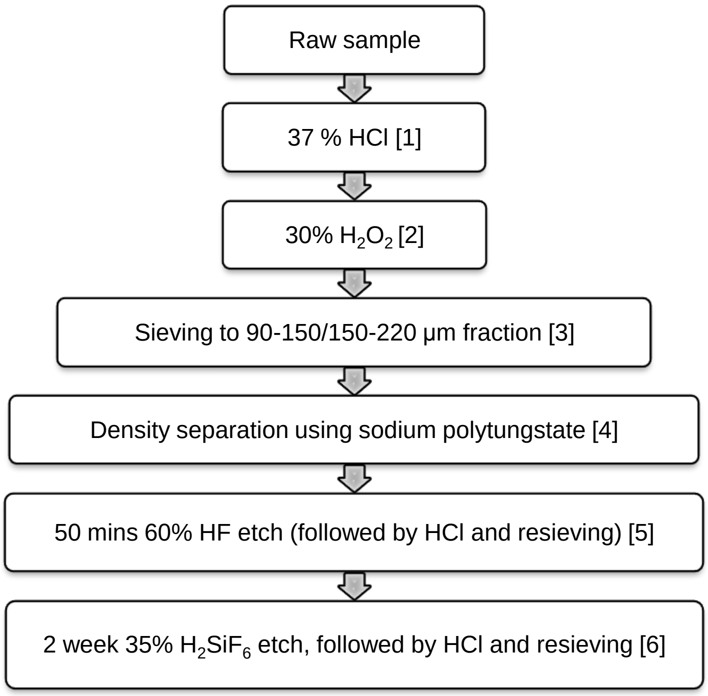

Figure 7.1: Full preparation procedure of quartz samples prior to D_e measurement. At each partial preparation stage [*i*], sample was extracted for D_e measurement.

following the same temperature and timing protocols. A SAR protocol (Murray and Wintle, 2000, 2003) and double-SAR protocol which incorporated an additional 125 °C IR-bleach (830 nm stimulation) before OSL measurement (Banerjee et al., 2001; Roberts, 2007) were used for fully and partially prepared samples. A dose recovery test using sample UAE10/3/16 showed no significant difference in recovered dose between a 50 s and 100 s 125 °C IR bleach; a 50 s IR bleach was therefore used to reduce measurement time. Quality assurance ratios of zero-dose, recycling and IR depletion were incorporated into the full SAR protocol; only aliquots with ratios within ±10% were included in D_e estimation. Recycling and zero-dose ratios were relaxed for partially prepared samples due to the higher number of measurements that would have been necessary if more stringent ratios were used; all aliquots were within 30% and 10% of unity/zero respectively. Dose recovery results were within ±10% of the given dose for all fully prepared samples, with four of the five named samples within ±5%.

The dose rates used for age calculations are the same as those calculated in Chapter 4.

7.2.2. Standardised growth curve (SGC) construction

A regional SGC was constructed using the standardised luminescence signals (Equation 7.1) from six fully prepared samples collected from the north-eastern Rub' al Khali (UAE10/1/2; 1/11; 1/20; 2/19; 3/2; 3/5), none of which will be further analysed in this paper in order to avoid circularity. 903 datapoints from 150 measured aliquots comprising eight regenerative dose points up to 60 Gy were used to create the growth curve. Roberts and Duller (2004) use the following general equation to describe the growth of the standardised OSL signal (*I*) with dose, *D*:

$$I = I_0 + I_\infty\left(1 - e^{-D/D_0}\right)$$

(Eq. 7.2)

where I_∞ is the saturated signal, D_0 is the characteristic dose, and I_0 deals with offset from zero at zero dose. Below ~125 Gy this single saturating exponential is adequate to describe the dose response of quartz (Roberts and Duller, 2004). This equation was used to fit the datapoints of the standardised OSL signal of the six samples described above, and hence construct the regional SGC used in this study (Figure 7.2).

The SGC constructed by Roberts and Duller (2004) was also used in this study by using their calculated I_∞, I_0 and D_0 values to assess the applicability and time efficiency of utilising a 'general' (region-independent) SGC. The values for I_∞, I_0 and D_0 using these two alternative curves are shown in Table 7.2.

Table 7.2: SGC parameters for the 'regional' SGC constructed in this study and the 'general' SGC, presented by Roberts and Duller (2004). Equation 7.2 is used for SGC construction.

Data set	I_0	I_∞	D_0
This study	0.03 ± 0.2	38.2 ± 1.2	41.2 ± 2.6
Roberts & Duller (2004)	0.03 ± 0.1	51.7 ± 0.6	55.1 ± 1.3

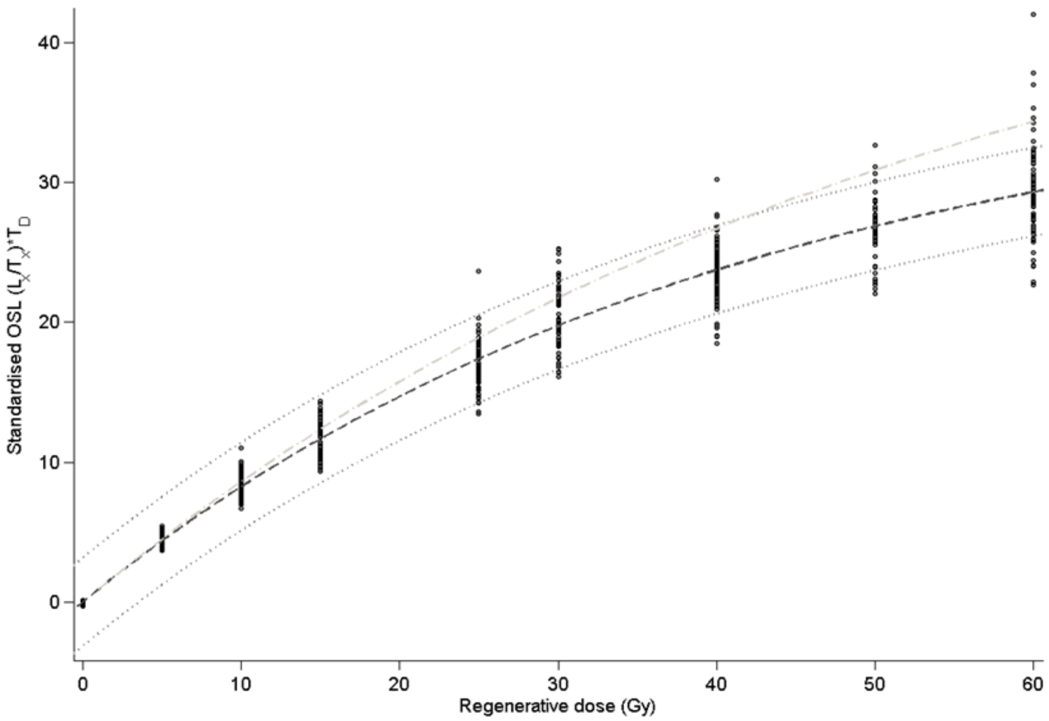

Figure 7.2: SGC constructed using 903 datapoints of the measured blue OSL signal of fully prepared regional samples according to Equation 7.2. 95% confidence intervals are shown by dashed lines. The grey dash-dot line shows the curve produced using the parameters of Roberts and Duller (2004).

D_e values were calculated and compared using both individually constructed growth curves using full SAR and double-SAR protocols, and the regional and general SGCs. The quality assurance ratios described in the section above were not used to remove aliquots from the calculation of the D_e when the SGC was used because, given the main advantage of this method is to reduce measurement time, under usual circumstances this information would be unavailable. The standardised first regeneration signal of each aliquot was compared to the corresponding dose point on the SGC and the resulting ratio was used for 'correction' of the natural standardised signal with uncertainties added in quadrature, using a fractional error of 15% on the SGC (i.e. the D_e was calculated as proportional to the dose response of each aliquot relative to the SGC, as suggested by Burbidge et al., 2006), before interpolating the corrected standardised natural signal to calculate the D_e. To do this, Monte

Carlo sampling was used (for each aliquot, 5000 random natural standardised signals, I_0, I_{Max} and D_0 values were generated to solve Equation 7.2 for D and calculate the mean and standard deviation of the resultant distribution, which were used as the D_e and uncertainty for each aliquot respectively). The accuracy of D_e estimates produced using the regional SGC was tested by the calculation of a D_e value for each individual aliquot of stage-6 UAE10/1/1 (i.e. fully prepared), using the SGC methodology as described above. The use of an SGC produced D_e estimates within errors of that calculated using the full SAR protocol and individually constructed growth curves. Sample D_e estimates were calculated using the central age model (Galbraith et al., 1999) when an individual dose response curve was constructed, or by using the relative weighted mean and standard error when calculated using a SGC, as larger uncertainties on the individual aliquot D_e estimations produced unfeasibly large overdispersion values despite overlapping uncertainties (due to numerical instabilities during calculation).

D_e estimates from partially prepared samples are compared to 'target D_e' values of fully prepared samples using the full SAR measurement procedure and individually constructed

Table 7.3: A summary of D_e measurement and calculation protocols used in this paper, and their description within the main text.

Description within main text	**Preparation stages measured**	**D_e measurement conditions**	**D_e calculation**
SAR	All stages	Minimum 3 regeneration points & zero-dose, IR depletion and recycling ratios; blue OSL	Individual growth curve
Double-SAR	HCl-only	Minimum 3 regeneration points & zero-dose, IR depletion and recycling ratios; post-IR blue OSL	Individual growth curve
post-IR OSL SGC	HCl-only	Natural & 1 regeneration point; post-IR blue OSL	Regional SGC
post-IR OSL general SGC	HCl-only	Natural & 1 regeneration point; post-IR blue OSL	SGC using independent parameters (Roberts & Duller, 2004)

dose response curves (where the ratio $r=D_e$/'target D_e'; these values are presented in Table 7.1). The different D_e measurement and calculation protocols used in this paper, and their description within the main text, are summarised in Table 7.3.

7.2.3. Component fitting

The quartz OSL signal has been shown to be the sum of several exponentials each corresponding to a component of different luminescence properties, such as the fast, medium and slow, described due to their relative decay rates. The dominance of the different components varies substantially between samples (e.g. Bailey et al., 1997; Jain et al., 2003). The behaviour of these components has been shown to be relatively consistent between studies (e.g. Durcan and Duller, 2011; Jain et al., 2003; Singarayer and Bailey, 2003). The use of linearly-modulated OSL (LM-OSL), where stimulation power is increased linearly during OSL measurement, enables the components to be more easily distinguished, but is time-consuming for measuring many geological samples. Separating several first-order components from continuous wave OSL (CW-OSL) by curve-fitting, assuming linear combination and using fixed parameters characterising the components, has the potential for more widespread incorporation into dating protocols (Cunningham and Wallinga, 2009). The photoionization cross-section has been shown to be strongly dependent on wavelength (Singarayer and Bailey, 2004). The difference between the component decay rates increases with increasing wavelength; green (~525 nm) light is therefore more useful for fitting the components than the conventional blue (~470 nm) light used for OSL dating of quartz samples (Bailey et al., 2011; Singarayer and Bailey, 2004).

For component fitting of samples UAE10/1/1 and 1/8, green diodes were used in order to enhance the fitting protocol. Component fitting is achieved using a Levenberg-Marquardt algorithm, implemented in custom-written software written by Diana Bailey (2009). An iterative fit method was conducted on the fully prepared samples to find the most appropriate number of components and constraints to produce the best fit for the samples. Upper and lower limits of decay rate ratios for three components found to give the most appropriate fit were 1.1-0.9, 0.4-0.1 and 0.01-0 respectively, which are similar to the average ratios used by Cunningham and Wallinga (2009) and to the relative cross-sections of the fast, medium, and slow2 components determined by Jain et al. (2003). Component fitting of fully prepared samples show that the quartz OSL signal of these samples are dominated by the fast component (Figure 7.3). Tightening and widening the constraint for the fast component (using 1.01-0.99, 1.05-0.95 and 1.2-0.8), together with using broader slower component constraints, were also investigated as techniques to “force” the fit to the fastest quartz component to varying degrees. The trials produced similar results, and so constraints of 1.1-0.9 and broad ranges for the medium and slow components (0.8-0) were

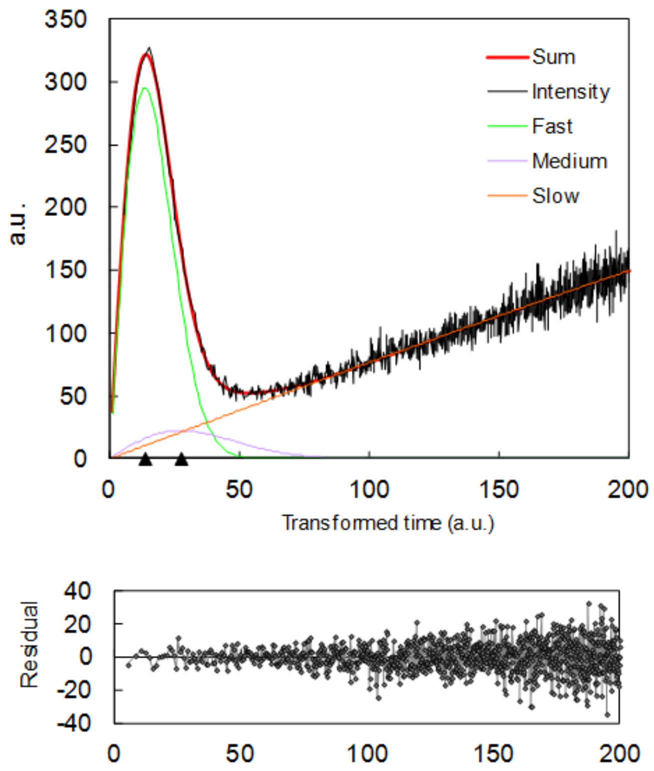

Figure 7.3: An example of component fitting for the natural signal (L_n) a fully prepared sample. The blue OSL signal is dominated by the fast component. The arrows on the x-axis indicate the peaks of the fast and medium components.

used to guide the fitting of partially prepared samples. These samples were measured using the double-SAR protocol in order to reduce the contribution of feldspar to the OSL signal prior to fitting. The L_x/T_x values of the isolated fast component were then used to calculate the D_e using a general SGC.

7.3. Results

7.3.1. Comparing preparation stages using the SAR protocol

Significant contributions of feldspar in the measured blue OSL signals were inferred in the partially prepared samples with slower OSL decay rates compared to the fully prepared samples (Figure 7.4a), and low IR depletion ratios before HF treatment (Duller, 2003). Raw samples exhibited a large degree of scatter in calculated (L_x/T_x) dose response data, and for the majority of aliquots the D_e could not be calculated. For samples that had been treated, before stage-6 (H_2SiF_6 treatment) the additional preparation steps yielded negligible difference in the D_e estimates calculated using a SAR protocol (Figure 7.4b). Hereafter, samples having received the minimum preparation treatment of HCl (preparation stage-1) will be investigated, given the similarity of D_e estimates for all preparation stages before H_2SiF_6 treatment, with the purpose of minimising the preparation time as much as possible.

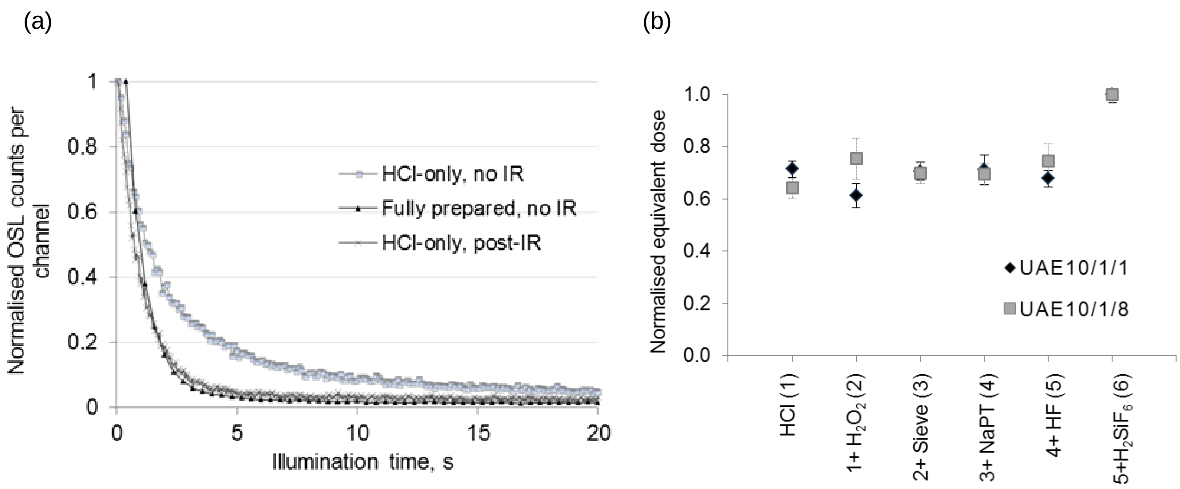

Figure 7.4: An example of: (a) Normalised decay curves for aliquots of HCl-only treated (OSL and post-IR OSL) and fully prepared sample UAE10/1/1 (OSL). (b) Normalised ratio of HCl-only to fully prepared D_e of samples UAE10/1/1 and 1/8 measured at each preparation stage (Figure 7.1), using a SAR protocol and blue OSL signal. At least 8 aliquots were included in the D_e calculation at each stage for each sample.

HCl-only D_e estimates are within 40% of the target D_e for all five samples investigated when using the SAR protocol (Table 7.4). The greatest underestimation is for the oldest samples: sample UAE10/1/1 has a ratio of HCl-only D_e to target D_e of 0.71; sample UAE10/1/8 of 0.63. Anomalous fading of the feldspar signal component is a possible explanation of this underestimation of D_e, which is less noticeable in the younger samples. A suitable OSL measurement protocol is therefore required for D_e estimation which is suitable for samples of all ages, and this is the focus of the following section.

7.3.2. HCl-only treated samples using the double-SAR protocol

Table 7.4 compares *r* for the SAR and double-SAR protocols. As the oldest samples, applying the standard SAR protocol to samples UAE10/1/1 and 1/8 gave a significant underestimation of the D_e values. The additional 125 °C IR-bleach in the double-SAR protocol appears to at least partially correct for this problem, as the D_e estimation for sample UAE10/1/1 is within errors of the fully prepared D_e value, although sample UAE10/1/8 is still underestimated by 17% (Table 7.4). One aliquot of UAE10/1/8 has unusually high natural and regenerative IRSL signals (~10 times higher than other aliquots of this sample). The post-IR OSL decay and thermoluminescence (TL) curve shapes indicate that the signal is not characteristic of a quartz sample, compared to those from 'typical' aliquots of the same HCl-only treatment and a fully prepared sample, and therefore is interpreted as dominated by feldspar (Figure 7.5). The D_e estimate (calculated using a regional SGC) from this aliquot is underestimated (65% of the target D_e). It is inferred that due to high feldspar presence in some of the samples, the IR-bleach is insufficient to remove the feldspar contribution to the OSL signal. In samples where the feldspar contribution is relatively low, the IR bleach preceding OSL measurement is sufficient to remove a large proportion of the feldspar signal and/or feldspar is present in some but not all of the measured aliquots.

Table 7.4: D_e estimates for five partially prepared samples using individually constructed growth curves and regional and general SGCs, and their ratio to fully prepared samples. *r* is the ratio between the particular measurement protocol and the fully prepared D_e value [1]; values in italics are within 10% of the 'target' D_e. All OSL and post-IR OSL measurements were made using blue diodes. Calculations [1-3] were made using dose response curves constructed from applying the full (double) SAR procedure to all aliquots (using the central age model), whilst [4-5] are calculated using the regional and general SGCs respectively (using the relative weighted mean and standard error).

D_e (Gy)		UAE10/1/1	n	*r*	UAE10/1/8	n	*r*	UAE10/3/16	n	*r*	UAE10/3/17	n	*r*	UAE10/3/18	n	*r*
Fully prepared (SAR) [1]		**34.79 ± 0.97**	29	-	**34.28 ± 1.25**	24	-	**15.32 ± 0.52**	22	-	**14.51 ± 0.51**	28	-	**5.07 ± 0.28**	13	-
HCl only	SAR [2]	24.87 ± 1.09	10	0.71	21.65 ± 1.39	12	0.63	13.78 ± 0.71	14	*0.90*	11.16 ± 0.63	14	0.77	4.10 ± 0.2	16	0.81
	d-SAR [3]	34.15 ± 1.54	11	*0.98*	28.29 ± 2.16	11	0.83	14.29 ± 1.10	11	*0.93*	13.23 ± 0.78	14	*0.91*	4.83 ± 0.18	12	*0.95*
	d-SAR SGC [4]	31.61 ± 1.24	4	*0.91*	26.15 ± 1.67	8	0.76	14.02 ± 1.02	17	*0.92*	14.82 ± 1.04	19	*1.02*	4.73 ± 0.14	16	*0.93*
	d-SAR R&D [5]	33.02 ± 1.64	10	*0.95*	27.87 ± 1.38	14	0.81	14.34 ± 0.92	18	*0.98*	14.34 ± 0.92	19	*0.99*	4.73 ± 0.14	16	*0.93*

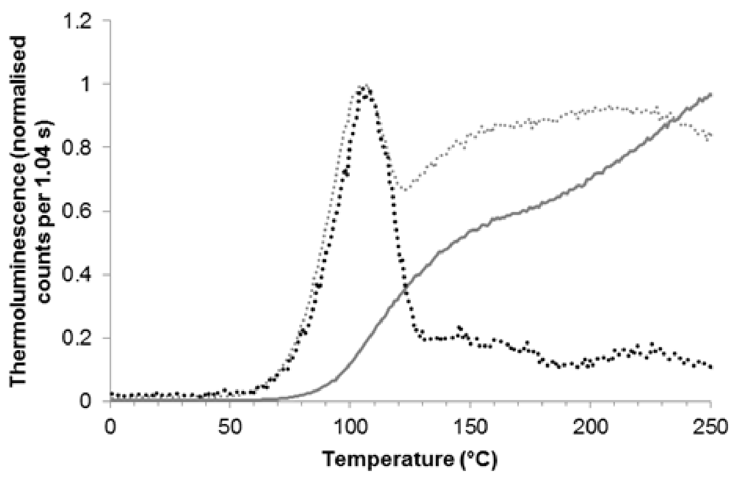

Figure 7.5: Normalised TL curves for HCl-only treated (grey) and fully prepared (black) aliquots of sample UAE10/1/8 respectively. 'Typical' aliquots are shown with a dashed line, whilst the solid line shows an aliquot with an inferred high feldspar component. The 110 °C TL peak is distinctive in two 'typical' aliquots, although the signal after this peak is higher in the partially treated sample compared to the fully prepared sample, indicative of the presence of feldspar or other luminescent minerals.

There is a range of both over- and under-estimating behaviour of the 'slow' post-IR OSL signals, shown by no correlation between the time required for the post-IR OSL signal to deplete by 50% (the half-life) and *r*. The behaviour leading towards an inaccurate D_e estimation appears unpredictable and difficult to relate to an exact mechanism (e.g. contamination by feldspars, quartz grain coatings, and/or the presence of other luminescent materials). Figure 7.6 shows a clear difference in the nature of the sample material when raw, treated with HCl-only and when fully prepared, indicating that there could be a range of materials contributing the OSL signal in the HCl-only treated samples. The range of underlying reasons for the incorrect D_e estimation makes the identification of unsuitable aliquots using rejection criteria problematic.

In order to further investigate the different contributions to the variability in D_e of partially prepared samples, HCl-treated quartz and feldspar for samples UAE10/1/1 and 1/8 were separated using sodium polytungstate densities of 2.68 and 2.58 g cm^{-3} and the post-IR OSL signals were measured individually (Figure 7.7). Dose recovery ratios (using the double-

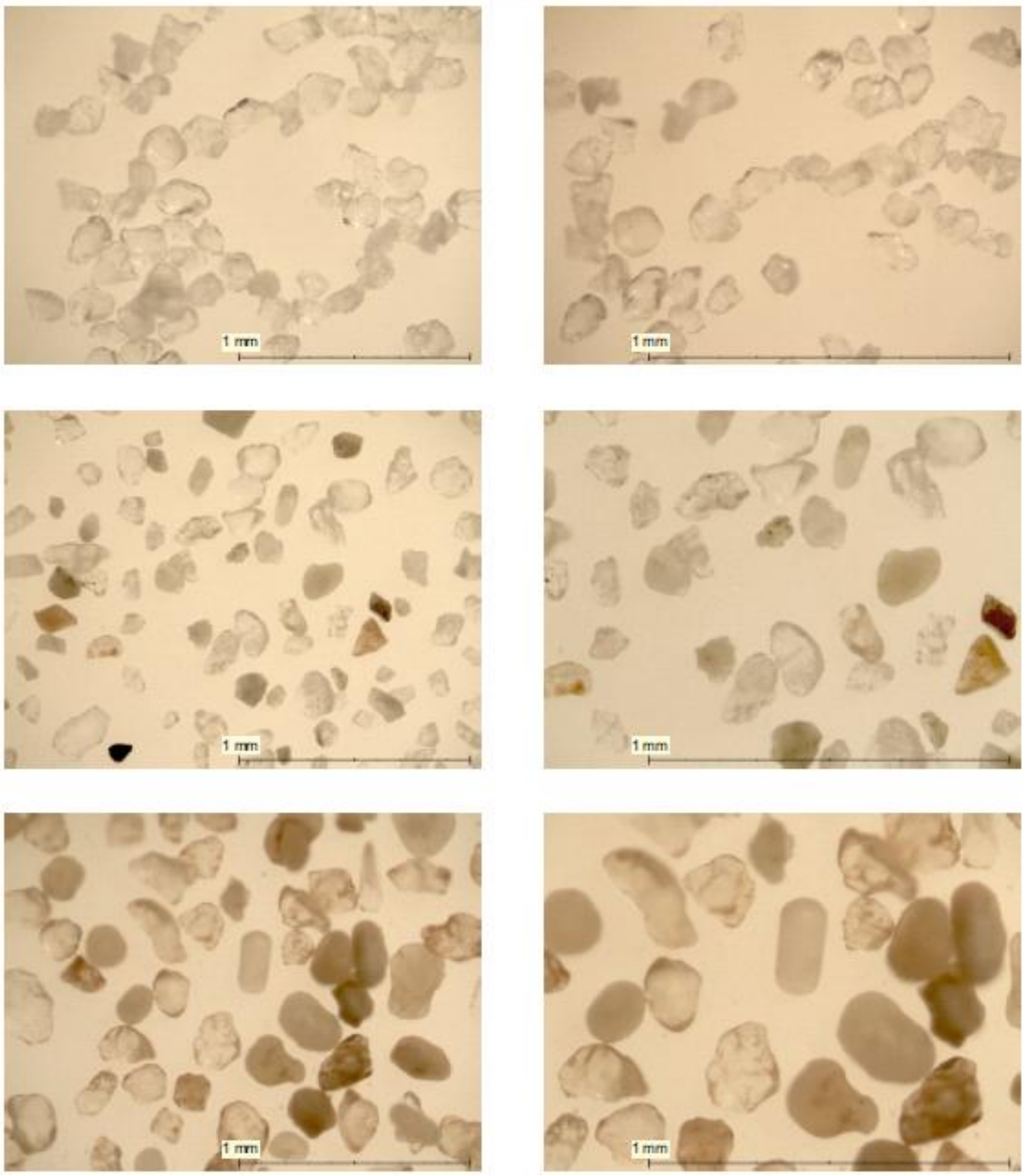

Figure 7.6: Microscopy images of sample UAE10/1/8 having undergone different stages of preparation, at 50x (left) and 80x (right) magnification. Top: fully prepared (preparation stage-6). Middle: HCl-only treatment (preparation stage-1). Bottom: raw sample.

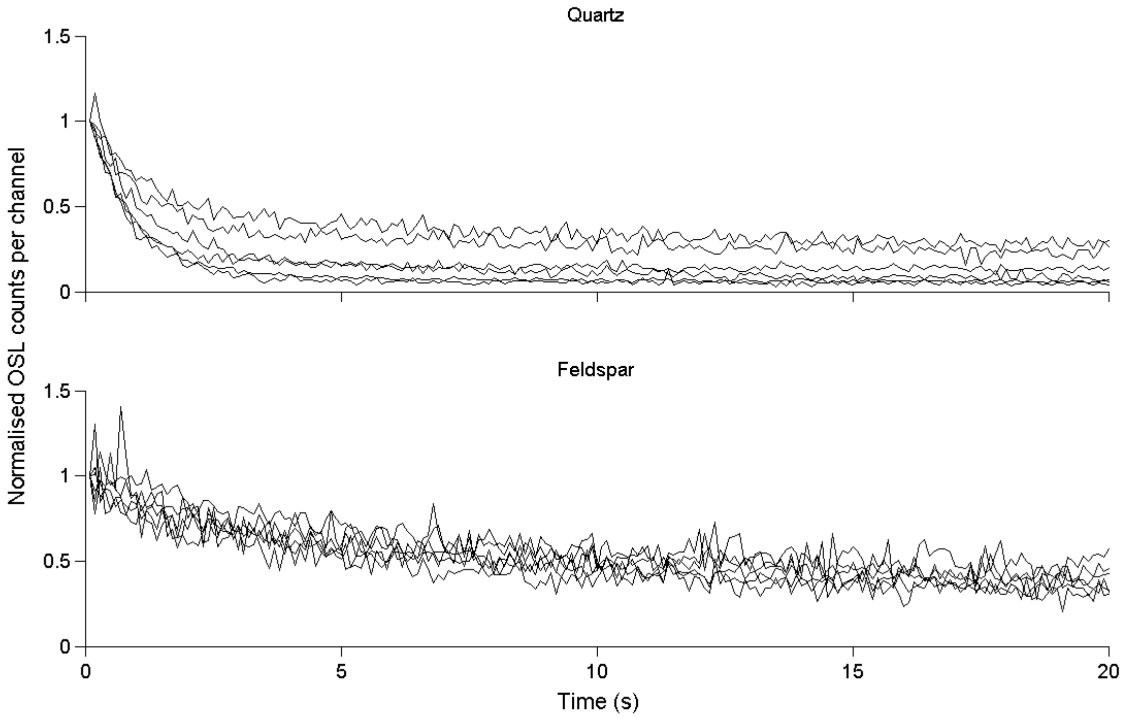

Figure 7.7: Normalised post-IR OSL decay curves for six aliquots of sample UAE10/1/8 that have been HCl-treated and separated using sodium polytungstate. Top: 2.58-2.68 g cm^{-3}, inferred to be dominantly quartz. Bottom: <2.58 g cm^{-3}, inferred to be dominantly feldspar.

SAR protocol) were higher for feldspar than quartz, yet D_e estimates were underestimated (Table 7.5). These results indicate that feldspar presence can explain the additional scatter and underestimation of D_e values for some samples, and that an IR bleach prior to blue OSL measurement, whilst adequate for most samples, is not always sufficient to give a quartz-dominated signal. The two additional floatation steps using sodium polytungstate and following the double-SAR protocol produces a cleaner quartz signal with D_e estimates within 15% of the target D_e for these samples.

Despite the above discussion of the variability of D_e estimates for individual aliquots, the majority of final sample D_e estimates (calculated using the central age model) for HCl-only treated material are within 10% of fully prepared D_e values (and within errors). For most of the measured aliquots, the IR-bleach appears to remove the OSL signal from non-quartz minerals to a suitable level so that the post-IR OSL signal is predominately quartz, as

Table 7.5: D_e and dose recovery ratios for HCl-treated and density separated samples UAE10/1/1 and 1/8 (fully prepared D_e values of 34.79±0.97 and 34.28±1.25 Gy respectively). Material in the range 2.58-2.68 g cm^{-3} is inferred to be dominantly quartz, material <2.58 g cm^{-3} is inferred to be dominantly feldspar.

Sample	**Feldspar (<2.58 g cm^{-3})**			**Quartz (2.58-2.68 g cm^{-3})**		
	***D*e**	**OD**	**DR**	***D*e**	**OD**	**DR**
UAE10/1/1	27.87 ± 1.89	0.23 ± 0.05	1.17	30.53 ± 1.98	0.22 ± 0.05	1.01
UAE10/1/8	29.04 ± 2.18	0.19 ± 0.06	1.20	31.53 ± 1.51	0.15 ± 0.04	1.02

shown by the similarity of decay curve shape to a fully prepared sample in Figure 7.4a. The standard errors of each sample D_e estimate are relatively low, at less than 10%. For the majority of these samples, the double-SAR protocol is therefore sufficient in providing D_e values close enough to the target D_e for the requirement of range-finder estimates. For new samples for which feldspar concentrations are unknown or thought to be high, it is advisable to incorporate a heavy density separation to further isolate the quartz prior to post-IR OSL measurement.

7.3.3. D_e calculation using a SGC

In order to assess the utility of the SGC approach, D_e estimates were calculated for the post-IR blue OSL L_x/T_x values from the same aliquots of HCl-only treated samples measured in Section 7.3.2 using the regional and general SGCs (rather than individually constructed growth curves that were described in the previous section). Using a 'general' SGC provides the possibility of decreasing throughput time further, by not requiring the measurement of fully prepared samples to construct a 'regional' SGC. To test this, the parameters proposed by Roberts and Duller (2004) have been applied to the same (natural and regenerative point) data as fitted using the regional SGC.

The D_e estimates for all samples are within errors of the target D_e values (Table 7.4), except for sample UAE10/1/8, which is within 20% of the target D_e when using the SGC parameters of Roberts and Duller (2004). Using the general SGC produces D_e estimations r values closest to unity, although the difference between estimates calculated using the two growth curves when using corrected standardised OSL signals is small. Without correcting the natural signal using a regeneration point, there is a tendency towards underestimation of the D_e. Uncertainties on the individual aliquot D_e estimates are therefore larger using the SGC compared to when calculated using individual dose response curves, due to the magnification of uncertainties by correcting for underestimation in addition to the incorporation of a 15% fractional error on the SGC (Section 7.2.2), but this does not significantly contribute to the uncertainty on the estimation of the sample D_e.

The distribution of r for the measured aliquots of the five samples is shown in Figure 7.8. The dose response of each aliquot is not always proportional to the natural signal at any given dose (e.g. an aliquot may have a large standardised L_x/T_x value relative to the SGC, but a natural standardised OSL signal lower than the mean of the aliquots). This is to be expected, given the expected variability in natural dose (due to heterogeneous dosimetry for example), variability in dose response form (above that expected due to sensitivity change), and random measurement errors. Correcting for the individual aliquot dose response using one regenerative response (as described in Section 7.2.2) improves the estimated sample (i.e. average) D_e in the present case, which was otherwise underestimated when correction was not used, indicating that these deviations are not systematic and that correction is appropriate. However, this process resulted in larger uncertainties, and led to problems calculating the D_e for Monte Carlo variants due to inevitably poor dose response characteristics for some dose response curves. This effectively results in a ‘filtering’ process, removing aliquots least suitable for application of a SGC (i.e. those requiring greater correction), but had no effect for samples other than UAE10/1/1, for which only four aliquots could be used to calculate D_e estimates using the regional SGC. For unknown

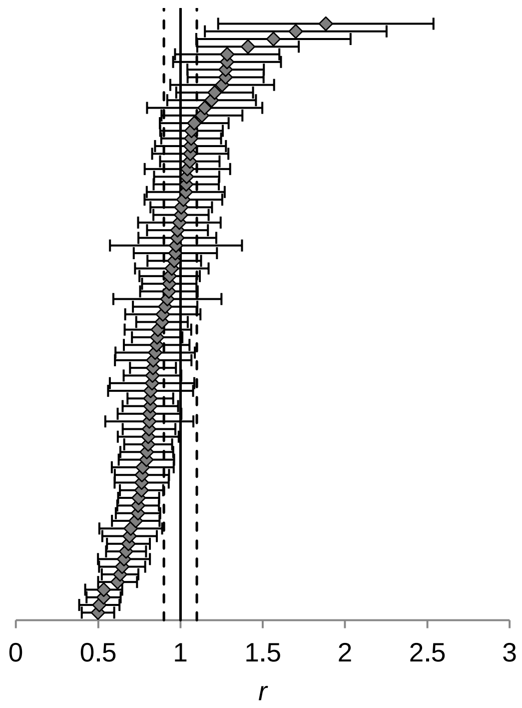

Figure 7.8: Distribution of *r* for all aliquots of samples UAE10/1/1, 1/8, 3/16, 3/17 and 3/18 where D_e is calculated using an independent SGC, shown as calculation [5] in Table 7.4 (parameters from Roberts and Duller, 2004). The dashed lines show 10% of the 'target D_e'.

reasons, this problem affected use of the SGC constructed using regional samples more than the general SGC.

7.3.4. Component fitting of the partially prepared OSL signal

Table 7.6 presents D_e estimates for HCl-only treated samples UAE10/1/1 and 1/8 using green diodes for OSL measurement. Similar D_e estimates and magnitudes of standard errors are obtained when using the isolated fast component double-SAR signal for D_e calculation (SGC) as when using the IR-bleach alone (Table 7.4). A possible reason for why the D_e estimate using the fast component alone was not more accurate or precise is that there are other relatively 'quick' signals that are not removed by curve-fitting. Given the use of an IR-bleach prior to OSL measurement and the mix of over- and underestimating behaviour of individual aliquots, these signals may be from other minerals than feldspar. These results

Table 7.6: D_e estimates for samples UAE10/1/1 and 1/8 using green diodes [6-8] for OSL measurement compared to the fully prepared blue OSL D_e value ('target D_e', [1]) and *r* values [1]. [6] is based on D_e calculation using a full SAR procedure and individually constructed dose response curve for each aliquot (applying the central age model). [7-8] use the SGC parameters of Roberts and Duller (2004) to calculate the D_e and standard error (the relative weighted mean and standard error). The fast component only, isolated using the component fitting procedure described in Section 7.2.3, is used to calculated [8].

		UAE10/1/1	n	*r*	UAE10/1/8	n	*r*
Fully prepared (SAR) [1]		34.79 ± 0.97	29	-	34.28 ± 1.25	24	-
HCl only	**Green d-SAR [6]**	33.53 ± 1.95	20	*0.96*	27.14 ± 1.41	16	0.79
	Green d-SAR R&D SGC [7]	33.96 ± 2.70	20	*0.98*	23.59 ± 0.94	16	0.69
	Fast R&D SGC [8]	30.93 ± 1.92	14	0.89	25.83 ± 1.65	14	0.75

indicate that for partially prepared samples, fitting of the CW-OSL signal does not remove all unwanted contributions to the fast component used for D_e calculation, and that for these samples is no better than using the double-SAR protocol alone.

7.3.5. Trial application of HCl-only treated range-finder ages

The use of a general SGC and HCl-only treated material is the quickest method of D_e estimation investigated. The *r* values of twelve samples, prepared and measured using this method, are shown in Figure 7.9. The range-finder D_e estimates are within 15% of the fully prepared D_e for two-thirds of the samples, the remainder of which were underestimated (by a maximum of 21%).

The range-finder D_e values yield relatively low errors of <10% for >90% of the samples. For homogeneous material where the dose rates are fairly consistent, such as for the samples presented here, these are suitable for the purposes of distinguishing separate populations. For assessment, the ages for the five main samples investigated here are presented in Table 7.7, with their calculated errors. ICP-MS/AES measurements have been used to calculate the dose rate. However, for the rapid calculation of dose rate thick-source

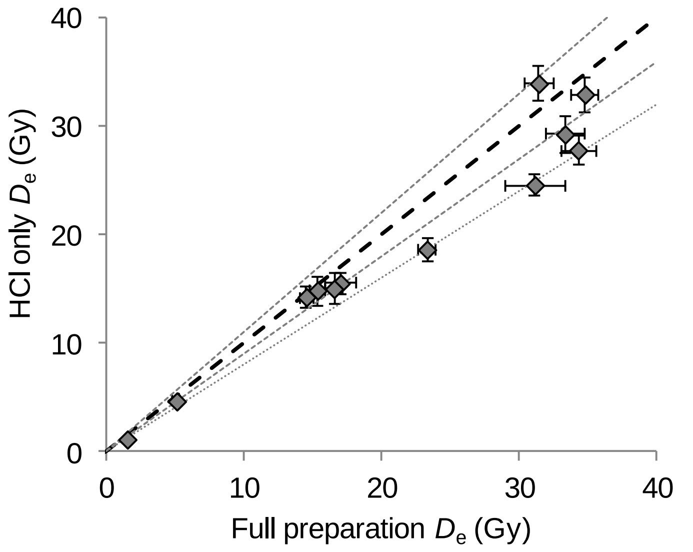

Figure 7.9: Comparison of D_e estimates for 12 samples using the most rapid preparation and measurement procedure (HCl-only, post-IR OSL signal, independent SGC) and the full preparation procedure (SAR protocol). The 1:1 line is shown, as well as 10% above and below, and 20% below (i.e. underestimation of the 'target D_e').

beta counting for 4 h is sufficient for a range-finder ages (Durcan et al., 2010; Roberts et al., 2009). These ages are within errors of those using fully prepared samples, apart from UAE10/1/8 (within 15%), with calculated errors of the same magnitude.

The application of a double-SAR protocol has enabled the identification of three age populations with D_e values of ~34, 15 and 5 Gy respectively that are present in the fully prepared and measured profile, using both individually constructed growth curves and an SGC, constructed using regional or geographically independent samples. The identification of these populations indicates that this method could be applied to a number of samples in order to identify age populations and target the chronological transitions for full preparation and OSL measurement.

If one were to estimate that sample preparation (all of the stages in Figure 7.1) for ~12 samples takes approximately 20 days, the shortened preparation procedure of HCl treatment requires just 1 day (increasing to two days if density separation is required). In addition,

Table 7.7: Age estimates for HCl-only treated samples using the SGC parameters described by Roberts and Duller (2004), and fully prepared sample ages.

Sample	Fully prepared age (ka)	n	HCl-only SGC age (ka)	n
UAE10/1/1	27.46 ± 2.75	29	27.37 ± 3.02	10
UAE10/1/8	27.39 ± 2.81	24	23.20 ± 2.50	14
UAE10/3/16	13.60 ± 1.33	22	13.54 ± 1.76	18
UAE10/3/17	11.34 ± 1.04	28	11.48 ± 1.22	19
UAE10/3/18	4.80 ± 0.60	13	4.64 ± 0.55	16

measurement time is reduced from approximately ~2 days to ~12 hours for each sample (dependent on source, age of sample etc). Therefore for every group of 12 samples, 37 days is saved (from 44 to 7) using the rapid preparation and measurement protocol presented here.

Three age groups were identified from the samples identified above. If it is hypothesised that this was the case in a core of 12 samples, 4-6 samples are likely required to be fully prepared, depending on where in the core the age transition is identified. In comparison to measuring all samples fully, a minimum of 6 days of measurement time would be saved in total. The higher the number of samples, the more efficient the use of range-finder ages will be. Often, multiple (tens of) cores are required from dunefields in order to distinguish signals that reflect widespread environmental change from more local dune processes (Telfer et al., 2010; Bailey and Thomas, In press; Chapter 6). Rapid preparation and measurement techniques make this possible, whereas previously more lengthy procedures made such high sampling resolution unfeasible.

7.4. Discussion

The majority of the D_e and age estimates within errors of fully prepared samples have been measured from HCl-only treated samples using a double-SAR protocol, reducing laboratory preparation time from ~20 days to one (until the reaction with HCl is complete). The possibility of using a SGC can significantly reduce machine run times, to a matter of hours rather than days for the full SAR protocol, depending on the age of the samples. A 'general' SGC has also successfully been applied to these samples, which would provide the quickest measurement protocol of range-finder D_e estimation. Previously, the application of SGCs to different regions has been found to correlate less well than when applied to samples from the same geographical region in which they were constructed (e.g. Telfer et al., 2008). However, we find that using an independent growth curve, here that defined by Roberts and Duller (2004), can provide D_e estimates within errors of D_e values from fully prepared samples measured using a full SAR protocol, and provide indistinguishable (or better) D_e estimates to those produced by a regional SGC. In practice, these time savings in the preparation and measurement protocols mean that a large number of samples can first be rapidly treated with HCl, the post-IR blue OSL signal measured using a shortened double-SAR protocol, and D_e estimated by applying an independent SGC before then deciding which samples require full preparation and measurement, rather than the inefficiency of committing time and resources to all samples if this is unnecessary for the context of a particular suite of samples.

The suitability of this preparation and measurement protocol will be dependent upon the nature of the material being dated; this level of preparation most likely marks the minimum suitable for dating. It is emphasised that these age estimates should not be used as final ages but solely as a guide within the laboratory to allow the possibility of a more systematic approach to preparing and dating samples. The age of sample UAE10/1/8 has been underestimated by ~20% (when using an independent SGC), despite successful application of this protocol to other samples from the same location, highlighting that this approach does not yield the same success for all samples. Material less dominated by quartz may require additional preparation, such as that put forward by Roberts et al. (2009). The method applied in this paper has the benefit of avoiding the use of HF, which, whilst often a rapid preparation stage, can be more hazardous and requires more stringent safety procedures.

The secondary advantage of this increase in sample throughput is a wider allowance for the consideration of sampling strategy. In Chapter 4 it was shown that dune bounding surfaces, representing breaks in accumulation, do not always align with chronologically significant hiatuses identifiable by OSL dating. This finding goes against the assumption that it is feasible to 'target' sampling utilising solely bounding surfaces in dunes, particularly for sites new to be studied where the nature of dune accumulation in terms of temporal variability cannot yet be inferred. Range-finder dating provides a practical approach that lies between the two problematic strategies. Significant samples can be preliminarily dated, with the scope that if dune stratigraphy is visible, this technique can be used in tandem with utilising bounding surfaces; whilst their chronological significance at the precision level of OSL dating cannot be assumed, bounding surfaces nonetheless represent breaks in accumulation and for which targeting provides the only way to increase the precision of the dating of hiatuses in dune accumulation.

7.5. Conclusions

The potential of using partially prepared samples as range-finder ages has been investigated. Raw material could not be dated, as reported elsewhere. However, D_e values within 15% of the target D_e have been measured for two-thirds of samples using HCl-only treated material when dated using a double-SAR protocol and a region-independent SGC. The application of both a SGC constructed using samples from the region and an independent SGC provided similar D_e estimates. Those samples for which D_e estimates are not within 15% of the target D_e are underestimated. This underestimation is attributed to the presence of feldspars and other luminescent minerals, such that the IR bleach prior to OSL measurement is not sufficient to allow for a post-IR OSL signal that is dominated by the quartz signal. Deconvolution of the CW-OSL curve, stimulated using green diodes, did not provide an improved alternative method. These results are encouraging for increasing throughput of OSL samples, potentially allowing for significantly higher sampling resolution, and allowing for a more thorough assessment of the representativeness of sampling strategy.

SECTION 3: IMPLICATIONS

8 Interpreting and modelling Late Quaternary dune accumulation in the southern Arabian Peninsula

Paper Five: Carly L. Leighton, Richard M. Bailey, David S.G. Thomas

Submitted to *Quaternary Science Reviews*

Abstract

One of the most fundamental questions in the reconstruction of Quaternary dryland environmental conditions is: what do dune OSL ages mean in terms of palaeoenvironmental change? This paper investigates the relationship between dune chronological records and external environmental forcing in the southern Arabian Peninsula during the last 30 ka. Aeolian records from the region are reviewed with reference to other regional palaeoenvironmental proxies, and these findings are related to both a qualitative and modelled assessment of dune response to the aeolian system state of the northeastern Rub' al Khali. The model replicates a range of features of the regional dune chronology when forced by three external parameters (sediment supply, sediment availability, and transport capacity), including extensive regional dune accumulation during the late Pleistocene-Holocene transition and reduced activity during the early Holocene humid period. Dune chronologies incorporate the influence of both external forcing parameters and localised short-term factors included as stochastic processes. Thick sedimentary units most likely represent external forcing conditions conducive to aeolian sediment transport and deposition, but at the same time these factors may be represented by periods of erosion of sediment at different sites. Confident interpretation of past environmental conditions is therefore not possible based on results from individual stratigraphic records. Sampling at multiple locations is needed in order to distinguish dune accumulation and preservation due to external forcing from stochastic processes of dune development.

8.1. Introduction

8.1.1. Dune chronologies as palaeoenvironmental tools

Whilst past climatic conditions can be established by the analysis of a range of proxies from different archives, the terrestrial response to these changes are generally more sparsely recorded and less well understood. In drylands in particular, different (geo)proxies may appear to reveal seemingly contradictory responses to climatic forcing as a function of local environmental and geomorphological context, including spatial and temporal variability in sensitivity (Thomas and Burrough, 2012). Often the relationships between climatic forcing and the processes recorded by different proxies are complex or variable through time, including the relationship between dune activity and aridity (e.g. Chase, 2009; Roskin et al., 2011). In addition, apparent contradictions may reflect actual regional spatial and temporal variability in climate and differences in proxy responses. For example, this is recorded in the spatial distribution of summer monsoonal rainfall noted in both proxy records and modern observations along the west coast of India (Sarkar et al., 2000). Or this may occur as a result of rapid and abrupt climatic events that may not be clearly captured in proxy records due to the precision of the chronometric methods used to date them (Boulter et al., 2010; Thomas and Burrough, 2012). Therefore, for an event-based chronology largely determined by rapid and/or spatially isolated environmental fluctuations, the interpretation of events must correspond to the scale of the processes occurring if the record is not to be falsely interpreted as reflecting climatic changes at larger scales. Variability in the geomorphic signal should therefore be expected and not ignored (Thomas and Burrough, 2012), with increasing recognition of the importance of context and localised responses to forcing in the interpretation of palaeoenvironmental records.

Desert sand dunes have the potential to provide important and extensive records of the response of drylands to past climatic changes. The accumulatory (although discontinuous) nature of linear dune development (Munyikwa, 2005; Wiggs, 2001) may allow for changes in accumulation rate and/or the nature of sediment accumulation, such as intervals of palaeosol development (Fitzsimmons and Telfer, 2008; Fitzsimmons et al., 2007), to be recorded. The application of optically stimulated luminescence (OSL) dating to dunes has enabled chronologies of dune accumulation and preservation to be correlated with other archives of environmental change, often in regions where other records of palaeoenvironmental change are scarce. However, this has not been without debate (Chase, 2009; Thomas, 2013). The interpretation of chronologies is problematic given the discontinuous nature of dune sedimentary structures, the numerous forcing factors influencing dune development, and variable sensitivity of aeolian processes to environmental forcing.

8.1.2. Factors influencing dune chronologies

Isolating forcing factors and deciphering the environmental conditions under which accumulation and preservation preferentially occur over erosion is difficult due to the influence of numerous forcing factors on the aeolian record, including temperature, wind strength, direction and variability, precipitation, sediment supply, and human activity (e.g. Chase and Thomas, 2006, 2007; Forman et al., 2005; Goudie et al., 2000a; Preusser, 2009; Roskin et al., 2011; Yang et al., 2012). Bailey and Thomas (submitted) describe the problem as one of successive ‘filtering’, whereby the information of initial forcing is transformed through geomorphological response and depositional and erosional processes to produce the sedimentary sequence available for dating and interpretation. The interaction of these factors to ‘produce’ dune structures is not straightforward. Geomorphic response is nonlinear and may vary under similar climatic forcing at different times (Boulter et al., 2010). Reworking and erosion of units further complicates matters, as preservation is not solely a function of environmental conditions at the time of deposition, but also those subsequently. In addition, where the palaeoenvironmental record is relatively well known, its use in aiding interpretation may run the risk of circularity.

To aid the interpretation of dune stratigraphic records in terms of past climatic conditions, some authors have considered forcing factors as a number of simplified components. For example, Kocurek's (1998) model of aeolian system response uses a sequence stratigraphic approach to understand changes in aeolian accumulation and preservation in the Sahara. Dune accumulation and preservation is based on the height of the accumulation surface over time and relative sediment flux rates. The accumulation surface rises, is bypassed or falls when there is a positive, neutral and negative sediment budget respectively. The preservation of units is dependent on the availability of preservation space and sediment state, defined by sediment supply, sediment availability and transport capacity (Kocurek and Lancaster, 1999). Distinguishing which of these factors is the dominant cause of accumulation and preservation (or of the absence of units) is difficult, and perhaps impossible, given their interrelated nature. For example, preservation potential, due to changes in sea level and precipitation, has been used to explain site differences in dune chronologies from the southern Arabian Peninsula (Stokes and Bray, 2005), whilst sediment supply has been interpreted by others as the most important control (Preusser, 2009). Kocurek and Lancaster (1999) attempt the separation of these influences by the quantification of sediment state components in the Mojave Desert. Whilst the quantification of natural systems is not always possible, the authors argue that this framework provides a rigorous approach to assessing the sediment state of aeolian systems and the relative importance of external influences. A modelling approach may therefore be useful in order to assess which combinations of forcing components could have resulted in the formation of the preserved sedimentary record.

Several papers have noted differences between the chronologies of sampled records at both the dune and dunefield scales as a result of local controls (Chapter 6; Cohen et al., 2010; Stokes and Bray, 2005; Telfer and Thomas, 2007). In light of this, how records can most appropriately be amalgamated and apparent conflicts reconciled is an important consideration. Chapter 6 reported a regional signal of dune accumulation and preservation, achieved by calculating net accumulation rates for dune chronologies across the northeastern United Arab Emirates (UAE). This approach is deemed more appropriate than many frequency-based graphic methods of data presentation, as the plotting of multiple age groups makes visible the corroboration of records from different sites. Further, the incorporation of depth information reduces the dominant influence of sampling resolution on the interpretation of ages. Regional patterns can be identified over localised dune responses, but the requirement of using numerous sampling sites and sampling at high resolution were highlighted as important for the effectiveness of this approach.

Given these findings, this paper investigates the relationship between dune chronological records and environmental forcing. A fundamental question in the reconstruction of Quaternary dryland environments is: what do dune OSL ages mean in terms of palaeoenvironmental change? The aim of this paper is to answer this question in the southern Arabian Peninsula, a region with a relatively well-dated and well-understood palaeoclimate record, in order to elucidate the controls upon accumulation and preservation during the last 30 ka. Whilst there are many examples of process-based dune research and palaeoenvironmental studies that use dune records to infer past climatic conditions, there is (as far as we are aware) no research that brings together these two approaches to understanding dunes as records of environmental change. This will be achieved by reviewing aeolian and other terrestrial palaeoenvironmental records for the region, and relating these findings to both a qualitative and a modelled assessment of the dune response to the aeolian system sediment state of the northeastern Rub’ al Khali.

8.2. Regional setting

Dunes of the Rub' al Khali (which covers parts of Saudi Arabia, UAE, Yemen and Oman) and the Wahiba Sands (southern Oman) (Figure 8.1) have been intensively dated, with over 300 luminescence ages published.

The Rub' al Khali is hyperarid, generally receiving on average less than 50 mm annual rainfall (Edgell, 2006). Within the UAE, there is a gradient of increasing precipitation and

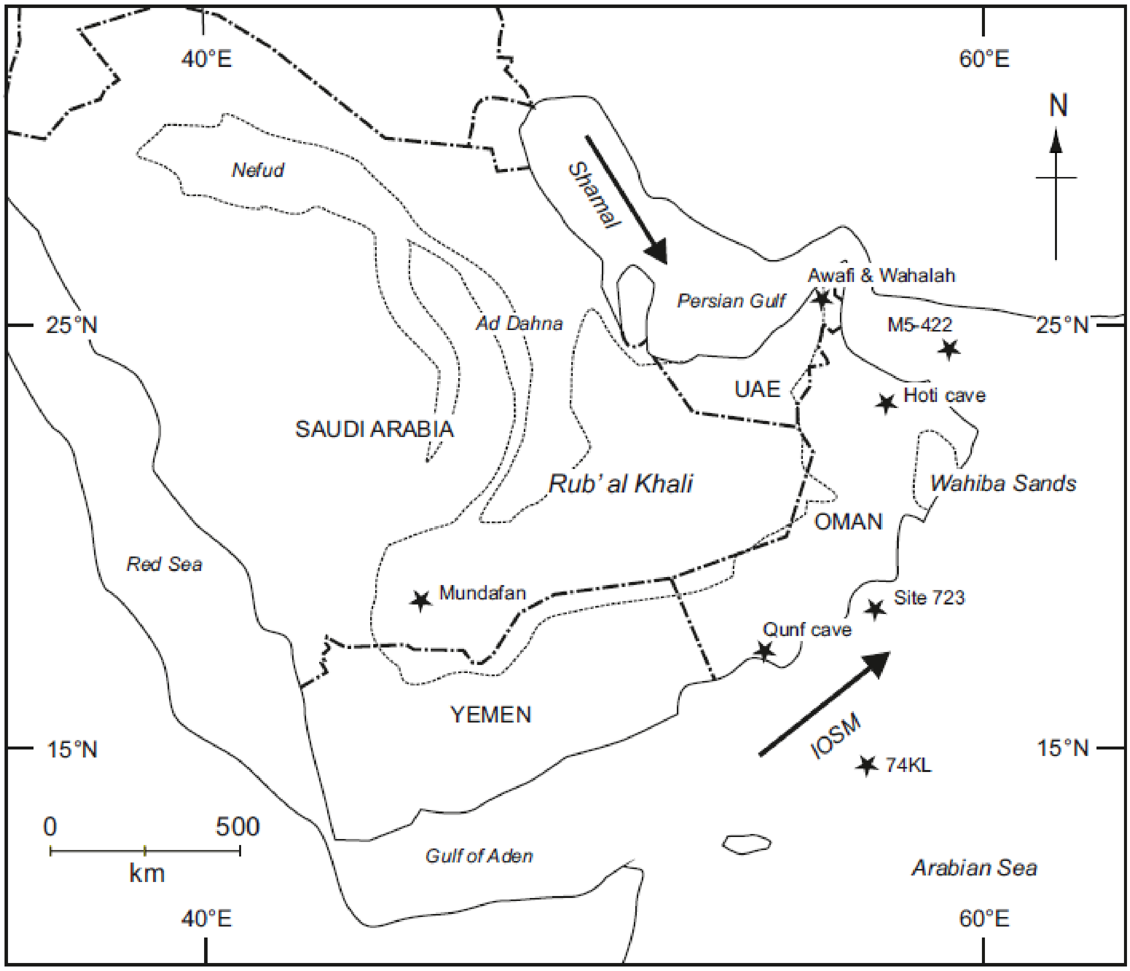

Figure 8.1: Location map of the southern Arabian Peninsula. The main wind directions of present-day *Shamal* and Indian Ocean Summer Monsoon (IOSM) are shown. Starred sites show the location of previously sampled marine (Cullen et al., 2000; Gupta et al., 2003; Sirocko et al., 1993; 2000), palaeolake (McClure, 1976; Parker et al., 2004; 2006; Preston, 2011; Preston et al., 2012; Rosenberg et al., 2011) and speleothem sites (Burns et al., 2001; Neff et al., 2001; Fleitmann et al., 2007) discussed in the main text.

decreasing temperature towards the northeast (Böer, 1997). Two dominant wind systems have influenced the dune systems in the southern Arabian Peninsula during the Late Quaternary through variations in strength, position and associated precipitation. The northwesterly *Shamal* has a clockwise path across Arabia and the Persian Gulf. Blowing from the north-northwest in the UAE, it is the dominant wind for sand transport in the Arabian deserts (Edgell, 2006; Glennie and Singhvi, 2002). Southwesterly Indian Ocean Summer Monsoon (IOSM) winds presently blow along the southern coast of the Arabian Peninsula during the summer months and are the dominant wind system influencing the Wahiba Sands (Edgell, 2006; Glennie, 1998).

The region's palaeoclimate has been reconstructed using a range of palaeoenvironmental archives, including marine cores, speleothems and lacustrine records (e.g. Fleitmann et al., 2003b; Gupta et al., 2003; Parker et al., 2006; Schulz et al., 1998), which will be further discussed in the following sections. Evidence of significant climatic changes during the Late Quaternary, including in patterns of atmospheric circulation, provides a good test of the response of dune systems to rapid and relatively well resolved palaeoenvironmental change.

8.3. Large-scale controls on dune accumulation and preservation

Aeolian system sediment state is defined by sediment supply, sediment availability and transport capacity (Kocurek and Lancaster, 1999). These three components have been simplified in the following discussion to describe changes in the large-scale controls on aeolian system processes in the region; sea level changes in the Persian Gulf, moisture, and the strength of the northwesterly winds respectively.

8.3.1. Sediment supply

The region's Late Quaternary dune record has been interpreted by Goudie et al. (2000a), Glennie and Singhvi (2002) and Preusser (2009) as significantly contributed to by changes in sediment supply, as a result of major sea level changes. The Persian Gulf is shallow, with a maximum depth today of ~90 m (Williams and Walkden, 2002) and average depth of ~35 m (Lambeck, 1996). During the last glacial maximum (LGM), sea level was 120-130 m lower than at present and thus the floor of the Gulf was exposed to subaerial processes (Lambeck, 1996; Williams and Walkden, 2002). Sediments were deflated and transported to the Rub' al Khali by the *Shamal* winds, resulting in the high calcareous content of the coastal dunes in the UAE (Garzanti et al., 2003). By the LGM the sediments may have become cemented by calcite or stabilised by vegetation, and deflation therefore reduced (Preusser, 2009; Teller et al., 2000). However, OSL ages from marine deposits of Zeugen along the northern UAE coastline indicate that the Gulf floor may not have been completely dry during the LGM (Wood et al., 2012), and hence supply and availability of sediments from the Gulf may have been more variable during the last glacial than previously thought.

Following the LGM rising sea level led to the marine incursion of the Persian Gulf. This event has previously been modelled to have started by 12.4 ^{14}C ka BP[4], with much of the seafloor exposed until ~8 ^{14}C ka BP[5] (Lambeck, 1996). Teller et al. (2000) tentatively align rapid rises in Gulf sea level at 12-11.5 and 9.5-8.5 ^{14}C ka BP[6] with meltwater pulses (MWP) 1a and 1b at ~14.1 and 11.3 ka respectively (Bard et al., 2010; Stanford et al., 2006). Inundation would not have been spatially uniform, with the western basin filling later (Lambeck, 1996). Sea level transgression led to increased sediment production before refilling was sufficient to reduce sediment supply. Sea level then peaked at 1-2 m above

[4] ~14.5 cal. ka BP (^{14}C ages calibrated on IntCal09 curve using OxCal 4.1, Bronk Ramsey, 2009a)
[5] ~8.9 cal. ka BP
[6] ~13.9-13.4 cal. ka BP and ~10.7-9.5 cal. ka BP

present level at ~5.5 ^{14}C ka BP[7] before returning to present level after ~2.3 ^{14}C ka BP[8] (Edgell, 2006; Williams and Walkden, 2002).

8.3.2. Transport capacity

During glacial periods the *Shamal* winds blew from the west-northwest and were stronger and less curved, as evidenced by dune bedding orientations (Glennie, 1998; Glennie et al., 2002). Magnesium content in Arabian Sea core 74KL, most likely from palygorskite and dolomite minerals transported as dust from the Arabian Peninsula, is interpreted as representing maximum aridity and strength of the northwesterlies between 18-16 cal. ka BP, which aligns with Heinrich event 1 (H1;~16.9 ka) (Sirocko, 2000). During the LGM the IOSM was weaker and its influence less significant (Pourmand et al., 2004; Sirocko, 2000).

8.3.3. Sediment availability

Some of the first radiocarbon dates from the Rub' al Khali were from interdune lacustrine sequences at Mundafan and five other sites in the southwestern Arabian Peninsula (McClure, 1976). Two main periods of lake development were identified at 36-17 ^{14}C ka (concentrated in 30-21 ^{14}C ka) and 9-6 ^{14}C ka[9]. However, the earlier humid phase is suggested to be an underestimation of age as a result of contamination by younger ^{14}C (Glennie and Singhvi, 2002; Preusser, 2009; Rosenberg et al., 2011). Revisiting the original sites, Rosenberg et al. (2011) found no evidence of a late Pleistocene wet period, with humid phases dated using radiocarbon, OSL and amino acid racemization (AAR) at ~125 ka, 100 ka, and 80 ka in addition to the early Holocene. Dating of lacustrine sediments at sites in Oman and the Nefud desert support these findings (Rosenberg et al., 2012, 2013). However, lacustrine sediments near Jebel Faya have been dated (using OSL) to earlier in

[7] ~6.3 cal. ka BP
[8] ~2.3 cal. ka BP
[9] 41.2-20.1 cal. ka BP (34.7-25.1 cal. ka BP) and 10.2-6.8 cal. ka BP respectively.

MIS 3 (~61-58 ka), which has been aligned with an intensification of the IOSM at ~58 ka (Parton et al., 2013). There is therefore still some uncertainty over the timing and extent of relatively more humid periods during MIS 3.

In addition to the two humid phases identified by McClure (1976), undated lacustrine sediments at Awafi indicate a wet phase between 18-13 ka, based upon the dating of overlying dune and underlying basal sands (Goudie et al., 2000a; Parker, 2009). A third set of lacustrine sediments at Mundafan have also been dated to ~15.0-11.5 ^{14}C ka BP[10] (McClure, 1976), and in Saudi Arabia speleothem growth has been dated to ~15.8 ka (Fleitmann et al., 2004). However, other records show no indication of an increase in moisture during this time interval (Burns et al., 2001; Fuchs and Buerkert, 2008; Rosenberg et al., 2011), including speleothem records in Oman and Yemen.

One interpretation of this evidence is that this debated pluvial in parts of the southern Arabian Peninsula is the result of the increasing influence of a northerly source of moisture at about 16 ka. This hypothesis is supported by a rise in lake levels at Lake Lisan, a precursor lake to the Dead Sea (Stein et al., 2010). Alternatively, the possible wet phase has also been hypothesised to align with the Bölling-Allerød interstadial (15-13 ka) (Parker, 2009). This suggestion is supported by evidence of re-strengthening of the IOSM between ~15-13 ka prior to the Younger Dryas, when monsoon strength rose rapidly and aeolian input in the Arabian Sea fell (Pourmand et al., 2004; Schulz et al., 1998). Given the lack of records supporting the presence of a wet interval during the late glacial-interglacial transition and imprecise chronologies, it is difficult to choose one interpretation over the other. However, the underlying mechanism has important implications for understanding dune accumulation and preservation during this time interval.

[10] 18.2-13.3 cal. ka BP

Following the LGM when the monsoon was weak, the IOSM strengthened in a series of abrupt steps at ~16, 13, 11.5, 9.5 and 9.1 ka to a peak strength and northward-most extent in the early Holocene, before weakening gradually from ~8.5 ka until the present (Overpeck et al., 1996; Sirocko, 2000; Sirocko et al., 1993; Thamban et al., 2007). Depleted groundwater isotopic values during the Holocene and previous interglacials indicate that a greater proportion of precipitation was sourced from the southern Indian Ocean than at present (Fleitmann et al., 2003b). A series of palaeoenvironmental sites and different proxies (each with their respective lag times) across southern Arabia track the latitudinal migration of the IOSM: ~11 ka in the lowlands of Yemen (Lézine et al., 2007); ~10.5 ka in southern Oman; ~10.1 ka in northern Oman (Fleitmann and Matter, 2009); ~8.5 ka in the UAE (Parker et al., 2004, 2006). The period of fastest speleothem growth from Hoti Cave, northern Oman, is between ~8.3-7.9 ka (Neff et al., 2001). The aligned timing of lacustrine and speleothem records in Southern Oman and Yemen indicates an abrupt arid-humid transition (Lézine et al., 2010). The *onset* of the early Holocene humid phase and impact on the terrestrial environment are therefore fairly well corroborated across a range of records.

The IOSM then gradually weakened and its mean position moved southwards towards its present zone of influence, although there is some need for conciliation of the timing of these changes. Marine core 74KL shows an increase in dolomite input at ~8.6 ka, indicating that the location of the ITCZ had moved sufficiently southwards for dust deflated from northern Arabia and the Gulf to be transported to the western Arabian Sea (Sirocko, 2000; Sirocko et al., 1993). Dust transport to this location initially halted at ~9.9 ka (Sirocko et al., 1993), which is after the recorded increase in precipitation at Hoti Cave and before the establishment of permanent lacustrine conditions at Awafi. Sedimentation rates in the Hajar Mountains fell at ~8 ka (Fuchs and Buerkert, 2008), whilst lacustrine records in Yemen lowlands indicate desiccation at ~7 ka (Lézine et al., 2010). However, in contrast to these indications of the monsoon weakening in the early Holocene, lakes persisted at Awafi, Wahalah and in the highlands of Yemen until the mid-Holocene (Lézine et al., 2010; Parker et al., 2006; Preston, 2011). Fuchs and Buerkert (2008) suggest that the reduction in sedimentation rate could be due to a gradual reduction in rainfall intensity below a significant threshold to produce sufficient sediment. The discrepancy between records may also be explained by higher groundwater levels at coastal sites and runoff from the highlands (Lézine et al., 2010). There is an abrupt increase in $\delta^{18}O$ values at ~6.3 ka at Hoti Cave to ~1‰ below modern values, explained by the influence of a northerly source of precipitation on more northerly located records, whilst at Qunf Cave (southern Oman) the decline is more gradual (Fleitmann et al., 2007). These apparently misaligned signals may therefore reflect a gradual reduction in strength and influence of the IOSM from ~8 ka, the varying spatial influence of alternative moisture sources, and the differing sensitivities of these palaeoenvironmental proxies.

Lakes were present but intermittent between 5.9-3.7 ka at Wahalah and 5.9-4.1 ka at Awafi (Parker et al., 2006; Preston, 2011). Aridity between 5.9-5.1 ka appears more sustained than the brief arid fluctuations during the early Holocene humid phase, and is also marked by the lowest levels of human activity in the region (Preston et al., 2012). Awafi and Wahalah lakes were then desiccated at ~4.1 and 3.7 ka respectively (Preston, 2011; Preston et al., 2012). This event appears to be regionally extensive, as it aligns with an increase in terrigeneous dust input to a marine core from the Gulf of Oman at 4.2 ka (Cullen et al., 2000) (Figure 8.4c), a reduction in Indus river discharge at 4.2 ka (Staubwasser et al., 2003), and a period without speleothem growth in Hoti Cave between 5.3-2.6 ka (Fleitmann et al., 2003b). The lake at Awafi was temporarily re-established between 4-3 ka (although these sediments have not been precisely dated), suggesting a brief return to wet conditions (Parker et al., 2004); an interpretation corroborated by indications of a weaker monsoon in marine cores (Lückge et al., 2001; Sarkar et al., 2000).

These large-scale environmental changes will be discussed further in the following sections and related to the regional aeolian record.

8.4. Aeolian records

Dune chronologies from the northeastern Rub' al Khali have been presented in a number of recent studies (Chapters 4 and 6; Atkinson et al., 2011, 2012; Goudie et al., 2000a; Parker and Goudie, 2007; Parker et al., 2006). These were reviewed and presented as net accumulation rates in Chapter 6, in order to establish a regional chronology of dune activity. The *net* accumulation rate represents the average rate that a *preserved* depth of sediment was deposited (i.e. continuous deposition is assumed in the calculation of the net accumulation rate, although it is recognised that over the relevant time interval both deposition and erosion occurred). This method of presentation includes depth information, and hence does not solely rely on frequency of sampled ages for interpretation. Ages from Liwa and the Wahiba Sands (Preusser et al., 2002, 2005; Radies et al., 2004; Stokes and Bray, 2005) have been incorporated in addition to those presented in Chapter 6 to produce Figure 8.2. Each bar represents an age group, which is a clustering of adjacently sampled ages within errors of each other, at a specific site. The 'as sampled' accumulation rate is calculated as the difference in depth between the upper and lower samples in the age group divided by the time interval between the mean ages of the oldest and youngest samples. The 'minimum interval' net accumulation rate is calculated by the minimum depth interval (as above) divided by the minimum time interval over which the unit could have accumulated, which is calculated as a one standard error interval above and below the relative weighted mean age (an homogeneity test is used to justify this assumption, Galbraith, 2003); otherwise the 'as sampled' time interval and rate is used.

During the last 30 ka dune OSL ages indicate regional accumulation (indicated by overlapping peaks) centred on ~30-26.5, 22.5-18, 16-9, 6-2.7, 2.1-1.6, 1.1 and 0.7 ka.

However, the scarcity of corroborated ages before ~16 ka means that more ages are needed in order to distinguish peaks from sampling bias (Chapter 6). This is in part inevitable for older ages due to accessibility of sampling and the expectation of reduced preservation with increasing age (Telfer et al., 2010). It should be noted that wide peaks do not necessarily equate to more significant deposition, as the age interval may reflect large age uncertainties which 'blur' different age groups; the individual age groups will therefore span a larger time interval than if the ages were more precise. As discussed above, each interval represents a net, or average, accumulation rate, including periods of higher deposition rates and erosional periods, and not a continuous period of accumulation. The 'true' intervals of accumulation of the sampled sections are likely to be somewhere in between Figures 8.2a and b, representing the 'minimum interval' and 'as sampled' net accumulation rates respectively.

Major accumulation between ~16-9 ka proved persistent across multiple sites, and

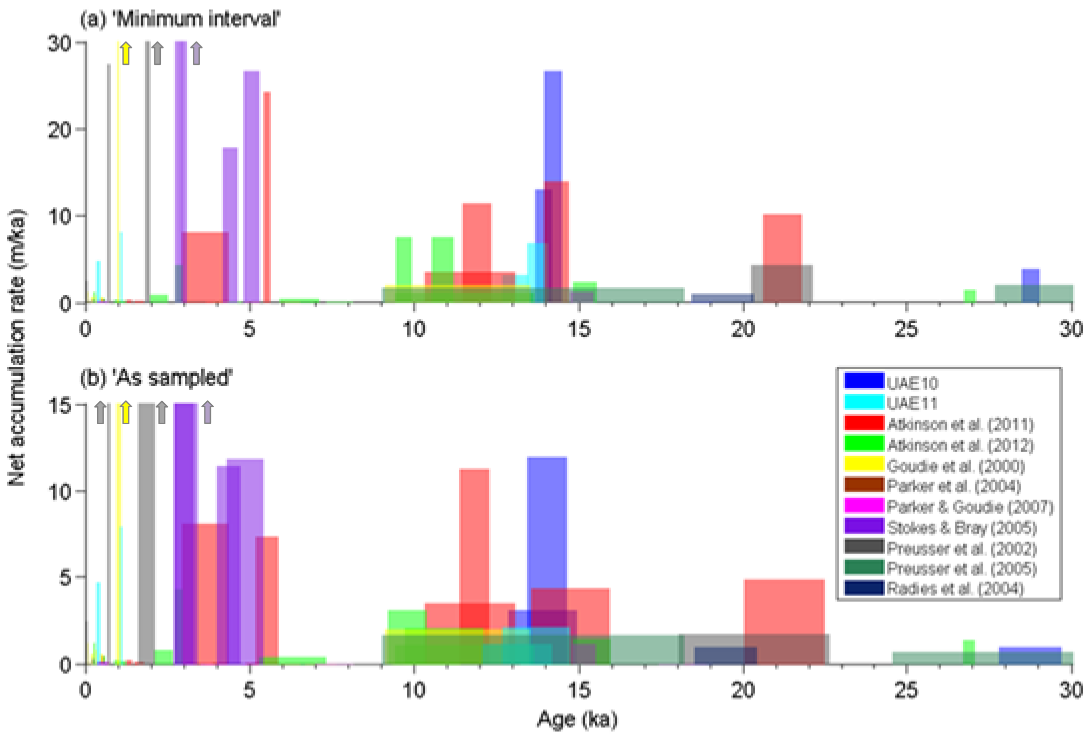

Figure 8.2: Net accumulation rates from dune sites in the southern Arabian Peninsula: (a) 'minimum interval' net accumulation rate; (b) 'as sampled' net accumulation rate.

represents the most continuous period of major accumulation across the southern Arabian Peninsula. Following a reduction in accumulation rates between ~9-6 ka, there is an increase in aeolian deposition and preservation, with multiple sites recording high accumulation rates at ~5.5-2.7 ka and sporadic activity until the present. The more variable nature of accumulation in the late Holocene is likely in part to be a result of the greater precision of these younger ages, which correspondingly reduces the time interval of each age group whilst increasing the net accumulation rate (Chapter 6). In other words, if these depositional units were sampled and dated several millennia into the future following further aeolian deposition, lower precision on the age groups could produce apparently longer age intervals with lower net accumulation rates. The relatively small number of ages and low accumulation rates recorded in Liwa during the late Pleistocene-Holocene transition is likely the result of low vertical sampling resolution.

An advantage of utilising this method of data presentation is that the individual studies are shown and site differences can be identified. Figure 8.3 shows the spatial distribution of net accumulation rates by site. There is significant variability in chronologies between sites, although there is no age group that is only sampled at one location. This indicates that whilst local factors determine whether erosion or deposition dominates at individual sites, a regional signal is apparent and can be identified when chronologies are combined.

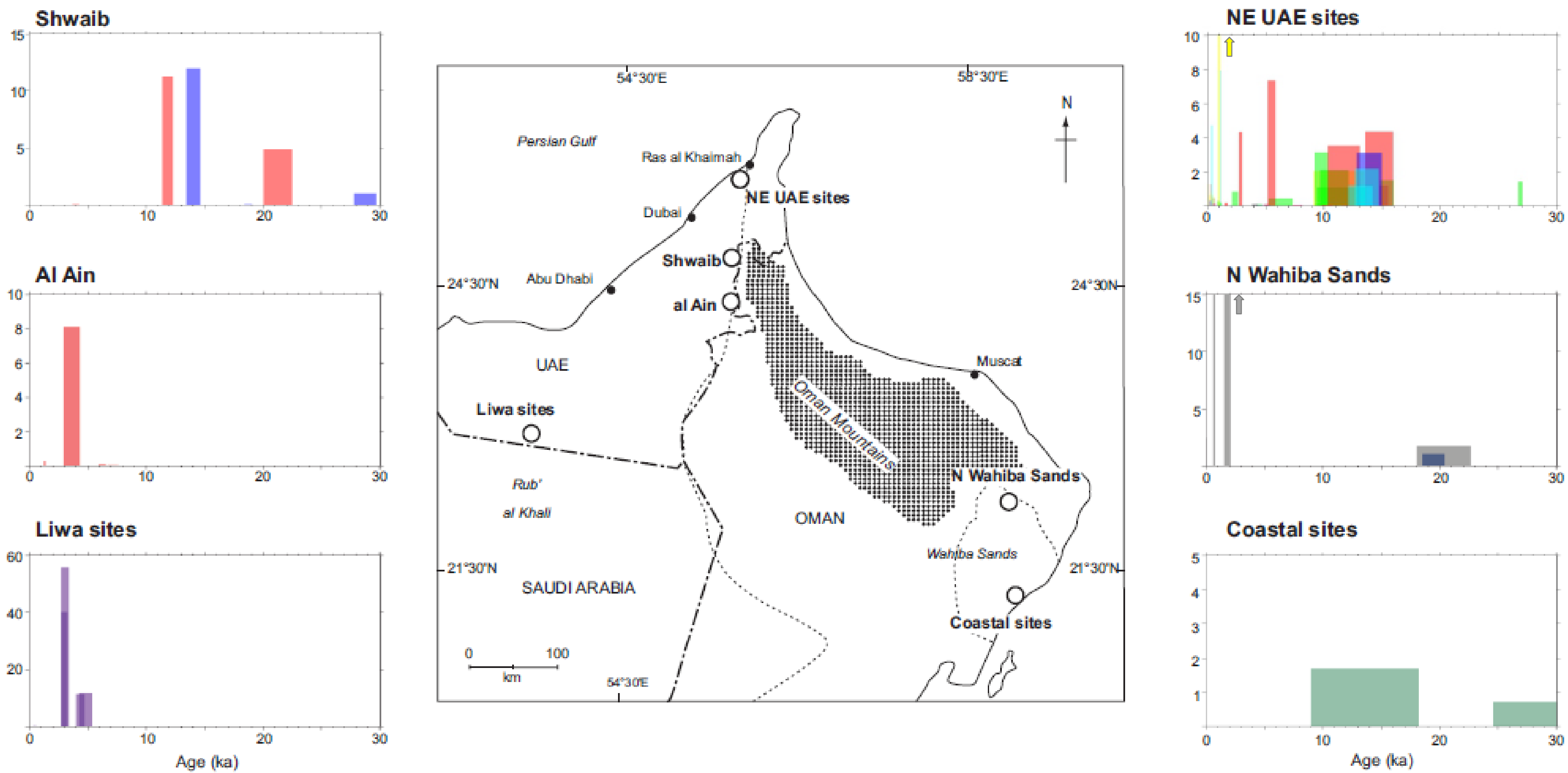

Figure 8.3: Changes in 'as sampled' net accumulation rate by site in the southern Arabian Peninsula. See Figure 8.2 for key.

8.5. Matching the dune record and the environmental history

Palaeoenvironmental proxy records represent responses to external forcing that are spatially and temporally variable. For example, large environmental forcing and/or relatively low proxy sensitivity to forcing will result in a largely externally forced signal. This section will review a number of records with a focus on attempting to explain the dune accumulation record in terms of past climatic factors.

8.5.1. Late Pleistocene (30-11 ka)

Activity v. preservation

Dune accumulation during the last glacial is recorded at ~30-26.5 and 22.5-18 ka, indicating that sufficient sediment was available for significant accumulation by aeolian processes. Figure 8.2 shows a reduction in net accumulation rate between ~24.5-22.5 ka ('as sampled', or ~26.5-22 ka 'minimum interval'), which aligns in timing with Heinrich event 2 (H2; ~24 ka). The Gulf was exposed and regional marine records show high levels of dust transport (Schulz et al., 1998; Sirocko et al., 1991); hence it is unlikely that this hiatus is due to limited sediment supply or availability. Teller et al. (2000) suggest that sediment may have been cemented or stabilised by the time of the late Pleistocene, but if this were the case more aeolian activity would be expected during windier periods when the threshold for sediment entrainment was more likely to have been breached, rather than vice versa (as seen in the record). It is therefore inferred that increased activity as a result of strengthened winds was not preserved extensively. Net accumulation was determined by local conditions conducive to preservation. The subsequent reduction in transport capacity following H2 allowed for more widespread preservation between ~22.5-18 ka. During the period of maximum dust transport to the Arabian Sea ~18-16 ka (Sirocko et al., 1996) there is also a reduction in net accumulation rate. It is therefore argued that some regional events, such as

Heinrich events, can be noticeable in the dune record by their absence. During the last glacial, preservation potential was a key determinant in the production of the sedimentary record.

The amalgamated signal provides a more continuous record than the individual chronological profiles alone, but it is unavoidable that the contribution of sampling resolution to the signal increases with age, as a result of fewer ages and lower precision on these ages. Addition of new research to data in this format will allow for comparison of records and enable reconsideration of previous interpretations.

Humid periods during the late glacial-Holocene transition

There remains debate over the occurrence, timing and extent of humid periods during MIS 2 and 3 (Section 8.3.3). Interestingly, there is a period of dune accumulation between ~30-26.5 ka at Shwaib (Chapter 4), Tawi Asmar in the northeastern Rub' al Khali (Atkinson et al., 2012, 2013), and at Qahid (coastal Wahiba Sands) (Preusser et al., 2005). This activity is only recorded at some sites, suggesting that the local context provided environmental conditions more conducive to activity and/or preservation at some but not all places within the system, although sampling resolution at these time intervals may also be insufficient to have captured the full distribution of activity (Chapter 6). In the regional archives this period aligns with fluctuations in monsoon strength, including a small peak at ~28-27 ka following Heinrich event 3 (H3; ~31 ka) (Pourmand et al., 2004; Schulz et al., 1998), accumulation in the Negev (Roskin et al., 2011), and, globally, a rapid fluctuation in dust transport (Mayewski et al., 1997).

Two possible interpretations of this period give controlling influence to moisture and windiness respectively. Firstly, a relatively short period of wetter conditions (in comparison to, say, the early Holocene humid period), unlikely to have been significant enough for lake presence across the region but sufficient to restrict entrainment and enable an increase in preservation of aeolian accumulation. Alternatively, a reduction in wind strength between H2 and H3 may have been sufficient at some sites for net deposition of sediment and preservation. Given a period of preserved dune accumulation at ~22-18 ka (Figure 8.2), the latter interpretation is thought most likely. A large number of different sites collaborating high net accumulation rates between ~16-9 ka suggests increased dune accumulation and preservation during the late Pleistocene-Holocene transition. There is a hint of bimodality in the regional dune record during this interval (Figure 8.2), and it would be interesting to test the persistence of this distribution further, and particularly its alignment with the undated lacustrine sediments at Awafi (Section 8.3.3), by dating this interval at specific sites using high resolution sampling. The Younger Dryas (~12.9 ka) is thought to have been less regionally extensive than H1 (Roskin et al., 2011), but has been correlated with increased aridity (Fuchs and Buerkert, 2008) and strengthened northwesterly winds (Pourmand et al., 2004; Sirocko, 2000). Together with increasing sediment supply as sea level in the Arabian Gulf began to rise this may have allowed for significant aeolian activity to be preserved, unlike during H1 and H2.

8.5.2. Holocene environmental changes

The influence of the IOSM on the northeastern Rub' al Khali at ~9 ka is marked in the dune record by an abrupt fall in net accumulation (Figure 8.2), prior to the presence of lacustrine sediments at Awafi and Wahalah at ~8.5 ka (Parker et al., 2004, 2006; Preston et al., 2012). Significant late Pleistocene accumulation prior to this transition, with no resolvable increase in accumulation before the hiatus, implies that preservation was not a limitation on accumulation in the late glacial/Holocene transition.

Throughout the Holocene several intervals of weak summer monsoon have been identified (Figure 8.4a), some of which have been correlated to climatic changes in the North Atlantic (Gupta et al., 2003, 2005; Staubwasser et al., 2002; Thamban et al., 2007). Arid intervals

Figure 8.4 has been removed due to Copyright restrictions

Figure 8.4: Comparison of the aeolian record with other palaeoenvironmental proxies for the last 12 ka. (a) Marine core *G. bulloides* data from Arabian Sea marine core 723 (Gupta et al. 2003), grey bands indicate periods of weak summer monsoon; (b) Speleothem records from Hoti Cave (H5), North Oman in blue (Neff et al., 2001) and Qunf Cave in black (Fleitmann et al., 2007). Where the values are unknown from Hoti Cave speleothem growth is shown as a straight line on the modern VPDB value; (c) Dolomite from marine core M5-422 in the Gulf of Oman (Cullen et al., 2000); (d) Geochemical record from palaeolake Awafi (Preston et al., 2012). Red bars are periods of aridity; lines indicate original authors' classified stratigraphic units; (e) 'As sampled' net accumulation rate, see Figure 8.2 for key.

have also been identified by the presence of aeolian sediments in lacustrine deposits at Awafi and Wahalah (Figure 8.4d) (Parker et al., 2006; Preston, 2011; Preston et al., 2012). This evident climatic variability implies that records of dune accumulation, even during the early Holocene humid period, should be unsurprising. Net accumulation rates are nonetheless relatively low during this period. Rapid environmental changes cannot be precisely identified nor resolved within the assimilated geomorphic signal, which in this case is dominated by a major regional climatic shift (i.e. the incursion of the IOSM). A relatively high threshold of dune activation is likely to be required for aeolian activity to be preserved as significant peaks in the net accumulation rate record.

Section 8.3.3 described several types of palaeoenvironmental archives that record the weakening and southwards migration of the IOSM. The 'as sampled' net accumulation rate record shows an increase in activity from ~5.8 ka (Figure 8.4e), which follows an increase in terrigenous sediment input at Awafi and Wahalah at ~5.9 ka (Parker et al., 2006), indicating a relatively rapid response to falling moisture levels and increasing availability of sediment.

The presence of shallow lakes reveals a brief shift to more pluvial conditions (although more variable than during the early Holocene) between 5.1-4.1 ka at Awafi and 5-4.6 ka at Wahalah, suggested to reflect an increase in precipitation from mid-latitude westerly systems (Parker et al., 2006; Preston, 2011). Dune records from northeastern UAE show a reduction in accumulation rate between ~5.2-4.3 ka (Figure 8.2). However, there is evidence of dune accumulation in Liwa during this time (Stokes and Bray, 2005). Further samples may refine this interpretation as a regional or localised humid event. The regional aridification inferred to have led to the desiccation of lakes at Awafi and Wahalah at ~4 and 3.7 ka respectively appears to have been too rapid to be identifiable within the dune record.

After ~2.7 ka some sites record very rapid net accumulation rates (e.g. Goudie et al., 2000a), whilst at others the rates are low. Towards the top of these deposits at some sites, the units are thin and there is a lack of clear stratigraphy (Chapter 4; Atkinson et al., 2012). This more extreme pattern of variability in net accumulation rates than recorded previously could be due to: preservation biased towards younger ages at a few sites, as units are sampled before future subsequent erosion; higher rates due to increased precision of younger ages (Section 8.4); and/or to actual variability in aeolian activity that is resolvable at higher dating precision, such as due to climatic fluctuations (e.g. Lückge et al., 2001; McLaren et al., 2009). Since ~1.5 ka climatic and environmental conditions were probably similar to present (Lückge et al., 2001).

8.5.3. Summary

As a result of the possibility that different hiatuses can represent no accumulation (as may be the case for the early Holocene) or no preservation (possibly during the last glacial and Heinrich events), interpretation of the aeolian dune chronological record is not straightforward. Further, chronological imprecision and proxy sensitivity complicate aligning different records. The above discussion shows that dune chronologies *can* be understood in relation to past climatic changes, and that the record generally reflects broad patterns of environmental conditions well. However, there are aspects of the regional palaeoenvironmental record for which the dune record is too imprecise or sparse to help decipher at this time, requiring further investigation (including high resolution sampling) to allow full interpretation of past environmental change. The next section will assess the potential role of numerical modelling in addressing some of these problems.

8.6. Modelling aeolian system sediment state

8.6.1. Model description

The framework of aeolian system sediment state (Section 8.3; Kocurek and Lancaster, 1999) will be used to evaluate the relative importance of environmental factors that have contributed to the preserved dune record in the southern Arabian Peninsula. Following the qualitative description given in the preceding sections, a more rigorous approach to assessing aeolian system sediment state is introduced here. Sediment supply, sediment availability and transport capacity have been modelled to show change in height of the accumulation surface over the last 30 ka using a numerical model described by Bailey and Thomas (submitted). The model calculates whether erosion or deposition takes place on a surface at each time step, and hence the change in surface height over time.

The model input parameters of sediment supply, wind energy and moisture controls used here are based upon the qualitative interpretation described in Section 8.3, and shown in Figure 8.5 and Table 8.1. These simplified large-scale changes in the forcing parameter inputs, depicted over the past 30 ka, do not reflect the full level of variability expected to have occurred at finer resolutions, given the difficulties in quantifying these components for natural aeolian systems (Kocurek and Lancaster, 1999). The input forcing factors describe regional changes derived from a range of palaeoenvironmental archives, described in Sections 8.3 and 8.5, in order to test whether these environmental forcing factors are sufficient to produce the regional dune record shown in Figure 8.2. The windspeed background level is 7±1.5 m/s (the threshold of sediment entrainment is 6.4 m/s for the model described by Bailey and Thomas, submitted). Peaks in windspeed at 31, 24, 16.9 and 12.9 ka represent H3-1 events and the Younger Dryas respectively. A reduction in windspeed centred on 8.5 ka represents when the mean summer position of the ITCZ was

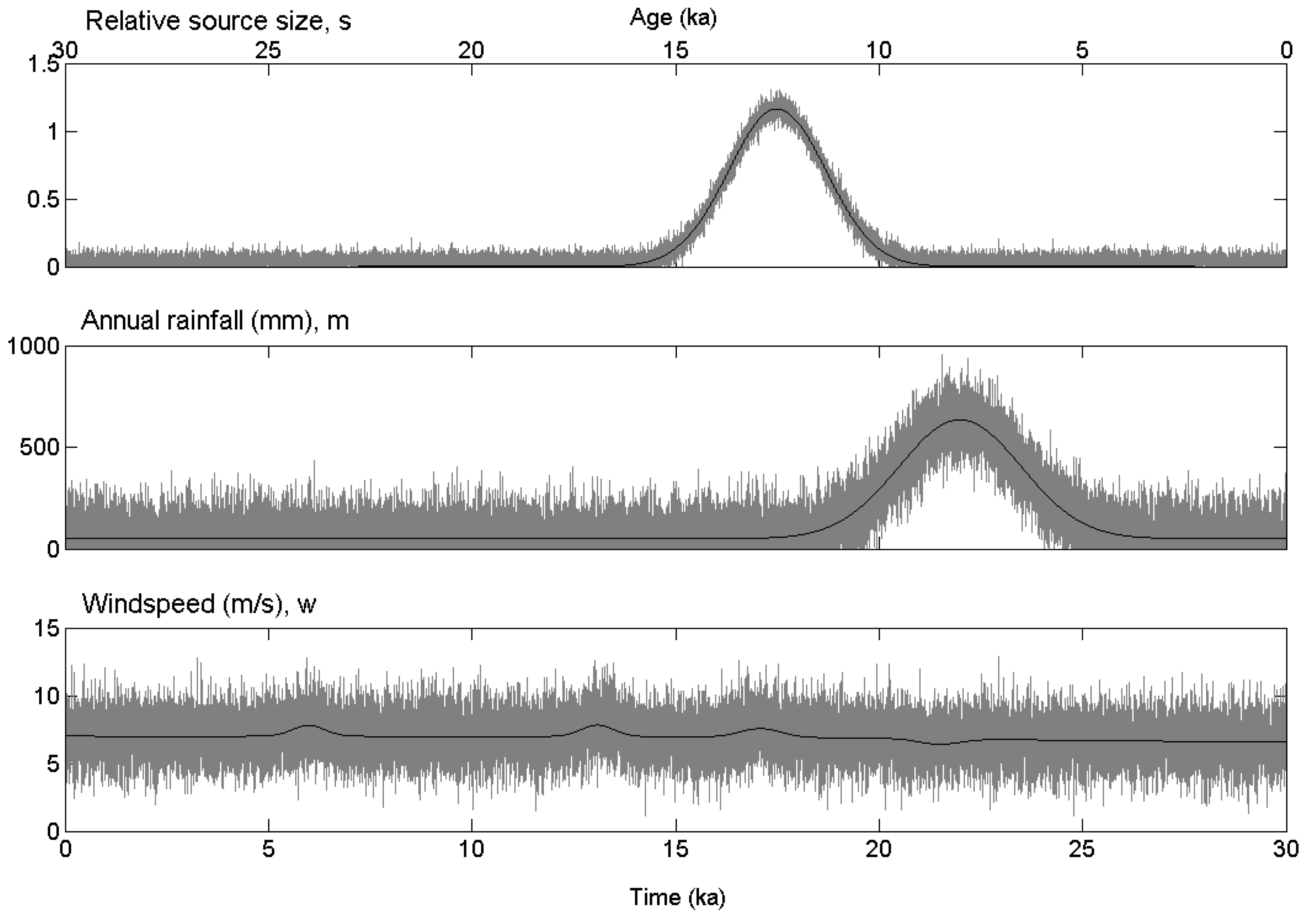

Figure 8.5: Model input parameters over 30 ka. Sediment supply is low with a peak centred on 12 ka. Sediment availability is represented in the model by moisture level, with a peak centred on 8.5 ka. Changes in transport capacity are represented by the strength of the northwesterly winds. Windspeeds are high during the last glacial compared to the Holocene, and lowest during the early Holocene humid phase. Maxima occur at H1-3 and the Younger Dryas.

Table 8.1: Summary of input parameters for model, run for 30 ka. Changes in forcing parameters (peaks and troughs) are described by a normal distribution, with the standard deviation [s.d.] referring to the peak width. The forcing parameters are shown graphically in Figure 8.5.

Sediment state parameter	Related model variable	Background level	Noise	Time of variable peak [s.d.] (ka)	Approximate mean deviation from background
Sediment supply	Relative source size	0	±0.05	12 [1.2]	+1.2
Sediment availability	Moisture (mm)	50	±100	8.5 [1.5]	+600
Transport capacity	Windspeed (m/s)	7	±1.5	31 [0.4] 24 [0.4] 16.9 [0.4] 12.9 [0.5] 8.5 [0.5]	+1 +1 +1 +0.5 -0.5

located over the southern Arabian Peninsula, and northerly sand-transporting winds are therefore inferred to be reduced. The mean external sediment supply background level is zero except from a peak centred on 12 ka (a 2 sigma interval of 14.4-9.6 ka), aligning with the transgression of the Persian Gulf (Lambeck, 1996). The increase in precipitation centred on 8.5 ka aligns with the presence of lakes across the region during the early-mid Holocene (Parker et al., 2004, 2006; Preston et al., 2012). In the absence of more precise palaeoclimatic reconstructions, 'best guess' estimates have been made of these key parameters. Therefore, whilst the model cannot be interpreted in a strictly quantitative manner, the results indicate the nature of dune response at different time periods.

Noise is included for all of the input parameters, which is representative of short-term events and interannual variability. A random component, ε, controls the extent of localised erosion and deposition through time ($\varepsilon=0$ represents a balance between erosion and deposition; $\varepsilon>0$ leads to deposition; and $\varepsilon<0$ leads to erosion of the surface). Here, a value range of $\varepsilon=0.02\pm0.5$ was used. Multiple repeats using the same underlying model parameters (but including randomness within the model so that each individual set of forcing conditions is unique) were used to mimic sampling numerous profiles within the same dunefield.

8.6.2. Results

The stratigraphic histories of individual modelled profiles (Figure 8.6) are dominated by random oscillations in controlling parameters rather than regional climatic forcing for large time periods during the last 30 ka. However, a rapid increase in surface height between ~13-11 ka and a chronological hiatus between ~10-5 ka are persistent dune responses across the multiple model runs (Figure 8.7). These patterns align well with the measured OSL dune chronologies from the northeastern Rub' al Khali (Figure 8.2).

Firstly, an interval of rapid accumulation between 13-11 ka tends to lie within a longer period of rapid, although irregular, accumulation. During high windspeed events, increased sediment deposition in some model runs is accompanied by increased erosion in other model runs (both responses a result of greater sediment transport potential). The preserved net accumulation is a function of the relative balance of depositional and erosional processes, which is partly determined by stochastic forcing and therefore expected to vary locally. During the high windspeed event of the Younger Dryas between ~13-11 ka the surface height increases much more substantially in all model runs with little or no net erosion of the surface, indicating that the concurrent increase in sediment supply is important in allowing for the preservation of sediment transported during the high windspeed event. H1-2 display a less obvious pattern across the different model runs, as sediment supply is low and stochastic forcing plays a larger role in determining dune response.

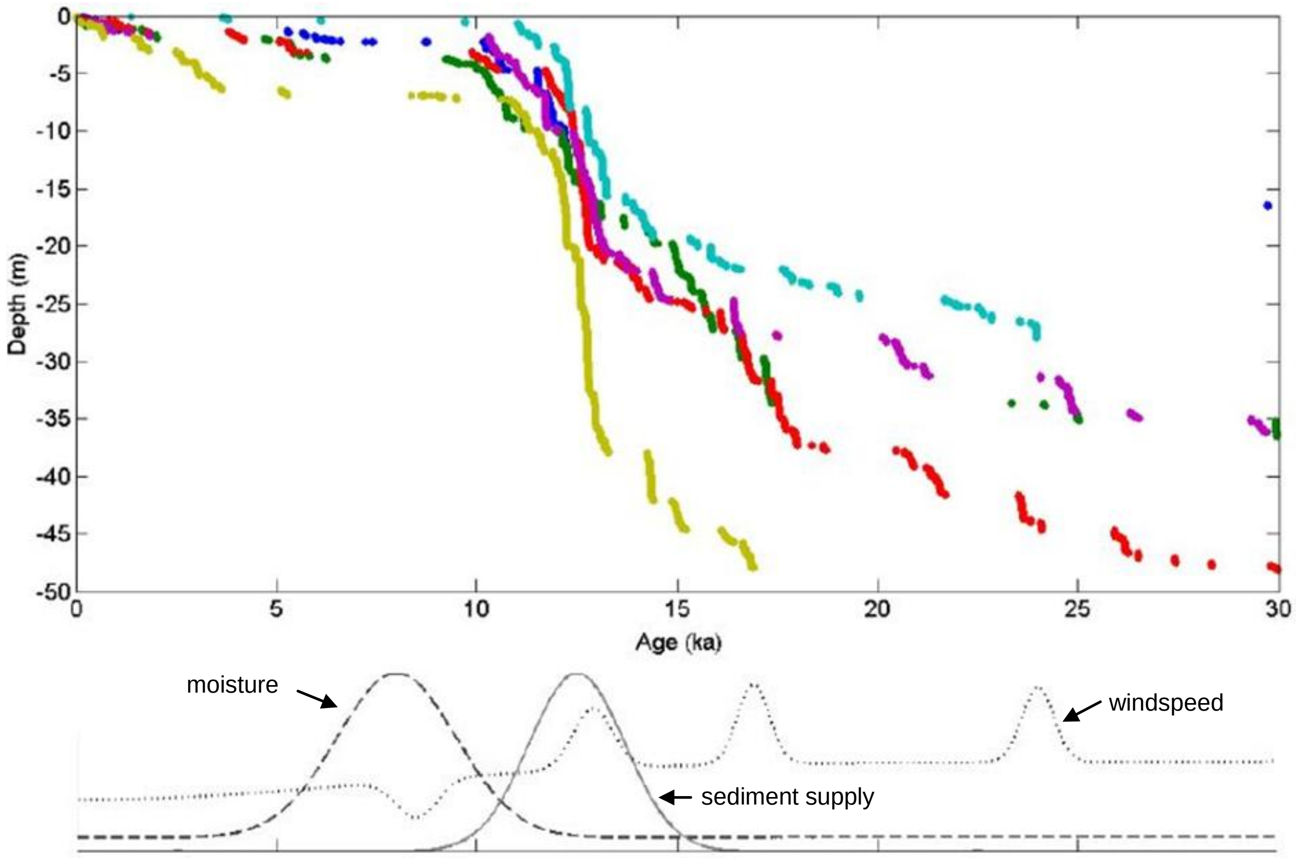

Figure 8.6: Simulated preserved depth of deposited sediment (m) over the last 30 ka. Outputs from six model runs with the same mean input parameters are shown. The normalised smoothed forcing parameters are given below: windspeed (dotted line); sediment supply (continuous line); and moisture (dashed line).

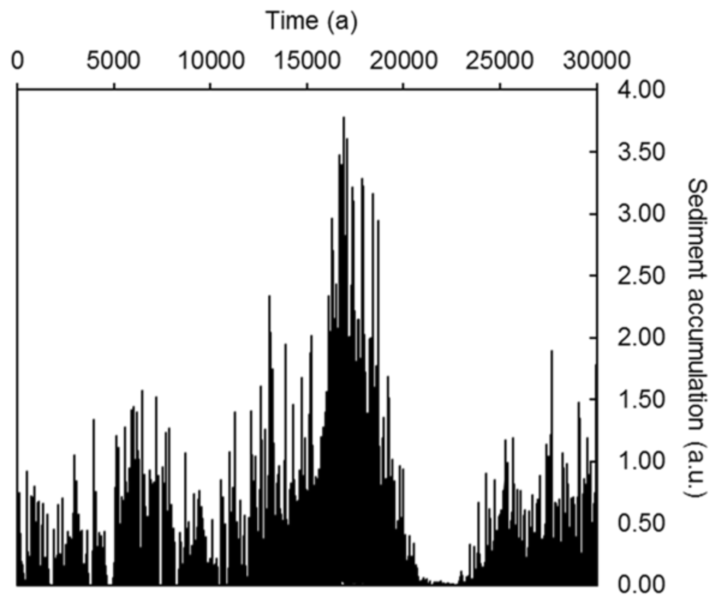

Figure 8.7: Simulated summed accumulation rate over 30 ka. The mean input parameters are the same as those presented in Table 8.1 for 20 model runs. Note the x-axis shows time progression within the model, rather than age.

The second noticeable interval of agreement across both model and preserved dune records is a hiatus in accumulation that aligns with increased moisture during the early Holocene humid period. During this interval reduced sediment availability appears to be the key controlling influence on aeolian activity, as the interval of reduced net accumulation exceeds the period of reduced transport capacity (Figure 8.6). Modern observations indicate that moisture, together with its influence on vegetation cover, is the dominant control on entrainment until sufficient dryness that wind velocity determines entrainment (Lancaster and Baas, 1998; Wiggs et al., 1995, 2004). It is postulated that at larger scales this relationship between moisture and aeolian activity may also hold true, and when there are low moisture levels, wind strength and sediment supply play a more dominant role in determining preservation potential. Resumed accumulation in the model results begins from ~6 ka with sporadic preserved activity, although at a much slower rate than during the late Pleistocene-Holocene transition. Whether ages are preserved during the early Holocene within the model depends primarily on the extent of erosion that occurs following the humid period. As a result of stochastic forcing (noise), aeolian activity can occur when moisture levels are high, as supported by field evidence (e.g. Parker et al., 2006). However, this modelled accumulation is unlikely to be of substantial thickness, and hence unlikely to be preserved unless there is little or no erosion subsequently.

Aside from these two identifiable periods within the modelled 30 ka time interval, the rest of the time period shows more variable accumulation and preservation, with multiple model runs showing distinctly different dune development histories. Under the same relatively stable external forcing parameters, the different dune chronologies are mainly a response to stochastic forcing. This significant variability in the output hinders interpretation of forcing conditions from chronologies alone.

8.6.3. Implications for sampling and interpreting dune chronologies

In the above discussion, model outputs are presented as the depth of preserved sediment resulting from changes in three forcing parameters. However, only limited amounts of this preserved sediment are sampled when dune sediments are dated. Therefore Figure 8.8 shows the chronologies that would result from sampling the six model outputs, which represent different sampled dune profiles, at 0.5 m vertical intervals. It is clear that whether the sampling resolution is sufficient is dependent upon the dune accumulation rate at any particular time, and therefore without continuous sampling thin chronological units may be missed. Under the conditions modelled here, 0.5 m vertical sampling resolution was sufficient to capture most units. However, allowing for uncertainty on the ages (here calculated as 8% of the age) results in separate periods of accumulation becoming indistinguishable within the sampled dune chronology. This is also apparent in the associated ‘as sampled’ net accumulation rates shown in Figure 8.9. Rapid fluctuations are therefore unlikely to be resolved by OSL dating, as shown by Bailey and Thomas (submitted), and under-sampling may result in the misinterpretation of apparent

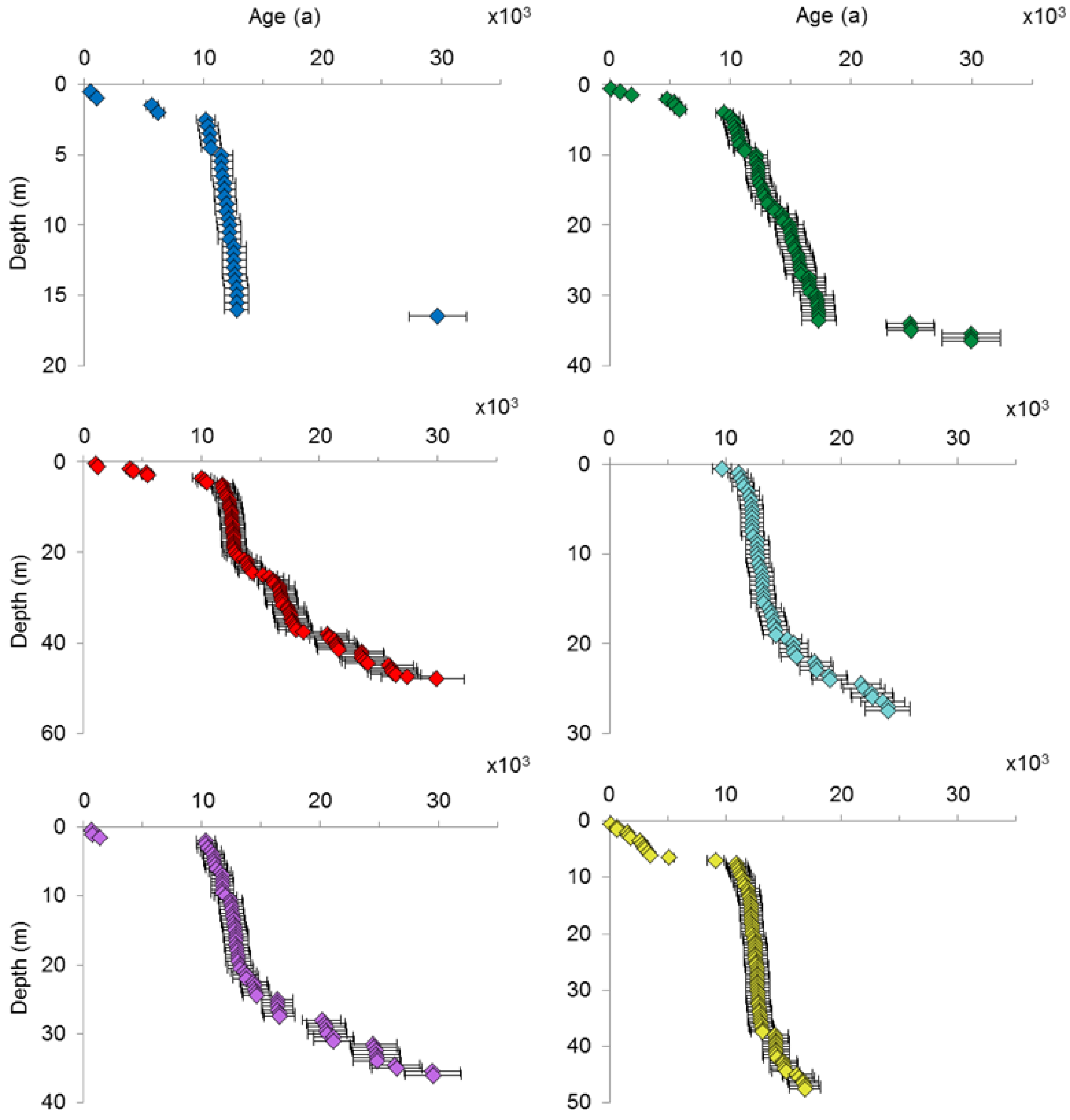

Figure 8.8: Sample output (age vs depth) at 0.5 m vertical sampling intervals for the six model runs (using the same colour coding) shown in Figure 8.6. Note the different scales of the y-axis.

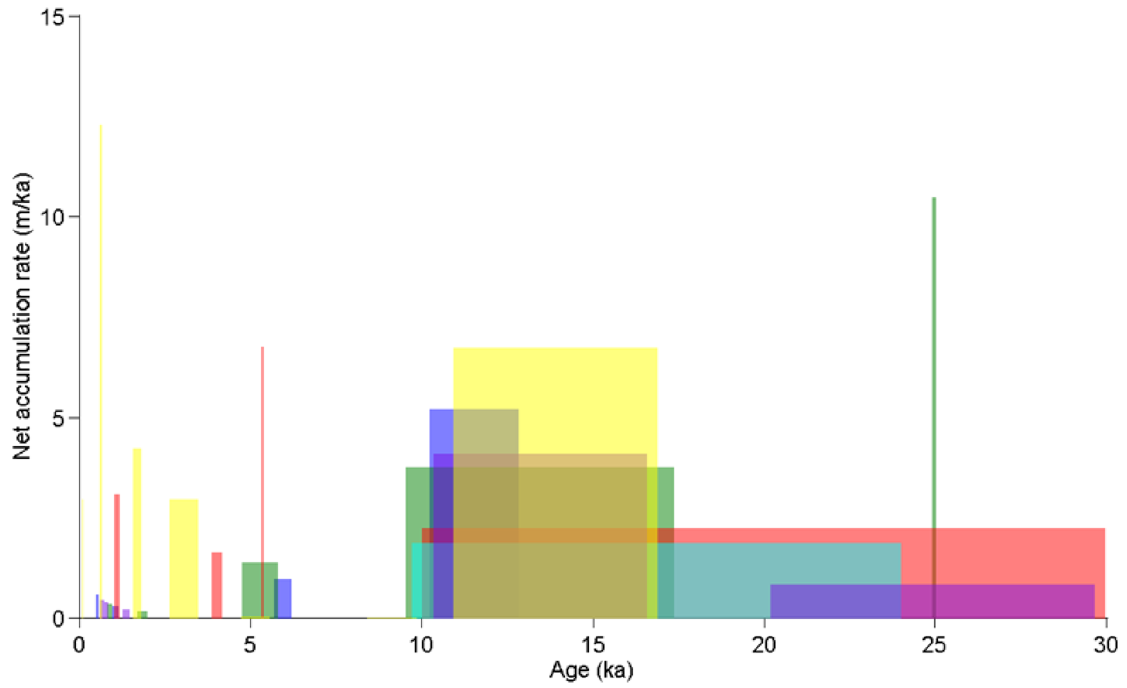

Figure 8.9: 'As sampled' net accumulation rate using 0.5 m sampling intervals of the same runs as shown in Figures 8.6-8.7.

hiatuses as periods of erosion or low levels of aeolian activity. False assumptions of the meaningfulness of apparent peaks of accumulation are then a likely consequence, as noted by Stone and Thomas (2008).

Multiple sampling profiles from the numerous model runs produce quite different sampled chronologies, a function of the noise in both the input parameters and the localised erosion/deposition component. This supports previous assertions from both the field (e.g. Chapter 6) and models (Telfer et al., 2010) that numerous sampling profiles are required in order to capture an inherent variability in chronologies for more persistent patterns reflecting external forcing to be identified.

Units that represent low accumulation rates are likely to only be preserved if they are not followed by a large erosional event. Younger ages are therefore more likely to be prevalent in dune chronologies than older ones, and the interpretation of dune accumulation rates must take this into account.

An important question following on from this discussion is whether or not the thickness of a unit is necessarily significant in terms of palaeoenvironmental conditions. A dune OSL age represents a period when surface dune height has risen (accumulation) and then been preserved. Periods of major accumulation occur at individual sites when environmental conditions are conducive to high rates of sediment transportation and deposition, i.e. in particularly 'active' points in space and time. However, not all sites can be expected to show the same pattern of dune accumulation and preservation. During intervals when transport capacity is high both erosion and deposition will be more likely to occur, and so extensive sediment deposition may take place at the same time as significant erosion at other sites. 'Active' aeolian systems are likely to have spatially variable dune chronologies, shown by both thick sedimentary units and erosional bounding surfaces. A thick unit does therefore not necessarily mean that the unit will be spatially extensive. For example, Figures 8.8a and 8.8e show 0 m and >11 m of sediment sampled respectively between 17-13 ka. Comparable field evidence is present at Shwaib, where both a ~12 m unit and a hiatus have been dated to between 23-20 ka (Chapter 6; Atkinson et al., 2011). Therefore, a thick unit (tens of metres) may not be spatially extensive in particularly dynamic aeolian systems. It is inferred that thick chronological units are the result of external forcing creating conditions for high levels of sand transport, and that spatial variability in the balance between erosion and deposition locally creates a high degree of spatial variability in unit thickness. The inverse of this is that little or no accumulation does not necessarily represent non-deposition, as a chronological hiatus may represent a contemporaneous or later erosional event. Less 'active' systems may display more consistency in chronologies between profiles in terms of absolute rates of accumulation, as it is unlikely that such thick units will be deposited. But spatial variability is still to be expected, as even though erosional processes may be reduced, the sedimentary units are likely to have been thinner to start with. Multiple sampling profiles are a practical way of trying to address the implications of this hypothesis in the field.

8.7. Conclusion: What do dune OSL ages mean?

A complex picture of past climatic and environmental change in the southern Arabian Peninsula has been described. Modelling changes in three external parameters (sediment supply, sediment availability, and transport capacity) based on evidence from other regional proxies of palaeoclimatic change in the southern Arabian Peninsula over the last 30 ka produces a dunefield history that replicates a range of features of the regional dune chronology, including high net accumulation rates after ~17 ka and a hiatus in activity during the early Holocene humid period.

The early Holocene humid period is clear across a range of proxies, and is marked in the aeolian record by an abrupt reduction in net accumulation rate. It is suggested that aeolian activity is limited once a threshold of moisture has been passed. There is evidence of aeolian activity occurring contemporaneously with temporary lake presence, although rapid events cannot be precisely deciphered in the aeolian record. Uncertainty (1 sigma errors) on ages also means that rapid climatic fluctuations cannot necessarily be identified within longer periods of accumulation. It is therefore necessary to utilise stratigraphy and other palaeoenvironmental proxies, as OSL ages from dunes alone cannot be relied upon to identify rapid climatic fluctuations. When interpreting dune OSL chronologies it must be recognised that they are a function of both sampling strategy and dating precision.

An extensive period of aeolian activity between 16-9 ka marks the transition from late glacial into the Holocene, and its dominance within the chronology is attributed to coeval increases in sediment supply and transport capacity. Preservation potential, due to low sediment supply and high windspeeds, during the late Pleistocene is interpreted as the main limitation on the sedimentary record during the last glacial, reflected in the sedimentary record by a reduction in net accumulation rate during high windspeed events. Within the Holocene ~6 ka is suggested as a period of increasing aeolian activity following a breached threshold of sediment availability as moisture levels fell. The last 4 ka have seen a relatively stable environment, with aeolian activity occurring throughout, but less extensively preserved than during the late Pleistocene.

During periods when external forcing is relatively stable, dune chronologies tend to represent stochastic processes. When these forcing conditions are conducive to ‘active’ aeolian systems (i.e. high sediment availability, sediment supply, and transport capacity) both erosional and depositional processes are more likely to take place, and hence thick sedimentary units can occur at the same time as chronological hiatuses in other dune records. At times less conducive to these processes, more spatially extensive signals may be identifiable in the regional record, although accumulation rates are unlikely to be as high. The larger the uncertainties on OSL ages, both due to precision of dating and insufficient sampling resolution, the more difficult it may be to distinguish these influences when using dunes as palaeoenvironmental archives.

To address these issues, acknowledgement of them is required at all stages of the research process. Sampling using narrow vertical intervals is necessary in order for discrete periods of accumulation not be falsely identified and for thin units to not be missed. Multiple sampling profiles are needed in order to distinguish dune accumulation and preservation due to external forcing from stochastic processes of dune development. Unusually thick chronological units most probably are indicative of accumulation as a result of conducive external forcing conditions, but will not always be preserved at all locations. Thin units/hiatuses may or may not represent a large amount of accumulation, as erosional events are difficult to identify from the dune record alone, although the use of multiple sampling sites allows this problem to be partially addressed.

9 Conclusions

9.1. Introduction

The purpose of this chapter is to summarise the main findings, assess to what extent the research questions have been answered and discuss the implications of these findings for future research using sand dunes as palaeoenvironmental archives. The contribution of this thesis to the understanding of the terrestrial environmental history of the southern Arabian Peninsula will also be discussed.

9.2. Representativeness of dune OSL chronologies

I. Are dune chronologies representative of the preserved stratigraphy at the dune and dunefield scales?

9.2.1. Dune scale

Dune chronologies are a function of sampling strategy as well as past environmental conditions. In order to investigate the broader question of what dunes can contribute to our understanding of past environmental change, the effect of under-sampling needs to be negligible, or at least recognised and appropriately acknowledged when dune chronologies are interpreted. Suitable sampling protocols must necessarily represent a compromise between high sampling coverage and financial and time constraints.

Using dune stratigraphy (specifically, bounding surfaces) to 'target' sampling for OSL dating was investigated in Chapter 4, and the implications discussed further in Chapter 5. It was found that hierarchical dominance of bounding surfaces within two-dimensional exposures of dune stratigraphy does not necessarily align with chronological significance, i.e. not all bounding surfaces (a stratigraphical distinction) are unconformities (a chronological distinction) at scales resolvable by the precision of OSL dating. Hierarchies (e.g. Brookfield, 1977; Kocurek, 1981) may be useful for sampling purposes when the area over which stratigraphic features reach is visible, but this is not always the case. Here, bounding surfaces cannot be traced fully and hence cross-cutting relationships are incompletely known (such as those studied in Chapter 4), despite the visibility of the dune internal structure by two-dimensional exposures. The designation of 'major' bounding surfaces that are assumed to be representative of chronological variability of dune accumulation and preservation is then dependent on relatively arbitrary categorisations. These assumptions may not be valid, as it has been shown that visibly major bounding surfaces that extend tens of metres may not be chronologically significant (e.g. UAE10/2), whilst less distinctive bounding surfaces can be (e.g. UAE10/1). Fundamentally, dune records are discontinuous, accumulation rates are variable, and the dune processes underlying sediment erosion and deposition may be indistinguishable in the sedimentary record. A bounding surface may represent one or several erosional events, and what is removed is unknown (Munyikwa, 2005). Future research using three-dimensional viewing techniques, such as the application of GPR profiling, is required in order to test whether 'super surfaces' (Kocurek, 1988) can be identified and the assumption that OSL sampling around 'major' bounding surfaces using this method is a valid one.

A fractal approach to thinking about dune stratigraphy is perhaps appropriate, as discussed by Miall (2012). Deposition is discontinuous and the apparent incompleteness of the record depends on the scale of analysis, as shown by Mandelbrot's (1983) 'Cantor bar' model, which built on work of the earlier mathematician Georg Cantor (Figure 10.1; Miall, 2012). The 'Cantor bar' model describes the division of a continuous bar (which represents an event) into an infinite number of discrete bars as the scale of analysis increases. The set is created by dividing the bar into thirds and removing the central bar, so the relationship between the bars and gaps is the same at each scale of analysis (Gleick, 1997). As Miall (2012: 4) states, "[t]he concept of continuous deposition has no theoretical or evidential

Figure 9.1 has been removed due to Copyright restrictions

Figure 9.1: Cantor bar model of Mandelbrot (1983). At each stage the middle third (using a gap size of 1/3) of each bar is removed, so that the relationship between bar and gap is the same at each scale of analysis. This process of division can be repeated infinitely, resulting in the Cantor dust set.

basis… Continuity is a scale-related assumption". Fractals have been described in many natural phenomena, such as the rings of Saturn and the coastline of Britain (Gleick, 1997; Mandelbrot, 1983). Applying this approach to the calculation of a sedimentation rate shows that the rate is dependent on the scale of analysis: if an erosional surface is recognisable, the sedimentation rate of the smaller periods of accumulation will be greater than the rate of the entire section as the hiatus is included in the calculation (Plotnick, 1986 in Miall, 2012). Miall (2012) investigates the relationship between stratigraphy and temporal scale further, focussing on how sedimentation rates can be used to assign stratigraphic units (and associated inferred processes) to an appropriate time scale for analysis and introducing the term 'sedimentation rate scales', within which sedimentation rates can be compared. However, as Chapters 4 and 5 show, the designation of different 'scales' of bounding surfaces is not always possible. Whilst allostratigraphy and fractal theory may provide appropriate frameworks to describe dune stratigraphy and critique assumptions of continuity, their applicability to sampling is more limited.

The above discussion relates to the representativeness of a particular approach to sampling for OSL dating; 'targeting' bounding surfaces as stratigraphic features that are assumed to have chronological significance. In Chapter 6 it was shown that different chronologies are produced when multiple sampling profiles were dated across an individual dune. Whilst accumulation between ~16-12 ka is notable in all three profiles, the presence of the younger units is more variable and highlights that the persistence of units, and therefore the likely correlation of different sampling profiles, depends on the local context of accumulation and preservation. One profile therefore cannot be extrapolated and scaled spatially to be representative of the preserved sedimentary structure at the dune scale.

9.2.2. Dunefield scale

If different chronologies are produced using different sampling profiles at the dune scale, as described above, one would expect increased variability at the dunefield scale as the contextual differences between sites also increase. It is clear that individual chronological profiles reflect a localised response to forcing. The importance of amalgamating data in order to build an aeolian dunefield response signal from multiple chronological profiles is necessary in order to move beyond a local signal and the stochastic processes of reworking.

The use of multiple profiles is particularly important for trying to decipher the significance of chronological hiatuses. A hiatus within an individual profile may just as likely be a product of erosion than of a reduction in accumulation. However, if another, second, record from a different but nearby location within the dunefield indicates significant accumulation that is contemporaneous to the hiatus in the first record, then this must have occurred under conditions conducive to the prior transport and deposition of a significant quantity of sediment. So, periods of significant accumulation are potentially easier to interpret than gaps in the record, and may be used to aid the interpretation of hiatuses by assimilating multiple chronological profiles. The presence of a hiatus in accumulation/preservation at the same time across a number of sampling profiles provides support to the hypothesis that the hiatus was a regional event, and not simply a result of reworking of sediment at one particular site. How to then interpret this hiatus is still a difficult question to answer, and is addressed in Section 9.3.

9.2.3. Implications for future research: sampling and measurement

One implication of the results presented in this thesis is that research that does not meet certain criteria with regards to sampling should probably not be included in regional reviews and assessments of dune activity, or at the least interpreted with caution. Future research should aim to use high vertical sampling resolution and multiple sampling profiles across the area of interest. The amalgamation of data from several studies is important: whilst interpretations regarding external environmental forcing cannot be made using *individual* profiles, aspects of the chronologies reflecting local dune processes may be distinguished when profiles are compared. Past interpretations that are based on inadequate sampling should be regarded with caution. It may be appropriate to re-assess the aeolian record in a number of regions according to the fulfilment of these criteria. In summary, if sampling is insufficient (i.e. under-sampling is a problem), then the extent to which results are extrapolated should be questioned. Establishing whether under-sampling is a problem is also difficult. If data is added that does not significantly change the regional accumulation record then it can be inferred that sampling resolution is sufficient, but in practice this may not be a feasible approach. By amalgamating records, sampling at high resolution at multiple locations, and interpreting records whilst recognising their associated sampling limitations, the chances of under-sampling may be minimised.

These findings have practical implications for sampling protocols. Unless *all* bounding surfaces are bracketed, targeting OSL samples selectively based on hierarchical dominance within the visible two-dimensional stratigraphy may be an inappropriate way of increasing dating efficiency. Dune stratigraphic features are not unique to particular environmental histories. In some situations portable OSL readers may be suitable to provide a guide to where to sample in the field. The use of portable OSL readers in desert dune settings has not yet been reported in published research, although they have been successfully used by Munoz-Salinas et al. (2011) and Munyikwa et al. (2012) to assess the suitability of fluvial sediments for luminescence dating and to identify stratigraphic breaks of postglacial dunes respectively. However, where readers are not available and/or appropriate for particular sites, such as where there are not different lithologies with characteristic luminescence properties or homogeneous dose rates (Munyikwa et al., 2012), there may not be a suitable methodology for sampling selectively in the field. Chapter 7 investigated one practical approach to addressing these requirements. Range-finder dating increases laboratory throughput by reducing processing time (and expense) during sample preparation and measurement. Whilst unfortunately not increasing efficiency in the field, this protocol does enable samples to be targeted for full preparation and dating procedures in a laboratory setting once some chronological information is known, and may allow for sampling to be conducted at high resolution in the knowledge that the number of samples will be reduced at a later stage.

9.3. Interpretation of dune OSL chronologies

II. How can dune chronologies be most appropriately interpreted to reconstruct reliable records of Quaternary dryland environmental conditions?

9.3.1. Appropriate use of datasets

OSL chronologies are a function of both sampling strategy and dating precision. Palaeoenvironmental interpretations can only be made once there is confidence that the dune chronology is an accurate reflection of the underlying dune sedimentary structure, the requirements and limitations of which are discussed in the preceding section.

In Chapter 6 a new method for presenting dunefield OSL chronologies as net accumulation rates was introduced. The incorporation of accumulation thicknesses within these calculations means that there is less significance simply based on frequency, or presence/absence, of ages. This is one attempt to move away from interpretations that are dependent on sampling resolution: whether a sedimentary unit is sampled twice or twenty times does not alter the net accumulation rate of the sampled profile. Another key advantage of the method proposed is that study sites can be identified separately as well as viewed within the whole dataset, so that the convergence of chronologies across different sites, or conversely the isolation of anomalous site accumulation/preservation histories, is visible. This method of presenting dune OSL chronologies is therefore more suitable than other widely used alternatives in addressing the problems faced as a result of the spatially and temporally variable nature of dune accumulation and preservation processes.

An important issue for consideration in the assimilation of regional OSL ages is whether the different datasets being used are comparable and of sufficient quality. Issues implicit in D_e and dose rate determinations are relevant here, such as the measurement protocol followed, whether quality assurance ratios were used to identify unsuitable samples, and the number of aliquots used in D_e estimation (Thomas and Burrough, in preparation). Sampling resolution is probably the most important consideration and highlights the importance of research question 1. Comparing studies using a range of criteria, including the vertical sampling interval used in the field and the OSL dating procedures followed in the laboratory, may be a difficult task based upon somewhat arbitrary designations, but could contribute towards recognition of the need for periodic reassessment of older data in light of more recent technological developments.

The reduction in the level of precision that can be achieved for older OSL ages (because 1 sigma errors tend to be greater than 8% of the final age determination, and claims for less have been questioned on statistical grounds, e.g. Guérin et al., 2013) means that the significance of certain periods of aeolian activity over others cannot be discerned: as precision decreases, absolute net accumulation rates will fall. A recent study, using the same numerical model as described in Chapter 8, indicates that rapid fluctuations in precipitation, affecting sand transport and accumulation, cannot be identified within dune OSL chronologies before ~30 ka due to the overlapping of age uncertainties (given as 8%) (Bailey and Thomas, submitted). These findings are supported by Chapters 4, 6 and 8, which showed, using stratigraphy and comparison with other records respectively, that OSL dating of dunes cannot resolve rapid climatic fluctuations. Other palaeoenvironmental records are therefore required, and the more so the older the record that is being investigated.

9.3.2. Palaeoenvironmental interpretations

The construction of a regional aeolian dataset allowed for its comparison with other records of palaeoenvironmental change in Arabia in Chapter 8. A period of regional high net accumulation has been identified between ~16-9 ka followed by the Holocene humid period, ~9-6 ka, when accumulation rates were low. The record at other times however allows for less confident interpretation.

The underlying controls of aeolian system state, defined as sediment supply, sediment availability and transport capacity, were modelled in Chapter 8. The aim of this exercise was to investigate whether the current understanding of dune processes and the system sediment state of the region is sufficient to produce the aeolian chronological record found in the southern Arabian Peninsula. The main characteristics of the aeolian record, including rapid net accumulation rates between 16-9 ka and a hiatus during the early Holocene, were present in multiple model runs, indicating that these major aspects of the signal are explainable by regional climatic and environmental changes.

The distinct hiatus during the Holocene humid period indicates the importance of moisture as a threshold on aeolian activity at the dunefield scale. The transition appears to have occurred rapidly, indicated by the recorded timings of increased moisture in a range of palaeoenvironmental records across the southern Arabian Peninsula (e.g. Fleitmann and Matter, 2009; Lézine et al., 2007; Parker et al., 2004, 2006), and is reflected by a sudden reduction in aeolian accumulation at the same time as lake presence in the northeastern UAE (Section 8.5.2; Parker et al., 2004, 2006; Preston et al., 2012). However, the shift towards drier conditions and increasing aeolian activity in the mid-Holocene was spatially more variable and mediated by local contexts (Figure 6.2; Sections 6.3.4 and 8.5.2).

Whilst the early Holocene humid period is fairly well constrained within the aeolian record, other hiatuses do not appear to be concurrent with recorded periods of increased moisture. For example, during MIS 3 reduced net accumulation aligns in timing with Heinrich events (Section 8.5.1). Marine cores show a correlation between changes in circulation patterns over the region, recorded by reduced upwelling as a result of a weaker IOSM and increased terrestrial dust content, and cold events in the North Atlantic, including Heinrich events, (Gupta et al., 2003; Pourmand et al., 2004; Schulz et al., 1998; Sirocko, 2000).

It has been suggested by other authors (Boulter et al., 2010; Chase, 2009; Chase and Thomas, 2006; Lancaster, 2008; Stone and Thomas, 2008) that dune OSL ages may be less likely in some contexts to represent ‘peak aridity’ than changes in other controls on aeolian activity. In Chapter 8 it was proposed that whilst moisture is a strong inhibitor of aeolian activity, preservation potential, which is the interactive result of sediment availability, sediment supply and transport capacity, was an important control on the extent of accumulation and preservation of aeolian sequences in southern Arabia during MIS 3. Periods of low preservation potential occur when sediment output is greater than sediment input, but the environmental causes underlying this situation are complex. Fluctuations in sediment supply and transport capacity are particularly important when moisture levels are reduced. For example, high rates of accumulation were simulated in the model when high transport capacity coincided with the presence of an external sediment supply, but without this supply of sediment the preserved net accumulation was more dependent on stochastic processes (Section 8.6.2). The use of generalised terms such as 'arid' and 'humid', imply relative stability and may allow for changes in other forcing factors, which may heavily characterise the aeolian record more than changes in moisture at some times, to be overlooked. Sediment supply, sediment availability and transport capacity all play a role and their respective dominance in determining preserved dune record is temporally and spatially variable.

The variability of the modelled chronological profiles across multiple model runs allowed for the impact of stochastic processes to be assessed. When the external forcing parameters are low (i.e. not conducive to high levels of aeolian activity), the combined record is dominated by stochastic processes which inherently vary between model runs (interpreted as the equivalent of using multiple sampling profiles). When the forcing parameters are high both erosional and depositional processes are enhanced, whilst these stochastic processes still occur. However the extent of accumulation found at some sites is unlikely to occur under such stochastic forcing conditions when external parameters are low. Distinguishing these different environmental conditions using individual dune OSL chronologies *alone* is impossible, although by utilising different profiles, the range of net accumulation rates are likely to be larger when forcing parameters are high (i.e. there is greater likelihood that deposited units will be thicker when sediment supply/sediment availability/transport capacity are high).

Reconstruction of past environmental conditions is complicated because there are numerous controls underlying dune activity, and different combinations of them can result in similar results (i.e. convergence/equifinality). For example, at any one period of time an increase in sediment supply *or* sediment availability *or* transport capacity could result in the thickness of accumulating sediment increasing (although note that the relationships between these variables and aeolian accumulation can be complex; for example an increase in windspeed may result in increased erosion of sediment at a location and hence a reduction in accumulation thickness). The similar result of these different mechanisms represents convergence in the sedimentary record, with the implication that, by utilising the OSL chronology *alone*, cause cannot be deciphered. However, the extent of preservation of this unit will depend on the specific combination from the infinite possible combinations of these primary controls that could occur *after* this one snapshot in time. The preserved sedimentary record as a whole is a unique product of the environmental history of the period of its formation, with similar events (e.g. increase in sediment supply resulting in increasing accumulation) resulting in different stratigraphy (divergence) because it is not solely the sum of events that are independently recorded: the environmental conditions of the time after a unit is deposited determine its existence within the record as much as those when the unit was first deposited. At the same time therefore, the dune sedimentary record shows convergence and divergence that complicates interpretation of the underlying environmental controls on accumulation and preservation processes.

Combining datasets partly allows for consideration of the extensiveness of aeolian system response by identifying periods of accumulation that are consistent across multiple sites. For example, this is possible for the high rates of net accumulation across sites during the late Pleistocene-Holocene transition in Arabia, which aligns with records of high sediment supply, sediment availability and windspeed. When accumulation rates are lower or sampling resolution is insufficient, the comparison of a period of time to another in absolute terms (low rates or, more importantly, dated units not corroborated at different sites) may lead to the interpretation that a period of time is governed by stochastic activity and accumulation/preservation is insignificant. However, these conclusions, based upon the comparison of absolute values of accumulation rates over time, may not be valid, as geomorphic sensitivity to external forcing varies over time. Whilst net accumulation rates are an attempt to provide a more quantitative comparison of the amount of accumulation at different sites and over time, the method of calculation relies on certain assumptions (discussed in Chapter 6), as well as the complexities of sampling dependency discussed above. This method is proposed as a more appropriate tool of presenting and collating datasets than commonly used approaches such as probability density functions (PDFs), but an acknowledgement of the assumptions underlying its calculation is required for palaeoenvironmental interpretations to be valid.

But do these limitations matter? In the simplest of terms, the presence of a particular sedimentary unit within a dune implies that environmental conditions were conducive for aeolian sediments to be deposited at that place and at that time. If found at several sites, that interpretation can be widened to being valid at multiple sites rather than only one, enabling extrapolation of findings to a larger spatial area. Even if accumulation rates are lower and/or not preserved to the same extent as units deposited at other time intervals, these general conclusions can still be held, even if comparisons over time cannot be made. Individual records allow for interpretations specific in space and time; combined datasets allow for whether broad terrestrial environmental conditions allowed for aeolian deposition and preservation or not. Dunes, as palaeoenvironmental archives, provide concurrently very specific *and* very general information. Ultimately, the mechanisms underlying the changes seen in the aeolian chronological record are not well known, and an absolute comparison of activity over time is not possible without additional information. Whilst dune chronologies are accurate records of terrestrial palaeoenvironmental change, they are not precise. Therefore other palaeoenvironmental records are needed in order to fill the gaps. For example, based upon comparison with other regional palaeoenvironmental archives including marine cores, lacustrine sediments and speleothems, the chronological hiatuses within the dune record in the early Holocene and MIS 3 can be distinguished, and aligned with increased moisture (and hence reduced activity) and reduced preservation respectively.

The requirement for external information is of course necessary in the interpretation of other palaeoenvironmental archives as these limitations (and others) are also valid, but perhaps the complications hindering the use of dune records are more acknowledged. These conclusions re-emphasise the importance of pooling information from different sources to enable the bigger environmental picture to be established. Given the importance of comparing dune chronologies to other palaeoenvironmental records, and generally comparing datasets within Quaternary science, more research is needed to investigate more rigorous methods of comparing and collating different datasets from different palaeoenvironmental records.

9.3.3. The value of dune chronologies as palaeoenvironmental archives

The discussion above highlights the need for other palaeoenvironmental records to interpret dune chronological records, so what additional information can aeolian records provide to justify their use in reconstructing past environments?

Dune records provide terrestrial records of the *geomorphic* response to past climatic and environmental changes. In drylands, the terrestrial palaeoenvironmental record is often sparse over time and space. Archives are inherently discontinuous, and so a holistic approach to understanding the environmental system is required. Dunefields are also spatially extensive in comparison to other terrestrial records that are only present in individual locations, such as speleothems. Dunes therefore provide an archive that can spatially link discrete terrestrial sites and fill in the gaps of other records which tend to be indicators of wetter conditions. For example, the transition out of the early Holocene humid period in the southern Arabian Peninsula is complex, with different records showing different sensitivities to increasing aridity (e.g. Fuchs and Buerkert, 2008). The timing of this climatic shift is shown by increasing aeolian activity after ~6 ka at some but not all sites (Figure 8.4), affirming other research that shows the reduction in precipitation post-6 ka was gradual (Fleitmann et al., 2003a, 2007; Parker et al., 2006) and the response of the terrestrial environment at the small-scale varied depending on environmental context (e.g. Boulter et al., 2010; Preusser, 2009).

More generally, understanding how aeolian systems actually respond to climatic change is important for predicting the impact of future changes on dryland environments. The use of a stratigraphic model in Chapter 8 tied the palaeoenvironmental record to dune processes. It is through this type of approach that our current understanding of the aeolian response to external forcing can be evaluated. The forcing parameters used in the model in Chapter 8 are based on large-scale and generalised changes in aeolian system sediment state. As knowledge of the past changes that occurred in the parameters of sediment supply, sediment availability and transport capacity develops through continuing palaeoenvironmental research, modelling the processes of dune response may be undertaken in more detail. Increasing use and development of modelling alongside the use of sand dunes in palaeoenvironmental studies is required to aid interpretation of dune chronologies and provide a link to studying geomorphic responses to future scenarios of climatic change in drylands.

9.4. The terrestrial environmental history of the southern Arabian Peninsula

This project focused on an examination of past environmental conditions during the last 30 ka because of the age of the primary samples presented and the lack of samples dating from earlier times (Section 2.4). Accumulation is recorded at ~30-26, 22.5-18, 16-9, 6-2.7, 2.1-

1.6, 1.1 and 0.7 ka (based on 'as sampled' net accumulation rates presented in Section 8.4). It is important to note that aeolian accumulation and preservation need not (and can be considered unlikely to) have been continuous during these broad periods, as unresolvable periods of erosion or non-deposition will be included in the calculation of the net accumulation rate.

Due to their alignment with Heinrich events 1 (~16.8 ka) and 2 (~24 ka), when high magnesium content in marine core 74KL is interpreted as evidence of strong northwesterly winds (Sirocko, 2000), the gaps in the record during the last glacial are inferred to be a result of low preservation potential. However, more OSL ages are required prior to ~16 ka in order to distinguish peaks and troughs in the accumulation record from those due to sampling bias (Section 6.3.1).

In Chapter 8 the complexity of the relationship between windiness and dune development processes was highlighted. Substantial accumulation during the Younger Dryas was replicated by the model when the sediment supply was increased (to represent production of sediment during the incursion of the Persian Gulf) concurrent to transport capacity. Without an external source of sediment available to transport, stochastic processes play a larger role in determining erosion or accumulation and hence more spatial variability of chronologies between sites can be expected. Individual dunes record the result of the interaction between windspeed, sediment availability and supply, and local environmental conditions. Higher windspeeds increase the likelihood for erosion, but if deposition is favoured (for example within a local topographical depression) there is more entrained sediment to be potentially deposited.

Within the last 16 ka, when the regional chronology can be most securely separated from issues associated with sampling resolution, three intervals of aeolian activity have been discerned. Extensive aeolian activity at a number of sites occurred between ~16-9 ka.

Marking the transition from the late Pleistocene into the Holocene, this time interval appears to have been particularly conducive to region-wide aeolian activity and accumulation. This period aligns with an increase in both sediment supply and transport capacity, and was replicated by modelling these controls in Chapter 8.

The reduction in accumulation rates between ~9 and 6 ka aligns with the early Holocene humid period, which is independently recorded in other terrestrial palaeoenvironmental records in the region (e.g. Fleitmann et al., 2007; Lézine et al., 2007; Parker et al., 2006; Preston et al., 2012). Due to the clear transition at the onset of the early Holocene humid period seen in Figure 8.4, and supporting field research demonstrating the importance of moisture as a control on grain entrainment at smaller scales (Wiggs et al., 2004), a threshold of moisture above which aeolian activity is negligible is inferred to have been crossed at ~9 ka. OSL ages are recorded at three sites in the northeastern UAE during this period (Chapter 6), but net accumulation rates are consistently low. Since ~6 ka an increase in aeolian activity occurred. It is thought that within the last ~4 ka the environment has been relatively stable, with aeolian activity occurring throughout but less extensively preserved than during the late Pleistocene-Holocene transition.

The apparent duration of intervals of preserved accumulation and absolute net accumulation rates cannot be compared easily to aeolian accumulation and preservation occurring at other periods of time (given the problems discussed in Section 6.3). However, the number of sites with units dated to the late Pleistocene-Holocene transition, the thicknesses of these sampled units compared to more modern accumulation, and the modelling exercise presented in Chapter 8, provide reasons to cautiously argue that environmental conditions were more conducive to extensive and significant thicknesses of accumulation and preservation than during the later Holocene. This could be a result of both reduced sediment supply, as the sea level within the Persian Gulf reached its present levels (Lambeck, 1996;

Teller et al., 2000; Williams and Walkden, 2002), and/or weaker *Shamal* winds (Glennie and Singhvi, 2002) in the late Holocene.

The spread of aeolian records in southern Arabia remains relatively sparse, both in space and time, despite a number of recent studies (e.g. Atkinson et al., 2011, 2012, 2013). Most sites have been located in northeastern UAE, Liwa and the Wahiba Sands (e.g. Atkinson et al., 2011; Bray and Stokes, 2003; Goudie et al., 2000a; Preusser et al., 2002, 2005), principally due to accessibility. Important questions persist, in terms of understanding the climatic history of the region and for interpreting palaeoenvironmental archives. Extending the aeolian chronological record further and collecting data from a wider area of the Rub' al Khali therefore remains a relevant objective for future research.

Dune and aeolianite ages in Liwa and the Wahiba Sands extend to MIS 5 (Preusser et al., 2002; Stokes and Bray, 2005). Bray and Stokes (2004; Stokes and Bray, 2005) and Preusser (2009) put forward different explanations of the dune OSL chronologies in Liwa and the Wahiba Sands. The former suggest that differences in preservation potential between the sites are most significant in determining the aeolian record, whilst the latter contests the importance of differences in sediment supply. However, these long records tend to use wider vertical sampling intervals. For example, Preusser et al. (2002) use sample approximately every 3 m when drilling to a maximum depth of 144 m. The findings presented in this thesis emphasise the importance of sampling resolution. More research aiming to extend the chronological record is needed in order to elucidate the extent to which the current record is dependent upon sampling. Rigorous sampling, in line with the suggestions from this research project, may enable any differences between the chronologies to be more comprehensively explained.

This thesis has addressed some of the fundamental questions underlying the interpretation of dune OSL chronologies and raised a few more, which are relevant and important irrespective of the study area. The importance of using multiple sampling profiles, to avoid under-sampling, has been highlighted, and a practical way of doing this in the laboratory has been suggested. A new method of presenting dunefield datasets has been introduced that attempts to avoid the pitfalls of currently used methods. In focusing upon the Late Quaternary palaeoenvironmental record in southern Arabia, these questions have been addressed, for the first time, explicitly and in a region where the climatic changes of the Late Quaternary are relatively well known. The regional dune chronological record has been used in conjunction with a numerical model to interpret aeolian dune responses to changes in forcing parameters. In doing so, aspects of the aeolian record that are under-represented in this region have been highlighted. The climatic, environmental and archaeological history of this region tells a changeable and fascinating story and is deservedly receiving increasing attention by researchers; hopefully future research will aim to further fill some of the gaps in our understanding in the reconstruction of past climatic change in drylands.

Bibliography

Adamiec, G.S.T., Aitken, M., 1998. Dose-rate conversion factors: update. Ancient TL 16: 37–50.

Ager, D.V., 1973. The nature of the stratigraphical record . Wiley, New York.

Ahmed, E.A., Soliman, M.A., Alsharhan, A.S., Tamer, S., 1998. Mineralogical characteristics of the Quaternary sand dunes in the eastern province of Abu Dhabi, United Arab Emirates. In: Alsharhan, A.S., Glennie, K.W., Whittle, G.L., Kendall, C.G.S., (Eds.), Quaternary Deserts and Climatic Change, A.A. Balkema, Rotterdam, pp. 279–291.

Aitken, M.J., 1998. An Introduction to Optical Dating. Oxford University Press, Oxford

Al-Farraj, A., Harvey, A.M., 2000. Desert pavement characteristics on wadi terrace and alluvial fan surfaces: Wadi Al-Bih, U.A.E. and Oman. Geomorphology 35 : 279–297.

Anderson, D.M., Prell, W.L., 1993. A 300 kyr record of upwelling off Oman during the late Quaternary - Evidence of the Asian southwest monsoon. Paleoceanography 8 : 193–208.

Anton, D., 1983. Modern Eolian Deposits of the Eastern Province of Saudi Arabia. In: Brookfield, M.E., Ahlbrandt, T.S., (Eds.), Developments in Sedimentology: Eolian Sediments and Processes, v. 38 , Elsevier, Amsterdam, pp. 365–378.

Armitage, S.J., Jasim, S.A., Marks, A.E., Parker, A.G., Usik, V.I., Uerpmann, H-P., 2011. The Southern Route “Out of Africa”: Evidence for an Early Expansion of Modern Humans into Arabia. Science 331 : 453–456.

Atkinson, O.A.C., Thomas, D.S.G., Goudie, A S., Bailey, R.M., 2011. Late Quaternary chronology of major dune ridge development in the northeast Rub' al-Khali, United Arab Emirates. Quaternary Research 76, 93-105.

Atkinson, O.A.C., Thomas, D.S.G., Goudie, A.S., Parker, A.G., 2012. Holocene development of multiple dune generations in the northeast Rub’ al-Khali, United Arab Emirates. The Holocene 22 : 179–189.

Atkinson, O.A.C., Thomas, D.S.G., Parker, A.G., Goudie, A.S., 2013. Late Quaternary humidity and aridity dynamics in the northeast Rub’ al-Khali, United Arab Emirates: Implications for early human dispersal and occupation of eastern Arabia. Quaternary International 300: 292-301.

Bagnold, R.A., 1941. The Physics of Blown Sand and Desert Dunes. Methuen & Co. Ltd., London.

Bagnold, R.A., 1953. The surface movement of blown sand in relation to meteorology. Research Council of Israel Special Publication 2: 89–96.

Bailey, D.J.E., 2009. Development of LM OSL analysis techniques for application to optical dating. DPhil thesis, University of Oxford.

Bailey, R.M., 2001. Towards a general kinetic model for optically and thermally stimulated luminescence of quartz. Radiation Measurements 33: 17–45

Bailey, R.M., 2010. Direct measurement of the fast component of quartz optically stimulated luminescence and implications for the accuracy of optical dating. Quaternary Geochronology 5 : 559–568.

Bailey, R.M., McKeever, S.W.S., (Unpublished). The physical basis of luminescence dating.

Bailey, R.M., Smith, B.W., Rhodes, E.J., 1997. Partial bleaching and the decay form characteristics of quartz OSL. Radiation Measurements 27 : 123–136.

Bailey, R.M., Thomas, D.S.G., (2013). A quantitative approach to understanding dated dune stratigraphies. Earth Surface Processes and Landforms, DOI: 10.1002/esp.3471.

Bailey, R.M., Yukihara, E.G., McKeever, S.W.S., 2011. Separation of quartz optically stimulated luminescence components using green (525 nm) stimulation. Radiation Measurements 46 : 643–648.

Baker, G.S., Jordan, T.E., Pardy, J., 2007. An introduction to ground penetrating radar (GPR). In: Baker, G.S., Jol, H.M., (Eds.), Stratigraphic Analyses Using GPR. Geological Society of America Special Paper, pp. 1–18.

Ballarini, M., Wallinga, J., Wintle, A.G., Bos, A.J.J., 2007. A modified SAR protocol for optical dating of individual grains from young quartz samples. Radiation Measurements 42 : 360–369.

Banerjee, D., Murray, A.S., Bøtter-Jensen, L., Lang, A., 2001. Equivalent dose estimation using a single aliquot of polymineral fine grains. Radiation Measurements 33 : 73–94.

Bard, E., Hamelin, B., Delanghe-Sabatier, D., 2010. Deglacial meltwater pulse 1B and Younger Dryas sea levels revisited with boreholes at Tahiti. Science 327 : 1235–7.

Barth, H-J., 2001. Characteristics of the wind regime north of Jubail, Saudi Arabia, based on high resolution wind data. Journal of Arid Environments 47 : 387–402.

Bateman, M.D., Boulter, C.H., Carr, A.S., Frederick, C.D., Peter, D., Wilder, M., 2007. Preserving the palaeoenvironmental record in Drylands: Bioturbation and its significance for luminescence-derived chronologies. Sedimentary Geology 195, 5-19.

Bateman, M.D., Thomas, D.S.G., Singhvi, A.K., 2003. Extending the aridity record of the Southwest Kalahari: current problems and future perspectives. Quaternary International 111 : 37–49.

Bengtsson, L., Enell, M., 1986. Chemical Analysis. In: Berglund, B.E., (Ed.), Handbook of Holocene palaeoecology and palaeohydrology. Wiley, Chichester, pp. 423–451

Berndtsson, R., Nodomi, K., Yasuda, H., Persson, T., Chen, H., Jinno, K., 1996. Soil water and temperature patterns in an arid desert dune sand. Journal of Hydrology 185: 221–240.

Besler, H., 1982. The north-eastern Rub' al Khali within the borders of the United Arab Emirates. Zeitschrift fur Geomorphologie 26 : 495–504.

Blockley, S.P.E., Ramsey, C.B., Lane, C.S., Lotter, A.F., 2008. Improved age modelling approaches as exemplified by the revised chronology for the Central European varved lake Soppensee. Quaternary Science Reviews 27 : 61–71

Blott, S., 2000. Gradistat v.4.0.

Böer, B., 1997. An introduction to the climate of the United Arab Emirates. Journal of Arid Environments 35 : 3–16.

Boggs, S., 2006. Principles of Sedimentology and Stratigraphy. 4th ed. Pearson Prentice Hall, Upper Saddle River

Botter-Jensen, L., Andersen, C.E., Duller, G.A.T., Murray, A.S., 2003a. Developments in radiation, stimulation and observation facilities in luminescence measurements. Radiation Measurements 37 : 535–541.

Bøtter-Jensen, L., McKeever, S.W.S., Wintle, A.G., 2003b. Optically Stimulated Luminescence Dosimetry. Elsevier, Oxford

Boulter, C., Bateman, M.D., Frederick, C.D., 2010. Understanding geomorphic responses to environmental change: a 19 000-year case study from semi-arid central Texas, USA. Journal of Quaternary Science 25 : 889–902.

Bray, H.E., Bailey, R.M., Stokes, S., 2002. Quantification of cross-irradiation and cross-illumination using a Risø TL/OSL DA-15 reader. Radiation Measurements 35: 275–280.

Bray, H.E., Stokes, S., 2003. Chronologies for Late Quaternary barchan dune reactivation in the southeastern Arabian Peninsula. Quaternary Science Reviews 22 : 1027–1033.

Bray, H.E., Stokes, S., 2004. Temporal patterns of arid-humid transitions in the south-eastern Arabian Peninsula based on optical dating. Geomorphology 59 : 271–280.

Bretzke, K., Armitage, S.J., Parker, A.G., Walkington, H., Uerpmann, H-P., 2013. The environmental context of Paleolithic settlement at Jebel Faya, Emirate Sharjah, UAE. Quaternary International, DOI: 10.1016/j.quaint.2013.01.028.

Bristow, C.S., Bailey, S.D., Lancaster, N., 2000. The sedimentary structure of linear sand dunes. Nature, 406, 56-59.

Bristow, C.S., Duller, G.A.T., Lancaster, N., 2007a. Age and dynamics of linear dunes in the Namib Desert. Geology 35 : 555–558.

Bristow, C.S., Jones, B.G., Nanson, G.C., Hollands, C., Coleman, M., Price, D.M., 2007b. GPR surveys of vegetated linear dune stratigraphy in central Australia: Evidence for linear dune extension with vertical and lateral accretion. In: Baker, G.S., Jol, H.M. (Eds.), Stratigraphic Analyses Using GPR, Geological Society of America Special Paper, Boulder, Vol. 432, pp. 19-33.

Bristow, C.S., Lancaster, N., Duller, G.A.T., 2005. Combining ground penetrating radar surveys and optical dating to determine dune migration in Namibia. Journal of the Geological Society 162, 315-321.

Bristow, C.S., Push, J., Goodall, T., 1996. Internal structure of aeolian dunes in Abu Dhabi determined using ground-penetrating radar. Sedimentology 43 : 995–1003.

Bronk Ramsey, C., 1995. Radiocarbon calibration and analysis of stratigraphy: The OxCal program. Radiocarbon 37, 425-430.

Bronk Ramsey C., 2001. Development of the radiocarbon calibration program. Radiocarbon 43: 355–363.

Bronk Ramsey, C., 2008. Deposition models for chronological records. Quaternary Science Reviews 27, 42–60.

Bronk Ramsey, C., 2009a. Bayesian analysis of radiocarbon dates. Radiocarbon 51(1), 337-360.

Bronk Ramsey, C., 2009b. Dealing with offsets and outliers in radiocarbon dating. Radiocarbon 51(3), 1023-1045.

Brookfield, M.E., 1977. The origin of bounding surfaces in ancient aeolian sandstones. Sedimentology, 24, 303-332.

Bullard, J.E., Thomas, D.S.G., Livingstone, I., Wiggs, G.F.S., 1995. Analysis of linear sand dune morphological variability, southwestern Kalahari desert. Geomorphology 11 : 189–203.

Bullard, J.E., Thomas, D.S.G., Livingstone, I., Wiggs, G.F.S., 1997. Dunefield activity and interactions with climatic variability in the southwest Kalahari Desert. Earth Surface Processes and Landforms 22 : 165–174.

Bulur, E., 2000. A simple transformation for converting CW-OSL curves into LM-OSL curves. Radiation Measurements 32 : 141–145.

Burbidge, C.I., Duller, G.A.T., Roberts, H.M., 2006. D-e determination for young samples using the standardised OSL response of coarse-grain quartz. Radiation Measurements 41 : 278–288.

Burbidge, C.I., Sanderson, D.C.W., Housley, R.A., Jones, P.A., 2007. Survey of Palaeolithic sites by luminescence profiling, a case study from Eastern Europe. Quaternary Geochronology 2: 296–302.

Burns, S.J., Fleitmann, D., Matter, A., Neff, U., Mangini, A., 2001. Speleothem evidence from Oman for continental pluvial events during interglacial periods. Geology 29 : 623–626.

Burns, S.J., Matter, A., Frank, N., Mangini, A., 1998. Speleothem-based paleoclimate record from northern Oman. Geology 26 : 499–502.

Burrough, S.L., Thomas, D.S.G., Shaw, P.A., Bailey, R.M., 2007. Multiphase quaternary highstands at lake Ngami, Kalahari, northern Botswana. Palaeogeography Palaeoclimatology Palaeoecology 253 : 280–299.

Buylaert, J.P., Murray, A.S., Thomsen, K.J., Jain, M., 2009. Testing the potential of an elevated temperature IRSL signal from K-feldspar. Radiation Measurements 44 : 560–565.

Carlson, A.E., 2010. What Caused the Younger Dryas Cold Event? Geology 38 : 383–384.

Chase, B., 2009. Evaluating the use of dune sediments as a proxy for palaeo-aridity: A southern African case study. Earth-Science Reviews 93 : 31.

Chase, B.M., Thomas, D.S.G., 2006. Late Quaternary dune accumulation along the western margin of South Africa: distinguishing forcing mechanisms through the analysis of migratory dune forms. Earth and Planetary Science Letters 251, 318-333.

Chase, B.M., Thomas, D.S.G., 2007. Multiphase late Quaternary aeolian sediment accumulation in western South Africa: Timing and relationship to palaeoclimatic changes inferred from the marine record. Quaternary International 166, 29-41.

Chen, G-Q., Yi, L., Xu, X-Y., Yu, H-J., Cao, J-R., Su, Q., Yang, L-H., Xu, Y-H., Ge, J-Y., Lai, Z-P., 2013. Testing the standardized growth curve (SGC) to OSL dating coastal sediments from the south Bohai Sea, China. Geochronometria 40 : 101–112.

Chiang, J.C.H., Bitz, C.M., 2005. Influence of high latitude ice cover on the marine Intertropical Convergence Zone. Climate Dynamics 25: 477–496.

Choi, J., Duller, G.A.T., Wintle, A.G., 2006. Analysis of quartz LM-OSL curves. Ancient TL 24 : 9–20.

Christensen, J.H., Hewitson, B., Busuioc, A., Chen, A., Gao, X., Held, I., Jones, R., Kolli, R.K., Kwon, W-T., Laprise, R., Magaña Rueda, V., Mearns, L., Menéndez, C.G., Räisänen, J., Rinke, A., Sarr, A., Whetton, P., 2007: Regional Climate Projections. In: Solomon, S., Qin, D., Manning, M., Chen, Z., Marquis, M., Averyt, K.B., Tignor, M., Miller, H.L., (Eds.), Climate Change 2007: The Physical Science Basis. Contribution of Working Group I to the Fourth Assessment Report of the Intergovernmental Panel on Climate Change, Cambridge University Press, Cambridge.

Clark-Balzan, L.A., Candy, I., Schwenninger, J-L., Bouzouggar, A., Blockley, S.P.E., Nathan, R., Barton, R.N.E., 2012. Coupled U-series and OSL dating of a Late Pleistocene cave sediment sequence, Morocco, North Africa: Significance for constructing Palaeolithic chronologies. Quaternary Geochronology 2012 : 53–64.

Clemens, S.C., Prell, W.L., 2003. A 350,000 year summer-monsoon multi-proxy stack from the Owen Ridge, Northern Arabian Sea. Marine Geology 201 : 35–51.

Cohen, T.J., Nanson, G.C., Larsen, J.R., Jones, B.G., Price, D.M., Coleman, M., Pietsch, T.J., 2010. Late Quaternary aeolian and fluvial interactions on the Cooper Creek Fan and the association between linear and source-bordering dunes, Strzelecki Desert, Australia. Quaternary Science Reviews 29 : 455–471.

Cullen, H.M., Demenocal, P.B., Hemming, S., Hemming, G., Brown, F.H., Guilderson, T., Sirocko, F., 2000. Climate change and the collapse of the Akkadian empire: Evidence from the deep sea. Geology 28 : 379–382.

Cunningham, A.C., DeVries, D.J., Schaart, D.R., 2012. Experimental and computational simulation of beta-dose heterogeneity in sediment. Radiation Measurements 47 : 1060–1067.

Cunningham, A.C., Wallinga, J., 2009. Optically stimulated luminescence dating of young quartz using the fast component. Radiation Measurements 44 : 423–428.

Cunningham, A.C., Wallinga, J., 2010. Selection of integration time intervals for quartz OSL decay curves. Quaternary Geochronology 5 : 657–666.

Daniels, D.J., 2005. Ground Penetrating Radar. In: Chang, K., (Ed.), Encyclopedia of RF and Microwave Engineering. Wiley, Hoboken, pp. 1833–1846.

Davies, C.P., 2006. Holocene paleoclimates of southern Arabia from lacustrine deposits of the Dhamar highlands, Yemen. Quaternary Research 66 : 454–464.

Derickson, D., Kocurek, G.A., Ewing, R.C., Bristow, C.S., 2008. Origin of a complex and spatially diverse dune-field pattern, Algodones, southeastern California. Geomorphology 99 : 186–204.

Duller, G.A.T., 2003. Distinguishing quartz and feldspar in single grain luminescence measurements. Radiation Measurements 37 : 161–165.

Duller, G.A.T., 2008. Single-grain optical dating of Quaternary sediments: why aliquot size matters in luminescence dating. Boreas 37 : 589–612.

Duller, G.A.T., Bøtter-Jensen, L., 1993. Luminescence from potassium feldspars stimulated by infrared and green light. Radiation Protection Dosimetry 47 : 683–688.

Duller, G.A.T., Bøtter-Jensen, L., Murray, A.S., Truscott, A.J., 1999. Single grain laser luminescence (SGLL) measurements using a novel automated reader. Nuclear Instruments and Methods in Physics Research Section B: Beam Interactions with Materials and Atoms 155 : 506–514.

Durcan, J.A., Duller, G.A.T., 2011. The fast ratio: A rapid measure for testing the dominance of the fast component in the initial OSL signal from quartz. Radiation Measurements 46 : 1065–1072.

Durcan, J.A., Roberts, H.M., Duller, G.A.T., Alizai, A.H., 2010. Testing the use of range-finder OSL dating to inform field sampling and laboratory processing strategies. Quaternary Geochronology 5, 86-90.

Edgell, H. S., 2006. Arabian Deserts: Nature, Origin and Evolution. Springer, Dordrecht.

El-Sayed, M., 1999. Sedimentological characteristics and morphology of the aeolian sand dunes in the eastern part of the UAE, a case study from Ar Rub' Al Khali. Sedimentary Geology 123 : 219–238.

Ewing, R.C., Kocurek, G.A., 2010. Aeolian dune-field pattern boundary conditions. Geomorphology 114 : 175–187.

Fairbanks, R.G., 1989. A 17,000-year glacio-eustatic sea level record: influence of glacial melting rates on the Younger Dryas event and deep-ocean circulation. Nature 342 : 637–642.

Feathers, J.K., Rhodes, E.J., Huot, S., McAvoy, J.M., 2006. Luminescence dating of sand deposits related to late Pleistocene human occupation at the Cactus Hill Site, Virginia, USA. Quaternary Geochronology 1, 167-187.

Fitzsimmons, K.E., 2007. Morphological variability in the linear dunefields of the Strzelecki and Tirari Deserts, Australia. Geomorphology 91 : 146–160.

Fitzsimmons, K.E., Rhodes, E.J., Magee, J.W., Barrows, T.T., 2007. The timing of linear dune activity in the Strzelecki and Tirari Deserts, Australia. Quaternary Science Reviews 26, 2598-2616.

Fitzsimmons, K.E., Telfer, M.W., 2008. Sedimentary history and the interpretation of late Quaternary dune records: Examples from the Tirari Desert, Australia and the Kalahari, South Africa. Chungara-Revista De Antropologia Chilena 40, 295-308.

Fleitmann, D., Burns, S.J., Mangini, A., Mudelsee, M., Kramers, J., Villa, I., Neff, U., Al-Subbary, A.A., Buettner, A., Hippler, D., Matter, A., 2007. Holocene ITCZ and Indian monsoon dynamics recorded in stalagmites from Oman and Yemen (Socotra). Quaternary Science Reviews 26 : 170–188.

Fleitmann, D., Burns, S.J., Mudelsee, M., Neff, U., Kramers, J., Mangini, A., Matter, A., 2003a. Holocene forcing of the Indian monsoon recorded in a stalagmite from Southern Oman. Science 300 : 1737–1739.

Fleitmann, D., Burns, S.J., Neff, U., Mangini, A., Matter, A., 2003b. Changing moisture sources over the last 330,000 years in Northern Oman from fluid-inclusion evidence in speleothems. Quaternary Research 60 : 223–232.

Fleitmann, D., Burns, S.J., Pekala, M., Mangini, A., Al-Subbary, A., Al-Aowah, M., Kramers, J., Matter, A., 2011. Holocene and Pleistocene pluvial periods in Yemen, southern Arabia. Quaternary Science Reviews 30 : 783–787.

Fleitmann, D., Matter, A., 2009. The speleothem record of climate variability in Southern Arabia. Comptes Rendus Geoscience 341 : 633–642.

Fleitmann, D., Matter, A., Pint, J.J., Al-Shanti, M.A., 2004. The speleothem record of climate in Saudi Arabia. Saudi Geological Survey, Open-File Report. Available from: http://www.i-pi.com/~ingham/saudicaves/OF-2004-8.pdf

Forman, S.L., Marín, L., Pierson, J., Gómez, J., Miller, G.H., Webb, R.S., 2005. Aeolian sand depositional records from western Nebraska: landscape response to droughts in the past 1500 years. The Holocene 15 : 973–981.

Fuchs, M., Buerkert, A., 2008. A 20 ka sediment record from the Hajar Mountain range in N-Oman, and its implication for detecting arid–humid periods on the southeastern Arabian Peninsula. Earth and Planetary Science Letters 265 : 546–558.

Galbraith, R.F., 2003. A simple homogeneity test for estimates of dose obtained using OSL. Ancient TL 21, 75-77.

Galbraith, R.F., 1990. The radial plot: Graphical assessment of spread in ages. International Journal of Radiation Applications and Instrumentation. Part D. Nuclear Tracks and Radiation Measurements 17 : 207–214.

Galbraith, R.F., 1998. The trouble with “probability density” plots of fission track ages. Radiation Measurements 29 : 125–131.

Galbraith, R.F., 2010. On plotting OSL equivalent doses. Ancient TL 28, 1-9.

Galbraith, R.F., Green, P.F., 1990. Estimating the component ages in a finite mixture. International Journal of Radiation Applications and Instrumentation. Part D. Nuclear Tracks and Radiation Measurements 17 : 197–206.

Galbraith, R.F., Roberts, R.G., 2012. Statistical aspects of equivalent dose and error calculation and display in OSL dating: An overview and some recommendations. Quaternary Geochronology 11 : 1–27.

Galbraith, R.F., Roberts, R.G., Laslett, G.M., Yoshida, H., Olley, J.M., 1999. Optical dating of single and multiple grains of quartz from jinmium rock shelter, northern Australia, part 1, Experimental design and statistical models. Archaeometry 41 : 339–364.

Galbraith, R.F., Roberts, R.G., Yoshida, H., 2005. Error variation in OSL palaeodose estimates from single aliquots of quartz: a factorial experiment. Radiation Measurements 39 : 289–307.

Gardner, R.A.M., 1988. Aeolianites and marine deposits of the Wahiba Sands: character and palaeoenvironments. Journal of Oman Studies Special Report No. 3 : 75–94.

Garzanti, E., Ando, S., Vezzoli, G., Dell'Era, D., 2003. From rifted margins to foreland basins: Investigating provenance and sediment dispersal across desert Arabia (Oman, UAE). Journal of Sedimentary Research 73 : 572–588.

Gleick, J., 1997. Chaos: making a new science. Minerva, London

Glennie, K.W., 1998. The desert of southeast Arabia: A product of Quaternary climatic change. In: Alsharhan, A.S., Glennie, K.W., Whittle, G.L., Kendall C.G.S.C., (Eds.), Quaternary Deserts and Climatic Change, A.A. Balkema, Rotterdam, pp. 279–291.

Glennie, K.W., Singhvi, A.K., 2002. Event stratigraphy, paleoenvironment and chronology of SE Arabian deserts. Quaternary Science Reviews 21 : 853–869.

Glennie, K.W., Singhvi, A.K., Lancaster, N., Teller, J.T., 2002. Quaternary climatic changes over southern Arabia and the Thar Desert, India. In: Clift, P.D., Kroon, D., Gaedicke, C., Craig, J., (Eds.), The Tectonic and Climatic Evolution of the Arabian Sea Region, Geological Society, London, pp. 301–316.

Goodall, T.M., 1995. The geology and geomorphology of the Sabkhat Matti region (United Arab Emirates): a modern analogue for ancient desert sediments from north-west Europe. PhD thesis, University of Aberdeen.

Goudie, A.S., Colls, A., Stokes, S., Parker, A., White, K., Al-Farraj, A., 2000a. Latest Pleistocene and Holocene dune construction at the north-eastern edge of the Rub Al Khali, United Arab Emirates. Sedimentology 47, 1011-1021.

Goudie, A.S., Parker, A.G., Al-Farraj, A., 2000b. Coastal Change in Ras Al Khaimah (United Arab Emirates): a Cartographic Analysis. The Geographical Journal 166 : 14–25.

Grine, F.E., Bailey, R.M., Harvati, K., Nathan, R.P., Morris, A.G., Henderson, G.M., Ribot, I., Pike, A.W.G., 2007. Late Pleistocene human skull from Hofmeyr, South Africa, and modern human origins. Science 315 : 226–9.

Groucutt, H.S., Petraglia, M.D., 2012. The prehistory of the Arabian peninsula: deserts, dispersals, and demography. Evolutionary Anthropology 21 : 113–25.

Guérin, G., Mercier, N., 2012. Preliminary insight into dose deposition processes in sedimentary media on a scale of single grains: Monte Carlo modelling of the effect of water on the gamma dose rate. Radiation Measurements 47 : 541–547.

Gupta, A.K., Anderson, D.M., Overpeck, J.T., 2003. Abrupt changes in the Asian southwest monsoon during the Holocene and their links to the North Atlantic Ocean. Nature 421, 354-357.

Gupta, A.K., Das, M., Anderson, D.M., 2005. Solar influence on the Indian summer monsoon during the Holocene. Geophysical Research Letters 32, 1-4.

Gutteridge, P.E., 2008. Who needs lithostratigraphy? Geoscientist 18.

Hadley, D.G., Brouwers, E.M., Bown, T.M., 1998. Quaternary paleodunes, Arabian Gulf coast, Abu Dhabi Emirate: Age and paleoenvironmental reconstruction. In: Alsharhan, A.S., Glennie, K.W., Whittle, G.L., Kendall, C.G.S.C., (Eds.), Quaternary Deserts and Climatic Change, A.A. Balkema, Rotterdam, 123–140.

Harari, Z., 1996. Ground-penetrating radar (GPR) for imaging stratigraphic features and groundwater in sand dunes. Journal of Applied Geophysics 36 : 43–52.

Heiri, O., Lotter, A.F., Lemcke, G., 2001. Loss on ignition as a method for estimating organic and carbonate content in sediments: reproducibility and comparability of results. Journal of Paleolimnology 25, 101-110.

Hollands, C.B., Nanson, G.C., Jones, B.G., Bristow, C.S., Price, D.M., Pietsch, T.J., 2006. Aeolian-fluvial interaction: evidence for Late Quaternary channel change and wind-rift linear dune formation in the northwestern Simpson Desert, Australia. Quaternary Science Reviews 25: 142–162.

Hughes, P.D., 2010. Geomorphology and Quaternary stratigraphy: The roles of morpho-, litho-, and allostratigraphy. Geomorphology 123 : 189–199.

Hunter, R.E., 1977. Basic types of stratification in small eolian dunes. Sedimentology 24, 361-387.

Hunter, R.E., Richmond, B.M., Rho Alpha, T., 1983. Storm-controlled oblique dunes of the Oregon coast. Geological Society of America Bulletin 94 : 1450.

Huntley, D.J., Lian, O.B., 2006. Some observations on tunnelling of trapped electrons in feldspars and their implications for optical dating. Quaternary Science Reviews 25 : 2503–2512.

Ivanochko, T.S., Ganeshram, R.S., Brummer, G-J.A., Ganssen, G., Jung, S.J.A., Moreton, S.G., Kroon, D., 2005. Variations in tropical convection as an amplifier of global climate change at the millennial scale. Earth and Planetary Science Letters 235 : 302–314.

Jacobs, Z., Wintle, A.G., Duller, G.A.T., 2003. Optical dating of dune sand from Blombos Cave, South Africa: I—multiple grain data. Journal of Human Evolution 44 : 599–612.

Jain, C., Murray, A.S., Bøtter-Jensen, L., Wintle, A.G., 2005. A single-aliquot regenerative-dose method based on IR (1.49 eV) bleaching of the fast OSL component in quartz. Radiation Measurements 39 : 309–318.

Jain, M., Ankjærgaard, C., 2011. Towards a non-fading signal in feldspar: Insight into charge transport and tunnelling from time-resolved optically stimulated luminescence. Radiation Measurements 46 : 292–309.

Jain, M., Murray, A.S., Bøtter-Jensen, L., 2003. Characterisation of blue-light stimulated luminescence components in different quartz samples: implications for dose measurement. Radiation Measurements 37 : 441–449.

Jansen, E., Overpeck, J., Briffa, K.R., Duplessy, J-C., Joos, F., Masson-Delmotte, V., Olago, D., Otto-Bliesner, B., Peltier, W.R., Rahmstorf, S., Ramesh, R., Raynaud, D., Rind, D., Solomina, O., Villalba, R., Zhang, D., 2007. Palaeoclimate. In: Solomon, S., Qin, D., Manning, M., Chen, Z., Marquis, M., Averyt, K.B., Tignor, M., Miller, H.L., (Eds.), Climate Change 2007: The Physical Science Basis. Contribution of Working Group I to the Fourth Assessment Report of the Intergovernmental Panel on Climate Change. Cambridge University Press, Cambridge.

Juyal, N., Singhvi, A.K., Glennie, K.W., 1998. Chronology and paleoenvironmental significance of Quaternary desert sediment in southeastern Arabia. In: Alsharhan, A.S., Glennie, K.W., Whittle, G.L., Kendall, C.G.S.C., (Eds.), Quaternary Deserts and Climatic Change, A.A. Balkema, Rotterdam, pp. 315-326.

Kocurek, G. 1981. Significance of interdune deposits and bounding surfaces in aeolian dune sands. Sedimentology 28, 753-780.

Kocurek, G., 1988. First-order and super bounding surfaces in eolian sequences – Bounding surfaces revisited. Sedimentary Geology 56, 193-206.

Kocurek, G.A., 1996. Desert Aeolian Systems. In: Reading, H.G. (Ed.), Sedimentary Environments: Processes, Facies and Stratigraphy. Blackwell Science, Oxford, pp. 125-153.

Kocurek, G.A., 1998. Aeolian system response to external forcing factors - A sequence stratigraphic view of the Saharan region. In: Alsharhan A.S., Glennie K.W., Whittle G.L., Kendall C.G.S.C., (Eds.), Quaternary Deserts and Climatic Change. A.A. Balkema, Rotterdam, pp. 327-338.

Kocurek, G., Ewing, R.C., 2005. Aeolian dune field self-organization - implications for the formation of simple versus complex dune-field patterns. Geomorphology 72 : 94–105.

Kocurek, G., Havholm, K.G., 1993. Eolian sequence stratigraphy - a conceptual framework. In: Weimer, P., Posamentier, H.W. (Eds.), Siliclastic Sequence Stratigraphy: Recent Developments and Applications. American Association of Petroleum Geologists, Tulsa, Vol. 492, pp. 393-409.

Kocurek, G., Lancaster, N., 1999. Aeolian system sediment state: theory and Mojave Desert Kelso dune field example. Sedimentology 46(3), 505-515.

Kocurek, G., Lancaster, N., Carr, M., Frank, A., 1999. Tertiary Tsondab Sandstone Formation: preliminary bedform reconstruction and comparison to modern Namib Sand Sea dunes. Journal of African Earth Sciences 29 : 629–642.

Kutzbach, J.E., 1981. Monsoon Climate of the Early Holocene: Climate Experiment with the Earth's Orbital Parameters for 9000 Years Ago. Science 214 : 59–61.

Lai, Z.P., Brückner, H., 2008. Effects of Feldspar Contamination on Equivalent dose and the Shape of Growth Curve for OSL of Silt-Sized Quartz Extracted from Chinese Loess. Geochronometria 30 : 49–53.

Lai, Z.P., 2006. Testing the use of an OSL Standardised Growth Curve (SGC) for D-e determination on quartz from the Chinese Loess Plateau. Radiation Measurements 41 : 9–16.

Lambeck, K., 1996. Shoreline reconstructions for the Persian Gulf since the last glacial maximum. Earth and Planetary Science Letters 142 : 43–57.

Lancaster, N., 1982. Linear dunes. Progress in Physical Geography 6 : 475–504.

Lancaster, N., 1985. Variations in wind velocity and sand transport on the windward flanks of desert sand dunes. Sedimentology 32, 581–593.

Lancaster, N., 1988. Controls of eolian dune size and spacing. Geology 16 : 972–975.

Lancaster, N., 2008. Desert dune dynamics and development: insights from luminescence dating. Boreas 37 : 559–573.

Lancaster N. 2011. Desert dune processes and dynamics. In: Thomas, D.S.G (Ed.), Arid Zone Geomorphology: Process, Form and Change in Drylands. Wiley-Blackwell, Oxford, 487–516.

Lancaster, N., Baas, A., 1998. Influence of vegetation cover on sand transport by wind: Field studies at Owens Lake, California. Earth Surface Processes and Landforms 23 : 69–82.

Lancaster, N., Kocurek, G.A., Singhvi, A., Pandey, V., Deynoux, M., Ghienne, J.F., Lo, K., 2002. Late Pleistocene and Holocene dune activity and wind regimes in the western Sahara Desert of Mauritania. Geology 30 : 991–994.

Lézine A-M., Robert, C., Cleuziou, S., Inizan, M.L., Braemer, F., Saliège, J.F., Sylvestre F., Tiercelin, J.J., Crassard, R., Méry, S., Charpentier, V., Steimer-Herbet, T., 2010. Climate change and human occupation in the Southern Arabian lowlands during the last deglaciation and the Holocene. Global and Planetary Change 72 : 412–428.

Lézine, A-M., Tiercelin, J.J., Robert, C., Saliege, J.F, Cleuziou, S., Inizan, M.L., Braemer, F., 2007. Centennial to millennial-scale variability of the Indian monsoon during the early Holocene from a sediment, pollen and isotope record from the desert of Yemen. Palaeogeography Palaeoclimatology Palaeoecology 243 : 235–249.

Livingstone, I., 1988. New models for the formation of linear sand dunes. Geography 73 : 105–115.

Livingstone, I., 1989. Monitoring surface change on a Namib linear dune. Earth Surface Processes and Landforms 14 : 317–332.

Livingstone, I., 2003. A twenty-one-year record of surface change on a Namib linear dune. Earth Surface Processes and Landforms 28 : 1025–1031.

Livingstone, I., Wiggs, G.F.S., Weaver, C.M., 2007. Geomorphology of desert sand dunes: A review of recent progress. Earth-Science Reviews 80 : 239–257.

Lomax, J., Hilgers, A., Radtke, U., 2011. Palaeoenvironmental change recorded in the palaeodunefields of the western Murray Basin, South Australia - New data from single grain OSL-dating. Quaternary Science Reviews 30 : 723–736.

Lückge, A., Doose-Rolinski, H., Khan, A.A., Schulz, H., Von Rad, U., 2001. Monsoonal variability in the northeastern Arabian Sea during the past 5000 years: geochemical evidence from laminated sediments. Palaeogeography Palaeoclimatology Palaeoecology 167 : 273–286.

Mandelbrot, B.B., 1983. The fractal geometry of nature. W.H. Freeman and Company, New York.

Mayewski, P.A., Meeker, L.D., Twickler, M.S., Whitlow, S., Yang, Q., Lyons, W.B., Prentice, M., 1997. Major features and forcing of high-latitude northern hemisphere atmospheric circulation using a 110,000-year-long glaciochemical series. Journal of Geophysical Research 102 : 26345–26366.

McClure, H.A., 1976. Radiocarbon chronology of late Quaternary lakes in the Arabian Desert. Nature 263 : 755–756.

McFarlane, M.J., Eckardt, F.D., Ringrose, S., Coetzee, S.H., Kuhn, J.R., 2005. Degradation of linear dunes in Northwest Ngamiland, Botswana and the implications for luminescence dating of periods of aridity. Quaternary International 135 : 83–90.

McLaren, S.J., Al-Juaidi, F., Bateman, M.D., Millington, A.C., 2009. First evidence for episodic flooding events in the arid interior of central Saudi Arabia over the last 60 ka. Journal of Quaternary Science 24 : 198–207.

Miall, A.D., 2012. A new uniformitarianism: stratigraphy as just a set of “frozen accidents”. Preprint in preparation for Geological Society, London, Symposium “Strata and Time”.

Millard, A.R., 2006. Bayesian analysis of Pleistocene chronmetric methods. Archaeometry 48 : 359–375.

Millard, A.R., 2008. A critique of the chronometric evidence for hominid fossils: I. Africa and the Near East 500-50 ka. Journal of human evolution 54 : 848–74.

Munoz-Salinas, E., Bishop, P., Sanderson, D.C.W., Zamorano, J.J., 2011. Interpreting luminescence data from a portable OSL reader: three case studies in fluvial settings. Earth Surface Processes and Landforms 36, 651-660.

Munyikwa, K., 2005. The role of dune morphogenetic history in the interpretation of linear dune luminescence chronologies: a review of linear dune dynamics. Progress in Physical Geography 29, 317-336.

Munyikwa, K., Brown, S., Kitabwalla, Z., 2012. Delineating stratigraphic breaks at the bases of postglacial eolian dunes in central Alberta, Canada using a portable OSL reader. Earth Surface Processes and Landforms 37 : 1603–1614.

Murphy, M.A., Salvador, A., 1999. International Stratigraphic Guide - An abridged version. Available from: http://www.stratigraphy.org/index.php/ics-stratigraphicguide

Murray, A.S., Roberts, R.G., 1997. Determining the burial time of single grains of quartz using optically stimulated luminescence. Earth and Planetary Science Letters 152 : 163–180.

Murray, A.S., Roberts, R,G., 1998. Measurement of the equivalent dose in quartz using a regenerative-dose single-aliquot protocol. Radiation Measurements 29 : 503–515.

Murray, A. S., Wintle, A. G., 2000. Luminescence dating of quartz using an improved single-aliquot regenerative-dose protocol. Radiation Measurements 32, 57–73.

Murray, A.S., Wintle, A.G., 2003. The single aliquot regenerative dose protocol: potential for improvements in reliability. Radiation Measurements 37 : 377–381.

NACSN, 2004. North American Stratigraphic Code. AAPG Bulletin 89 : 1547–1591.

Naidu, P.D., Malmgren, B.A., 1996. A High-resolution record of Late Quaternary upwelling along the Oman Margin, Arabian Sea based on planktonic foraminifera. Paleoceanography 11 : 129–140.

Nanson, G.C., Chen, X.Y., Price, D.M., 1992. Lateral migration, thermoluminescence chronology and colour variation of longitudinal dunes near Birdsville in the Simpson Desert, central Australia. Earth Surface Processes and Landforms 17 : 807–819.

Nathan, R.P., Thomas, P.J., Jain, M., Murray, A.S., Rhodes, E.J., 2003. Environmental dose rate heterogeneity of beta radiation and its implications for luminescence dating: Monte Carlo modelling and experimental validation. Radiation Measurements 37 : 305–313.

Neff, U., Burns, S.J., Mangini, A., Mudelsee, M., Fleitmann, D., Matter, A., 2001. Strong coherence between solar variability and the monsoon in Oman between 9 and 6 kyr ago. Nature 411 : 290–293.

Olley, J.M., Murray, A., Roberts, R.G., 1996. The effects of disequilibria in the uranium and thorium decay chains on burial dose rates in fluvial sediments. Quaternary Science Reviews 15 : 751–760.

Olley, J.M., Pietsch, T., Roberts, R.G., 2004. Optical dating of Holocene sediments from a variety of geomorphic settings using single grains of quartz. Geomorphology 60 : 337–358.

Olley, J.M., Roberts, R.G., Murray, A.S., 1997. Disequilibria in the uranium decay series in sedimentary deposits at Allen’s Cave, Nullarbor Plain, Australia: Implications for dose rate determinations. Radiation Measurements 27 : 433–443.

Overpeck, J., Anderson, D., Trumbore, S., Prell, W., 1996. The southwest Indian Monsoon over the last 18 000 years. Climate Dynamics 12 : 213–225.

Parker, A.G., 2009. Pleistocene Climate Change in Arabia: Developing a Framework for Hominin Dispersal over the Last 350 ka. In: Petraglia, M.D., Rose, J.I., (Eds.), The Evolution of Human Populations in Arabia: Paleoenvironments, Prehistory and Genetics, Springer, London, pp. 39–49.

Parker, A.G., Eckersley, L., Smith, M.M., Goudie, A.S., Stokes, S., Ward, S., White, K., Hodson, M.J., 2004. Holocene vegetation dynamics in the northeastern Rub' al-Khali desert, Arabian Peninsula: a phytolith, pollen and carbon isotope study. Journal of Quaternary Science 19, 665-676.

Parker, A.G., Goudie, A.S., 2007. Development of the Bronze Age landscape in the southeastern Arabian Gulf: new evidence from a buried shell midden in the eastern extremity of the Rub’ al-Khali desert, Emirate of Ras al-Khaimah, U.A.E. Arabian Archaeology and Epigraphy 18 : 132–138.

Parker, A.G., Goudie, A.S., Stokes, S., White, K., Hodson, M.J., Manning, M., Kennet, D., 2006. A record of Holocene climate change from lake geochemical analyses in southeastern Arabia. Quaternary Research 66, 465-476.

Parteli, E.J.R., Duran, O., Tsoar, H., Schwammle, V., Herrmann, H.J., 2009. Dune formation under bimodal winds. Proceedings of the National Academy of Sciences of the United States of America 106 : 22085–22089.

Parton, A., Farrant, A.R., Leng, M.J., Schwenninger, J-L., Rose, J.I., Uerpmann, H-P., Parker, A.G., 2013. An Early MIS 3 Pluvial Phase in Southeast Arabia: Climatic and Archaeological Implications. Quaternary International, DOI: 10.1016/j.quaint.2013.02.016.

Pietsch, D., Kühn, P., 2012. Early Holocene paleosols at the southwestern Ramlat As-Sab’atayn desert margin: New climate proxies for Southern Arabia. Palaeogeography, Palaeoclimatology, Palaeoecology 365-366, 154-165.

Pourmand, A., Marcantonio, F., Schulz, H., 2004. Variations in productivity and eolian fluxes in the northeastern Arabian Sea during the past 110 ka. Earth and Planetary Science Letters 221 : 39–54.

Powers, R.W., Ramirez, L.F., Redmond, C.D., Elberg, E.L., 1966. Geology of the Arabian Peninsula: Sedimentary Geology of Saudi Arabia. U.S. Geological Survey Professional Paper, pp. 1–147.

Prescott, J.R., Hutton, J.T., 1994. Cosmic ray contributions to dose rates for luminescence and ESR dating: Large depths and long-term time variations. Radiation Measurements 23 : 497–500.

Preston, G.W., 2011. From nomadic herder-hunters to sedentary farmers: the relationship between climate, environment and human societies in the United Arab Emirates from the Neolithic to the Iron Age. PhD thesis, Oxford Brookes University.

Preston, G.W., Parker, A.G., Walkington, H., Leng, M.J., Hodson, M.J., 2012. From nomadic herder-hunters to sedentary farmers: The relationship between climate change and ancient subsistence strategies in south-eastern Arabia. Journal of Arid Environments 86 : 122–130.

Preusser, F., 2009. Chronology of the impact of Quaternary climate change on continental environments in the Arabian Peninsula. Comptes Rendus Geoscience 341 : 621–632.

Preusser, F., Kasper, H.U., 2001. Comparison of dose rate determination using high-resolution gamma spectrometry and inductively coupled plasma-mass spectrometry. Ancient TL 19 : 19–23.

Preusser, F., Radies, D., Driehorst, F., Matter, A., 2005. Late quaternary history of the coastal Wahiba Sands, Sultanate of Oman. Journal of Quaternary Science 20 : 395–405.

Preusser, F., Radies, D., Matter, A., 2002. A 160,000-year record of dune development and atmospheric circulation in southern Arabia. Science 296 : 2018–2020.

Prospero, J.M., Lamb, P.J., 2003. African droughts and dust transport to the Caribbean: climate change implications. Science 302 : 1024–7.

Pugh, J.M., 1997. The Quaternary desert sediments of the Al Liwa area, Abu Dhabi.. PhD thesis, University of Aberdeen.

Radies, D., Hasiots, S.T., Preusser, F., Neubert, E., Matter, A., 2005. Paleoclimatic significance of Early Holocene faunal assemblages in wet interdune deposits of the Wahiba Sand Sea, sultanate of Oman. Journal of Arid Environments 62 : 109–125.

Radies, D., Preusser, F., Matter, A., Mange, M., 2004. Eustatic and climatic controls on the development of the Wahiba Sand Sea, Sultanate of Oman. Sedimentology 51 : 1359–1385.

Räsänen, M.E., Auri, J.M., Huitti, J. V., Klap, A.K., Virtasalo, J.J., 2009. A shift from lithostratigraphic to allostratigraphic classification of Quaternary glacial deposits. GSA Today 19 : 4–11.

Reffet, E., Du Pont, S.C., Hersen, P., Douady, S., 2010. Formation and stability of transverse and longitudinal sand dunes. Geology 38 : 491–494.

Reichart, G.J., DenDulk, M., Visser, H.J., VanderWeijden, C.H., Zachariasse, W.J., 1997. A 225 kyr record of dust supply, paleoproductivity and the oxygen minimum zone from the Murray ridge (northern Arabian sea). Palaeogeography Palaeoclimatology Palaeoecology 134 : 149–169.

Rhodes, E.J., Ramsey, C.B., Outram, Z., Batt, C., Willis, L., Dockrill, S., Bond, J., 2003. Bayesian methods applied to the interpretation of multiple OSL dates: high precision sediment ages from Old Scatness Broch excavations, Shetland Isles. Quaternary Science Reviews 22, 1231-1244.

Risø DTU., 2009. Guide to “The Risø Single grain laser OSL system”. Roskilde.

Roberts H.M., 2007. Assessing the effectiveness of the double-SAR protocol in isolating a luminescence signal dominated by quartz. Radiation Measurements 42 : 1627–1636.

Roberts, H.M., Duller, G.A.T., 2004. Standardised growth curves for optical dating of sediment using multiple-grain aliquots. Radiation Measurements 38, 241-252.

Roberts, H.M., Durcan, J.A., Duller, G.A.T., 2009. Exploring procedures for the rapid assessment of optically stimulated luminescence range-finder ages. Radiation Measurements 44, 582-587.

Roberts, H.M., Wintle, A.G., 2001. Equivalent dose determinations for polymineralic fine-grains using the SAR protocol: application to a Holocene sequence of the Chinese Loess Plateau. Quaternary Science Reviews 20 : 859–863.

Roberts, H.M., Wintle, A.G., 2003. Luminescence sensitivity changes of polymineral fine grains during IRSL and [post-IR] OSL measurements. Radiation Measurements 37 : 661–671.

Rosenberg, T.M., Preusser, F., Blechschmidt, I., Fleitmann, D., Jagher, R., Matter, A., 2012. Late Pleistocene palaeolake in the interior of Oman: a potential key area for the dispersal of anatomically modern humans out-of-Africa? Journal of Quaternary Science 27 : 13–16.

Rosenberg, T.M., Preusser, F., Fleitmann, D., Schwalb, A., Penkman, K., Schmid, T.W., Al-Shanti, M.A., Kadi, K., Matter, A., 2011. Humid periods in southern Arabia: Windows of opportunity for modern human dispersal. Geology 39 : 1115–1118.

Rosenberg, T.M., Preusser, F., Risberg, J., Plikk, A., Kadi, K.A., Matter, A., Fleitmann, D., 2013. Middle and Late Pleistocene humid periods recorded in palaeolake deposits of the Nafud desert, Saudi Arabia. Quaternary Science Reviews 70 : 109–123.

Roskin, J., Tsoar, H., Porat, N., Blumberg, D.G., 2011. Palaeoclimate interpretations of Late Pleistocene vegetated linear dune mobilization episodes: evidence from the northwestern Negev dunefield, Israel. Quaternary Science Reviews 30 : 3364–3380.

Rubin, D.M., 1990. Lateral migration of linear dunes in the Strzelecki Desert, Australia. Earth Surface Processes and Landforms 15 : 1–14.

Rubin, D.M., Hesp, P.A., 2009. Multiple origins of linear dunes on Earth and Titan. Nature Geoscience 2 : 653–658.

Rubin, D.M., Hunter, R.E., 1983. Reconstructing bedform assemblages from compound crossbedding. In: Brookfield, M.E., Ahlbrandt, T.S., (Eds.), Eolian sediments and processes. Developments in sedimentology, Vol. 38, pp. 407-428.

Rubin, D.M., Hunter, R.E., 1985. Why deposits of longitudinal dunes are rarely reconized in the geologic record. Sedimentology 32, 147-157.

Ruddiman, W.F., 2001. Earth’s climate: past and future. W.H. Freeman and Company, Basingstoke.

Sanderson, D.C.W., Bishop, P., Houston, I., Boonsener, M., 2001. Luminescence characterisation of quartz-rich cover sands from NE Thailand. Quaternary Science Reviews 20 : 893–900

Sanderson, D.C.W., Bishop, P., Stark, M.T., Spencer, J.Q., 2003. Luminescence dating of anthropogenically reset canal sediments from Angkor Borei, Mekong Delta, Cambodia. Quaternary Science Reviews 22 : 1111–1121

Sanderson, D.C.W., Murphy,S., 2010. Using simple portable OSL measurements and laboratory characterisation to help understand complex and heterogeneous sediment sequences for luminescence dating. Quaternary Geochronology 5, 299-305.

Sanlaville, P., 1992. Changements climatiques dans la Peninsule Arabique durant le Pleistocene Superieur et l'Holocene. Paleorient 18 : 5–26.

Santisteban, J.I., Mediavilla, R., Lopez-Pamo, E., Dabrio, C.J., Zapata, M.B.R., Garcia, M.J.G., Castano, S., Martinez-Alfaro, P.E., 2004. Loss on ignition: a qualitative or quantitative method for organic matter and carbonate mineral content in sediments? Journal of Paleolimnology 32 : 287–299.

Sarkar, A., Ramesh, R., Somayajulu, B.L.K., Agnihotri, R., Jull, A.J.T., Burr, G.S., 2000. High resolution Holocene monsoon record from the eastern Arabian Sea. Earth and Planetary Science Letters 177 : 209–218.

Schulz, H., Von Rad, U., Erlenkeuser, H., 1998. Correlation between Arabian Sea and Greenland climate oscillations of the past 110,000 years. Nature 393 : 54–57.

Selley, R.C., 1985. Ancient Sedimentary Environments. 3rd Ed. Chapman and Hall, London.

Shackleton, N.J., 1987. Oxygen isotopes, ice volume and sea level. Quaternary Science Reviews 6 : 183–190.

Shakun, J.D., Burns, S.J., Fleitmann, D., Kramers, J., Matter, A., Al-Subary, A., 2007. A high-resolution, absolute-dated deglacial speleothem record of Indian Ocean climate from Socotra Island, Yemen. Earth and Planetary Science Letters 259 : 442–456.

Siddall, M., Rohling, E.J., Almogi-Labin, A., Hemleben, C., Meischner, D., Schmelzer, I., Smeed, D.A., 2003. Sea-level fluctuations during the last glacial cycle. Nature 423, 853-858.

Singarayer, J.S., Bailey, R.M., 2003. Further investigations of the quartz optically stimulated luminescence components using linear modulation. Radiation Measurements 37 : 451–458.

Singarayer, J.S., Bailey, R.M., 2004. Component-resolved bleaching spectra of quartz optically stimulated luminescence: preliminary results and implications for dating. Radiation Measurements 38 : 111–118.

Singhvi, A.K., Sharma, Y.P., Agrawal, D.P., 1982. Thermoluminescence dating of sand dunes in Rajasthan, India. Nature 295 : 313–315.

Sirocko, F., 2000. Processes controlling trace element geochemistry of Arabian Sea sediments during the last 25,000 years. Global and Planetary Change 26 : 217–303.

Sirocko, F., Garbe-Schonberg, D., McIntyre, A., Molfino, B., 1996. Teleconnections Between the Subtropical Monsoons and High-Latitude Climates During the Last Deglaciation. Science 272 : 526–529.

Sirocko, F., Sarnthein, M., Erlenkeuser, H., Lange, H, Arnold, M., Duplessy, J.C., 1993. Century-scale events in monsoonal climate over the past 24,000 years. Nature 364 : 322–324.

Sirocko, F., Sarnthein, M., Lange, H., Erlenkeuser, H., 1991. Atmospheric summer circulation and coastal upwelling in the Arabian Sea during the Holocene and the last glaciation. Quaternary Research 36 : 72–93.

Solymar, L., Walsh, D., 1984. Lectures on the electrical properties of materials. Oxford University Press, Oxford.

Spooner, N.A., 1994a. On the optical dating signal from quartz. Radiation Measurements 23 : 593–600.

Spooner, N.A., 1994b. The anomalous fading of infrared-stimulated luminescence from feldspars. Radiation Measurements 23 : 625–632.

Stanford, J.D., Rohling, E.J., Hunter, S.H., Roberts, A.P., Rasmussen, S.O., Bard, E., McManus, J., Fairbanks, R.G., 2006. Timing of meltwater pulse 1a and climate responses to meltwater injections. Paleoceanography 21, 1-9.

Staubwasser, M., Sirocko, F., Grootes, P.M., Erlenkeuser, H., 2002. South Asian monsoon climate change and radiocarbon in the Arabian Sea during early and middle Holocene. Paleoceanography 17, 1-12.

Staubwasser, M., Sirocko, F., Grootes, P.M., Segl, M., 2003. Climate change at the 4.2 ka BP termination of the Indus valley civilization and Holocene south Asian monsoon variability. Geophysical Research Letters 30 : 1425–1429.

Stein, M., Torfstein, A., Gavrieli, I., Yechieli, Y., 2010. Abrupt aridities and salt deposition in the post-glacial Dead Sea and their North Atlantic connection. Quaternary Science Reviews 29 : 567–575.

Stevens, T., Armitage, S.J., Lu, H.Y., Thomas, D.S.G., 2007. Examining the potential of high sampling resolution OSL dating of Chinese loess. Quaternary Geochronology 2 : 15–22.

Stokes, S., Bray, H.E., 2005. Late pleistocene eolian history of the liwa region, Arabian Peninsula. Geological Society of America Bulletin 117 : 1466–1480.

Stone, A.E.C., Thomas, D.S.G., 2008. Linear dune accumulation chronologies from the southwest Kalahari, Namibia: challenges of reconstructing late Quaternary palaeoenvironments from aeolian landforms. Quaternary Science Reviews 27, 1667-1681.

Telfer, M.W., 2011. Growth by extension, and reworking, of a south-western Kalahari linear dune. Earth Surface Processes and Landforms 36 : 1125–1135.

Telfer, M.W., Bailey, R.M., Burrough, S.L., Stone, A.E.S., Thomas, D.S.G., Wiggs, G.S.F., 2010. Understanding linear dune chronologies: Insights from a simple accumulation model. Geomorphology 120, 195-208.

Telfer, M.W., Bateman, M.D., Carr, A.S., Chase, B.M., 2008. Testing the applicability of a standardized growth curve (SGC) for quartz OSL dating: Kalahari dunes, South African coastal dunes and Florida dune cordons. Quaternary Geochronology 3, 137-142.

Telfer, M.W., Thomas, D.S.G., 2007. Late Quaternary linear dune accumulation and chronostratigraphy of the southwestern Kalahari: implications for aeolian palaeoclimatic reconstructions and predictions of future dynamics. Quaternary Science Reviews 26 : 2617–2630.

Teller, J.T., Glennie, K.W., Lancaster, N., Singhvi, A.K., 2000. Calcareous dunes of the United Arab Emirates and Noah's Flood: the postglacial reflooding of the Persian (Arabian) Gulf. Quaternary International, 68, 297-308.

Thamban, M., Kawahata, H., Rao, V.P., 2007. Indian summer monsoon variability during the holocene as recorded in sediments of the Arabian sea: Timing and implications. Journal of Oceanography 63 : 1009–1020.

Thomas, D.S.G., 2011. Arid environments: their nature and extent. In: Thomas, D.S.G (Ed.), Arid Zone Geomorphology: Process, Form and Change in Drylands. Wiley-Blackwell, Oxford, pp. 3–16.

Thomas, D.S.G., 2013. Reconstructing paleoenvironments and palaeoclimates in drylands: what can landform analysis contribute? Earth Surface Processes and Landforms 38 : 3–16.

Thomas, D.S.G., Burrough, S.L., 2012. Interpreting geoproxies of late Quaternary climate change in African drylands: implications for understanding environmental and early human behaviour. Quaternary International 253, 5-17.

Thomas, D.S.G., Knight, M., Wiggs, G.F.S., 2005. Remobilization of southern African desert dune systems by twenty-first century global warming. Nature 435, 1218-1221.

Thomas, D.S.G., Leason, H.C., 2005. Dunefield activity response to climate variability in the southwest Kalahari. Geomorphology 64 : 117–132.

Thomas, D.S.G., Shaw, P.A., 2002. Late Quaternary environmental change in central southern Africa: new data, synthesis, issues and prospects. Quaternary Science Reviews 21, 783-797.

Thomas, D.S.G., Wiggs, G.F.S., 2008. Aeolian system responses to global change: challenges of scale, process and temporal integration. Earth Surface Processes and Landforms 33 : 1396–1418.

Thomsen, K.J., Murray, A.S., Jain, M., Bøtter-Jensen, L., 2008. Laboratory fading rates of various luminescence signals from feldspar-rich sediment extracts. Radiation Measurements 43: 1474–1486.

Tseo, G., 1993. Two types of longitudinal dune fields and possible mechanisms for their development. Earth Surface Processes and Landforms 18 : 627–643.

Tsoar, H., 1983. Dynamic processes acting on a longitudinal (seif) sand dune. Sedimentology 30, 567–578.

Tsoar, H., 1984. The formation of seif dunes from barchans - a discussion. Zeitschrift für Geomorphologie 28 : 99–103.

Tsoar, H., 1989. Linear dunes - forms and formation. Progress in Physical Geography 13 : 507–528.

Tsoar, H., 2001. Types of aeolian sand dunes and their formation. In: Balmforth, N.J., Provenzale, A., (Eds.), Geomorphological Fluid Mechanics, Springer-Verlag, London, 403–429.

Tsoar, H., Blumberg, D.G., Stoler, Y., 2004. Elongation and migration of sand dunes. Geomorphology 57, 293–302.

UNEP, 1992. World Atlas of Desertification . Edward Arnold, London.

Wang, X., Dong, Z., Zhang, J., Qu, J., 2004. Formation of the complex linear dunes in the central Taklimakan Sand Sea, China. Earth Surface Processes and Landforms 29: 677–686.

Wang, X., Yang, Y., Dong, Z., Zhang, C., 2009. Responses of dune activity and desertification in China to global warming in the twenty-first century. Global and Planetary Change 67 : 167–185.

Wang, Y., Cheng, H., Edwards, R.L., He, Y., Kong, X., An, Z., Wu, J., Kelly, M.J., Dykoski, C.A., Li, X., 2005. The Holocene Asian monsoon: links to solar changes and North Atlantic climate. Science 308 : 854–857.

Washington, R., Bouet, C., Cautenet, G., Mackenzie, E., Ashpole, I., Engelstaedter, S., Lizcano, G., Henderson, G.M., Schepanski, K., Tegen, I., 2009. Dust as a tipping element: the Bodele Depression, Chad. Proceedings of the National Academy of Sciences of the United States of America 106 : 20564–71.

Washington, R., Thomas, D.S.G., 2011. Future climate change and arid zone geomorphology. In: Thomas, D.S.G (Ed.), Arid Zone Geomorphology: Process, Form and Change in Drylands. Wiley-Blackwell, Oxford, pp. 599-610.

Wasson, R.J., Hyde, R., 1983. Factors determining desert dune type. Nature 304 : 337–339.

Wiggs, G.F.S., 2001. Desert dune processes and dynamics. Progress in Physical Geography 25, 53–79.

Wiggs, G.F.S., Baird, A.J., Atherton, R.J., 2004. The dynamic effects of moisture on the entrainment and transport of sand by wind. Geomorphology 59 : 13–30.

Wiggs, G.F.S., Thomas, D.S.G., Bullard, J.E., 1995. Dune mobility and vegetation cover in the southwest Kalahari Desert. Earth Surface Processes and Landforms 20 : 515–529.

Williams, A.H., Walkden, G.M., 2002. Late Quaternary highstand deposits of the southern Arabian Gulf: a record of sea-level and climate change. In: Clift, P.D., Kroon, D., Gaedicke, C., Craig, J. (eds). The Tectonic and Climatic Evolution of the Arabian Sea Region, London, pp. 371–386.

Wintle, A.G., Murray, A.S., 2000. Quartz OSL: Effects of thermal treatment and their relevance to laboratory dating procedures. Radiation Measurements 32 : 387–400.

Wintle, A.G., Murray, A.S., 2006. A review of quartz optically stimulated luminescence characteristics and their relevance in single-aliquot regeneration dating protocols. Radiation Measurements, 41, 369-391.

Wood, W.W., Bailey, R.M., Hampton, B.A., Kraemer, T.F., Lu, Z., Clark, D.W., James, R.H.R., Al Ramadan, K., 2012. Rapid late Pleistocene/Holocene uplift and coastal evolution of the southern Arabian (Persian) Gulf. Quaternary Research 77 : 215–220.

Wood, W.W., Imes, J.L., 1995. How wet is wet? Precipitation constraints on late Quaternary climate in the southern Arabian Peninsula. Journal of Hydrology 164 : 263–268.

Wopfner, H., Twidale, C.R., 2001. Australian desert dunes: wind rift or depositional origin? Australian Journal of Earth Sciences 48 : 239–244.

Yang, L., Lai, Z.P., Long, H., Zhang, J., 2011. Construction of a quartz OSL standardised growth curve (SGC) for aeolian samples from the Horqin dunefield in northeastern China. Geochronometria 38 : 391–396.

Yang, L., Wang, T., Zhou, J., Lai, Z.P., Long, H., 2012. OSL chronology and possible forcing mechanisms of dune evolution in the Horqin dunefield in northern China since the Last Glacial Maximum. Quaternary Research 78 : 185–196.

Yokoyama, Y., Lambeck, K., De Deckker, P., Johnston, P., Fifield, L., 2000. Timing of the Last Glacial Maximum from observed sea-level minima. Nature 406 : 713–6.

Zander, A., Degering, D., Preusser, F., Kasper, H.U., Bruckner, H., 2007. Optically stimulated luminescence dating of sublittoral and intertidal sediments from Dubai, UAE: Radioactive disequilibria in the uranium decay series. Quaternary Geochronology 2 : 123–128.

Zhang, R., Kan, M., Kawamura, T., 2005. Numerical study of the formation of transverse dunes and linear dunes. Journal of the Physical Society of Japan 74 : 599–604.

Appendix A: Author contributions

The papers incorporated within this thesis have been co-authored with supervisors. The majority of the work presented is my own work. The account below describes my contribution (CL) and that of my supervisors and co-authors (DT and RB) to the papers.

Sampling in the field was conducted by CL, RB and DT. CL prepared, dated and conducted all laboratory work (unless stated explicitly in the thesis) for all samples. RB gave technical advice of laboratory and modelling procedures conducted for Paper 4 (Chapter 7). The numerical model used in Paper 5 (Chapter 8) was written by RB. CL conducted all model runs described in the paper. CL conducted all data analysis. CL wrote all of the papers, and drew all figures and tables. All papers were discussed between CL, RB and DT, and comments were incorporated into the papers.

Appendix B: Investigating the application of ground penetrating radar in aeolian sediments

B.1 Introduction

'Radar stratigraphy' has been defined as the "the study of stratigraphy and depositional facies as interpreted from radar data using seismic stratigraphic principles" (Jol and Bristow, 2003: 23, modified from Mitchum et al., 1977). The application of ground penetrating radar (GPR), which enables the subsurface to be imaged, within dunefields has provided the enticing prospect of using dune structures to guide and aid interpretation of OSL dating. This short study will examine the use of GPR within various dunefields and describe the use of this technique in the UAE.

Aeolian dunes have been successfully imaged using GPR in many different dunefields (e.g. Bristow et al., 1996, 2000, 2005; Harari, 1996). Different internal structures can be expected to be seen in different types of dunes, as a result of spatial and temporal variability of depositional processes. These structures have been used to further understanding of the dynamics of dune development (e.g. Bristow et al., 2000, 2007a, 2007b).

Bristow et al. (2000) conducted GPR surveys along the crest of a sinuous dune in the northern Namib Sand Sea, holding the assumption that spatial differences in internal stratigraphy were a result of the elongation of the dune northwards over time. The prevalence of bimodal dipping and sets of cross-stratification as the size of the dune increased were interpreted by the authors as representing the development and migration of superimposed bedforms along the primary dune. The revealed structural asymmetry of sinuous linear dunes in the Namib and Simpson Deserts has been used to infer lateral migration of their forms and support Rubin's (1990) hypothesis of dune asymmetry (Bristow et al., 2000, 2007b).

GPR profiling has also been used to provide a relative chronology that can be used to guide OSL sampling (e.g. Bristow, 2004; Bristow et al., 2005; Li and Fan, 2011). Further, this has enabled estimations of rates to be attributed to dune processes (Bristow et al., 2005, 2007a). Reflections are assumed to represent isochronous surfaces, and hence "successive radar sequences can be used to construct a relative chronology following the laws of superposition and cross-cutting relations" (Bristow et al., 2005: 317). OSL dating and sedimentological analysis along the length of linear dunes have been used to investigate whether downwind elongation or wind-rifting is the dominant process of linear dune extension. Case studies of individual dunes have yielded evidence of both forms of formation and elongation (Bristow et al., 2007b; Hollands et al., 2006), supporting Telfer's (2011) hybrid model of linear dune formation (Section 1.3.1).

B.2 GPR profiling

B.2.1 The physics of GPR

GPR utilises the propagation of electromagnetic (EM) waves and the EM properties of the subsurface to map buried reflector surfaces. The GPR unit consists of transmitting and receiving antennae. An EM pulse generated by the transmitting antenna is directed into the subsurface and scattered when it reaches a reflector. The reflected wave is recorded by the receiving antenna at the surface (Baker et al., 2007). The subsurface structure can then be assessed in the field; GPR hence provides a non-destructive and potentially rapid tool to target subsurface sedimentary structures for OSL dating.

The propagation of EM waves is determined by the *relative permittivity* (also known as the dielectric constant) of a material; hence, reflections are generated at boundaries where there is a change in relative permittivity. Relative permittivity is "the ability of a material to store and then permit the passage of EM energy when a field is imposed on the material" (Baker et al., 2007: 1). When exposed to an external electric field, the atoms in a dielectric material are subject to molecular orientation and an internal EM field which balances the imposed external field is created. Energy loss occurs during this process, and so permittivity is represented as storage (real number) and dissipation (imaginary number, related to electrical conductivity) components. Relative permittivity (dimensionless) can be described as:

$$\varepsilon_r = \varepsilon/\varepsilon_0$$

(Eq. B.1)

where ε is permittivity, and ε_0 is the permittivity of free space (both in F m^{-1}).

Table B.1: Electrical properties of typical materials at 80-120 MHz. (Modified from Baker et al., 2001, and Neal, 2004, with data from Daniels et al. 1995; Davis and Annan, 1989; van Heuteren et al., 1998; Theimer et al., 1994; van Overmeeren, 1994).

Table B.1 has been removed due to Copyright restrictions

The *travel time* is the time for the EM wave to travel from the transmitting antenna to the receiving antenna and is determined by the *propagation velocity* of the wave, which is dependent upon the relative permittivity of the material. The propagation velocity of the atmosphere near sea level is 0.3 m ns^{-1} (Table B.1). In earth materials the velocity is lower in comparison a result of higher relative permittivity values; in the range of 0.05 to 0.15 m ns^{-1}, with dry sand between 0.12-0.17 m ns^{-1} (Baker et al., 2007). When the propagation velocity of the subsurface material is known, this is used to calculate the depth of the reflector. The subsurface being profiled is most likely to be heterogeneous, with materials of varying relative permittivity, and so the level of heterogeneity of the material is important in determining the level of the signal in relation to background scatter in the signal whilst anisotropic characteristics may distort the image (Daniels, 2005).

Propagation velocity (and therefore wavelength) is determined by the relative permittivity of the material, whilst the amplitude and attenuation of the wave is determined by the *magnetic permeability* (μ, a measure of how energy is stored and dissipated in a material when exposed to an external magnetic field) and *electrical conductivity* (a measure of electron transport in a material subject to an external electric field) of the material (Baker et al., 2007). These relationships can be described by:

$$\lambda = v/f$$

(Eq. B.2)

$$v = \frac{c}{\sqrt{\varepsilon_r}}$$

(Eq. B.3)

where v =velocity (m s^{-1}), λ =wavelength (m), c =speed of light in a vacuum (m s^{-1}), f =frequency (Hz). The greatest resolution that can be achieved is one quarter of the wavelength, which is known as the Nyquist sampling interval (Jol and Bristow, 2003). In order for EM waves to propagate, the frequency of the wave must be greater than the material's transition frequency (dependent on both relative permittivity and electrical conductivity of the material).

- As relative permittivity increases, propagation velocity decreases. This allows shorter wavelengths, and hence higher resolution.
- As magnetic permeability increases, attenuation increases. In most sediments which are not ferromagnetic magnetic permeability is low: $\mu \approx \mu_0$.
- As electrical conductivity increases, attenuation increases. Electrical conductivity is important in the calculation of the attenuation constant of a material:

$$\alpha \approx \frac{\sigma}{2}\sqrt{\frac{\mu_r \mu_0}{\varepsilon_r \varepsilon_0}} \approx \sqrt{\pi f \mu_r \mu_0 \sigma}$$

(Eq. B.4)

where α=attenuation constant (Np m^{-1}) and σ=electrical conductivity (S m^{-1}) (Baker et al., 2007).

Therefore GPR is most effective, with the deepest penetration depth, in materials that are electrically and magnetically resistive, such as sands and gravels (Baker et al., 2007). The depth of profiling is limited by attenuation of the electromagnetic wave, due to losses in the electric and magnetic fields (Daniels, 2005).

In general, sand provides an ideal material for EM propagation due to its electrical resistivity. Davis and Annan (1989) state that in materials such as sand with conductivities less than 1 mS m^{-1} depths of up to 50 m have been demonstrated. Lower frequencies allow for greater depth, whilst higher frequencies, with shorter wavelengths, enable greater vertical resolution. Most sedimentary studies use frequencies in the range of 50-500 MHz (Jol and Bristow, 2003). Water content has been shown to have the most significant effect on the permittivity of sediments, and changes in permeability as a result of textural variability at bedding set boundaries result in the imaging of bounding surfaces in dune sediments (Bristow, 2004) .

However, some problems encountered demonstrate the difficulties of using GPR even in dry sand. Attenuation of the EM signal across the Simpson Desert, Australia, has been linked to high clay and silt content and traces of iron (Bristow et al., 2007b). Whilst Harari (1996) reached depths of greater than 35 m when using a 100 MHz antenna, and ~9 m depth using a 500 MHz antenna in studies of aeolian dunes in Saudi Arabia and Australia, no bounding surfaces were detected in the Eastern Province of Saudi Arabia where internal structures were known to be present. This led the authors to conclude that GPR is not effective in detecting surfaces that are defined by variations in grain packing density alone. Additionally, difficulty in correlating bounding surfaces in Liwa, UAE, highlights the complexity of subsurface structures (Bristow et al., 1996).

B.2.2 Field protocols

Of the four main types of scattering, spectral reflection scattering is the most important used in GPR profiling (Baker et al., 2007). The angle of incidence is equal to the angle of reflection (Figure B.1a), whilst the energy not reflected will be refracted into the underlying surface, producing a record of several reflections each representing a change in EM properties. The characteristics of a reflected EM wave are a function of antennae orientation, electrical properties of materials surrounding interface, and the angle of incidence (dependent on antennae separation and depth) (Baker et al., 2007).

EM wave propagation is described by Maxwell's equations. The GPR transmitter transmits an electric field (*E)*, from which a magnetic field (*H)* is generated, which in turn generates an electric field. The repetition of these processes produces propagating EM waves. Most GPR systems create linearly polarised waves, where the electric and magnetic fields, which are perpendicular to each other, do not rotate over time (Baker et al., 2007). The electric field is parallel to the long axis of the antennae whilst magnetic field is perpendicular to the long axis (Figure B.1b). A perpendicular broadside antennae orientation will generate *EH* polarization (perpendicularly polarized), which tends to have a higher signal-to-noise ratio than the alternative, *EV*, polarization (Baker et al., 2007).

In bistatic mode the two antennae are separate units. Common offset (CO) mode is the most common measurement protocol for profiling subsurface structures. The antennae are separated by a fixed distance and together are moved along the survey line by a fixed step size (the distance between each data collection point). This distance should be less than the Nyquist sampling interval, in order to avoid spatial aliasing. Typically for a 100 MHz survey a step size of 0.25 m is used (Jol and Bristow, 2003). Step size presents a limit on horizontal resolution due to the time needed to complete survey lines; most studies do not use a step size of less than 0.1 m due to the time required for survey measurement.

Figure B.1 has been removed due to Copyright restrictions

Figure B.1: (a) Typical reflected paths off two horizontal subsurfaces from the transmitter (T) to the receiver (R). (b) Perpendicular broadside antennae orientation of T and R along survey line Y. *E* and *H* show the electric and magnetic vectors respectively. Z is the vertical plane of incidence. Redrawn from Baker et al. (2007).

Survey lines within a grid should be orientated to be parallel and perpendicular to the sedimentary dip direction (Jol and Bristow, 2003). Systematically surveying in a grid pattern allows the construction of a radar image using 2 or 3-dimensions. If using a 3-D grid, survey line spacing involves another compromise between time of survey and horizontal resolution; small areas are often covered due to the time needed to collect and process the data (Bristow, 2004).

B.3 A GPR investigation in the northeastern Rub' al Khali

B.3.1 Data collection and interpretation

GPR transects were conducted at sites near the Emirates Highway, Falaj Al Moalla, and Shwaib (Figure B.2) using a RAMAC GPR from MALA GeoScience and 50, 100 and 200 MHz antennae frequencies (antenna separation 2 m, 1 m and 60 cm respectively) in CO mode. The GPR surveys were led by Dr Oliver Sass and Johannes Stangl from the University of Graz, as part of fieldwork undertaken in March 2011.

Before data collection, it is important to know the size and nature of the subsurface target, and ground conditions at the site in order to choose the appropriate measurement strategy (e.g. antennae orientation, separation and frequency, step size) (Jol and Bristow, 2003). The propagation velocity of a specific subsurface material is calculated by conducting a common-midpoint (CMP) test. The antennae are first placed side by side along the survey line and the distance between them, keeping the midpoint fixed, is then incrementally increased. The velocity is calculated by utilising the increasing travel time of the ground wave from a subsurface horizontal interface. Corrections and processing procedures can also be made to enhance the signal and reduce noise and distortion (Harari, 1996).

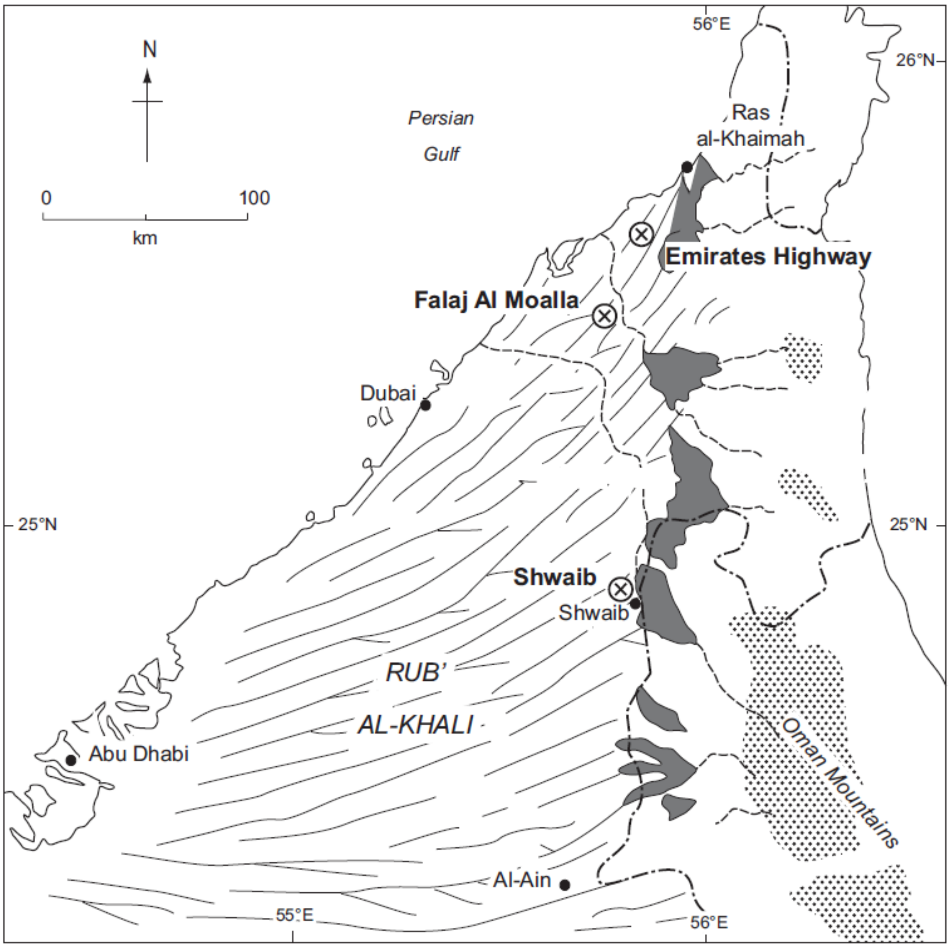

Figure B.2: Map of site locations in the UAE where GPR surveys were conducted. Trends of linear megaridges and major alluvial fans are shown. Adapted from Atkinson et al. (2011).

Surface samples from the UAE and other locations where GPR has both been successfully and unsuccessfully applied (provided by Dr Charlie Bristow, University of Birkbeck) were analysed in the laboratory. Particle size analysis was conducted using the method described in Section 3.3. In addition, the electrical conductivity of the samples was measured, and the samples were sent for clay analysis using XRD (described below).

B.3.2 Electrical conductivity

Electrical conductivity (EC) was measured using samples from sites where ground penetrating radar (GPR) profiling was conducted. There are numerous methods used to measure the EC of soil, which makes comparison of published values problematic. EC can be measured in the field, as if often the case for agricultural purposes (e.g. Grisso et al., 2009), although it is not widely used due to the dependence upon the soil-water content at the time of measurement (Rhoades, 1978 in Miller and Curtin, 2008). In the laboratory EC can be measured using either saturation paste extracts (EC_e) or, as increasingly used due to the time and skill required to use saturated pastes, fixed ratio extracts (commonly 1:1, 1:2, 1:5) (Miller and Curtin, 2008). When relative rather than absolute comparisons of conductivity are needed, ratio extracts can be of use (Rhoades, 1982). In this study, a fixed soil:water ratio extract of 1:5 ($EC_{1:5}$) was used. Air-dry sand (5 g) was weighed and the appropriate volume of deionized water (25 ml) was added. The solution was shaken for 1 h prior to measurement at room temperature. An ORION 150 conductivity meter was calibrated using standard calibration solutions before measurement of the mixtures. Readings of conductivity, salinity and total dissolved solids (TDS) were taken. Temperature is automatically corrected for by the probe.

B.3.3 X-ray diffraction

X-ray diffraction (XRD) is used to identify and characterise crystalline substances, including clay minerals. It has been used as a technique in this thesis to further investigate the nature of the sediments at sites where GPR has been successfully or unsuccessfully applied. X-rays are focused at a sample and the scattered beam is detected. Constructive interference, or diffraction, depends upon the nature of the crystal structure of the sample. The condition for diffraction is given by the Bragg equation:

$$n\lambda = 2d \sin\theta$$

(Eq. B.5)

where n is an integer representing the order of the diffraction peak, λ is wavelength of the x-ray, d is the inter-plane distance within a crystal lattice, and θ is the scattering angle (UC Santa Barbara Materials Research Laboratory, 2013). Therefore the XRD patterns are directly related to the atomic distances of the material and peaks in can be used to identify the present crystals (phases).

> "…every crystalline substance gives a pattern; the same substance always gives the same pattern; and in a mixture of substances each produces its pattern independently of the others." (Hull, 1919 in Scintag Inc., 1999)

The area under each peak in the diffraction pattern is related to the amount of each phase within the sample (Scintag Inc., 1999). The XRD results discussed below were conducted at the University of Birkbeck.

B.3.4 Results and discussion

Dry sand is a material for which GPR is usually effective, as it is both electrically and magnetically resistive (Baker et al., 2007) and has been applied successfully previously in the UAE (Bristow et al., 1996). However, subsurface reflectors were not identified despite it known that there *is* clear internal structure at these sites from the visible exposures. Although greater depths were reached at Falaj Al Moalla and Shwaib, attenuation was high at all sites (e.g. Figure B.3).

In Saudi Arabia, the application of GPR to dunes found similar problems regarding the lack of structure resolved by the GPR, despite the known presence of dune internal structure. This has been attributed to the structures being solely defined by changes in packing density (Harari, 1996). Another possible reason is the lack of moisture in the sands after a drier than average winter, which made changes in moisture content negligible between the sedimentary sets. However, if this were the case it would be expected for the EM waves to propagate with little attenuation until there was enough moisture for a reflection to be identified, but no measurable structures at depth indicate that there is significant attenuation of the signal (Sass, pers. comm.).

Figure B.3 has been removed due to Copyright restrictions

Figure B.3: A GPR transect at Falaj al Mualla, using 100 MHz antenna frequency, corrected for topography. The noisy signal is inferred to be a result of high attenuation. A small number of bounding surfaces are identifiable, but not to the extent that these results can be used to guide OSL sampling.

Conductivity values of 5-11 mS m^{-1} for the UAE samples (A-D in Tables B.2 and B.3) are significantly larger than the range of the 0.01 mS m^{-1} 'typical' value of unsaturated sand suggested by Neal (2004). Comparison of surface and subsurface samples at the same site (B and C respectively) shows higher conductivity in the interdune compared to the crest. Whilst conductivity values are dependent on the method of measurement (particularly sample:water ratio), which are not explicitly stated in the examples shown in Table B.1, these results indicate that electrical conductivity may be an explanation for high attenuation in these sediments.

Additional samples from locations where GPR has been successful or unsuccessful were also analysed using the same laboratory methods to enable a direct comparison. The conductivity values for the UAE samples are between ~3 and 10 times higher than those of samples from other locations (Tables B.2 and B.3), which are in the range of ~1-2 mS m^{-1}. Attenuation as a result of high electrical conductivity of the sand in this part of the Rub' al Khali is therefore a likely explanation for the unsuccessful application of GPR. It is inferred

Table B.2: List of samples used for sedimentological analyses and GPR suitability at the respective sites. Four samples are from the UAE (A-D) and four samples are from other locations (provided by Professor Charlie Bristow, University of Birkbeck).

Listing in Table	Site/sample	GPR suitability
A	Emirates Highway (UAE11/1/1)	Poor
B	Falaj Al Moalla (crest)	Poor
C	Falaj Al Moalla (interdune)	Poor
D	Shwaib (UAE10/2/19)	Poor
E	Australia	Poor
F	Algeria	Good
G	Morocco	Good
H	Namibia	Good

Table B.3: EC and particle size data for GPR samples listed in Table B.2. Particle size components (using the classification of Blott, 2000) are given in percentages. TDS represents total dissolved salts. The thick horizontal line separates sites where GPR was unsuccessfully (above) and successfully (below) applied.

Site	EC (mS m^{-1})	Salinity (‰)	TDS (mg l^{-1})	Mean particle size (µm)	Sorting (s.d.)	V. coarse sand	Coarse sand	Med sand	Fine sand	V. fine sand	Silt
A	5.49	0.0	26	187	1.64	1.3	2.1	24.4	51.0	21.1	0.2
B	6.93	0.0	33	185	1.43	-	-	20.3	65.5	14.2	-
C	10.96	0.1	57	174	1.54	-	0.4	20.3	56.3	22.8	0.2
D	5.93	0.0	28	182	1.51	-	0.1	22.3	58.8	18.8	0.1
E	1.90	0.0	9	208	2.01	-	4.5	35.5	40.8	12.0	7.2
F	1.06	0.0	5	307	1.60	-	15.3	51.5	29.9	3.2	-
G	1.85	0.0	9	288	1.29	-	1.2	69.9	28.9	-	-
H	1.46	0.0	7	281	1.29	-	1.0	66.2	32.8	-	-

that this is as a result of coastal sediment influx, as there is greater penetration depth at the sites located further inland and GPR has been successfully applied in the Liwa Basin (Bristow et al., 1996). This hypothesis will require more in-depth comparison of sediments within the northeastern Rub' al Khali in order to be tested.

Electrical conductivity is low for the Australian sand sample (E) and yet GPR was ineffective (Bristow et al., 2007b). An alternative reason for the high attenuation at this site, and suggested by Bristow et al., is high clay content. Clay minerals are layered silicate minerals (phyllosilicates) and are usually considered to be less than 2 μm in diameter (for example within the Wentworth, 1922, particle size classification). Clays with high cation-exchange capacities (CECs) tend to have surface conductivity (σ_s), which, together with pore fluid conductivity (σ_w), is related to the bulk electrical conductivity (σ).

The clay minerals identified by XRD analysis in each of the samples are shown in Table B.4. Montmorillonite, part of the smectite group, is identified in the Australian sample (Figure B.4b). As a result of their di- or trioctahedral 2:1 charged layer structure, clays of the smectite group tend towards extensive isomorphic substitution and high CECs (Hall, 1987). Montmorillonite has a CEC of 700-1000 meq kg^{-1} (measured at pH 7); high compared to chlorite (100-400 meq kg^{-1}), kaolinite (30-150 meq kg^{-1}) and palygorskite (200

Table B.4: Minerals present in the samples listed in Table B.2, identified by XRD analysis. The thick horizontal line separates sites where GPR was unsuccessfully (above) and successfully (below) applied. Tectosilicates (including feldspars) are indicated in italics, carbonates are underlined.

Site	***Albite***	***Andesine***	**Antigorite**	**Calcite**	**Chlorite**	**Dolomite**	**Kaolinite**	**Lepidocrocite**	***Microcline***	**Montmorillonite**	**Muscovite**	**Palygorskite**	***Quartz***	***Sanidine***	**Wadsleyite**
A			✓	✓	✓	✓		✓			✓	✓	✓		
B	✓		✓	✓	✓	✓			✓		✓		✓		
C			✓	✓	✓				✓			✓	✓		✓
D	✓			✓	✓	✓					✓	✓	✓		
E					✓		✓			✓	✓		✓	✓	
F				✓	✓						✓		✓		
G				✓					✓		✓		✓		
H	✓	✓			✓				✓		✓		✓		

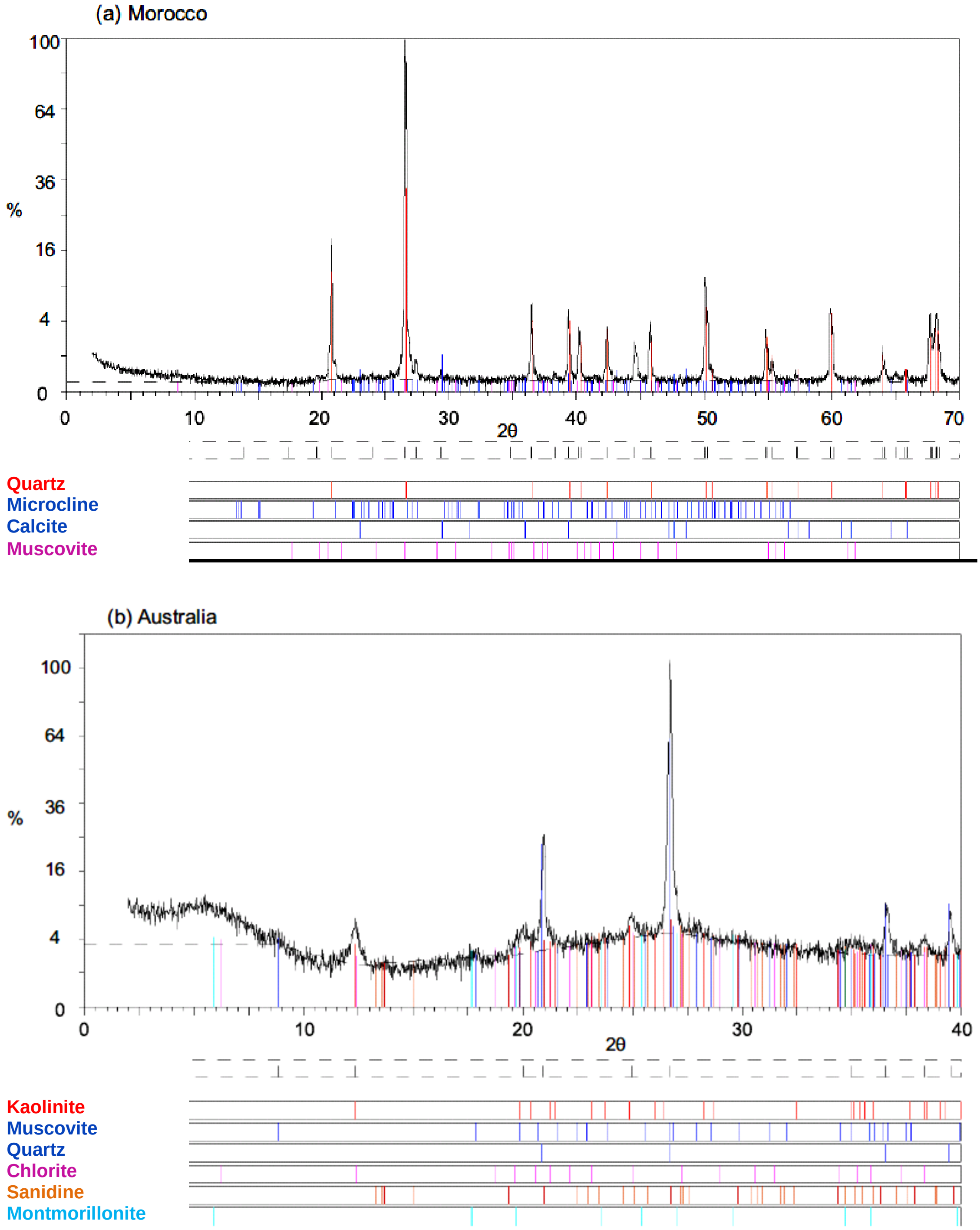

Figure B.4: XRD analysis of (a) Moroccan and (b) Australian sand samples, where GPR was successful and unsuccessful respectively. Counts have been converted to percentage intensity.

meq kg^{-1}) (Carroll, 1959). Smectite clays minerals are not present in any of the other samples, and the presence of montmorillonite, in addition to other clay minerals, in the Australian sample may explain the high attenuation levels of the sediment at this site.

The samples from the UAE are mainly composed of calcite and quartz. Chlorite is present at both good and bad GPR sites (Table B.4), and, given the similar CECs of chlorite and palygorskite, it is thought that these clay minerals must be present in large quantities in order to explain the high attenuation at these sites. Lepidocrocite, an iron oxyhydroxide, is present at the Emirates Highway. The presence of iron oxides has been associated with introducing complexity in GPR analyses (Van Dam and Schlager, 2000). However, ICP-AES analysis shows low concentrations, suggesting that this is probably not the main cause for the problems faced in the UAE.

B.3.5 Conclusions

An attempt to further develop the results put forward in this thesis by the use of GPR to image subsurface dune structures was ultimately unsuccessful. This is a result of high attenuation of the EM signal at three sites in the UAE. Sedimentological analyses and comparisons with sand samples from sites where the use of GPR has been both successful and unsuccessful on aeolian dunes indicate that the high attenuation was a result of high electrical conductivity. The presence of montmorillonite has been attributed as the cause of high EM attenuation at an Australian site where GPR surveys were largely ineffective (Bristow et al., 2007b). It is suggested that sedimentological analyses are conducted on samples prior to fieldwork, where feasible, and future work aims to do this by developing guidelines as to the identification of ‘good’ and ‘bad’ samples for using GPR.

These findings show that the application of GPR is not necessarily a solution to the problems of blind sampling. In addition, concerns over the use of bounding surfaces as indicators of significant temporal hiatuses (Chapters 4 and 5) also suggest that the importance of GPR data in both guiding and interpreting OSL studies may be overestimated.

B.3.6 Appendix bibliography

Atkinson, O.A.C., Thomas, D.S.G., Goudie, A S., Bailey, R.M., 2011. Late Quaternary chronology of major dune ridge development in the northeast Rub' al-Khali, United Arab Emirates. Quaternary Research, 76, 93-105.

Baker, G.S., Jordan, T.E., Pardy, J., 2007. An introduction to ground penetrating radar (GPR). In: Baker, G.S., Jol, H.M., (Eds.), Stratigraphic Analyses Using GPR. Geological Society of America Special Paper, pp. 1–18.

Blott, S., 2000. Gradistat V.4.0.

Bristow, C.S., 2004. GPR in sediments: Recent advances in stratigraphic applications. In: Slob, E.C., Yarovoy, A., Rhebergen, J., (Eds.), Proceedings of the Tenth International Conference on Ground Penetrating Radar, Delft, The Netherlands, pp. 569-573.

Bristow, C.S., Bailey, S.D., Lancaster, N., 2000. The sedimentary structure of linear sand dunes. Nature, 406 , 56-59.

Bristow, C.S., Duller, G.A.T., Lancaster, N., 2007a. Age and dynamics of linear dunes in the Namib Desert. Geology 35 : 555–558.

Bristow, C.S., Jones, B.G., Nanson, G.C., Hollands, C., Coleman, M., Price, D.M., 2007b. GPR surveys of vegetated linear dune stratigraphy in central Australia: Evidence for linear dune extension with vertical and lateral accretion. In: Baker, G.S., Jol, H.M., (Eds.), Stratigraphic Analyses Using GPR. Geological Society of America Special Paper, Vol. 432, pp. 19-33. Boulder.

Bristow, C.S., Lancaster, N., Duller, G.A.T., 2005. Combining ground penetrating radar surveys and optical dating to determine dune migration in Namibia. Journal of the Geological Society, 162, 315-321.

Bristow, C.S., Push, J., Goodall, T., 1996. Internal structure of aeolian dunes in Abu Dhabi determined using ground-penetrating radar. Sedimentology 43 : 995–1003.

Carroll, D., 1959. Ion exchange in clays and other minerals. Geological Society of America Bulletin 70 : 749.

Van Dam, R.L., Schlager, W., 2000. Identifying causes of ground-penetrating radar reflections using time-domain reflectometry and sedimentological analyses. Sedimentology 47 : 435–449.

Daniels, D.J., 2005. Ground Penetrating Radar. In: Chang K (Ed.), Encyclopedia of RF and Microwave Engineering. Wiley, Hoboken, pp. 1833–1846.

Davis, J.L., Annan, A.P., 1989. Ground-penetrating radar for high-resolution mapping of soil and rock stratigraphy. Geophysical Prospecting 37 : 531–551.

Hall, P.L., 1987. Clays: their significance, properties, origins and uses. In: Wilson, M.J., (Ed.), A Handbook of Determinative Methods in Clay Mineralogy. Blackie: Glasgow.

Harari, Z., 1996. Ground-penetrating radar (GPR) for imaging stratigraphic features and groundwater in sand dunes. Journal of Applied Geophysics 36 : 43–52.

Hollands, C.B., Nanson, G.C., Jones, B.G., Bristow, C.S., Price, D.M., Pietsch, T.J., 2006. Aeolian-fluvial interaction: evidence for Late Quaternary channel change and wind-rift linear dune formation in the northwestern Simpson Desert, Australia. Quaternary Science Reviews 25: 142–162.

Jol, H.M., Bristow, C.S., 2003. GPR in sediments: advice on data collection, basic processing and interpretation, a good practice guide. In: Bristow, C.S., Jol, H.M. (Eds.), Ground Penetrating Radar in Sediments. Geological Society: London, pp. 9–27.

Li, S-H, Fan, A., 2011. OSL chronology of sand deposits and climate change of last 18 ka in Gurbantunggut Desert, northwest China. Journal of Quaternary Science 26 : 813–818.

Neal, A., 2004. Ground-penetrating radar and its use in sedimentology: principles, problems and progress. Earth Science Reviews 66 : 261–330.

Rubin, D.M., 1990. Lateral migration of linear dunes in the Strzelecki Desert, Australia. Earth Surface Processes and Landforms 15 : 1–14.

Telfer, M.W., 2011. Growth by extension, and reworking, of a south-western Kalahari linear dune. Earth Surface Processes and Landforms 36 : 1125–1135.

Wentworth, C.K., 1922. A scale of grade and class terms for clastic sediments. Journal of Geology 30 : 377–392.